

Water Absorption and Performance Degradation of Natural Fiber Reinforced Thermoplastic  
Composites

by

Nicole Lee M. Robertson

A thesis submitted in partial fulfillment of the requirements for the degree of

Doctor of Philosophy

in

Materials Engineering

Department of Chemical and Materials Engineering  
University of Alberta

© Nicole Lee M. Robertson, 2017

## ABSTRACT

Natural fiber reinforced polyethylene biocomposites are an environmentally friendly alternative to non-biodegradable thermoplastic materials. The addition of natural fibers to polyethylene improves mechanical properties such as tensile modulus and tensile strength. Unlike thermoplastics, biocomposites are water absorbant due to the presence of natural fibers. Biocomposites mechanical properties degrade when exposed to water. Immersion in water shortens the product life of biocomposites and limits their use in many applications. However, a shorter product life is advantageous for some applications because early degradation reduces the material's environmental impact.

The work herein explores long-term water immersion (6000+ hours) of injection molded hemp and wood pulp fiber reinforced polyethylene. Both low density polyethylene (LDPE) and high density polyethylene(HDPE) were tested, each with three fiber fill fractions. The comprehensive dataset collected for this project allowed for conclusions to be drawn about the effect of fiber type, content and distribution as a function of immersion time to predict water absorption. The extent of mechanical degradation was proven to be dependent on the quantity of water absorbed. A model was developed to predict the percentage of water absorbed over a long time scale that accounts for fiber degradation to enable the prediction of changes to the mechanical properties. The prediction of the rate and magnitude of water absorption by natural fiber thermoplastic composites will allow designers to understand, and account for, the degradation of the material's mechanical properties over time.

## ACKNOWLEDGEMENTS

My doctoral program has been an expansion of creative thought of both physical and social systems. Now, I can think “outside the box”! This journey has developed my ability to think creatively and reflect pragmatically. I’d like to acknowledge and thank those individuals who have contributed by either sharing their vastly different research topics, engaging in deep reflective discussions or coaching to step outside my comfort zone. First and foremost thank you to my supervisors John A. Nychka & John D. Wolodko, for your mentorship as an educator, researcher and engineer. Thank you for believing in me until I finally began to believe in myself. I’ll forever think “what would John say?”

Thank you for everyone who has been directly or inadvertently involved in my work. My apologies to those whose contributions are not directly captured within these acknowledgements. I had the privilege of interfacing with 5 distinct research groups at AITF, 4 laboratory groups within the University of Alberta and two government institutions, Alberta Agriculture and National Research Council. Along with the support of from both my industry colleagues to finish my dissertation while working full time.

Thank you to the Advanced Material group at Alberta Innovates Technology Futures. A few specific individuals include Lisa Sopkow, Ron Rau and Jim Melnichuk. Lisa Sopkow thank you for teaching me how to work safely and efficiently in the lab and modelling how to handle tough situations in the workplace. You have been a great role model. I will never be able to thank you enough for all the extra hours you worked off the clock. Without your dedication to help, my degree would not have been possible. Another special thank you to Ron Rau for taking me under your wing and continually feeding my curiosity of mechanical testing and plastics. Lastly, Jim Melnichuk thank you for teaching me how to think about both sides of the coin, and for teaching me how to make your famous jigs!

Thank you to the following mentors who have supported me throughout my program. Thank you:

- Jim Sawada for pushing me when I didn’t know I needed it, and for providing daily perspective and encouragement.
- Theo Hengsbach for contribution of countless hours in setting up the injection molder, troubleshooting the manufacturing issues and educating me on the art of it. Your friendship and mentorship will always be greatly appreciated.

- Renee Polziehn for the opportunity to work with you engaging the graduate student body in development of teaching and learning. Thank you for your mentorship and continued support.
- Terri Funk for encouraging me to pursue a higher level of education and providing an employment opportunity prior to the completion of my degree. Your belief in my abilities has meant so much. I am the confident individual that I am today because of you.

Thank you to those individuals who have assisted with this final dissertation: 1) Layne Huber for his work on an illustrator drawing and 2) Robyn Braun for her expertise, dedication and kindness editing portions of this work.

Thank you to my committee members, Dr. Reg Eadie and Dr. Philip Choi for your guidance throughout the years. Both of you have provided me with so much opportunity professionally and personally. I am very grateful to have had the opportunity to work with both of you. It has been such an honour and privilege.

Lastly, thank you to all of my friends for including me in your journey. A few specific individuals include: 1) JP Whan for your unwavering support 2) Katherine Jonsson for your continued insight and friendship 3) Michal Zielinski thank you for starting this journey with me – your friendship is invaluable, 4) Terry Runyon who has enabled the seemingly impossible in and out of the lab, and 5) lastly the numerous other team mates of the Materials Interface group whose feedback has helped push me to answer even more questions.

# TABLE OF CONTENTS

Abstract .....	ii
Acknowledgements .....	iii
List of Figures .....	ix
List of Tables .....	xxi
Definition of Parameters .....	xxiv
Abbreviations.....	xxvi
1. Introduction.....	1
1.1 Significant Contributions.....	4
References.....	5
2. Background.....	7
2.1 Constituent material properties used in Biocomposites.....	8
2.1.1 Natural Fibers Reinforcement .....	9
2.1.2 Thermoplastic Matrix.....	16
2.2 Manufacturing of Biocomposite Materials .....	20
2.2.1 Processing Natural Fibers.....	20
2.2.2 Mixing.....	21
2.2.3 Molding & Finishing.....	23
2.3 Mechanisms Of and Effects from Water Absorption .....	25
2.3.1 Influences on Water Absorption.....	26
2.3.2 Mechanisms for Water Absorption.....	28
2.4 Water Absorption Models .....	34
2.4.1 Fickian Diffusion.....	37
2.4.2 Dual Stage Fickian Diffusion.....	39
2.4.3 Anomalous Diffusion.....	40
2.4.4 Percolation Theory .....	40
2.5 Effect of Water Absorption on Mechanical Properties.....	43
2.6 Conclusions.....	46
References.....	47
3. Experimental Design & Description.....	52
3.1 Manufacturing Methods.....	52

3.1.1	Raw Materials .....	53
3.1.2	Raw Fiber Processing .....	54
3.1.3	Compounding of Biocomposites .....	55
3.1.4	Injection Molding .....	58
3.1.5	Machined Samples .....	59
3.2	Evaluation of Materials .....	61
3.2.1	Gas Pycnometry .....	62
3.2.2	Water Immersion – Gravimetric Measurements.....	64
3.2.3	Mechanical Tensile Tests .....	66
3.2.4	Fluorescent Macrophotography.....	67
3.2.5	Scanning Electron Microscopy.....	68
3.2.6	Image Analysis – Area Fiber Fraction .....	70
3.2.7	Natural Fiber Water Content.....	74
3.2	References.....	75
4.	Impact of Water on Mechanical Properties .....	77
4.1	Determination of Volume Fraction.....	77
4.1.1	Evaluation of Polyethylene Density.....	79
4.1.2	Evaluation of Fiber Densities .....	80
4.1.3	Biocomposite Evaluation .....	82
4.2	Water Absorption of Tensile Specimens .....	86
4.3	Mechanical Properties .....	88
4.3.1	Representative Engineering Stress-Strain Curves .....	88
4.3.2	Modulus.....	91
4.3.3	Yield Strength .....	97
4.3.4	Ultimate Tensile Strength.....	101
4.3.5	Elongation at Break & Toughness .....	105
4.4	Reversibility of Mechanical Degradation .....	113
4.4.1	Modulus Loss .....	113
4.4.2	Tensile Yield Strength Loss.....	115
4.4.3	Ultimate Tensile Strength Loss.....	116
4.4.4	Elongation at Break & Toughness Loss.....	117
4.5	Fracture Mode Assessment.....	119

4.5.1	Polymer .....	119
4.5.2	Fiber .....	120
4.5.3	Biocomposite .....	121
4.6	Summary .....	124
	References.....	128
5.	Phenomenon, Mechanism and Predictive Water Absorption Model in Biocomposites..	130
5.1	Visual characterization of Biocomposites .....	131
5.1.1	Assessment of Surface Area Percent Fiber .....	133
5.2	Comprehensive Water Absorption Curves.....	139
5.2.1	Matrix.....	139
5.2.2	Hemp Reinforced Biocomposites .....	140
5.2.3	Wood Pulp Reinforced Biocomposites .....	141
5.2.4	Fiber Volume Fraction & Maximum Water Absorption .....	142
5.2.5	Overview of Water absorption of Fiber Reinforced Biocomposites .....	144
5.3	Reversibility of Water Absorption – Drying .....	145
5.3.1	Surface Fiber Degradation.....	145
5.3.2	Gravimetric Quantification of Fiber Loss .....	147
5.4	Analysis of Current Water Absorption Models.....	151
5.4.1	Transport of Water by Pressure .....	152
5.4.2	Diffusion.....	153
5.4.3	Interconnectivity .....	157
5.5	Dual Phase Diffusion Absorption with Decay Model.....	162
5.5.1	Initial Mass Absorption Term .....	163
5.5.2	Bulk Water Absorption Magnitude and Rate.....	168
5.5.3	Long Term Fiber Decay.....	175
5.6	Model Functionality .....	180
5.7	Chapter Summary .....	183
5.8	References.....	185
6.	Conclusions .....	186
6.1	Water Absorption .....	186
6.2	Mechanical Properties .....	188
6.3	Summary .....	190

7. Future Work.....	192
Bibliography By Chapter .....	194
Introduction References .....	194
Background References.....	196
Experimental Design & Description References .....	200
Impact of Water on Mechanical Properties References.....	201
Phenomenon, Mechanism and Predictive Water Absorption Model in Biocomposites References.....	203
Conclusions.....	203
Future Work.....	203
Appendices References.....	203
A. Appendix: Biocomposites Manufacturing Parameters .....	204
A.1 Calibration Feed Rate for Matrix and Fiber .....	204
A.2 Additional Fiber Processing Information .....	206
A.3 Summary of Extrusion Parameters .....	207
A.4 Summary of Injection Molding Parameters .....	208
A.5 Nitrogen Pycnometry Sensitivity of Minimum Volume .....	209
B. Appendix: Statistical Analysis of Uncertainty.....	210
B.1 Density Measurement – Uncertainty Analysis.....	210
B.2 Weight Measurements & normalized Weight Gain.....	213
B.3 Mechanical Properties – Uncertainty Analysis .....	215
References.....	216
C. Appendix: Mechanical Property Data Library .....	217
D. Appendix: Water Absorption Data Library.....	222
E. Appendix: Water Absorption Model Parameters.....	237
F. Appendix: Surface Exposed Fiber – Back Scattered SEM Image Analysis Results.....	241
F.1 Assessment of Percent Fiber on Manufactured Surfaces .....	241
F.2 Calculated Surface Area of Fiber.....	244



## LIST OF FIGURES

Figure 1.1 Consumption of thermoplastic over the last 40 years compared to steel. <i>Data graphed from Michal Biron, Thermoplastics and Thermoplastic Composites 2007</i> ). .....	1
Figure 2.1 Material science paradigm, traditional (left) to path dependency (right) to illustrate the relationship of structure, properties, processing, structure and performance for a material. Images used with permission from J.A. Nychka and G.D. Hibbard from [1]. .....	7
Figure 2.2 Classification of natural fibers, modified from [9].....	10
Figure 2.3 Chemical structures of cellulose, hemicelluloses and three phenolic building block structure of lignin redrawn from [12]. .....	11
Figure 2.4 Network of hydrogen bonds between cellulose chains, formation of crystalline cellulose micro fibrils and the helical arrangement of cellulose within natural fiber micro fibril [17] (left to right). Images reproduced with permission from [17]. .....	13
Figure 2.5 Hierarchical classification of natural fiber types from stem to micro fibril for bast fiber, flax. Image reproduced with permission from [20]. .....	13
Figure 2.6 Breakdown of consumption of thermoplastics by volume produced. Polyethylene is the largest produced thermoplastic. Data reproduced from [32]. .....	16
Figure 2.7 2013 world polyethylene demand, 81.8 million metric tons, by classification graphed from data in [34].....	17
Figure 2.8 Polyethylene chain and crystal structure, images modified from [35] and [18]. ....	17
Figure 2.9 Overview of the biocomposites manufacturing processes. ....	20
Figure 2.10 Overview of agricultural fiber processing methods for compounding. ....	21
Figure 2.11 Illustration of dispersion and distribution of a discontinuous phase (black). .....	22
Figure 2.12 Mechanistic pathways schematic of water absorption for a single fiber embedded within a matrix, a) structure prior to immersion, b) concurrent processes during water immersion, and c) the structure after drying. Adapted from [60]. .....	28
Figure 2.13 Demonstrates the low interconnectivity with only one cluster, not connected compared to multiple fiber clusters with different interconnected paths through the material. Image modified from [66]. .....	30
Figure 3.1 Process Flow Diagram of Manufacturing and Analysis Methods .....	52
Figure 3.2 As received (milled) fiber condition a) Hemp and b) Wood Pulp. ....	53

Figure 3.3 Equipment involved with natural fiber pelletization from left to right: Ohaus Moisture Analyzer[1], Amandus Kahl Die Face Mill with Rollers, and Wiley Mill. ....	54
Figure 3.4 Pelletized fiber condition a) Hemp and b) Wood Pulp along with a range of individual fiber bundle silhouettes (obtained from bright field transmitted optical light microscopy) in the top right. Image modified from [2]. ....	55
Figure 3.5 Thermo Scientific Twin Screw Extruder a) thermoplastic feeder, b) thermoplastic feeder port, c) natural fiber feeder, d) natural fiber feed port and e) vacuum port location....	56
Figure 3.6 Air cooling apparatus after extrusion compounding.....	56
Figure 3.7 Twelve variations of hemp fiber and wood pulp reinforced polyethylene biocomposites displayed in the same arrangement as Table 3.1. The left three columns are LDPE and the right three columns are HDPE variations.....	57
Figure 3.8 Left: BOY 22A Injection molder Right: Mold cavity with all three specimen types manufactured in one injection molded shot. ....	58
Figure 3.9 X-Y Izod Specimen Type showing fiducial markings (white lines) used for referencing locations in SEM characterization. ....	59
Figure 3.10 Cut edge(s) specimen types.....	60
Figure 3.11 Gas Pycnometer [6] (left) and Schematic of Pycnometer Chambers (right).....	62
Figure 3.12 Sample chamber filled with square biocomposite specimens .....	63
Figure 3.13 Freezer Mill (left) and sample tube with rod (right). ....	64
Figure 3.14 Water bath for tensile immersion specimens (at back right) and as molded flexural specimens. Specimens were stacked vertically (tensile) or placed inside glass vials (flexural, square, etc) to reduce area not in direct contact with the water immersion environment while ensuring the specimen remains submerged. ....	65
Figure 3.15 Schematic of Tensile Specimen (left) and typical stress strain curve for fiber filled biocomposite (right). Stress Strain curve is representative curve from HH45 prior to water immersion. ....	66
Figure 3.16 LH45(32.8) after immersion in UV water soluble dye. Left to right: 0 hour, 1 hour, and 24 hours. ....	68
Figure 3.17 Fracture Surface of LH15(9.4) without exposure to water immersion. ....	69
Figure 3.18 Representative BS SEM Images of 30wt% Hemp filled HDPE at each surface. Light grey regions are hemp fibers, as indicated by white arrows.....	69

Figure 3.19 Field of View on HH45(36.4) XY Izod Specimen. Notice the fiducial lines at left and bottom.....	70
Figure 3.20 Schematic of location of cut surfaces.....	71
Figure 3.21 Montage of Auto Threshold settings on the As Molded surface of 30wt% hemp filled HDPE.....	72
Figure 3.22 Comparison of backscattered and the corresponding IsoData thresholded micrograph at each surface for 30 wt% hemp filled HDPE. ....	73
Figure 3.23 (Left) Backscattered micrograph of glass silica beads and (right) IsoData thresholded imaged. ....	73
Figure 3.24 Glass vacuum chamber where salt solution filled the bottom of the container to produce a high humidity environment of 97.3%. Image from [20]. ....	74
Figure 4.1 Comparison of LDPE and HDPE as molded density determined by nitrogen pycnometry (filled) versus density provided on the technical data sheet (unfilled). The error bars represented a 99% confidence interval based on a proven normal distribution. ....	79
Figure 4.2 Comparison of mass density for Hemp fiber (left) and Wood Pulp (right) after different processing methods. Hemp exhibits higher variability to fiber preparation method than wood pulp as the magnitude of scatter between fiber forms is greater for hemp. The error bars represent a 99% confidence interval around the mean based on a proven normal distribution. ....	80
Figure 4.3 Transmitted bright field optical light microscope micrographs of hemp fiber processed by a) hammer milling and b) freezer milling methods. Freezer milling has reduced both fiber size and shape to maximize exposure of fiber closed pore volume.....	82
Figure 4.4 Comparison of manufactured target weight percent to actual weight percent, relative to the 1:1 relationship shown by $y=x$ . The actual weight percent fiber frequently does not match the targeted fiber content, especially as the fiber content increases. ....	84
Figure 4.5 Distribution of fiber volume fraction at each targeted fiber weight fraction from manufacturing. ....	85
Figure 4.6 Average moisture absorption as a function of time, hemp reinforced biocomposites (diamond) and wood pulp reinforced biocomposites (circle) tensile specimens. The colors designate the relative amount of fiber content, none (control) = grey, target 15 wt% low= green, target 30 wt% medium = blue and target 45 wt% high = purple. ....	86
Figure 4.7 Magnitude of water absorbed after 6552 hours immersion comparison between hemp fiber (diamond) and wood pulp (circle) in a) LDPE matrix and b) HDPE matrix. The colors	

designate the relative amount of fiber content, none (control) = grey, target 15 wt% low= green, target 30 wt% medium = blue and target 45 wt% high = purple. ....87

Figure 4.8 Representative stress versus strain curve for both HDPE and LDPE. HDPE demonstrates a greater tensile strength and ultimate tensile strength after which the specimen necks due to chain alignment at low strain rates where by the specimen does not break unlike LDPE which fractured. ....89

Figure 4.9 Representative engineering stress versus strain curves for low density polyethylene biocomposites a) hemp fiber and b) wood pulp reinforced. Increase in fiber content leads to an increase in tensile modulus and strength at the expense of loss of ductility. .... 90

Figure 4.10 Representative engineering stress versus strain curves for high density polyethylene biocomposites a) hemp fiber and b) wood pulp reinforced. The change in fiber content from low to medium results in an increase in elastic modulus but with a decrease in ductility. .... 90

Figure 4.11 Tensile Modulus as a function of fiber volume fraction for LDPE (unfilled symbols) and HDPE (filled symbols). Increase fiber content translates into an increase in tensile modulus. The colors designate the relative amount of fiber content as reported. .... 91

Figure 4.12 Tensile modulus as a function of water immersion time for all material variations. Observed continued decline after 168 hours immersion in modulus. The colors designate the relative amount of fiber content, none (control) = grey, target 15 wt% low= green, target 30 wt% medium = blue and target 45 wt% high = purple. .... 92

Figure 4.13 Tensile modulus versus absorbed water for all material variations. Increased mass gain led to decreased modulus, to varying degrees, in all biocomposite formulations. The colors designate the relative amount of fiber content, none (control) = grey, target 15 wt% low= green, target 30 wt% medium = blue and target 45 wt% high = purple. .... 93

Figure 4.14 Exponential decay, Equation 4.8 (dashed line), of normalized tensile modulus and percent mass gain of water for all biocomposite variations ..... 94

Figure 4.15 The average load carrying capability of the natural fibers by volume fraction of fiber at time 0 (light blue) and after 6552 hours (dark blue) for all material variations. For all variations except HW15, exposure time in an immersion environment resulted in a decrease in in situ fiber modulus. .... 96

Figure 4.16 Tensile yield strength as a function of fiber volume fraction for LDPE (unfilled symbols) and HDPE (filled symbols). Natural fibers provide additional strength to the biocomposite for all variations except wood pulp reinforced in high density polyethylene, HW. .... 97

Figure 4.17 Yield strength as a function of water immersion time for all material variations. Tensile yield strength declines with immersion time..... 98

Figure 4.18 Tensile yield strength verses percent water absorbed for all material variations. Tensile yield strength decreases as the percent mass gain of water increases. The colors designate the relative amount of fiber content, none (control) = grey, target 15 wt% low= green, target 30 wt% medium = blue and target 45 wt% high = purple. .... 99

Figure 4.19 Linear relationship, Equation 4.9 (dashed line), of normalized tensile yield strength and percent mass gain of water for all biocomposite variations. The colors designate the relative amount of fiber content, none (control) = grey, target 15 wt% low= green, target 30 wt% medium = blue and target 45 wt% high = purple. .... 100

Figure 4.20 Ultimate tensile strength as a function of fiber volume fraction for LDPE (unfilled symbols) and HDPE (filled symbols). No increase observed in UTS with the addition of natural fibers. The colors designate the relative amount of fiber content, none (control) = grey, target 15 wt% low= green, target 30 wt% medium = blue and target 45 wt% high = purple. .... 101

Figure 4.21 Ultimate tensile strength as a function of water immersion time for all material variations. Continued decline of ultimate tensile strength after 168 hours immersed. The colors designate the relative amount of fiber content, none (control) = grey, target 15 wt% low= green, target 30 wt% medium = blue and target 45 wt% high = purple. .... 102

Figure 4.22 Ultimate tensile strength versus percent water absorbed for all material variations a) hemp reinforced LDPE, b) hemp reinforced HDPE, c) wood pulp reinforced LDPE and d) wood pulp reinforced HDPE. Ultimate tensile strength decreases as the percent mass gain of water increases to a greater extent for HDPE based biocomposites than LDPE based. The colors designate the relative amount of fiber content, none (control) = grey, target 15 wt% low= green, target 30 wt% medium = blue and target 45 wt% high = purple. .... 103

Figure 4.23 Linear relationship, Equation 4.10 (dashed line), of normalized ultimate tensile strength and percent mass gain of water for all biocomposite variations. The colors designate the relative amount of fiber content, none (control) = grey, target 15 wt% low= green, target 30 wt% medium = blue and target 45 wt% high = purple..... 104

Figure 4.24 Elongation at break as a function of fiber volume fraction for LDPE (unfilled symbols) and HDPE (filled symbols). Increased fiber content results in a decrease in ductility represented by elongation at break. The colors designate the relative amount of fiber content, none (control) = grey, target 15 wt% low= green, target 30 wt% medium = blue and target 45 wt% high = purple. .... 106

Figure 4.25 Toughness as a function of fiber volume fraction for LDPE (unfilled symbols) and HDPE (filled symbols). The addition of natural fibers results in a sharp decrease in tensile toughness. The colors designate the relative amount of fiber content, none (control) = grey,

target 15 wt% low= green, target 30 wt% medium = blue and target 45 wt% high = purple.  
..... 107

Figure 4.26 Elongation at break (left) and Toughness (right) of LDPE as a function of immersion time. No observed trends were observed for LDPE in either elongation at break or toughness due to the scatter in the data. HDPE results are not reported as the virgin material did not fracture..... 108

Figure 4.27 Elongation at break as a function of water immersion time for all material variations. Duration of immersion does not alter the elongation at break..... 109

Figure 4.28 Toughness as a function of water immersion time for all material variations. Duration of immersion does not alter the biocomposite toughness. .... 109

Figure 4.29 Percent water absorbed verses elongation at break for all material variations. A slight increase in elongation at break was observed for medium (blue) and high (purple) fiber contents in HDPE; otherwise no trend is observed. .... 110

Figure 4.30 Toughness of each material variation with respect to water absorbed. No observed change in biocomposite tensile toughness with water immersion. The colors designate the relative amount of fiber content, none (control) = grey, target 15 wt% low= green, target 30 wt% medium = blue and target 45 wt% high = purple. .... 111

Figure 4.31 Normalized elongation at break relative to percent mass gain from water immersion, with Equation 4.11 graphed (dashed line). Linear increase in ductility with absorbed water without an observed increase in toughness. The colors designate the relative amount of fiber content, none (control) = grey, target 15 wt% low= green, target 30 wt% medium = blue and target 45 wt% high = purple where filled are HDPE variations and unfilled are LDPE..... 112

Figure 4.32 Normalized tensile modulus of specimens dried after 6552 hours of immersion, where grey is virgin, blue represents 15 wt%, green represents 30 wt% and purple represents 45 wt%. Permanent degradation in tensile modulus after prolonged immersion correlated with an observed mass loss. The colors designate the relative amount of fiber content, none (control) = grey, target 15 wt% low= green, target 30 wt% medium = blue and target 45 wt% high = purple. .... 114

Figure 4.33 Normalized tensile yield strength of specimens dried after 6552 hours of immersion, where grey is virgin, blue represents 15 wt%, green represents 30 wt% and purple represents 45 wt%. Permanent degradation observed in tensile yield strength for hemp fiber reinforced specimens. The colors designate the relative amount of fiber content, none (control) = grey, target 15 wt% low= green, target 30 wt% medium = blue and target 45 wt% high = purple. .... 115

Figure 4.34 Normalized ultimate tensile strength of specimens dried after 6552 hours of immersion, where grey is virgin, blue represents 15 wt%, green represents 30 wt% and purple represents 45 wt%. Permanent degradation in the ultimate tensile strength for hemp fiber reinforced specimens is observed; no significant change for wood pulp reinforced specimens is observed. The colors designate the relative amount of fiber content, none (control) = grey, target 15 wt% low= green, target 30 wt% medium = blue and target 45 wt% high = purple. .... 116

Figure 4.35 Normalized elongation at break of specimens dried after 6552 hours of immersion, where grey is virgin, blue represents 15 wt%, green represents 30 wt% and purple represents 45 wt%. Water immersion environment resulted in increased ductility. The colors designate the relative amount of fiber content, none (control) = grey, target 15 wt% low= green, target 30 wt% medium = blue and target 45 wt% high = purple..... 117

Figure 4.36 Normalized toughness of specimens dried after 6552 hours of immersion, where grey is virgin, blue represents 15 wt%, green represents 30 wt% and purple represents 45 wt%. Negligible changes in toughness observed with the exception of LH variations which gained additional toughness. The colors designate the relative amount of fiber content, none (control) = grey, target 15 wt% low= green, target 30 wt% medium = blue and target 45 wt% high = purple..... 118

Figure 4.37 Ductile fracture surface for both a) LDPE and b) HDPE near a reinforcing fiber. .... 119

Figure 4.38 Fiber fracture surfaces at different stages with regards to water immersion a) before exposure, b) after exposure c) exposed and dried..... 121

Figure 4.39 Fracture surface at 0 hours and 672 hours of immersion for a) LDPE, b) LH15 and c) LW15 where the white arrows identify the matrix and the black point to the natural fiber. LDPE changes from ductile to brittle with addition of natural fiber, however, when immersed in water, LDPE plasticizes as shown by smoother ductile surfaces elongated in multiple directions compared to the rough fibril surfaces observed when dry..... 122

Figure 4.40 Overview of all the normalize mechanical properties as a function of water absorbed, a) Modulus, b) yield tensile strength c) elongation at break and d) ultimate tensile strength. The degradation of mechanical properties are dependent on the water absorbed within the specimen for all material variations. .... 126

Figure 5.1 Time series of immersed UV dyed hemp (left) and wood pulp (right) filled low density polyethylene square specimens. The green dyed regions correspond only with fibers intersecting the surface of the specimen and the intensity increases with immersion time. 131

Figure 5.2 LH series (left) and LW series (right) after UV Dye Immersion of 1 week..... 132

Figure 5.3 Back scattered cross sectional assessment of fiber distribution from as molded surface, left, into the bulk biocomposite, right for a) LH30 and b)LH45. Note the increasing gradient in fiber concentration going from left to right in each image; the width of the fiber gradient is much smaller for LH45 (b) than LH30 (a) ..... 132

Figure 5.4 a) Schematic of the four types of surfaces: as-molded, as-molded perimeter, transverse and longitudinal cut. b) Green fluorescence maps the higher concentration of natural fibers on the cut surfaces relative to the molded of LH45 after 1 week immersion.. 133

Figure 5.5: Overview of the surface types and the corresponding accessible fiber on the biocomposite surface of variations: a)LH, b) HH, c) LW and d) HW. As-molded surfaces have less accessible fiber content which intersects the biocomposite surface..... 135

Figure 5.6 Relationship between fiber volume fraction and calculated percentage of fiber surface area with specimen geometries for all material variations;  $x = y$  dashed gray guideline for reference..... 136

Figure 5.7 Surface area of fiber, normalized longitudinal cut relative to molded surface (a) and normalized transverse cut relative to molded surface (b). Notice as the fiber volume fraction increases, the surface area of accessible fiber approaches a homogenous material with the same ratio of fibers on the longitudinal(left) and transverse (right) relative to the molded surface, represented with a near 1:1 ratio..... 137

Figure 5.8 Effect of one longitudinal cut on the absorption profile of HH30. By sectioning the specimen, a 2-fold increase in maximum mass gain was observed for this material combination. .... 138

Figure 5.9 Water Absorption of control matrix materials: a) HDPE (left) and b) LDPE (right) up to 9000 hours immersion time..... 139

Figure 5.10 Water Absorption of hemp fiber reinforced biocomposites for both HDPE (left) and LDPE (right) arranged from high fiber fill fractions (top) to lower fill fractions (bottom) up to 9000 hours immersion time. Higher volume fractions of fibers result in higher rates of water absorption and larger magnitudes of total water absorption. .... 140

Figure 5.11 Wood Pulp reinforced biocomposites with (left) LDPE and (right) HDPE arranged from high fiber fill fractions (top) to lower fill fractions (bottom). As for hemp (Figure 5.10) higher water absorption is associated with higher volume fractions of wood pulp fibers..... 142

Figure 5.12 Maximum magnitude of water absorbed during 6552 hours of immersion for all specimens as a function of fiber volume fraction. Hemp fiber reinforced biocomposites absorb a greater amount of water than wood pulp variations and the maximum amount absorbed increases linearly with fiber volume fraction with the exception of LH45..... 143



Figure 5.13 Two locations of hemp fiber present on an as-molded surface within high density polyethylene (HH45), imaged as a function of increasing time (left to right). The fiber degraded, and disappeared from the surface as a function of increase in immersion time..... 145

Figure 5.14 BS-SEM micrographs of high fiber fraction biocomposites surface morphology prior to and after 5 weeks of water immersion to demonstrate the loss of surface accessible fiber. Extent of fiber loss for all material variations due to water immersion. .... 147

Figure 5.15 Comparison of LDPE and HDPE percent dried mass after 6552 hours immersion based on fiber volume fraction for hemp (diamond) and wood pulp (circle)..... 149

Figure 5.16 Comparison of percent dried mass after 6552 hours immersion a) hemp and b) wood pulp reinforced biocomposites HDPE (filled) and LDPE (unfilled) based on ratio of accessible fiber surface area to specimen volume. Wood pulp biocomposites did not endure appreciable mass loss as did hemp fiber, the latter which is inversely proportional to the ratio of accessible fiber area to specimen volume. .... 149

Figure 5.17 Cross sectional illustration of natural fiber dissolution from the surface to the bulk material. Interconnection of natural fibers to the surface; it remains unknown and therefore so does the depth of interconnected fiber loss..... 150

Figure 5.18 Representative water absorption curves isolated from HH45 (purple diamond filled), HW45 (blue circle filled) and LW30 (maroon circle unfilled) all 4 cut specimen type. .... 151

Figure 5.19 Water Absorption of HH45 Flexural specimen type with both 50bar and 1 bar of pressure, negligible difference observed. .... 152

Figure 5.20 Fickian Diffusion for characteristics curves after 100 hours immersed adequately represents absorption in short immersion times..... 153

Figure 5.21 Fickian Diffusion coefficient displayed as a function of fiber volume fraction (a & b), percent fiber surface area (c & d), and accessible fiber area per volume (e & f) for hemp fiber variations (left) and wood pulp variations (right) for all specimen types except tensile bars. Linear increase in the Diffusion coefficient with an increase in accessible fiber surface area, except for LH45 variations,..... 154

Figure 5.22 Fickian Diffusion for characteristics curves after 9 weeks immersed. Fickian diffusion is unable to predict long term immersion for HH45 (purple diamond filled), HW45 (blue circle filled) and LW30 (maroon circle unfilled) all 4 cut specimen type..... 156

Figure 5.23 Dual Fickian Diffusion curve fit for characteristics curves are unable to capture continued water absorption LW30 (maroon circle unfilled) and HH45 (purple diamond filled) continued decrease..... 157

Figure 5.24 Experimentally calculated average fiber water content for wood pulp reinforced biocomposites, HDPE (filled) and LDPE (unfilled), relative to the maximum possible fiber water content in 97% relative humidity (dotted line). HW45 has the highest probability of possessing an interconnected fiber network..... 159

Figure 5.25 Experimentally calculated average fiber water content for hemp fiber reinforced biocomposites, HDPE (filled) and LDPE (unfilled), relative to the maximum possible fiber water content in 97% relative humidity (dotted line) and liquid immersion (dashed). The average fiber water content for LH45, HH45 and HH30 variations demonstrate greater water content than observed at 97.3% relative humidity which may suggest the possibility of an interconnected fiber network..... 159

Figure 5.26 Cross sectional view of LH45 square geometry after immersed in UV dye for 13,176 hours (1.5 years), specimen thickness 3.11mm. Minimal dye penetration observed around the perimeter..... 160

Figure 5.27 Representative water absorption curves isolated from HH45 (purple diamond filled), HW45 (blue circle filled) and LW30 (maroon circle unfilled) all 4 cut specimen type. .... 162

Figure 5.28 Model Dual Phase Absorption and Decay decoupled to show each function separately (left)..... 163

Figure 5.29 Contribution of initial absorption (blue short dash), bulk absorption (blue dash), and fiber decay (red dash) in the first 125 hours of absorption for the three characteristic curves; a) LW30, b) HW45 and c) HH45. .... 164

Figure 5.30 Linear dependency of parameter A on the accessible surface area fiber fraction of the biocomposite for a) hemp fiber variations and b) wood pulp variations..... 165

Figure 5.31 Relative contribution of parameter A compared to the maximum water absorbed for all specimen geometries..... 166

Figure 5.32 Parameter B as a function of accessible surface area fiber fraction for a) hemp fiber variations and b) wood pulp variations for all specimen geometries..... 167

Figure 5.33 The biocomposite initial absorption rate is controlled by the ratio of surface accessible fiber to specimen volume, with the exception of LH45 variations due to suspected interconnected fiber network. Dashed line is a best-fit curve, Eq. 5.7..... 167

Figure 5.34 Experimental correlation between maximum water absorbed and model parameter C..... 168

Figure 5.35 Parameter C assessed as a function of fiber volume fraction for a) hemp fiber variations and b) wood pulp variations for all specimen geometries. Dashed lines are best-fit curves as shown in equations 5.8 and 5.9 respectively..... 169

Figure 5.36 Parameter C assessed as a function of ratio of fiber accessible surface area fraction to specimen volume as a function of matrix type a) LDPE b) HDPE as well as a function of fiber type c) hemp variations and d) wood pulp variations. Dashed lines (c and d) are best-fit curves as shown in equations. 5.10 and 5.11 respectively..... 170

Figure 5.37 Parameter D assessed as a function of fiber volume fraction for a) hemp fiber variations and b) wood pulp variations for all specimen geometries. At higher fiber volume fractions, an exponential relationship reemerges in the bulk diffusion rate, variations HH45, HH30, LH45 and HW45. .... 171

Figure 5.38 Parameter D assessed as a function fiber surface area fraction (a & b) and ratio of fiber accessible surface area fraction to specimen volume (c & d) as a function of fiber type for hemp variations (a & c) and wood pulp variations (b & d). .... 173

Figure 5.39 Bulk biocomposite absorption rate is dependent on diffusion coefficient of the biocomposite if there is an interconnected structure. Dashed lines: interconnected (Eq. 5.12) and dispersed and distributed (Eq. 5.13)..... 174

Figure 5.40 Percent mass loss for a) hemp variations and b) wood pulp variations (right) as a function of percent fiber surface area for all specimen geometries. Note: LW cut geometries are not included..... 175

Figure 5.41 Parameter E variables for a) hemp fiber variations and b) wood pulp variations for all specimen geometries..... 176

Figure 5.42 Parameter E as a function of accessible surface area fiber fraction for a) hemp fiber variations and b) wood pulp variations for all specimen geometries. Dashed lines: are for equations 5.14, 5.15 and 5.16 for LH, HH and Wood Pulp respectively..... 177

Figure 5.43 Parameter F as a function of fiber volume fraction by both matrix type a) LDPE and b) HDPE as well as by fiber type c) Hemp fiber reinforced and d) Wood pulp reinforced for all specimen geometries..... 178

Figure 5.44 Parameter F as a function of accessible surface area fiber fraction for a) hemp fiber variations and b) wood pulp variations for all specimen geometries..... 179

Figure 6.1 Overview of all the normalize mechanical properties as a function of water absorbed, a) Modulus, b) yield tensile strength c) elongation at break and d) ultimate tensile strength. The degradation of mechanical properties are dependent on the water absorbed within the specimen for all material variations. The colors designate the relative amount of fiber content, target 15 wt% low= green, target 30 wt% medium = blue and target 45 wt% high = purple. .... 189

Figure 6.2 Overview of how fiber weight fraction can be translated into predict models of normalized mechanical properties from characterization of the material (purple boxes) and performance (blue boxes) completed within this work .....	190
Figure A.1 Example Calibration Curve of High Density Polyethylene Pellets .....	204
Figure A.2 Example of Wood Pulp Pelletized and Wiley milled gravimetric calibration curve with the error bars graphed with the standard deviation. ....	205
Figure A.3 Example of visual assessment between variations fiber forms of wood pulp (top down) velco punched, steam pelletized and pelletized without addition of moisture extruded with HDPE. From this trail, pelletized without moisture was selected to have promise dispersing into the melt. The black arrows point to locations with noticeable fiber clusters. ....	206
Figure A.4 Example calibration curve of high density polyethylene pellets.....	209

## LIST OF TABLES

Table 2.1: Classification of reasons and the factors for variability in natural fiber properties..	9
Table 2.2: Chemical composition and moisture content of natural fibers reported from [3, 5, 6, 15].....	12
Table 2.3: Common natural fiber types, mechanical properties and specific modulus and strength compared to E-glass. Data taken from [4, 5, 11, 22-24]. Selected fibers highlighted in green.....	14
Table 2.4: Water absorption parameters of common natural fibers utilized for biocomposites.....	15
Table 2.5: Overview of common thermoplastics and their permeability to water.....	18
Table 2.6: Overview of Mechanical Properties of Common Thermoplastics compiled from [41].....	19
Table 2.7 Comparison of common methods to mold biocomposites.....	23
Table 2.8 Comparison of mechanism of water absorption in literature .....	28
Table 2.9 Summary of diffusion coefficients calculated based on Fick's model for biocomposites subjected to long term water immersion conducted at temperatures between 23-30°C. ....	36
Table 2.10 Summary of assessment of mechanical properties of biocomposites.....	44
Table 3.1: Name and symbology convention for manufactured biocomposites.....	57
Table 3.2: Design of Experiments Overview .....	61
Table 3.3: Water Immersion Number of Replicates per Specimen Type .....	65
Table 3.4: Tensile Specimen Water Immersion Intervals .....	67
Table 4.1 Hemp filled Biocomposite Densities from Square Specimens.....	83
Table 4.2 Wood Pulp filled Biocomposite Densities from Square Specimens .....	83
Table 4.3 Name designation for manufactured biocomposites .....	84
Table 5.1: Characteristic curves classification of the type of diffusion cases, reported in terms of n, k and maximum content of water absorbed for 4 cut geometries assessed up to 100 hours.....	151
Table 5.2: Maximum Water Content of Natural Fibers.....	158

Table 6.1 Summary of model parameter as a function of material variation.....	187
Table A.1 - Summary of Extrusion Parameters.....	207
Table A.2 - Summary of Injection Molding Parameters .....	208
Table B.1 Overview of Quantifiable Uncertainty of Experimental Results.....	210
Table B.2 Variation in Density with an Ambient Air Temperature deviation during measurement.....	211
Table B.3 Variation in Percent Weight Gain with assumed residual water thickness.....	214
Table C.1 Matrix Material – LDPE and HDPE.....	217
Table C.2 Hemp Reinforced LDPE Biocomposites.....	218
Table C.3 Hemp Reinforced HDPE Biocomposites .....	219
Table C.4 Wood Pulp Reinforced LDPE Biocomposites.....	220
Table C.5 Wood Pulp Reinforced HDPE Biocomposites.....	221
Table D.1 Water Absorption for LDPE specimen types.....	223
Table D.2 Water Absorption for HDPE specimen types.....	224
Table D.3 Water Absorption for LH15 specimen types.....	225
Table D.4 Water Absorption for LH30 specimen types.....	226
Table D.5 Water Absorption for LH45 specimen types.....	227
Table D.6 Water Absorption for HH15 specimen types.....	228
Table D.7 Water Absorption for HH30 specimen types .....	229
Table D.8 Water Absorption for HH45 specimen types.....	230
Table D.9 Water Absorption for LW15 specimen types.....	231
Table D.10 Water Absorption for LW30 specimen types.....	232
Table D.11 Water Absorption for LW45 specimen types.....	233
Table D.12 Water Absorption for HW15 specimen types .....	234
Table D.13 Water Absorption for HW30 specimen types .....	235
Table D.14 Water Absorption for HW45 specimen types .....	236

Table E.1 Hemp fiber reinforced LDPE specimen model parameters.....	237
Table E.2 Wood Pulp reinforced LDPE specimen model parameters .....	238
Table E.3 Hemp fiber reinforced HDPE specimen model parameters .....	239
Table E.4 Wood Pulp reinforced HDPE specimen model parameters.....	240
Table F.1 Percent Fiber on each surface type for Hemp fiber reinforced LDPE .....	241
Table F.2 Percent Fiber on each surface type for Wood Pulp reinforced HDPE .....	242
Table F.3 Percent Fiber on each surface type for Hemp fiber reinforced HDPE.....	242
Table F.4 Percent Fiber on each surface type for Wood Pulp reinforced HDPE .....	243
Table F.5 Total Calculated Accessible Fiber for Hemp reinforced LDPE specimen types.....	245
Table F.6 Total Calculated Accessible Fiber for Wood Pulp reinforced LDPE specimens .....	246
Table F.7 Total Calculated Accessible Fiber for Hemp reinforced HDPE specimens .....	247
Table F.8 Total Calculated Accessible Fiber for Wood Pulp reinforced HDPE specimens.....	248

## DEFINITION OF PARAMETERS

$A_f$	Accessible Fraction of Fiber
$d_m$	Dial setting for the Matrix
$d_f$	Dial setting for the Fiber
$D$	Diffusion coefficient of biocomposite ( $\text{mm}^2/\text{s}$ )
$D_x$	Diffusion coefficient in the x plane including edge effects by sample length and width for a homogeneous material ( $\text{mm}^2/\text{s}$ )
$g$	Width (mm)
$h$	Thickness (mm)
$l$	Length (mm)
$n$	Number of replicates or iterations
$\mu\dot{m}_f$	Slope of fiber calibration curve
$\mu\dot{m}_m$	Slope of matrix calibration curve
$\dot{m}_f$	Mass flow rate of fiber (g/min)
$\dot{m}_m$	Mass flow rate of matrix (g/min)
$M_t$	Percent mass gain after immersion time (%)
$M_\infty$	Percent mass gain after infinite time (%)
$p$	Probability
$p_c$	Probability of critical fiber content
$P_B$	Number of Pixels Black
$P_W$	Number of Pixels White
$r$	radius (mm)
$SA_f$	Surface accessible fiber fraction (%) – equivalent to area fraction of fiber on biocomposite surface
$t$	Time immersed (seconds)
$v_f$	Volume of fiber ( $\text{cm}^3$ )



$V_f$	Volume fraction of fiber (%)
$v_m$	Volume of matrix (cm <sup>3</sup> )
$V_m$	Volume fraction of matrix (%)
$w_f$	Weight of fiber (g)
$W_f$	Weight fraction of fiber (%)
$w_m$	Weight of matrix (g)
$W_m$	Weight fraction of matrix (%)
$w_t$	Weight of biocomposite at an immersion time interval (g)
$w_i$	Initial weight of biocomposite (g)
$y_i$	Measured property (unit)
$\bar{y}$	Average property (unit)
$\bar{Y}$	Normalized property relative to time of exposure (%)
$\beta$	Critical static exponent, 0.42 for 3D crystal lattice
$\zeta$	Percolation factor (mm <sup>2</sup> )
$\rho_f$	Density of fiber (g/cm <sup>3</sup> )
$\rho_m$	Density of matrix (g/cm <sup>3</sup> )
$\theta_s$	Slope of $M_t$ verse $\sqrt{t}$

## ABBREVIATIONS

CI	confidence interval
FSP	fiber saturation point
LDPE	low density polyethylene
LH	low density polyethylene reinforced with hemp fiber
LW	low density polyethylene reinforced with wood pulp
HDPE	high density polyethylene
HH	high density polyethylene reinforced with hemp fiber
HW	high density polyethylene reinforced with wood pulp
MFI	melt flow index
PE	polyethylene
UTS	ultimate tensile strength

# 1. INTRODUCTION

Over the past few decades, there has been increased societal demand to consume sustainable materials. Plastic consumption has been rising since 1985, as shown in Figure 1.1. Although there are many societal benefits of plastics such as food and water packaging applications, utilization of this material to improve cost efficiency of disposable consumer products has led to a significant quantity of plastic litter [1]. The drastic increase in the quantity of plastic has contributed to the formation of five *garbage islands* [2, 3]. The increase in plastic consumption is one of the major causes of soil pollution[4, 5]. From the mounting evidence of environmental damage caused by plastic waste, it is imperative that sustainable materials replace today's non-renewable petroleum-based thermoplastics. A viable solution is to manufacture materials from renewable resources that degrade after service life into non-toxic pieces for reduced environmental impact. Degradable bio-derived biocomposites are one part of the solution due to their good specific mechanical properties, low cost, biocompatibility and environmental characteristics such as renewable, non-toxic, biodegradable, and low embodied energy versus glass fiber [6].

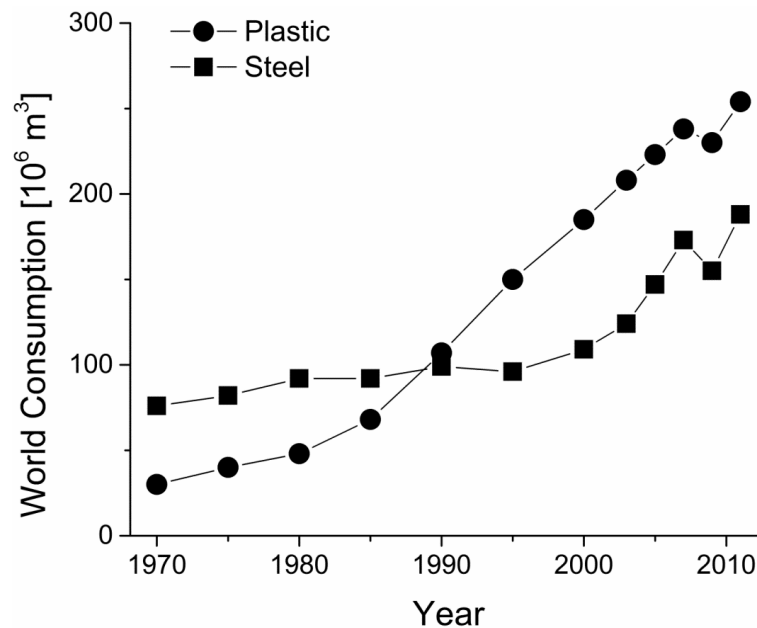


Figure 1.1 Consumption of thermoplastic over the last 40 years compared to steel. *Data graphed from Michal Biron, Thermoplastics and Thermoplastic Composites 2007).*

Degradable green biocomposites are defined as a combination of a bio-derived polymer matrix reinforced with natural materials that degrade when exposed to environmental elements such as water, sunlight and biological attack (microbial or fungal). Natural materials used for reinforcement include: plant fibers, animal fibers and mineral reinforcement. Plant-based natural fibers are produced with a variety of feedstocks from around the world and are sustainable, renewable, biodegradable and lightweight.

Degradable green biocomposites are difficult to study because the properties of both the natural fiber (reinforcement) and the polymer matrix are simultaneously affected by environmental conditions. Degradable bio-derived polymers (i.e., matrix materials) have been extensively studied to control both chemical composition and structure for desired properties. Indeed they are so well understood as to be commercially available. Therefore, the work of this herein focuses on the other component of green degradable biocomposites: **natural fiber response**. To decouple the natural fiber's contribution to degradation from a degradable plastic, a commercially available non-biodegradable synthetic thermoplastic polymer, polyethylene, was chosen as the matrix for a control.

Degradation is a process where the material physically breaks down and loses its desired mechanical, thermal, or visual properties over time. The three main ways of environmental degradation for biocomposites include water absorption, ultraviolet light (UV) weathering, and microbial and fungal attack. Water is present in all three degradation modes making it a constant factor in degradation for biocomposite materials. For this reason, degradation by **water immersion** is the focus of this work.

Traditionally, degradation caused from exposure to water has been viewed as a material limitation rather than an advantage. Exposure to water immersion and high humidity environments causes deleterious effects on biocomposite properties including mechanical degradation which can be advantageous after its service life. To use this known disadvantage as an environmental advantage, it is critical that the factors which influence both the mechanism and rate of absorption are understood.

Both the mechanical and moisture absorption properties of natural fiber thermoplastic composites have been extensively investigated over the past decade [7-22]. However, a consensus on the mechanism(s) of water absorption is required to predict long term performance. The prediction of the rate and magnitude of water absorption, generated

in this work, is critical to allow designers to understand, and account for, the degradation of the mechanical properties with time.

## 1.1 SIGNIFICANT CONTRIBUTIONS

The overarching objective of the research is to create a design space for engineers to better utilize natural fiber reinforced polyethylene biocomposites with tailored degradation rates in a water immersion environment. This work brings designers one step closer to utilizing biocomposites rather than traditional non-degradable non-renewable plastics. The accomplished research objectives are listed below with reference to the Chapters.

1. Comprehensive long term data set of both mechanical properties and water absorption for an array of fiber types as well as fiber contents for future research. (Appendix C and Appendix D)
2. Established the requirement and method to evaluate fiber volume fraction of manufactured biocomposite specimens. (Chapter 4)
3. Developed constitutive governing mathematical relationships to quantify the degradation of tensile mechanical properties dependent on the quantity of water absorbed from immersion environments. (Chapter 4)
4. Developed a mathematical model to predict kinetics of water absorption of a biocomposite as a function of immersion time to account for matrix type, fiber type, fiber volume fraction, surface accessible fiber, and accessible fiber surface area to specimen volume (Section 5)
  - a. Refined the assessment of accessible fiber ratio parameter.
  - b. Confirmed diffusion-based water absorption mechanism.
  - c. Natural fiber degradation captured into a long term water absorption model.
  - d. Model correlates short term experimental data into extrapolated long term prediction of water absorption to avoid the requirement for long term studies.

These models utilized in combination allow for the prediction of water absorption and mechanical properties in an immersion environment – over the entire immersion time up to 6500 hours. A design space has been constructed that allows a range of composites to be tailored for both short term and long term applications.

## REFERENCES

1. Andrady, A.L. and M.A. Neal, *Applications and societal benefits of plastics*. Philosophical Transactions of the Royal Society B: Biological Sciences, 2009. **364**(1526): pp. 1977-1984.
2. Zolfagharifard, E. *Watch humanity ruin the oceans: Nasa animation shows how vast 'garbage islands' have taken over the seas in the last 35 years*. 2015 March 31, 2017]; Available from: <http://www.dailymail.co.uk/sciencetech/article-3206442/Watch-humanity-ruin-oceans-Nasa-animation-shows-vast-garbage-islands-taken-seas-35-years.html>.
3. Parker, L. *First of Its Kind Map Reveals Extent of Ocean Plastic*. 2014 March 31, 2017]; Available from: <http://news.nationalgeographic.com/news/2014/07/140715-ocean-plastic-debris-trash-pacific-garbage-patch/>.
4. Lytle, C.I.G. *The great plastic tide*. 2016 April 2016 March 31, 2017]; Available from: <http://plastic-pollution.org/>.
5. *Pollution and Toxin: General*. 2016; Available from: <http://worldcentric.org/about-compostables/traditional-plastic/pollution>.
6. Dicker, M.P.M., P.F. Duckworth, A.B. Baker, G. Francois, M.K. Hazzard, and P.M. Weaver, *Green composites: A review of material attributes and complementary applications*. Composites Part A: Applied Science and Manufacturing, 2014. **56**: pp. 280-289.
7. Bavan, D.S. and G.C.M. Kumar, *Potential use of natural fiber composite materials in India*. Journal of Reinforced Plastics and Composites, 2010. **29**(24): pp. 3600-3613.
8. Ashori, A., *Wood-plastic composites as promising green-composites for automotive industries!* Bioresource Technology, 2008. **99**(11): pp. 4661-4667.
9. Mehta, G., A.K. Mohanty, K. Thayer, M. Misra, and L.T. Drzal, *Novel biocomposites sheet molding compounds for low cost housing panel applications*. Journal of Polymers and the Environment, 2005. **13**(2): pp. 169-175.
10. Chollakup, R., R. Tantatherdtam, S. Ujjan, and K. Sriroth, *Pineapple Leaf Fiber Reinforced Thermoplastic Composites: Effects of Fiber Length and Fiber Content on Their Characteristics*. Journal of Applied Polymer Science, 2011. **119**(4): pp. 1952-1960.
11. John, M.J. and S. Thomas, *Biofibres and biocomposites*. Carbohydrate Polymers, 2008. **71**(3): pp. 343-364.
12. Xu, Y., Q. Wu, Y. Lei, F. Yao, and Q. Zhang, *Natural Fiber Reinforced Poly(vinyl chloride) Composites: Effect of Fiber Type and Impact Modifier*. Journal of Polymers and the Environment, 2008. **16**(4): pp. 250-257.
13. Kim, S.J., J.B. Moon, G.H. Kim, and C.S. Ha, *Mechanical properties of polypropylene/natural fiber composites: Comparison of wood fiber and cotton fiber*. Polymer Testing, 2008. **27**(7): pp. 801-806.
14. Pan, M.-Z., D.-G. Zhou, J. Deng, and S.Y. Zhang, *Preparation and properties of wheat straw fiber-polypropylene composites. I. Investigation of surface treatments on the wheat straw fiber*. Journal of Applied Polymer Science, 2009. **114**(5): pp. 3049-3056.
15. Bourmaud, A. and S. Pimbert, *Investigations on mechanical properties of poly(propylene) and poly(lactic acid) reinforced by miscanthus fibers*. Composites Part A: Applied Science and Manufacturing, 2008. **39**(9): pp. 1444-1454.
16. Chand N., F.M., *Natural fibers and their composites*, in *Tribology of natural fiber polymer composites*, W.P. Limited, Editor 2008, CRC Press LLC: Boca Raton, FL. pp. 2-58.

17. Yao, F., Q.L. Wu, Y. Lei, and Y.J. Xu, *Rice straw fiber-reinforced high-density polyethylene composite: Effect of fiber type and loading*. Industrial Crops and Products, 2008. **28**(1): pp. 63-72.
18. Tajvidi, M. and A. Takemura, *Recycled Natural Fiber Polypropylene Composites: Water Absorption/Desorption Kinetics and Dimensional Stability*. Journal of Polymers and the Environment, 2010. **18**(4): pp. 500-509.
19. Salmah, H. and A. Faisal, *The Effect of Waste Office White Paper Content and Size on the Mechanical and Thermal Properties of Low-Density Polyethylene (LDPE) Composites*. Polymer-Plastics Technology and Engineering, 2010. **49**(7): pp. 672-677.
20. Mohanty, A.K., M. Misra, and L.T. Drzal, *Surface modifications of natural fibers and performance of the resulting biocomposites: An overview*. Composite Interfaces, 2001. **8**(5): pp. 313-343.
21. Faruk, O., A.K. Bledzki, H.-P. Fink, and M. Sain, *Biocomposites reinforced with natural fibers: 2000–2010*. Progress in Polymer Science, 2012. **37**(11): pp. 1552-1596.
22. Shinoj, S., S. Panigrahi, and R. Visvanathan, *Water absorption pattern and dimensional stability of oil palm fiber-linear low density polyethylene composites*. Journal of Applied Polymer Science, 2010. **117**(2): pp. 1064-1075.



## 2. BACKGROUND

The ultimate objective for material engineers is to predict and tailor materials performance. The material paradigm shown in Figure 2.1 illustrates two quintessential relationships between the four corner stones of material science: process, structure, property and performance. The first (at left) being the centralized theme of characterization to provide insight into each corner stone and secondly (at right) the path dependency of each corner stone which dictates the materials performance. The work herein focuses on the prediction of performance of natural fiber reinforced biocomposites after exposure to a water immersion environment by the characterization and assessment of each cornerstone.

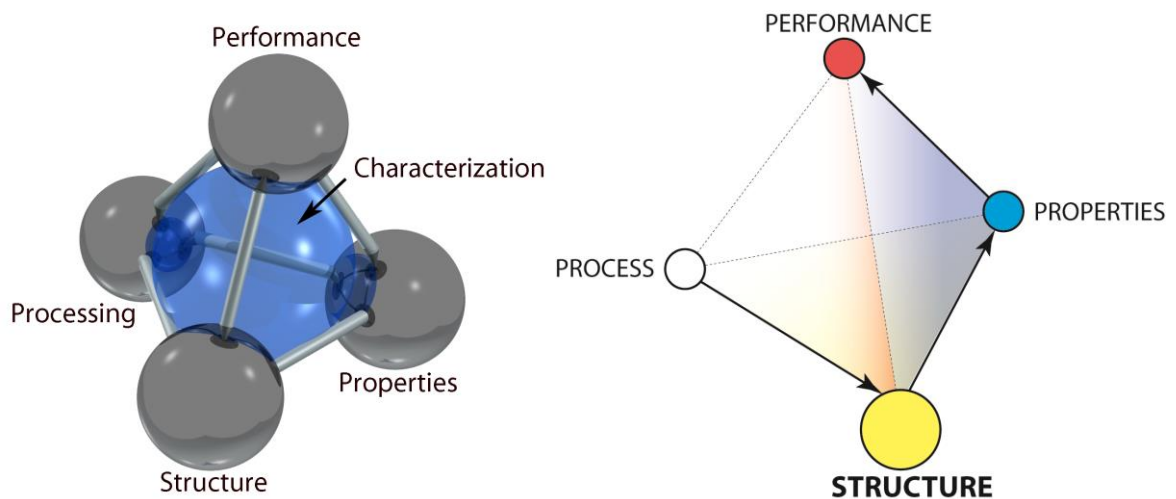


Figure 2.1 Material science paradigm, traditional (left) to path dependency (right) to illustrate the relationship of structure, properties, processing, structure and performance for a material. Images used with permission from J.A. Nychka and G.D. Hibbard from [1].

The information provided within the background creates a context for understanding water absorption in biocomposite materials and the subsequent impact on mechanical properties. Questions such as: What is a biocomposite? What are the constituent materials? What are the independent properties of those materials? How are each of those material properties combined within the biocomposite to impact performance? These questions lay the foundation for the following research questions to be investigated:

### **Research Question #1: How does water enter into the material?**

- How has water absorption been assessed?
- What factors are typically considered and what should be considered?

## **Research Question #2: How does water affect mechanical properties?**

- What methods have been used to assess the damage created by water absorption?
- What models exist to explain water's impact on mechanical properties?

The scope and definitions of constituent materials in biocomposites, manufacturing methods, and the impact of design choices made on the structure and processing as well as characterization methods to gain insight into how these materials react in different environments as well as in-service conditions will be explained herein. This section is laid out to introduce the reader to the individual properties of the constituent materials, and then insight into the processing - structure relationship through evaluation techniques relevant to this work. The second section will provide a background on the current state of mechanisms and models utilized to predict the water absorption (i.e., performance), of these biocomposite materials.

### **2.1 CONSTITUENT MATERIAL PROPERTIES USED IN BIOCOMPOSITES**

Biocomposites comprise two or more distinct constituent materials (insoluble in one another where one is naturally derived) that combined yield a new material with improved performance over individual components [2]. The two constituent materials are referred to as the matrix and reinforcement. The reinforcement provides additional properties over the matrix, typically mechanical strength or stiffness and is typically discontinuous in form when natural fibers are used. The matrix material is a continuous phase that binds the reinforcement together and transfers load onto the reinforcement. Biocomposite performance is dependent on the combination of constituent material properties as well as the structure created from the manufacturing process.

A brief overview of individual constituent materials and properties are provided in Sections 2.1.1 and 2.1.2 for context on the material selection. Highlights of known effects from manufacturing process are discussed in Section 2.2 along with context of how it relates to performance in water immersion environments. All biocomposites discussed herein are composed of plant derived natural fibers with a thermoplastic matrix.

### 2.1.1 NATURAL FIBERS REINFORCEMENT

The advantages of the use of natural fibers as a reinforcement over traditional materials such as glass fiber are: low cost, low density, high toughness, have the potential to be biodegraded, acceptable specific strength and specific modulus [3]. Typically, natural fibers are selected in combination with the matrix to increase strength to weight ratios, use of renewable products and most recently to promote biodegradation at the end of product life. Important properties of natural fibers used by designers include density, electrical resistivity, tensile strength, modulus, fracture toughness, thermal stability, moisture regain and crystallinity.

Disadvantages of natural fibers include variability in properties, and susceptibility to water absorption. Since natural fibers are produced by nature rather than a controlled synthetic manufacturing environment, variability is experienced in terms of quality, chemical composition and mechanical properties [4, 5]. Factors which influence variability are listed in Table 2.1.

Table 2.1: Classification of reasons and the factors for variability in natural fiber properties

<b>Reason</b>	<b>Factors</b>	<b>Ref.</b>
<b>Growth Environment</b>	<ul style="list-style-type: none"> <li>• Region and field location</li> <li>• humidity and precipitation</li> <li>• soil type</li> <li>• fertilization type(s) and quantity</li> <li>• season</li> <li>• cultivar (cultivated plant variety)</li> <li>• position of the fiber in the plant</li> <li>• plant age at harvest</li> </ul>	[4-6]
<b>Processing Damage</b>	<ul style="list-style-type: none"> <li>• method of fiber removal from plant</li> <li>• industrial processes or hand cultivation</li> </ul>	[6]
<b>Fiber Classification</b>	<ul style="list-style-type: none"> <li>• technical fiber or fiber bundles</li> </ul>	[6]
<b>Test Methods</b>	<ul style="list-style-type: none"> <li>• type of test</li> <li>• humidity</li> <li>• temperature</li> <li>• fiber cross-section measurement technique</li> <li>• rate (mechanical) or duration (absorption and chemical analysis) of test</li> <li>• accuracy of the testing equipment</li> </ul>	[6, 7]

Natural fibers are highly heterogeneous materials both physically and chemically [8], therefore a fundamental overview of nuances with natural fibers has been provided in terms of classification, chemical structure, structure, mechanical properties, and lastly water absorption characteristics.

### 2.1.1.1 CLASSIFICATION OF NATURAL FIBERS

Natural fibers are classified based on source either, plant, animal or mineral. Plant based natural fibers are the focus and are referred to as natural fibers herein afterwards. Fibers are categorized by both plant type and anatomical origin within the plant. The six main categories of agro-based plant fibers: wood fibers, straw fibers, seed/fruit, bast (stem), leaf and grass fibers are illustrated in Figure 2.2. Two fiber types selected were: 1) Hemp fiber – a common type of bast fiber with reported high mechanical properties and 2) Wood pulp – chemically purified and refined cellulose fiber utilized as a baseline.

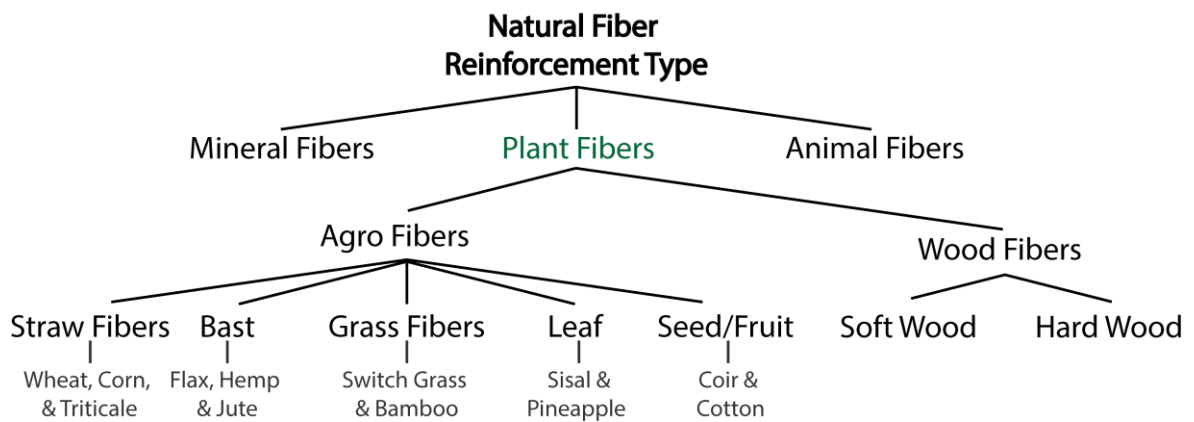


Figure 2.2 Classification of natural fibers, modified from [9].

### 2.1.1.2 CHEMICAL STRUCTURE

Properties such as density, ultimate tensile strength, modulus, and electrical resistivity are related to the chemical composition and internal structure of the fibers [5]. Natural fibers are composed of varying distributions of three main chemical compounds: 1) cellulose, 2) hemicelluloses and 3) lignin, see Figure 2.3. Additional chemical components exist such as pectins a polysaccharide that holds the fiber together and waxes that influence the fibers wettability and adhesion characteristics [10, 11]. The relative fraction of each compound is dependent on the plant type, cultivar, variation in growth environment as well as the method used to process the fiber. According to Mohanty [5], the chemical components responsible for

water absorption, in descending order are: Hemicellulose to cellulose to lignin to crystalline cellulose.

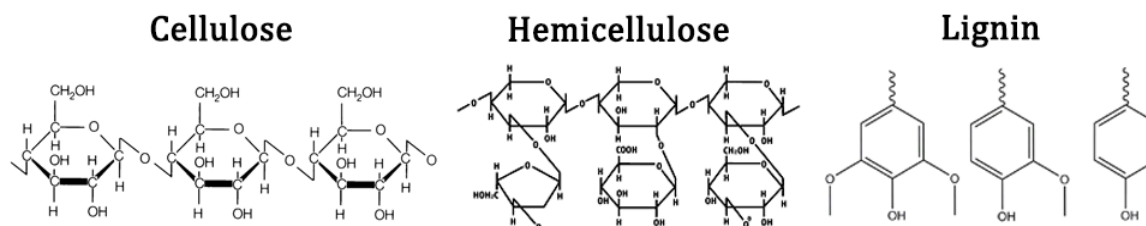


Figure 2.3 Chemical structures of cellulose, hemicelluloses and three phenolic building block structure of lignin redrawn from [12].

### CELLULOSE

Cellulose serves as the main structural component of the cell wall which provides strength and stability to the plant. Cellulose exhibits high modulus and tensile strength due to the crystalline packing of the linear polymer chains. Fiber types with high cellulose content are desired as the reinforcement type in for biocomposite. Cellulose is the predominant chemical constituent for hemp and wood pulp fibers.

Cellulose consists of D-anhydroglucose ( $C_6H_{11}O_5$ ) repeat units containing three hydroxyl groups with the repeat units joined by β-1,4 ether linkages at C<sub>1</sub> and C<sub>4</sub> positions [3, 13] as illustrated in Figure 2.3 as a linear polymer. The hydroxyl groups allow for the formation of both intramolecular hydrogen bonds inside the macromolecule itself and intermolecular hydrogen bonds among other constituents within the fiber such as cellulose, hemicellulose, and water soluble components [3]. These hydroxyl groups are also able to form hydrogen bonds with water, therefore classifying cellulose as hydrophilic (water attracting). Absorbed water is known to weaken the intra- and intermolecular hydrogen bonds within the fiber and decrease the overall mechanical properties. Cellulose content has associated with the primary pathway for water absorption within biocomposites.

### HEMICELLULOSE

Hemicellulose is very hydrophilic and is composed of multiple polysaccharides of 5- and 6-carbon ring sugars with branched pendant groups [13]. Hemicellulose is soluble in alkali solutions and is readily hydrolyzed [11]. Mechanically, hemicelluloses contribute little to the stiffness and strength of the fibers or individual cells.

## LIGNIN

Lignin is an amorphous and highly complex cross-linked molecular structure with aliphatic and aromatic constituents [13] as shown in Figure 2.3. The exact chemical nature remains obscure due to the difficulty associated with isolating the lignin from the native fiber state, but the majority of functional groups and units have been identified [3]. Lignin protects the carbohydrates from chemical and physical damage with compressive strength that stiffens the cell wall [10]. Due to the structural complexity of lignin, it is difficult for the majority of microorganisms to break it down. Certain species of fungi are capable of degrading lignin [14]. Lignin has been deemed the limiting step in the degradation of plant fibers. There are many different configurations of lignin whose properties range from water soluble (lignosulfonates) to insoluble (kraft lignin) in organic solvents such as acetone.

### COMMON FIBER TYPES COMPOSITIONS

Overviews of the chemical composition for common natural fibers used as reinforcement in thermoplastic biocomposites are displayed in Table 2.2. The natural fiber selected, hemp and wood pulp, have two of the highest cellulose contents.

Table 2.2: Chemical composition and moisture content of natural fibers reported from [3, 5, 6, 15]

<b>Fiber Type</b>	<b>Cellulose (wt%)</b>	<b>Hemicellulose (wt%)</b>	<b>Lignin (wt%)</b>	<b>Pectin (wt%)</b>	<b>Wax (wt%)</b>	<b>Moisture Content (%)<sup>1</sup></b>
<b>Wood Pulp</b>	99.9	-	-	-	-	-
<b>Coir</b>	36-43	0.15-0.25	41-45	3-4	-	8.0
<b>Cotton</b>	82.7	5.7	-	0.6	-	-
<b>Sisal</b>	67-79	10.0-14.2	8-11	10	2.0	11.0
<b>Jute</b>	61-71.5	13.6-20.4	12-13	0.2	0.5	12.6
<b>Hemp</b>	67.0-85.7	5.5-22.4	2.9-5.7	0.8-2.5	0.8	10.8
<b>Flax</b>	71	18.620.6	2.2	2.3	1.7	10.0

### **2.1.1.3 STRUCTURE**

Natural fibers comprise hollow linear structures with cellulose microfibrils wrapped in a helical pattern around the fiber axis and are held together by a lignin and hemicelluloses matrix, illustrated in Figure 2.4 [13]. Microfibrils do not have a homogenous uniform structure due to intrinsic imperfections as the fiber is naturally synthesized. The angle between the fiber axis and the crystalline microfibril wrap direction is called the

---

<sup>1</sup> Moisture content is defined as retained percentage of water at atmospheric conditions.

microfibrillar angle and correlates to the stiffness of the fiber [11]. The hollow structure, known as the “lumen”, introduces porosity into the biocomposite where water has the potential to accumulate.

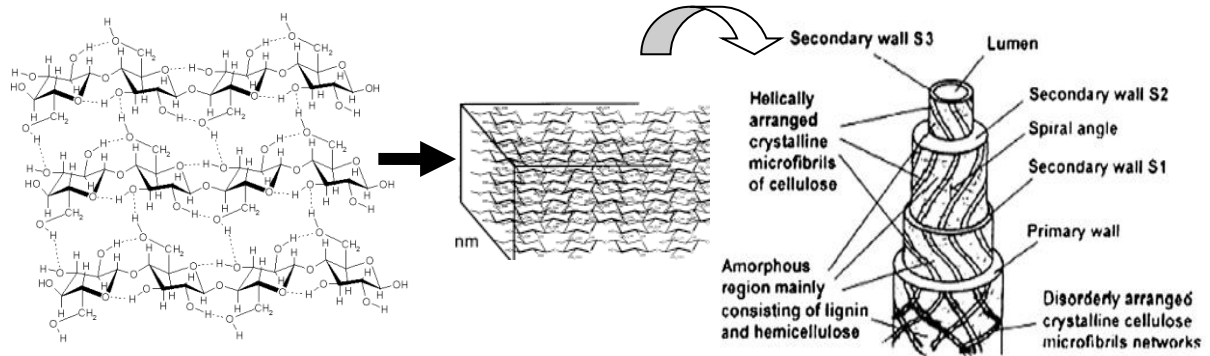


Figure 2.4 Network of hydrogen bonds between cellulose chains , formation of crystalline cellulose micro fibrils and the helical arrangement of cellulose within natural fiber microfibril [17] (left to right). Images reproduced with permission from [17].

Natural fibers have a hierarchy structure dependent on the level of processing from the macro-scale, the harvested fiber to the nano-scale, micro fibrils as shown in Figure 2.5. Fibers are rarely found as individual cells in the plant, but mostly assembled into bundles [4]. Müssig reported different strength values of the fiber dependent on whether a fiber, a bundle or a collective of fibers or a collective of bundles was tested [4, 18, 19].

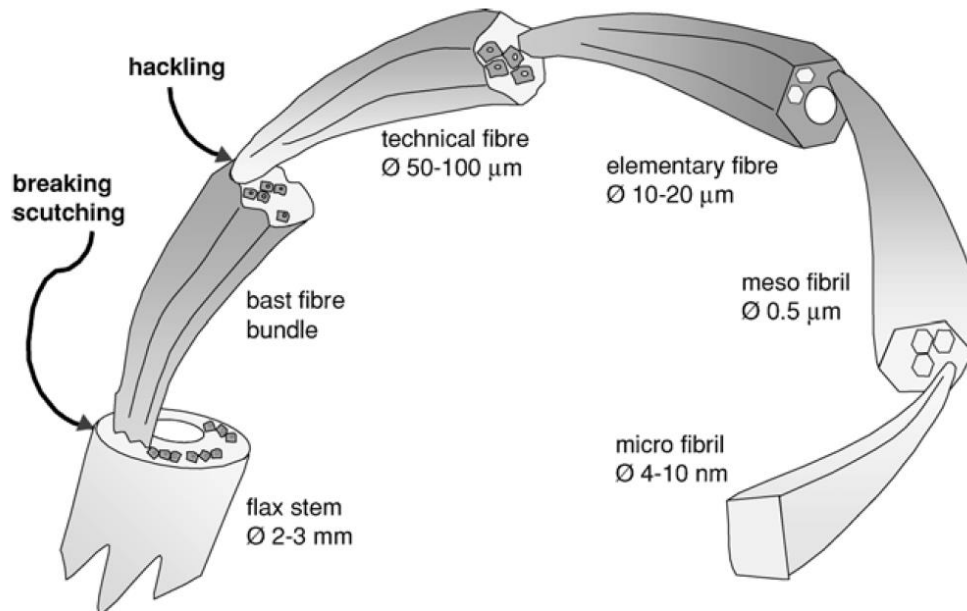


Figure 2.5 Hierarchical classification of natural fiber types from stem to micro fibril for bast fiber, flax. Image reproduced with permission from [20].

Natural fibers incorporated into thermoplastic biocomposites ranges from fiber bundles to meso fibrils in size depending on the processing methods used. These available processing methods can fractionate or separate lingo-cellulosic feedstocks (e.g. stalks or stems) into various fiber types and sizes, and but also can fibrillate the fibers which increase the surface area available for adhesion with the matrix [21].

#### 2.1.1.4 MECHANICAL PROPERTIES

The mechanical properties vary between types of natural fibers due to differences in both chemical composition and structure. Plant based fibers exhibit significant, natural, stochastic scatter in mechanical properties due to natural variability from factors listed in Table 2.1. Typical tensile properties of common natural fibers are compared to E-glass in Table 2.3. Bast fiber types, (i.e., jute, hemp and flax) exhibit the highest tensile modulus and tensile strength values. The majority of research has focused on bast fibers due to these mechanical properties as well as the feasibility of harvesting the fiber. The specific modulus of hemp has the ability to be equal to or greater than e-glass with a near comparable specific strength. Hemp fiber has the best potential as a reinforcement for a stiff biocomposite with a suitable tensile strength [4]. Although wood pulp has a low elongation at break, the specific modulus and specific strength are comparable to e-glass fiber. Both fibers were selected due to their mechanical performance. It is recommended to assess the viability of a particular natural fibers as a reinforcement by Ashby-type plots as established by Shah[22].

Table 2.3: Common natural fiber types, mechanical properties<sup>2</sup> and specific modulus and strength compared to E-glass. Data taken from [4, 5, 11, 22-24]. Selected fibers highlighted in green.

Fiber Type	Density (g·cm <sup>-3</sup> )	Tensile Modulus (GPa)	Tensile Strength (MPa)	Elongation at Break (%)	Specific Modulus (GPa/g·cm <sup>-3</sup> )	Specific Strength (MPa/g·cm <sup>-3</sup> )
Wood pulp <sup>3</sup>	1.3-1.5	40	10000	0.5-0.6	26-31	767
Coir	1.15-1.2	4-6	131-220	15-40	3.3-5.0	110-180
Cotton	1.5-1.6	5.5-13	287-800	3.0-10	3.7-8.4	190-530
Sisal	1.3 - 1.5	9.4-28	468-855	2.0-2.5	6.7 - 20	362 - 610
Jute	1.3 - 1.5	10-55	393-800	1.16-1.8	<b>7.1 - 39</b>	300 - 610
Hemp	1.48	58-70	550-1110	1.6-4.7	<b>39 - 47.3</b>	370 - 740
Flax	1.5	27.6 - 80	345-1830	1.2-3.2	<b>18.4-53</b>	230-1220
E-Glass	2.5	70	2000-3500	2.5	28	800-1200

<sup>2</sup> Variability in reported mechanical properties is due to factors listed in Table 2.1 such as specifying testing fiber bundles versus elementary fibers.

<sup>3</sup> Softwood pulp produced using Kraft separation method.



### 2.1.1.5 WATER ABSORPTION

Natural fibers absorb water due to their hydrophilic nature. Water is able to penetrate the fiber structure cellulose network of the fiber into the capillaries spaces between the fibrils. Water molecules may attach itself to chemical groups in the cellulose molecules such as the free hydroxyls. The introduction of water into the natural fiber destroys some of the rigidity as intramolecular bonds are broken between the fiber to form new bonds with the absorbed water. The decrease in intramolecular bonding permits the cellulose molecules to more freely resulting in a softened natural fiber that can easily change shape with application of an external force [25]. Furthermore, a strong relationship exists between the amorphous fraction of cellulose and the diffusion coefficient of water in cellulosic materials which indicates water molecules diffuse only through the amorphous part of cellulose samples [26]. Therefore, a higher the cellulose content does not necessarily translate into a higher affinity for water absorption, as it is dependent on the crystallinity of the cellulose within the natural fiber.

Natural fibers, independently, are difficult to study in immersion environments due to the measurement techniques. Typically, kinetics are assumed to be the same as the desorption kinetics. Lee's work cautioned desorption kinetics use as an indication of absorption as the kinetics of sorption occur at two separate time scales [27]. Céline [28, 29] and other researchers have explored the mechanism of water absorption of natural fibers and have argued a Fickian diffusion kinetic model for short exposure times, less than 100 hours. The exact mechanism and model for water absorption is debated based on the condition which the fiber was tested (i.e. relative humidity or immersion). In either case, natural fibers show a general good agreement with Fickian diffusion model. As Saikia [30] reported, the first stage of absorption obeys Fick's law of diffusion, the second stage of absorption represents non-Fickian diffusion. An overview of the reported diffusion coefficients are reported in Table 2.4

Table 2.4: Water absorption parameters of common natural fibers utilized for biocomposites.

<b>Fiber Type</b>	<b>Diffusion Coefficient (mm<sup>2</sup>/s)</b>	<b>Maximum Water Content (%)</b>	<b>Reference</b>
<b>Sisal</b>	2.14E-6	60.6	[29]
<b>Jute</b>	1.12E-6	67.8	[29]
<b>Hemp</b>	4.0E-4 to 5.2E-5	62-63	[29, 30]
<b>Flax</b>	7.80 E-05 to 1.19E-6	42.5 -62.5	[25, 29]

### 2.1.2 THERMOPLASTIC MATRIX

Thermoplastics represent approximately 90% by weight of all plastics consumed world-wide [31]. Thermoplastics are the primary contributor to *garbage islands* as the majority of thermoplastics are not able to environmentally degrade. The addition of natural fibers in these materials would allow a portion of the material to be renewable and degradable to limit the environmental impact.

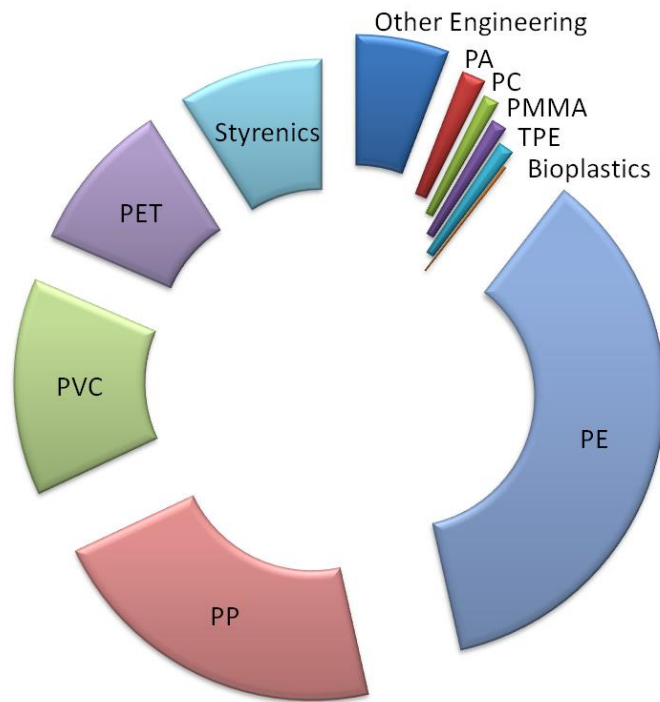


Figure 2.6 Breakdown of consumption of thermoplastics by volume produced. Polyethylene is the largest produced thermoplastic. Data reproduced from [32].

Thermoplastics matrices which have been combined with plant based natural fibers include polypropylene, polyvinylchloride, polyethylene terephthalate and bioplastic thermoplastics made from renewable resources such as polylactic acid. The world's most widely consumed thermoplastic by volume is polyethylene [31, 33], as shown in Figure 2.6. Therefore polyethylene is a suitable matrix to utilize the properties of natural fibers for a greener product in the intermediary timeframe until sufficient biodegradable materials exist.

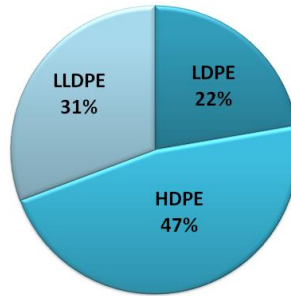


Figure 2.7 2013 world polyethylene demand, 81.8 million metric tons, by classification graphed from data in [34].

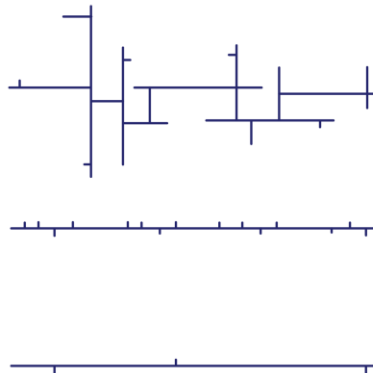
The majority of the market consists of three types of polyethylene: HDPE, LDPE and LLDPE [34] as shown in Figure 2.7. Despite being identical in chemical composition, the three classifications differ in performance and are used in different applications. The performance is dependent on differences in chain structure shown in Figure 2.8 which impacts the materials crystal structure as well as molecular weight and molecular weight distribution. Variation in molecular weight and branch structure of polyethylene are obtained through synthesis in different solvents and utilization of unique catalysts.

**a) Chain Structure**

**LDPE**  
Density = 0.915-0.935 g/cm<sup>3</sup>  
Melt Point = 105-115 °C

**LLDPE**  
Density = 0.90-0.93 g/cm<sup>3</sup>  
Melt Point = 100-130 °C

**HDPE**  
Density = 0.94-0.97 g/cm<sup>3</sup>  
Melt Point = 128-136 °C



**b) Crystal Structure**

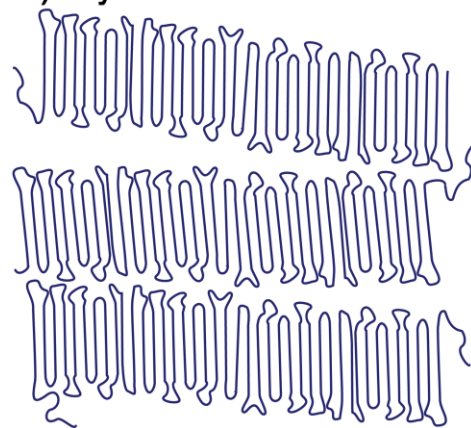


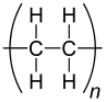
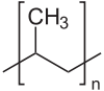
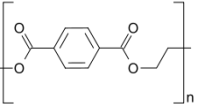
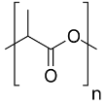
Figure 2.8 Polyethylene chain and crystal structure, images modified from [35] and [18].

Polyethylene is a semi-crystalline thermoplastic where by the polymeric chains align by folding onto themselves into a laminar crystal structure [33] shown in Figure 2.8b. The lower branch density of HDPE allows for an increase in crystallinity which results in a higher density (closer packing of atoms), decrease in free volume space within polymer, decrease in permeation rate and an increase in melting temperature as more energy is required to cause chain movement. The degree of crystallinity of semi-crystalline polymers affects most

properties, including transport coefficients [36]. The difference between low density and high density also impact mechanical properties and processability. Fotouh has suggested that matrices with higher crystallinity contents have greater stiffness contraction on the natural fiber during water absorption hence limiting the maximum amount of water absorbed by the biocomposite [37].

Both LDPE and HDPE are compared with other traditionally used thermoplastics such as polypropylene, polyethylene terephthalate and polylactic acid as displayed in Table 2.5 and Table 2.6. The ranges of properties reflect commercially available properties intended for various applications. HDPE has a higher mechanical strength and stiffness and tends to be used in application that require more durability whereas LDPE is more flexible and tougher [34]. HDPE has one of the lower vapour permeation rates whereas LDPE has one of the highest, despite contain the same repeat unit. Polyethylene's are on the lower end of tensile modulus while displaying a large magnitude of elongation before failure. Polyethylene has a theoretical molecular modulus of 300 GPa but only has a bulk modulus of only 1.0 GPa [33]. The high ductility coupled with the low modulus make polyethylene an excellent matrix to utilize natural fibers since they are brittle with a high specific modulus.

Table 2.5: Overview of common thermoplastics and their permeability to water

	Name	Repeat Unit	Crystal Structure[8]	Water Vapour Permeability [38] (g/ m <sup>2</sup> ·day)
HDPE	High density polyethylene		Semi-crystalline 60 – 80%	4.6 – 7.3
LDPE	Low density polyethylene		Semi-crystalline 30 – 50%	15.5 – 31.0
PP	Polypropylene		Semi-crystalline	5.9 – 23.3
PET	Polyethylene terephthalate		Semi-crystalline	15.5 – 27.9
PLA	Polylactic acid		Semi-crystalline	N/A

In addition to the advantageous mechanical properties and range in water vapour permeability to investigate the relationship between water absorption and its effect on mechanical properties, polyethylene has a major processing advantage. Polyethylene has one

of the lowest melt processing temperatures of common thermoplastics. Polyethylenes are typically processed between 190 - 200°C. A low processing temperature is advantageous for the incorporation of natural fibers as thermal degradation occurs between 190 - 330°C dependent on fiber type [39, 40]. The selection of polyethylene as the matrix reduces the likelihood of the natural fibers undergoing thermal degradation during the manufacturing process.

Table 2.6: Overview of Mechanical Properties of Common Thermoplastics compiled from [41]

<b>Name</b>	<b>Modulus (GPa)</b>	<b>Tensile Yield Strength (MPa)</b>	<b>Elongation at Break (%)</b>
HDPE	0.450 - 1.50	6.89 - 200	3 - 1900
LDPE	0.11 - 0.45	7.60 - 64.8	13.5 - 1000
PP	0.5 - 8.25	4 - 42.1	8 - 750
PET	0.14 - 21.9	21 - 105	1 - 300
PLA	0.52 - 4.6	16 - 60	0.5 - 19

In summary, Polyethylene was selected as the matrices within this work due to:

1. Investigate the influence of matrix permeation rates with the same chemical composition.
2. Evaluate the contribution of natural fiber reinforcement within the same polymer but with two sets of mechanical properties and the impact of absorbed water on those properties.

The use of two grades of polyethylene allowed the removal of the assumption regarding the interfacial bonds based on chemical differences. Also the selection of LDPE allows for the natural fiber contribution to be more apparent.

3. Commercially significant polymer which has established processability and manufacturing capabilities.

## 2.2 MANUFACTURING OF BIOCOSPOSITE MATERIALS

The manufacture of thermoplastic biocomposites requires three main stages of processing with an optional fourth stage, as outlined in Figure 2.9. The processing stages are listed below and the significance of each stage is reviewed within its section.

- (1) Process the natural fibers from its native form into a useable form by means of mechanical and/or chemical processes.
- (2) Combination of the raw materials (fiber and matrix) by a mixing method.
- (3) Form the biocomposite mixture into a final or near final product by a mold or die.
- (4) Optional: Finish the part by machining it into the final. This stage is dependent on the formation process selected.

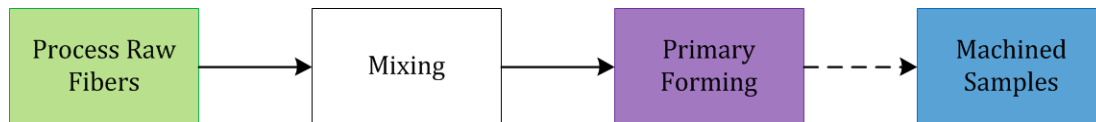


Figure 2.9 Overview of the biocomposites manufacturing processes.

### 2.2.1 PROCESSING NATURAL FIBERS

Natural fibers in their native form cannot be readily incorporated into a biocomposite; therefore they are processed to obtain the desired fiber structure, refer to Figure 2.5, for the selected mixing and/or molding process. There are numerous methods to extract natural fibers, dependent on plant type. Generally agricultural fibers are cut down by traditional farm equipment, decorticated and or retted followed by milling and or chemical treatment as shown in Figure 2.10. Decortication is a method that extracts the fibers by crushing and beating the plant material with blunt knives, then pressed and held against the scrapping action of the blade to remove the cellulosic material [42]. Retting is a method which allows biology to assist with the breakdown of the fiber structure by exposing the dying plant material to heat, water and UV rays to break down the fiber so it can be separated more easily. Both processes breakdown the fiber and inherently influence the mechanical properties of the fiber and can potentially introduce defects [6, 20]. Whereas, wood pulp is created from a combination of mechanical, thermal and chemical processes that results in a near pure cellulose fiber with a fine structure.

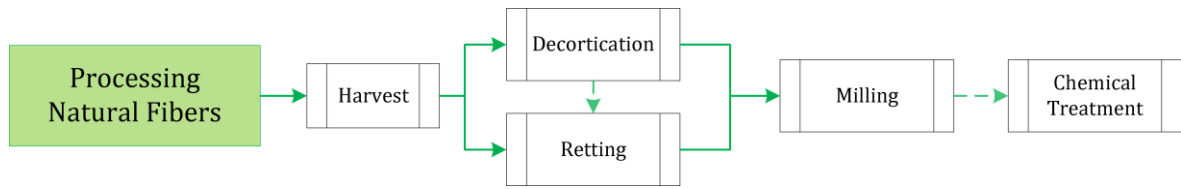


Figure 2.10 Overview of agricultural fiber processing methods for compounding.

For short fiber reinforced biocomposites, milling is typically executed to refine the fiber dimensions to be fed into the mixing equipment. Along with separating the fibers, milling also fibrillates and therefore maximizes the fiber surface area for increased interface with the matrix in the final manufactured biocomposite. An increase in the surface area of fiber-matrix interfaces increases the number of surfaces for load transfer to occur in the biocomposite.

The majority of plant based fibers face the same challenge, achieving a consistent feed rate using gravimetric feeders for high volume compounding processes. Fibrillated fibers especially become intertwined and clump in the gravimetric hopper. Fiber pelletization has been used by Peltola [43], Fotouh [37] and Robertson [44] as a solution to feed the natural fibers into the compounding process. A consistent feed rate of fiber into the mixing processes increases the likelihood of fiber distribution in the melt.

Finally, natural fibers can be treated with chemicals [3], and/or thermomechanical [45, 46] processes in an effort to increase the extent of bonding at the fiber-matrix interface. A number of fiber treatments have shown different levels of improved performance over fibers without treatment in terms of increased mechanical properties and a reduction in absorbed water. Fiber treatments have been extensively studied and were excluded from the study since fibers without treatment result in a worse case water absorption scenario.

### 2.2.2 MIXING

A method of mixing is required to combine the natural fiber with the matrix. Techniques such as compounding via extrusion, batch mixing and dry mixing can be used to combine natural fiber and thermoplastics. Extrusion is the most common method of mixing due to high volume and screw configuration adaptability. Extrudate (material after extrusion) can be used as the final product as a continuous shape or the extrudate can be pelletized and the pellets subsequently injection molded. A disadvantage associated with extrusion is an observed decrease in fiber aspect ratio due to gradual fiber breakage with increasing fiber contents [47]. There are three types of extruders: single, co-rotating and counter rotating twin screws.

Co-rotating extruders have demonstrated the best distribution and dispersion results and was the selected extruder type.

A major challenge in compounding biocomposites is achieving a well dispersed and distributed fiber, top right corner of Figure 2.11. A high degree of both distribution and dispersion ensure each microfibril bundle is encapsulated by matrix, limiting the ability to absorb water or negates fiber to fiber interconnectivity of water absorption. Also, a high degree of distribution and dispersion increases the surface area of the fiber-matrix interface for effective load transfer and uniform repeatable mechanical properties. "Recycling" the biocomposite by grinding and re-mixing reduced water absorption due to increased fiber distribution and reduced fiber size [48]. The extent of dispersion and distribution achieved from compounding directly influences the final microstructure and has been theorized to be the key to overall biocomposite water absorption of biocomposites[49]. The dispersion and distribution dictates biocomposite properties and performance.

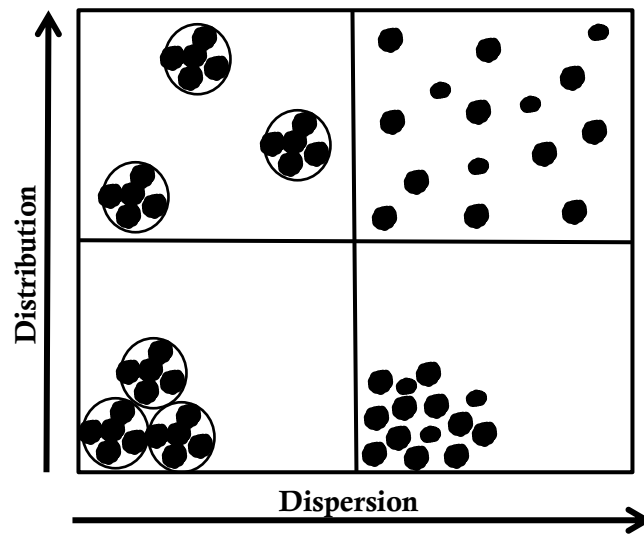


Figure 2.11 Illustration of dispersion and distribution of a discontinuous phase (black).

Fiber contents are designed based on mass balance calculations of material in (fiber and matrix) equalling the quantity of material out (biocomposite). The mass rate of the fiber relative to the mass rate of the matrix dictates the fiber content of the biocomposite. In most cases the rate of matrix versus fiber is controlled by two separate feeders into the extruder. In other cases, the matrix and fiber are mixed manually and feed into one hopper [50, 51]. The downfall with manual mixing prior to extrusion is the portion of fiber to matrix cannot be monitored nor controlled.



The fiber concentration is regarded as the single most important parameter influencing the composite properties [52]. The mass balance assumption has been proven incorrect in section 4.1 and must be verified by a secondary method due to manufacturing losses and/or inconsistencies. Fiber content is relevant to the prediction of mechanical properties and the quantity of water absorbed, and previous studies have based conclusion on unverified fiber contents [53, 54].

### 2.2.3 MOLDING & FINISHING

Three methods for molding a short fiber thermoplastic biocomposites mixtures are 1) solvent casting 2) compression molding [55] and 3) injection molding [55]. The advantages and disadvantages of these method are shown in Table 2.7. Injection molding was selected as the molding method for this work based on its commercial application as well as the ability to produce manufactured parts without further machining required. Forming processes such as compression molding typically require parts to be machined from a molded sheet compared to all “molded” surfaces with injection molding process. Chapter 5 explores how different levels of exposure of machined surfaces impact water absorption to simulate both other manufacturing methods and practice reasons to machine the part after molding. For example, a practical reason to machine a molded surface includes the addition of fasteners and fixtures, or cleaning up the flashing along a part edge.

Scientific Injection Molding by William J. Tobin is a guide on how to set up the injection mold process parameters to establish a processing window for the biocomposite material [56]. Molding high fiber content biocomposites is difficult due to the rheology within the mold, as the matrix material flows into the mold while the fiber remains solid. Therefore, an important parameter in selecting a matrix material is the melt flow index (MFI) of thermoplastic. The melt flow index is a standardized index as determined by ASTM D1238 [57] which is a measure of the ability of a thermoplastic to flow at a given temperature and pressure. The greater the MFI the easier the polymer flows within the mold to be able to manufacture high fiber fractions.

Table 2.7 Comparison of common methods to mold biocomposites.

<b>Forming Process</b>	<b>Advantages</b>	<b>Disadvantages</b>
Solvent Casting	Easy setup  Low material cost	Low fiber fraction contents Exposure to highly toxic solvents Small quantities only (0.01-1 kg)

		May require machining
Compression Molding	Automated process Part consolidation Random fiber orientation	Likelihood of entrapped air or voids Higher tooling costs May require machining
Injection Molding	Highly repeatable High production volume Low cost / unit Part consolidation	Long set up times Processing window of material may be difficult to determine Fiber alignment in direction of mold flow

The direction of polymer flow within the mold also correlates with the direction of fiber alignment. Cabral [47], observed for injection molding specimens at all fiber contents, fibers orientated along the mold fill direction in the outer layer with a more random orientation in the core. Random orientation of fibers cannot be achieved by this method. The effect of fiber alignment results in higher tensile properties in the mold flow direction compared to the perpendicular direction due to the alignment of fibers.

## 2.3 MECHANISMS OF AND EFFECTS FROM WATER ABSORPTION

Absorbed water has a multitude of effects on the biocomposite such as a discoloration, distortion in dimensions, reduction in strength, and reduction in stiffness. Controlling these effects by understanding their mechanism is the main drive for water absorption research. Research has not yet determined the extent of degradation on biocomposites' mechanical properties. The decline in properties with absorbed water has been referred to as the "main material limitation" as it limits the materials' durability. As a result, a plethora of work has been conducted to inhibit water absorption by compatibilization methods such as fiber treatments or compatibilizers additives for the matrix. The extent of water absorption has also been used as a proof of concept test for compatibilization methods [51]. Other researchers have looked at co-extrusion of a synthetic polymer coating to reduce, if not limit, water absorption to ensure product longevity. Manipulating water absorption in biocomposites was not the aim of the work, rather the study of mechanistic pathways of water absorption, and the long term prediction of water absorption and their subsequent mechanical properties.

There exist common challenges in utilizing the data within the existing literature:

- A. Volume fraction of fiber within the manufactured biocomposite is never experimentally determined. All fiber fractions reported are unverified in the as-molded state rather assumed from the targeted fraction;
- B. Differences in manufacturing methods correspond to differences in structure and types of manufacturing flaws, which influence both the mechanism of water absorption and the mechanical properties;
- C. Different materials, fiber types and matrix types, make it difficult to compare the properties of the biocomposites.

The observations within each study are valuable, but caution must be applied when extrapolating results from one study to another due to different manufacturing conditions and/or unverified fiber contents. An overview of trends within the literature observed for both water absorption and its effect on mechanical properties are outlined within the next two subsections.

### 2.3.1 INFLUENCES ON WATER ABSORPTION

Although water absorption is used as a frequent method to quantify the performance of a biocomposite formulation, few studies are dedicated to assessing the factors contributing to the response of the biocomposite to water immersion. General characteristics to quantify and compare water absorption are: (1) rate, (2) maximum water absorbed and (3) time to reach equilibrium. Duration of water immersion has ranged from 7 to 17,520 hours (140 weeks), with the majority of studies conducted within the first 336 hours (2 weeks). Variables impacting water absorption that have been investigated and the responding influence on water absorption are:

#### A. Fiber type

- Due to different fiber macrostructures, the natural fiber processing methods used and the chemical components of the fiber, the extent of water absorption is dependent on fiber type. Fibers within the same classification based on origin, 2.1.1.1 respond similarly such as bast fiber types – flax and hemp as well as types of kraft wood pulp.

#### B. Fiber content

- An increase in fiber content results in increased water absorption.

#### C. Fiber compatibilization method

D. Inconsistent results have been observed between various compatibilization methods with different fiber – matrix system. Some compatilization treatments result in both a decrease in the rate of absorption as well as the extent of saturation. Although other methods, only result in a rate reduction of water absorbed. Medium (immersion environments and/or exposure to relative humidity)

- Immersion environments show more deleterious effects on biocomposites than exposed to high humidity.

#### E. Temperature

- An increase in temperature results in an increased rate of water absorption lowering the time to reach equilibrium.
- Consensus within the field is that the Arrhenius equation 2.11, given in 2.4.2.1 relates the rate of absorption with temperature.

Beg & Pickering's [58] absorption curves for 40wt%, unverified fiber content, kraft pulp, with and without maleic anhydride poly propylene (MAPP) reinforced polypropylene, are similar

to the absorption curves in Chapter 5 of this study. There is an initial stage of water immersion followed by a secondary phase of absorption after the first 100 hours, with some samples not reaching maximum water absorption after 5712 hours (238 days). Even in a long-term absorption study of 1512 hours, the biocomposites still showed signs of continual increase, however the study was stopped[54]. Further, the kinetics were only assessed during initial absorption and a Fickian model was deemed an appropriate description of the model. The kinetics were only assessed during initial absorption and Fickian diffusion was deemed an appropriate model [54].

### 2.3.2 MECHANISMS FOR WATER ABSORPTION

Mechanism as defined by Merriam-Webster is “the fundamental processes involved in or responsible for an action, reaction, or other natural phenomenon” [59]. Much work has been completed to understand the phenomenon of water absorption by biocomposites in an immersion environment [49, 60, 61]. Mechanistic pathways and the evidence of the mechanisms that influence or dictate water absorption in natural fiber reinforced thermoplastic biocomposites are summarized in Table 2.8. Each mechanism as illustrated in Figure 2.12 has been defined and described in its respective section.

Table 2.8 Comparison of mechanism of water absorption in literature

Mechanism	Evidence	Ref.
Matrix	<ul style="list-style-type: none"> <li>▪ Mass uptake of polymer (PLA) [62]</li> <li>▪ Diffusion coefficient obtained for polymer PLA [62]</li> </ul>	[62]
Fiber	<ul style="list-style-type: none"> <li>▪ Increase fiber content increases water absorption</li> </ul>	[25, 44] [55, 62-64]
Fiber Interconnectivity	<ul style="list-style-type: none"> <li>▪ Critical fiber volume fraction[47]</li> </ul>	[47]
Fiber – Matrix Interface	<ul style="list-style-type: none"> <li>▪ Fiber treatment decreased water absorption [55, 63]</li> <li>▪ Disbondment at interface from shear stress caused by natural fiber swelling [55]</li> <li>▪ Measured interfacial distance [61]</li> </ul>	[55, 63, 64]
Unoccupied Volume (Cracks, Pores &/or Voids)	<ul style="list-style-type: none"> <li>▪ Poor interfacial bonding lead to an increase in micro voids[64]</li> </ul>	[25, 49, 63, 64]
Fiber Degradation	<ul style="list-style-type: none"> <li>▪ Mass loss after drying long term immersion specimen [62]</li> <li>▪ Fiber mass loss after 11 days of immersion [29]</li> <li>▪ Loss of fiber properties attributed to washing out of soluble components of fibers during immersion [62]</li> </ul>	[29, 62, 63]

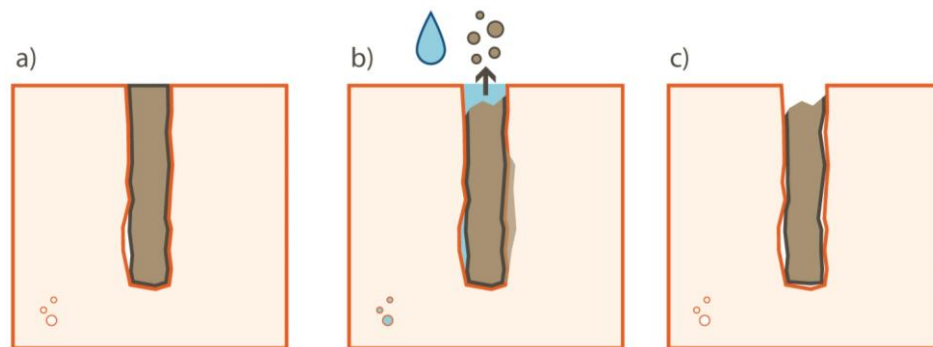


Figure 2.12 Mechanistic pathways schematic of water absorption for a single fiber embedded within a matrix, a) structure prior to immersion, b) concurrent processes during water immersion, and c) the structure after drying. Adapted from [60].

### **2.3.2.1 MATRIX**

The ability of a matrix to absorb water is dependent on the chemical structure of the polymer's repeat unit, and crystallinity as shown in Table 2.5. Polymers unable to form hydrogen bonds with water typically exhibit measured contact angles greater than 90° and therefore are classified as hydrophobic[65]. Hydrophobic polymer's lack a repeat unit with a dipole moment created from an unbalanced arrangement of highly electronegative atoms such as oxygen, capable of forming hydrogen bonds. Highly crystalline polymers also have low water absorption rates, as the water molecules are not able to penetrate the crystalline structure. Since polyethylene is a semi-crystalline hydrophobic polymer, water absorbed by the matrix is minuscule compared to natural fibers. Water absorption within the polyethylene matrix of a natural fiber composite is typically ignored in predictive models.

### **2.3.2.2 FIBER**

The predominant mechanistic pathway for biocomposites to absorb water is into the natural fiber. For a description of the water absorption mechanism within the fiber refer to section 2.1.1.5. Various authors are in agreement that the rate of water absorption and the maximum water content (saturation point) of a biocomposite are dictated by fiber type, fiber surface treatment and most importantly, fiber content. An increase in fiber content results in a higher rate of water absorption as well as a higher saturation limit of the biocomposite.

Analogous to Wang's description of accessible fiber content, an argument has been made for surface accessible fiber content as an access point for water to absorb into the biocomposite[49]. In this work, the surface accessible fiber area was quantified by secondary electron scanning microscopy and image analysis to capture the area travelled through by the flux of water. The maximum quantity of absorbed water in the biocomposite is dependent on both the fiber's capacity when embedded in a matrix and the extent to which surface fibers are connected to the bulk within the biocomposite.

### **2.3.2.3 FIBER – FIBER INTERCONNECTIVITY**

Fiber-fiber interconnectivity, defined as the direct contact between fibers, is dependent on the manufactured microstructure. At very low fiber content, individual fibers are more likely to be encapsulated by plastic than in contact with another fiber, reducing that fiber's ability to absorb water. The extent of connectedness increases with increased fiber volume content as illustrated in Figure 2.13 where the shaded squares represent the presence of fiber. The fiber content that connects fibers through thickness is called the “percolation threshold” or “critical

fiber content” [49]. At fiber contents greater than the critical content, fiber-fiber interconnectivity becomes the dominating mechanism of water absorption [49]. Unique properties emerge at the onset of macroscopic through thickness connectivity and are known as percolation properties. Different empirical parameters have been created to predict the content when the reinforcing phase has a connectivity path through the thickness of the materials and are outlined in section 2.4.2.1.

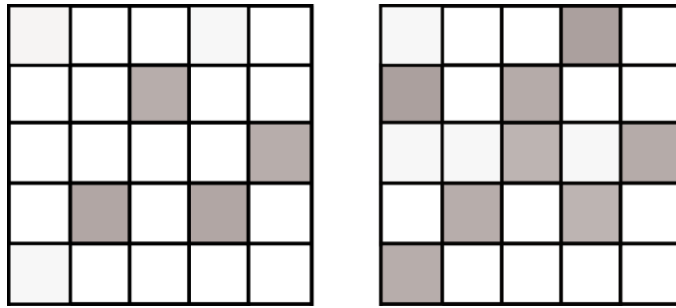


Figure 2.13 Demonstrates the low interconnectivity with only one cluster, not connected compared to multiple fiber clusters with different interconnected paths through the material. Image modified from [66].

High volume fiber fraction contents (>30%) [49] are difficult to achieve for injection-molded short fiber thermoplastics. As a result, it is unlikely that fiber through thickness interconnectivity is prevalent in the biocomposites studied here, although possible at the highest fiber fractions. However, this does not mean that the mechanism of water absorption is not dependent on the interconnected fibers from the surface into the bulk of the material. Interconnectivity is thought to be a major influencing mechanism because of the time required to reach “equilibrium.” The duration is thought to be determined by water diffusion through each fiber and then ‘jumping’ to the next interconnected fiber and so on and so on. The tortuosity of the pathway and its length influence the time for the biocomposite to reach equilibrium [49]. For jute reinforced polypropylene, Cabral [47] observed a clear distinction in the calculated diffusion coefficient above and below a critical fiber volume fraction.

#### 2.3.2.4 FIBER – MATRIX INTERFACE

Numerous journal articles reference water absorption at the fiber matrix interface due to incompatibility of hydrophilic fiber and hydrophobic matrix. The evidence to support this absorption pathway is an observed reduction in water absorption with a selected compatibilization treatment to improve the interfacial bond. Different successful methods have been found relative to the fiber type and treatment to reduce water absorption. Depending on the method deployed one or more characteristics of water absorption could be



impacted: a) rate of initial absorption (<100 hours) b) the maximum saturation content of the biocomposite c) the time taken to reach the maximum saturation content.

Natural fiber chemically treated prior to manufacturing has been theorized to increase interfacial adhesion at the fiber-matrix interface, thereby decreasing the water absorption [63]. The rate was found to change with surface treatments however the capacity, or maximum water content absorbed remained constant but required longer times to reach saturation. An increase in interfacial matrix-fiber bond is consistent with a reduction in the  $n$  values from Fickian diffusion,  $n = 0.5$ , to pseudo-Fickian diffusion,  $n > 0.5$  based on compatibilization method deployed [63].

Among all of these articles, the extent of dispersion has never been compared between treated fiber and a non-treated fiber. The reduction in water absorption may have been due to an increase in fiber dispersion within the matrix. If the fibers are more dispersed with a compatibilization method, then the biocomposite would also see a decrease in water absorption not just due to bonding at the interface but by separation of the fibers preventing the interconnectivity of the fiber network. Compatibilization methods were not utilized to provide a worst case for water absorption.

The effectiveness of the fiber-matrix interface has been also studied by both fluorescence spectroscopy and laser scanning confocal microscopy (LSCM) work. Forster resonance energy transfer (FRET) has illustrated, that when natural fibers aggregate, there is an absence of FRET indicating fiber-matrix interfacial gap [61]. The results from Zammarano's work indicate that the distance between the matrix and cellulosic fiber, the interfacial gap, is less than 10nm [61]. The interfacial gap validates that there is a sufficient space to be occupied by absorbed water molecules. Due to the width of the gap, 10nm compared to the macroscopic fiber bundles ranging from 1 – 500  $\mu\text{m}$ , it cannot be the main method for water absorption but rather part of the biocomposites' overall capacity to absorb water and provide room for the fiber to swell.

### **2.3.2.5 UNOCCUPIED VOLUME - CRACKS, PORES AND VOIDS**

Frequently, literature uses terminology such as cracks, pores and voids, almost interchangeably to describe unoccupied volume within the biocomposite. In theory, all of this unoccupied volume could be occupied by absorbed water. Each feature has a distinct

morphology from the various condition of how it was formed. A definition of each feature is provided along with the relevance to water absorption in biocomposites.

For the case of biocomposites, a crack is a linear fracture feature formed after the material has undergone deformation either from mechanical stress or from exposure to an environment. Natural fibers expand (swell) during water absorption. When embedded in a biocomposite the swelling is constrained by the matrix. Many authors theorize that the change in fiber diameter from the absorbed water causes the formation of cracks or micro-cracks within the matrix. For brittle matrices, such as thermosets, this is a plausible mechanism. However for ductile polymers, such as polyethylene, it is unlikely that the matrix would crack, as virgin material can withstand up to 150% strain at failure.

Pores and voids are features likely to be created during the manufacturing process. A pore is a type of manufacturing defect that has atmospheric pressure. A pore's surface morphology is a circular and smooth which would be observed on either a fracture surface or cross sectional assessment. Pores can be formed from trapped evolved gases such as evaporation of water vapour or solvent, or from entrapped air at a weld line during molding of thermoplastics. Whereas the word void comes from latin and implies 'unoccupied or vacant,' it differs from a pore in that the unoccupied volume has in it a vacuum from the way it was formed. The formation of a void is possible under mechanical deformation such as strain imposed from shrinkage after the molding process. For the purposes of the rest of the thesis, the main defect of concern for the presence of absorbed water is the pore volume within the biocomposite, as it is a location where water can accumulate within the material.

Special precautions should be taken especially when manufacturing biocomposites with natural fibers, which retain moisture from the atmosphere to reduce the likelihood in the formation of pore. Methods to reduce the likelihood of pore formation include: vacuum drying the raw materials as well as the pelletized extrudate, avoidance of a water bath to cool the extrudate after mixing, and addition of vacuum ports to draw off moisture that has evaporated from the natural fiber. The aforementioned precautions were undertaken in this study to reduce pore formation since the presence of pores within a composite is known to lead to increased absorbed water.

#### **2.3.2.6 FIBER DEGRADATION**

The majority of absorption research has been over short time scales. Therefore, fiber loss has not been an area of focus. Recently Céline has shown approximately a 4% irreversible mass loss after 11 days in a water immersion environment for natural fibers such as such as hemp, flax and sisal [29]. Natural fiber reinforced polyethylene biocomposites have reported up to 3% mass loss after 16 months [44], and up to 6.6% loss after 24 days of immersion[53]. Biocomposite mass loss has been attributed to fiber loss.

The effect of fiber loss during immersion can be observed in the biocomposite absorption curve depending on the fiber content and length of immersion. Water has a lower density than natural fibers, reference Table 2.3, and the replacement volume of lost fiber with water volume results in an apparent decrease in the percent mass absorption. Tajvidi [48] reported slight reduction in water absorption at long times which was confirmed by the lower weight after drying. In literature, the phenomenon is observed more often than an explanation is given[64].

The results from the work completed within uncovered fiber degradation from the surface of the biocomposite during long-term immersion. The purposed model has incorporated a term representing fiber degradation for predictive long term water absorption.

## 2.4 WATER ABSORPTION MODELS

**Adsorption** and **absorption** are two processes frequently discussed within the sorption literature related to natural fibers. Adsorption is classified as “surface bound” where water accumulates only on the surface as a thin monolayer, while absorption is a process where fluid penetrates or permeates directly into the bulk of the material. Adsorption and its associated models have been reported for relative humidity based experiments. While lessons from humid environments provide insight into the physics at the molecular level, specific mechanisms and models have been intentionally neglected here since the fundamental understanding of surface-only condition is not valid.

Diffusion, defined by Crank as the “process by which matter is transported from one part of a system to another as a result of random molecular motions” [67]. The process of random molecular motion can be visualized by how dye spreads over time. For biocomposites, water absorption literature has reached consensus and accepted diffusion as the fundamental process occurring in water absorption. The majority of studies either assume or prove Fickian diffusion as per equation 2.4, as shown in Table 2.9.

The mathematical theory of diffusion in **isotropic substances** is therefore based on the hypothesis that the rate of transfer of a substance through the unit area of a section is proportional to the concentration gradient measured normal to the section, shown in equation 2.1. The negative sign in the equation arises because diffusion occurs in the opposite direction to that of increasing concentration. Where  $J$  is the rate of flux, the quantity of substance transferred per unit area section,  $C$  is the concentration of diffusion substance, in this case water,  $x$  is the space coordinate measured section and  $D$  is the diffusion coefficient  $(\text{length})^2(\text{time})^{-1}$ .

$$J = -D \frac{dC}{dx} \quad (2.1)$$

$$\frac{dC}{dt} = -\frac{dJ_x}{dx} \quad (2.2)$$

Fick’s diffusion coefficient is a measure of the rate of a non-equilibrium mass transfer process when a concentration gradient exists. Depending on the context, diffusion coefficient has been referred to as mutual diffusion coefficient or interdiffusion coefficient [68]. If the diffusion coefficient is assumed to be constant (ie., independent of concentration and time),

combining equations 2.1 and 2.2 yields equation 2.3, known as Fick's second law of mass transfer. It describes how concentration evolves with time.

$$\frac{dc}{dt} = D \frac{d^2c}{dx^2} \quad (2.3)$$

An assumption about Fickian diffusion is that after a "short" time, it goes to steady-state for cases such a transport of penetrant molecules and in the other cases is in an unsteady state such as the kinetic sorption / desorption of penetrant in/out of bulk polymer bulk [69]. Fick's first and second laws are the basic formula to model both kinds of systems [67].

In some instances, diffusion is non-Fickian. According to the Fick's second law, the basic equation of mass uptake by a polymer can be given by Equation 2.4, where the exponent  $n$  refers to the type of diffusion mechanism, and  $k$  is constant which depends on the diffusion coefficient and thickness of film [69, 70]. Classification of diffusion can be created from the following:

$$\frac{M_t}{M_\infty} = kt^n \quad (2.4)$$

When:

$n < 0.5$	Pseudo-Fickian
$n = 0.5$	Fickian diffusion (also referred to as Case I)
$1 > n > 0.5$	Anomalous
$n = 1$	Case II
$n > 1$	Supercase II

Fickian diffusion (Case I) is often observed in the polymer system when the temperature is well above the glass transition temperature of the polymer ( $T_g$ )[69]. For reference, the glass transition temperature of polyethylene is  $-125^\circ\text{C}$  and that for polypropylene commonly used in the literature is  $0^\circ\text{C}$  [71]. Case II is the process of moving boundaries and linear sorption kinetics, which are opposed to Fickian with the initial boundary conditions. Case II and anomalous diffusion are usually observed for a polymer with a glass transition temperature higher than the experimental temperature. Both polyethylene and cellulose have a glass transition temperature below room temperature. Therefore, both types of diffusion are unlikely.

Table 2.9 Summary of diffusion coefficients calculated based on Fick's model for biocomposites subjected to long term water immersion conducted at temperatures between 23-30°C.

<b>Immersion (hours)</b>	<b>Confirmed Fickian (n~0.5)</b>	<b>Matrix Type(s)</b>	<b>Fiber Type(s)</b>	<b>Diffusion (mm<sup>2</sup>/s)</b>	<b>Ref.</b>
175	Yes (n=0.42-0.5)	PP	Kraft Pulp	1.4 – 8.8 E-07	[72]
175	Yes (n=0.5-.58)	PP	Sisal	0.8-3.8E-07	[72]
175	Yes (n=0.55-0.63)	PP	Coir	4.3-10.9 E-07	[72]
175	Yes (n=0.58-0.61)	PP	Luffa	3.1- 18.3E-07	[72]
240	Yes (n=0.34-0.36)	PP	Sisal	1.5-3.6 E-08	[55]
275	Yes (n=0.36-0.54)	PP	Palm Oil Fiber	2.8 – 18.7E-6	[63]
300	No	HDPE	Rice Husks	4.0-8.4 E-7	[49]
850	No	PP	Wood flour	5.0 E-6	[48]
850	No	PP	Bagasse	2.6 E-6	[48]
1512	Yes (n=0.35-0.43)	HDPE	Wood flour	3.2 – 9.5E-6	[54]
1512	Yes (n=0.43-0.57)	PP	Wood flour	2.8 – 6.6 E-6	[54]
1800	Yes (n=0.55-0.56)	PP	Newspaper	6.63-7.43 E-6	[64]
5040	No	PP	Flax	0.2-1.5 E-7	[73]
5712	No	PP	Kraft pulp	2.9 E-7	[58]
6576	Yes (n=0.49-0.67)	HDPE	Hemp	1.5 - 13.6 E-6	[37]
6576	Yes (n=0.40-0.45)	LDPE	Hemp	2.1 - 4.7 E-6	[37]
11,515	Yes	LDPE	Hemp	2.5 - 7.0 E-7*	[44]
11,515	Yes	LDPE	Flax	2.0 - 4.2 E-7*	[44]
11,515	Yes	LDPE	Wood pulp	1.4 – 2.2 E-7*	[44]
17,520	No	PLA	Flax	1.3 E-4	[62]

\*denotes diffusion coefficient was calculated from the data provided within reference.

Natural fiber reinforced thermoplastics typically comprise  $n$  values in the range of pseudo-Fickian to anomalous diffusion dependent on the fiber content, fiber surface treatment and specimen geometry. Kittikorn [63] demonstrated that unmodified oil palm fiber reinforced polypropylene absorbed water according to the Case I, Fickian diffusion, with  $n$  values of 0.36-0.54 at 23°C depending on the fiber content. Fotouh [37] determined that for hemp reinforced polyethylene, LDPE and HDPE,  $n$  values ranged from 0.4 to 0.67 for weight fractions from 10 – 40 wt%. Treated fibers showed  $n$  values in the pseudo-fickian region with values ranging from 0.19 – 0.34 [63]. The consensus in the field is that short term water absorption follows Fickian diffusion.

For diffusion-based models, an assumed equilibrium content is required for use with the model. However, the value is typically taken from the maximum content observed throughout the experiment. The maximum content may fall short of what it should be due to insufficient time to reach equilibrium and/or degradation of the natural fiber prior to establishment of equilibrium. Since natural fibers are known to degrade with time in immersion environments, the equilibrium content should therefore be taken critically and should be avoided for the assessment of models.

Common models to describe water absorption in biocomposites from immersion environments are based on molecular diffusion: Fick's diffusion, dual stage Fickian diffusion, time varying diffusion, anomalous diffusion and percolation theory.

#### 2.4.1 FICKIAN DIFFUSION

Fickian diffusion has been widely accepted in the field to predict the short term water absorption of natural fiber biocomposites. The international standards organization has a recommended practice, ISO 62, to determine absorption by plastics [74]. Key assumptions are made to utilize Fick's first law: infinite plate sheet, homogenous material, equal concentration gradients on both sides of the infinite sheet. These assumptions are possible due to the analytical solution of Fick's second law as a Gaussian function shown in equation 2.5.

$$c(x, t) = \frac{c_0}{2\sqrt{\pi Dt}} e^{-x^2/4Dt} \quad (2.5)$$

The solution for an infinite plate is shown in equation 2.6.

$$\frac{M_t}{M_\infty} = 1 - \sum_{n=0}^{\infty} \frac{4}{a^2 \alpha_n^2} e^{-D_1 \alpha_n^2 t} \quad (2.6)$$

Where  $M_t$  is the percent mass gain at time  $t$ , and is calculated as:

$$M_t = \frac{m_t - m_i}{m_i} \quad (2.7)$$

Where,

$m_t$  = mass at time (g)

$m_i$  = initial mass (g)

$t$  = Time (s)

By an approximation solution, equation 2.6 is simplified to equation 2.7.

$$M_t = \frac{4 * M_{\infty} * \sqrt{D}}{\sqrt{\pi} * h} * \sqrt{t} \quad (2.8)$$

Plot

$$y = \theta_s x; \quad (2.9)$$

$$\text{where } y = M_t, \quad x = \sqrt{t} \quad \text{and} \quad \theta_s = \frac{4 M_{\infty} \sqrt{D}}{\sqrt{\pi} * h} \quad (2.10)$$

The empirical solution for the diffusion coefficient of the material has been widely accepted [49, 75, 76] as shown in equation 2.10.

$$\therefore D = \pi \left[ \frac{h}{4M_{\infty}} \right]^2 \left[ \frac{M_2 - M_1}{\sqrt{t_2} - \sqrt{t_1}} \right]^2 \quad (2.11)$$

Where,

$M_t$  = Percent mass gain at time,  $t$ (%)

$t$  = Time (s)

$\theta_s$  = slope of  $M_t$  verse  $\sqrt{t}$

$M_{\infty}$  = Percent mass gain after infinite time (%)

$D$  = Coefficient of Diffusion ( $\text{mm}^2/\text{s}$ )

$h$  = thickness (mm)

The rate that moisture diffuses into or out any solid is governed by Fick's First Law, which says that the mass of moisture that passes through a cross-section, called the flux, is proportional to the concentration gradient of moisture  $dC/dx$ . The proportionality constant is the diffusion coefficient or diffusivity  $D$  ( $\text{mm}^2/\text{sec}$ ). Most problems in diffusion such as the fiber problem have a region where the concentration of moisture changes with time; Fick's first law is not useful in the case but Fick's second law describes the moisture absorption in fibers to determine the concentration as a function of time.

Shen and Springer [75] developed an equation to account for the edge effect from specimens which are of finite dimensions and of homogeneous material. Shen and Springers' equation has been widely adopted in the composite materials' literature due to its simplicity as a closer approximation from experimental data.



$$D_x = D \left(1 + \frac{h}{l} + \frac{h}{g}\right)^{-2} \quad (2.12)$$

Where,

h = thickness (mm)

l = length (mm)

g = width (mm)

$D_x$  = Diffusivity in the x plane including edge effects for homogenous material  $\left(\frac{mm^2}{s}\right)$

A strong consensus in the literature exists that the diffusion coefficient increases with temperature as per the Arrhenius equation 2.11 [55, 58, 72, 77]. Due to this established relationship, temperature was not a variable within the study.

$$D = D_0 e^{\left(\frac{-E_a}{RT}\right)} \quad (2.13)$$

Where,

$D$  = diffusion coefficient at a designated temperature ( $mm^2/s$ )

$D_0$  = diffusion coefficient constant ( $mm^2/s$ )

$T$  = temperature (K)

$R$  = universal gas constant,  $8.314 \times 10^6 \frac{kg \cdot mm^2}{s^2 \cdot K \cdot mol}$

$E_a$  = activation energy of diffusion  $\left(\frac{kg \cdot mm^2}{s^2 \cdot mol}\right)$

#### 2.4.2 DUAL STAGE FICKIAN DIFFUSION

Dual stage Fickian absorption has been used with moderate success to describe water absorption in natural fibers[29]. The diffusion rates found within a natural fiber were not drastically different than single stage Fickian diffusion [29]. Dual stage Fickian diffusion was applied to biocomposites, to apply the theory of a two staged process.

$$M_t = M_{\infty 1} \left(1 - \sum_{n=0}^{\infty} \frac{4}{a^2 \alpha_n^2} e^{-D_1 \alpha_n^2 t}\right) + M_{\infty 2} \left(1 - \sum_{n=0}^{\infty} \frac{4}{a^2 \alpha_n^2} e^{-D_2 \alpha_n^2 t}\right) \quad (2.14)$$

$$M_{\infty} = M_{\infty 1} + M_{\infty 2} \quad (2.15)$$

Where,

$M_{\infty}$  = Equilibrium water content after infinite time for process, 1, and process, 2, (%)

### 2.4.3 ANOMALOUS DIFFUSION

Anomalous diffusion as defined by an  $n$  value greater than 0.5 means the ratio of water absorbed is greater than half that with time. With cases of anomalous diffusion a few different situations may occur which increases the exponential factor to greater than 0.5, such as when an increase in pressure outside of a cylindrical polymer (cellulose) results in increased water absorption [78]. For the work within, explained in Chapter 5.4.1, the addition of external pressure had no effect on the rate or quantity of water absorbed of the manufactured biocomposites. Another reason for observed anomalous diffusion in natural fiber reinforced biocomposites could be concurrent absorption processes, as explained in the parallel exponential kinetic model.

#### 2.4.3.1 PARALLEL EXPONENTIAL KINETIC MODEL

A variation of dual stage Fickian diffusion, known as the parallel exponential kinetic (PEK) model, has also been reported [79] for natural fiber absorption when the initial moisture content is zero as shown in 2.13.  $M_t$  is the percent mass of absorbed water at time  $t$  of exposure to the environment. The sorption kinetic curve is composed of two exponential terms which represent a fast, 1, and a slow, 2, process having characteristic times of  $s_{t_1}$  and  $s_{t_2}$ . The water content at infinite time is represented by  $M_{\infty 1}$  and  $M_{\infty 2}$  associated with each respective process [79].

$$M_t = M_{\infty 1} \left(1 - e^{-t/s_{t_1}}\right) + M_{\infty 2} \left(1 - e^{-t/s_{t_2}}\right) \quad (2.16)$$

The use of the parallel exponential kinetic model is recent and has not gained adoption in the biocomposite field. One potential deterrent is the lack of methodology to establish the characteristic times of  $s_{t_1}$  and  $s_{t_2}$ .

### 2.4.4 PERCOLATION THEORY

The properties of a system which emerge at the onset of macroscopic through thickness interconnectivity are known as percolation properties [49]. For biocomposites, percolation requires fiber to fiber interconnectivity based on fiber volume fraction, fiber size and distribution-dispersion of the fibers. The fiber content from one edge to another is called the “percolation threshold” or “critical fiber content” and is designated as  $p_c$  (%). In other material systems, typical percolation threshold volume fractions range from 30-40% for a spherical particles range and decreases with cylinder-like morphologies, such as natural fibers [80].

For the volume fraction of fibers assessed within this study, it is probable that at the highest fiber volume fraction, percolation would occur. If the fiber content is greater than  $p_c$  then the probability that an additional fiber square belongs to the infinite cluster can be calculated by equation 2.17.

$$p_{\infty} \approx (V_f - V_{f_{critical}})^{\beta} \quad (2.17)$$

Where,

$p_{\infty}$  = probability that the fiber belongs to a cluster

$V_{f_{critical}}$  = critical fiber content at the onset of interconnectivity (%)

$V_f$  = specimen fiber content (%)

$\beta$  = critical static exponent, 0.42 for 3D crystal lattice

The percolation factor,  $\zeta$ , represents the amount of interconnectivity based on the fiber content and radius. The percolation factor is displayed in equation 2.18.

$$\zeta = \pi V_f r^2 \quad (2.18)$$

Where.

$\zeta$  = percolation factor ( $\text{mm}^2$ )

$V_f$  = volume fraction of fiber (%)

$r$  = average radius of fiber (mm)

#### **2.4.4.1 FICKIAN DIFFUSION COMBINED WITH PERCOLATION THEORY**

Different empirical parameters have been created to predict the content when the reinforcing phase has an interconnected path through the thickness of the material. Wang introduced the application of percolation theory to water absorption. A percolation model was developed to estimate the critical accessible fiber ratio [49]. Wang developed an empirical parameter “diffusion permeability coefficient”, DP, for biocomposites in order to determine the critical accessible fiber ratio,  $A_f$ , from experimental absorption data [49]. Future improvements to the model would include a) use of experimentally determined fiber saturation points for the specific fiber type and b) the use of fiber volume fraction to allow for utilization with various matrices and fiber types.

Accessible Fiber Ratio ( $A_f$ ):

$$A_f = \frac{M_\infty}{\frac{w_f}{100} \rightarrow FSP} \quad (2.19)$$

Diffusion i Permeability Coefficient (DP):

$$DP = \frac{\theta_s}{\sqrt{\frac{2 \cdot w_f}{100} - A_f}} = k (A_f - A_{f_{critical}}) \quad (2.20)$$

Where.

$M_t$  = Mass gain at time,  $t$ (%)

$M_\infty$  = Mass gain after infinite time,  $\infty$  (%)

$D$  = Coefficient of Diffusion ( $\frac{mm^2}{s}$ )

$t$  = Time (hours)

$\theta_s$  = slope of  $M_t$  verse  $\sqrt{t}$

$w_f$  = weight fiber content (wt%)

$FSP$  = Fiber Saturation Point – assumed 30% by Wang

The concepts proposed by Wang were significant in the advancement of water absorption prediction to capture interconnected fiber networks. Wang's key concept of the accessible fiber ratio was built one step forward for non-interconnected biocomposites with surface accessible fiber content. Unfortunately, Wang's model, like others, focuses only on the prediction of short term absorption data rather than the long term response.

## 2.5 EFFECT OF WATER ABSORPTION ON MECHANICAL PROPERTIES

Various mechanical test methods have been utilized to assess both biocomposite properties as well as the changes in those properties with exposure to water immersion. Common assessment methods include: a) tensile b) flexural and c) impact. Tensile properties were selected to determine the biocomposite properties for the following reasons: 1) a comparative body of knowledge exists, 2) mechanical models exist to predict properties, 3) they are the most frequently tested to compare materials, and 4) provides the most material information from a single test, including properties such as modulus, strength (yield and ultimate), strain to failure and an approximation of material toughness from the area underneath the stress-strain curve. Toughness is usually quantified by either IZOD or Charpy test methods, however with the small differences found for medium to high fiber contents [44], the area under the stress-strain curve sufficed to capture large changes in toughness.

Material properties are evaluated both in the elastic and the plastic region of the stress strain curve. All properties are dependent on the combination of each component and the interaction between them to transfer the load from the matrix onto the reinforcing fiber by means of the interface. Modulus is a bulk material property evaluated at the initial loading stage, the elastic region, of the stress-strain curve. The tensile yield strength evaluates the strength of the material at the transition from elastic deformation to plastic deformation. The ultimate tensile strength or strength at max load is evaluated in the plastic region where the biocomposite experiences the largest load. Strength evaluated at stress at max load is usually the same as the strength at break. The strength at break not only depends on the component properties but especially on the reinforcement dispersion within the matrix for effective load transfer at the interface.

Typically, the effect of water absorption on the mechanical properties has been assessed before and after immersion rather than as a function of immersion time [55, 58, 72]. Espert [72] observed a decrease in modulus, stress and strain at maximum load after 175 hours of immersion. Few studies [62] have investigated the change in properties as a function of immersion time. A summary of relevant thermoplastic natural fiber reinforced thermoplastics is displayed in Table 2.10 to identify the trend with absorbed water and to show which tests were measured as a function of time.

Table 2.10 Summary of assessment of mechanical properties of biocomposites.

<b>Immersion (hours)</b>	<b>Matrix Type(s)</b>	<b>Fiber Type(s)</b>	<b>Type of Test(s)</b>	<b>Function of time?</b>	<b>Decline?</b>	<b>Ref.</b>
175	PP	Kraft pulp	Tensile	Yes - 175 hours	Yes - E, $\sigma_{\max}$ & $\epsilon_{\max}$	[72]
240	PP	Sisal	Tensile	Yes - 72 hours	Yes - E & $\sigma$	[55]
5040	PP	Flax	Tensile	No	Yes - E & $\sigma$	[73]
5712	PP	Kraft pulp	Tensile Impact	No	Yes - E & $\sigma_{ys}$ No - $\epsilon_{\max}$ & Impact Strength	[58]
17,040	PLA	Flax	Tensile	Yes - 17,040 hours	Yes - E & $\sigma_{ys}$	[62]

Beg & Pickering [58] reported a remarked decrease in both yield strength and Young's modulus where indications of ductility increased with Charpy impact strength and strain at failure. Beg & Pickering and Joseph hypothesized that water molecules acted as a plasticizer in the biocomposite [55, 58].

For one biocomposite variation Duigou [62] reported that there was a decrease in mechanical properties with increased water absorbed. However, Duigou were not able to show that the degradation in mechanical properties was based on the natural fiber degrading since the matrix, PLA, absorbed water and underwent hydrolysis.

A few studies have correlated the normalized mechanical property as a function of water absorbed [25]. A correlation exists between increased water absorbed with an observed decline in both tensile modulus, and ultimate tensile strength. In Stamboulis' [25] work, a fiber treatment method was compared to an untreated fiber. The relative relationship between absorbed water and mechanical property changed with a potentially different interfacial condition. A relationship between both matrix and fiber types has not been established due to the lack of empirical data. The work within provides a comprehensive data set to establish relationships for both matrix and fiber type.

Duigou [62] not only evaluated the property retention with respect to immersion time and absorbed water but also evaluated the reversibility of the degradation. Both dried and wet tensile results were compared for all immersed times. Irreversible damage to both the modulus and ultimate tensile strength was observed after 30 and 15 days, respectively. Since biocomposite modulus is evaluated at the beginning of loading, where damage levels are low, modulus is more reversible than strength at break which depends on the failure properties of each component and the interaction between them [62]. Similar trends were found by

Arbelaiz; after immersion for 5040 hours irreversible damage was sustained for ultimate tensile strength and modulus [73]. Arbelaiz found that after immersion for 5040 hours, and compared to prior to immersion, the biocomposite lost both strength and modulus [73]. The extent of the irreversible degradation of the mechanical properties increased with increased fiber content [54].

Composite stiffness is strongly linked to the constituent properties and therefore also to their evolution during ageing. Despite this, the Young's modulus is obtained at the beginning of the loading where the damage levels are low. Strength at break depends on the failure properties of each component and especially on the interactions between them as well as, the reinforcements' dispersion on the damage accumulation induced by ageing.

Based on these studies, it can be stated that generally water absorption in biocomposites causes degradation on the mechanical properties. The effect of water absorption on the mechanical properties is based on the fiber volume fraction, fiber distribution-dispersion and fiber size [60]. This work adds to the body of knowledge by exploring how the accessible fiber ratio as proposed by Wang [49, 81] affects this degradation.

## 2.6 CONCLUSIONS

Common challenges such as a) unverified fiber contents, b) differences in manufacturing methods, c) differences in constituent materials and d) short term exposure studies have limited the establishment of mechanisms and models for water absorption. To overcome the common challenges with the literature, this work: a) established a reliable method to evaluate fiber volume fraction; b) & c) manufactured 12 variations of biocomposites at three weight fractions with two fiber types and two matrix types to assess changes in material without differences in manufacturing method; and d) executed long term testing for both tensile mechanical properties and water absorption.

Absorbed water has been known to cause deleterious effects on biocomposite mechanical properties. Literature has reported a decline in properties with immersion. In these few studies, only evaluated one fiber content and matrix. The work within this dissertation has established a global relationship for polyethylene based biocomposites that quantifies the degradation of tensile mechanical properties dependent on the quantity of water absorbed from immersion environments independent of fiber content or fiber type.

There is limited long-term absorption data available for most natural fiber types in thermoplastic matrices. The lack of long term data has led to a lack in the ability to predict material durability due to its' susceptibility to environmental degradation. A model was developed to predict long term immersion response as a function of of matrix type, fiber type, fiber fraction, accessible surface fiber ratio and immersion time..

This research provides a more detailed understanding of water absorption and its impact on tensile mechanical properties and will enable designers to utilize these evolving materials to reduce environmental impact [82].



## REFERENCES

1. Nychka, J.A. and G.D. Hibbard. *Rethinking the Materials Paradigm: A Bottom-Up Philosophy*. in *North American Materials Education Symposium - selected oral presentation (1 of 19 from over 100 submissions)*. 2016. University of California Berkeley, Berkeley, CA.
2. Rudin, A. and P. Choi, *Chapter 13 - Biopolymers*, in *The Elements of Polymer Science & Engineering (Third Edition)*2013, Academic Press: Boston. pp. 521-535.
3. Mohanty, A.K., M. Misra, and L.T. Drzal, *Surface modifications of natural fibers and performance of the resulting biocomposites: An overview*. *Composite Interfaces*, 2001. **8**(5): pp. 313-343.
4. Graupner, N., A.S. Herrmann, and J. Mussig, *Natural and man-made cellulose fibre-reinforced poly(lactic acid) (PLA) composites: An overview about mechanical characteristics and application areas*. *Composites Part a-Applied Science and Manufacturing*, 2009. **40**(6-7): pp. 810-821.
5. Mohanty, A.K., M. Misra, and G. Hinrichsen, *Biofibres, biodegradable polymers and biocomposites: An overview*. *Macromolecular Materials and Engineering*, 2000. **276**(3-4): pp. 1-24.
6. Hughes, M., *Defects in natural fibres: their origin, characteristics and implications for natural fibre-reinforced composites*. *Journal of Materials Science*, 2012. **47**(2): pp. 599-609.
7. Thomason, J.L. and J. Carruthers, *Natural fibre cross sectional area, its variability and effects on the determination of fibre properties*. *Journal of Biobased Materials and Bioenergy*, 2012. **6**(4): pp. 424-430.
8. Fernandes, E.M., J.F. Mano, and R.L. Reis, *5. Polyethylene Composites with Lignocellulosic Material*, in *Polyethylene-Based Blends, Composites and Nanocomposites*, V. P. M and M.J.M. Morlanes, Editors. 2015, John Wiley & Sons.
9. Mohanty, A.K., L.T. Drzal, and M. Misra, *Engineered natural fiber reinforced polypropylene composites: influence of surface modifications and novel powder impregnation processing*. *Journal of Adhesion Science and Technology*, 2002. **16**(8): pp. 999-1015.
10. Reddy, N. and Y. Yang, *Biofibers from agricultural byproducts for industrial applications*. *Trends in Biotechnology*, 2005. **23**(1): pp. 22-27.
11. John, M.J. and S. Thomas, *Biofibres and biocomposites*. *Carbohydrate Polymers*, 2008. **71**(3): pp. 343-364.
12. Luo, H. and M.M. Abu-Omar, *Chemicals From Lignin A2 - Abraham, Martin A*, in *Encyclopedia of Sustainable Technologies*2017, Elsevier: Oxford. pp. 573-585.
13. John, M.J. and R.D. Anandjiwala, *Recent developments in chemical modification and characterization of natural fiber-reinforced composites*. *Polymer Composites*, 2008. **29**(2): pp. 187-207.
14. Lu, X., M.Q. Zhang, M.Z. Rong, D.L. Yue, and G.C. Yang, *Environmental degradability of self-reinforced composites made from sisal*. *Composites Science and Technology*, 2004. **64**(9): pp. 1301-1310.
15. Summerscales, J., N.P.J. Dissanayake, A.S. Virk, and W. Hall, *A review of bast fibres and their composites. Part 1 – Fibres as reinforcements*. *Composites Part A: Applied Science and Manufacturing*, 2010. **41**(10): pp. 1329-1335.
16. *Hemicellulose*. Available from: <http://www.lentinplus.net/images/arabinoxylan.gif>.

17. Rong, M.Z., M.Q. Zhang, Y. Liu, G.C. Yang, and H.M. Zeng, *The effect of fiber treatment on the mechanical properties of unidirectional sisal-reinforced epoxy composites*. *Composites Science and Technology*, 2001. **61**(10): pp. 1437-1447.
18. Materials scientist, P.-a.u.k.s.R.Z.S.a.d.w.d.w., *Polymerketten\_-\_amorph\_und\_kristallin.svg*, Wikimedia Commons.
19. Müssig, J. and R. Martens, *Quality Aspects in Hemp Fibre Production—Influence of Cultivation, Harvesting and Retting*. *Journal of Industrial Hemp*, 2003. **8**(1): pp. 11-32.
20. Bos, H.L., M.J.A. Van Den Oever, and O.C.J.J. Peters, *Tensile and compressive properties of flax fibres for natural fibre reinforced composites*. *Journal of Materials Science*, 2002. **37**(8): pp. 1683-1692.
21. Mwaikambo, L.Y. and M.P. Ansell, *Chemical modification of hemp, sisal, jute, and kapok fibers by alkalization*. *Journal of Applied Polymer Science*, 2002. **84**(12): pp. 2222-2234.
22. Shah, D.U., *Natural fibre composites: Comprehensive Ashby-type materials selection charts*. *Materials and Design*, 2014. **62**: pp. 21-31.
23. Pickering, K.L., M.G.A. Efindy, and T.M. Le, *A review of recent developments in natural fibre composites and their mechanical performance*. *Composites Part A: Applied Science and Manufacturing*, 2016. **83**: pp. 98-112.
24. Cheung, H.-y., M.-p. Ho, K.-t. Lau, F. Cardona, and D. Hui, *Natural fibre-reinforced composites for bioengineering and environmental engineering applications*. *Composites Part B: Engineering*, 2009. **40**(7): pp. 655-663.
25. Stamboulis, A., C.A. Baillie, S.K. Garkhail, H.G.H. Van Melick, and T. Peijs, *Environmental Durability of Flax Fibres and their Composites based on Polypropylene Matrix*. *Applied Composite Materials*, 2000(7): pp. 273-294.
26. Nakamura, K., T. Hatakeyama, and H. Hatakeyama, *Studies on Bound Water of Cellulose by Differential Scanning Calorimetry*. *Textile Research Journal*, 1981. **51**(9): pp. 607-613.
27. Lee, J.M., J.J. Pawlak, and J.A. Heitmann, *Longitudinal and concurrent dimensional changes of cellulose aggregate fibrils during sorption stages*. *Materials Characterization*, 2010. **61**(5): pp. 507-517.
28. Celino, A., S. Fréour, F. Jacquemin, and P. Casari, *The hygroscopic behavior of plant fibers: a review*. *Frontiers in Chemistry*, 2014. **2**.
29. Céline, A., S. Fréour, F. Jacquemin, and P. Casari, *Characterization and modeling of the moisture diffusion behavior of natural fibers*. *Journal of Applied Polymer Science*, 2013. **130**(1): pp. 297-306.
30. Saikia, D., *Studies of Water Absorption Behavior of Plant Fibers at Different Temperatures*. *International Journal of Thermophysics*, 2010. **31**: pp. 1020-1026.
31. Biron, M., *Thermoplastics and Thermoplastics Composites*, 2007.
32. Biron, M., *2 - The Plastics Industry: Economic Overview*, in *Thermoplastics and Thermoplastic Composites (Second Edition)* 2013, William Andrew Publishing. pp. 31-131.
33. Osswald, T.A., *Polymer Processing* 1998, Munich: Hanser Publishers. 229.
34. Freedonia, *World Polyethylene*, in *World Collection* 2014.
35. McKeen, L.W., *9 - Polyolefins, Polyvinyls, and Acrylics*, in *Permeability Properties of Plastics and Elastomers (Third Edition)* 2012, William Andrew Publishing: Oxford. pp. 145-193.

36. Flaconnèche, B., J. Matrin, and M.H. Klopffer, *Permeability, Diffusion and Solubility of Gases in Polyethylene, Polyamide 11 and Poly(vinylidene fluoride)*. Oil & Gas Science and Technology, 2001. **56**(3): pp. 261-278.
37. Fotouh, A., J. Wolodko, and M. Lipsett, *Isotherm moisture absorption kinetics in natural-fiber-reinforced polymer under immersion conditions*. Journal of Composite Materials, 2015. **49**(11): pp. 1301-1314.
38. Plastics Design Library, S., *Permeability and Other Film Properties of Plastics and Elastomers*, 1995, William Andrew Publishing/Plastics Design Library.
39. Jasinska, I., *Analysis of thermal decomposition of selected natural fibres on the basis of visual changes during heating*. Industria Textila, 2016. **67**(5): pp. 287-291.
40. Robertson, N.M., J.A. Nychka, and J. Wolodko. *Standardized Thermal Analysis of Natural Fibers in Biocomposites*. in *Faculty of Engineering Graduate Research Symposium*. 2010. Edmonton, Alberta, Canada.
41. *MatWeb: Material Property Data*, 2017, MatWeb, LLC.
42. Chand N., F.M., *Natural fibers and their composites*, in *Tribology of natural fiber polymer composites*, W.P. Limited, Editor 2008, CRC Press LLC: Boca Raton, FL. pp. 2-58.
43. Peltola, H., E. Laatikainen, and P. Jetsu, *Effects of physical treatment of wood fibres on fibre morphology and biocomposite properties*. Plastics, Rubber and Composites. **40**: pp. 86-92.
44. Robertson, N.L.M., J.A. Nychka, K. Alemaskin, and J.D. Wolodko, *Mechanical performance and moisture absorption of various natural fiber reinforced thermoplastic composites*. Journal of Applied Polymer Science, 2013. **130**(2): pp. 969-980.
45. Mukhopadhyay, S. and R. Figueiro, *Physical Modification of Natural Fibers and Thermoplastic Films for Composites - A Review*. Journal of Thermoplastic Composite Materials, 2009. **22**(2): pp. 135-162.
46. Belgacem, M.N., Bataille P., & Sapiera S., *Effect of Corona Modification on the Mechanical Properties of Polypropylene/Cellulose Composites*. Journal of Applied Polymer Science, 1994. **53**: pp. 379 - 385.
47. Cabral, H., M. Cisneros, J.M. Kenny, A. Vázquez, and C.R. Bernal, *Structure-properties relationship of short jute fiber-reinforced polypropylene composites*. Journal of Composite Materials, 2005. **39**(1): pp. 51-65.
48. Tajvidi, M. and A. Takemura, *Recycled Natural Fiber Polypropylene Composites: Water Absorption/Desorption Kinetics and Dimensional Stability*. Journal of Polymers and the Environment, 2010. **18**(4): pp. 500-509.
49. Wang, W., *Moisture sorption and hygro-thermal expansion of natural fiber plastic composites (NFPC)*, 2005, University of Toronto (Canada): Canada. p. 103.
50. Awal, A., S.B. Ghosh, and M. Sain, *Development and morphological characterization of wood pulp reinforced biocomposite fibers*. Journal of Materials Science, 2009. **44**: pp. 2876-2881.
51. Li, X., L.G. Tabil, and S. Panigrahi, *A Study on Flax Fiber-reinforced Polyethylene Biocomposites*. Applied Engineering in Agriculture, 2009. **25**(4): pp. 525-531.
52. Agarwal, B.D., L.J. Broutman & Chandrashekhara K., ed. *Analysis and Performance of Fiber Composites*. 3rd ed. 2006, John Wiley & Sons Inc: New Jersey. 562.
53. Zykova, A.K., P.V. Pantyukhov, N.N. Kolesnikova, T.V. Monakhova, and A.A. Popov, *Influence of Filler Particle Size on Physical Properties and Biodegradation of Biocomposites Based on Low-Density Polyethylene and Lignocellulosic Fillers*. 2017: pp. 1-12.

54. Adhikary, K.B., S. Pang, and M.P. Staiger, *Long-term moisture absorption and thickness swelling behaviour of recycled thermoplastics reinforced with Pinus radiata sawdust*. Chemical Engineering Journal, 2008. **142**(2): pp. 190-198.
55. Joseph, P.V., M.S. Rabello, L.H.C. Mattoso, K. Joseph, and S. Thomas, *Environmental effects on the degradation behaviour of sisal fibre reinforced polypropylene composites*. Composites Science and Technology, 2002. **62**(10): pp. 1357-1372.
56. Tobin, W.J., *Scientific Injection Molding: The Qualifications, Startups, and Tryouts of Injection Molds*. Fourth Edition ed2010: WJT Associates LLC.
57. ASTM, *D1238-13 Standard Test Method for Melt Flow Rates of Thermoplastics by Extrusion Plastometer*, 2013, ASTM International: West Conshohocken, PA.
58. Beg, M.D.H. and K.L. Pickering, *Mechanical performance of Kraft fibre reinforced polypropylene composites: Influence of fibre length, fibre beating and hygrothermal ageing*. Composites Part A: Applied Science and Manufacturing, 2008. **39**(11): pp. 1748-1755.
59. *Definition of MECHANISM*, 2017, Merriam-Webster.
60. Azwa, Z.N., B.F. Yousif, A.C. Manalo, and W. Karunasena, *A review on the degradability of polymeric composites based on natural fibres*. Materials & Design, 2013. **47**: pp. 424-442.
61. Zammarano, M., P.H. Maupin, L.-P. Sung, J.W. Gilman, E.D. McCarthy, Y.S. Kim, and D.M. Fox, *Revealing the Interface in Polymer Nanocomposites*. ACS Nano, 2011. **5**(4): pp. 3391-3399.
62. Le Duigou, A., A. Bourmaud, P. Davies, and C. Baley, *Long term immersion in natural seawater of Flax/PLA biocomposite*. Ocean Engineering, 2014. **90**: pp. 140-148.
63. Kittikorn, T., E. Stromberg, M. Ek, and S. Karlsson, *Comparison of Water Uptake as Function of Surface Modification of Empty Fruit Bunch Oil Palm Fibres in PP Biocomposites*. Bioresources, 2013. **8**(2): pp. 2998-3016.
64. Shakeri, A. and A. Ghasemian, *Water Absorption and Thickness Swelling Behavior of Polypropylene Reinforced with Hybrid Recycled Newspaper and Glass Fiber*. Applied Composite Materials, 2010. **17**: pp. 183-193.
65. Nychka, J.A. and M.M. Gentleman, *Implications of wettability in biological materials science*. JOM, 2010. **62**(7): pp. 39-48.
66. *Percolation Theory and Forest Fires*. [cited 2017; Available from: <http://www1.coe.neu.edu/~emelas/NetForestFires.htm>.
67. Crank, J., *The Mathematics of Diffusion*. Second ed1975, Great Britain: Oxford University Press.
68. Rudin, A. and P. Choi, *Chapter 6 - Diffusion in Polymers*, in *The Elements of Polymer Science & Engineering (Third Edition)*2013, Academic Press: Boston. pp. 275-304.
69. Karimi, M., *Diffusion in Polymer Solids and Solutions*, in *Mass Transfer in Chemical Engineering Processes*, J.E. MarkoÅ, Editor 2011, InTech.
70. Alfrey Jr. T, G.E., Lloyd WG., *Diffusion in Glassy Polymers*. J Polym Sci: Part C 1966. **1966**(12).
71. MiSumi. *Plastic Molding Tutorial*. 2011 [cited 2017 August 5]; Available from: <http://www.misumi-techcentral.com/tt/en/mold/2011/12/106-glass-transition-temperature-tg-of-plastics.html>.
72. Espert, A., F. Vilaplana, and S. Karlsson, *Comparison of water absorption in natural cellulosic fibres from wood and one-year crops in polypropylene composites and its influence on their mechanical properties*. Composites Part A: Applied Science and Manufacturing, 2004. **35**(11): pp. 1267-1276.

73. Arbelaiz, A., B. Fernández, J.A. Ramos, A. Retegi, R. Llano-Ponte, and I. Mondragon, *Mechanical properties of short flax fibre bundle/polypropylene composites: Influence of matrix/fibre modification, fibre content, water uptake and recycling*. Composites Science and Technology, 2005. **65**(10): pp. 1582-1592.
74. ISO, 62 - *Plastics: Determination of water absorption*, 2008. p. 22.
75. Shen, C.-H. and G.S. Springer, *Moisture Absorption and Desorption of Composite Materials*. Journal of Composite Materials, 1976. **10**(1): pp. 2-20.
76. Jost, W., *Diffusion in Solids, Liquids, Gases*. 3rd ed. PHYSICAL CHEMISTRY: A series of monographs, ed. E. Hutchinson and P.V. Rysselberghe 1960, New York: Academic Press Inc.
77. Lin, Q.F., X.D. Zhou, and G. Dai, *Effect of hydrothermal environment on moisture absorption and mechanical properties of wood flour-filled polypropylene composites*. Journal of Applied Polymer Science, 2002. **85**(14): pp. 2824-2832.
78. ISO, 180 - *Plastics - Determination of Izod impact strength*, 2013. p. 10.
79. Xie, Y., C.A.S. Hill, Z. Jalaludin, S.F. Curling, R.D. Anandjiwala, A.J. Norton, and G. Newman, *The dynamic water vapour sorption behaviour of natural fibres and kinetic analysis using the parallel exponential kinetics model*. Journal of Materials Science, 2011. **46**(2): pp. 479-489.
80. Ambrozic, M., A. Dakskobler, M. Valant, and T. Kosmac, *Percolation threshold model and its application to the electrical conductivity of layered BaTiO<sub>3</sub>-Ni*. Materials Science-Poland, 2005. **23**(2): pp. 535-539.
81. Wang, W., M. Sain, and P.A. Cooper, *Study of moisture absorption in natural fiber plastic composites*. Composites Science and Technology, 2006. **66**(3-4): pp. 379-86.
82. Ashby, M.F., *13. Processes and Process Selection*, in *Materials Selection in Mechanical Design (4th Edition)*, Elsevier.

### 3. EXPERIMENTAL DESIGN & DESCRIPTION

This section describes the philosophy and methods used to manufacture, evaluate and analyze the biocomposite specimens, which allowed the investigation of long term water absorption and the deleterious impact on mechanical properties. Methods described herein were designed and optimized to produce consistent repeatable results. The experimental methods used are shown relative to the manufacturing stage illustrated in Figure 3.1.

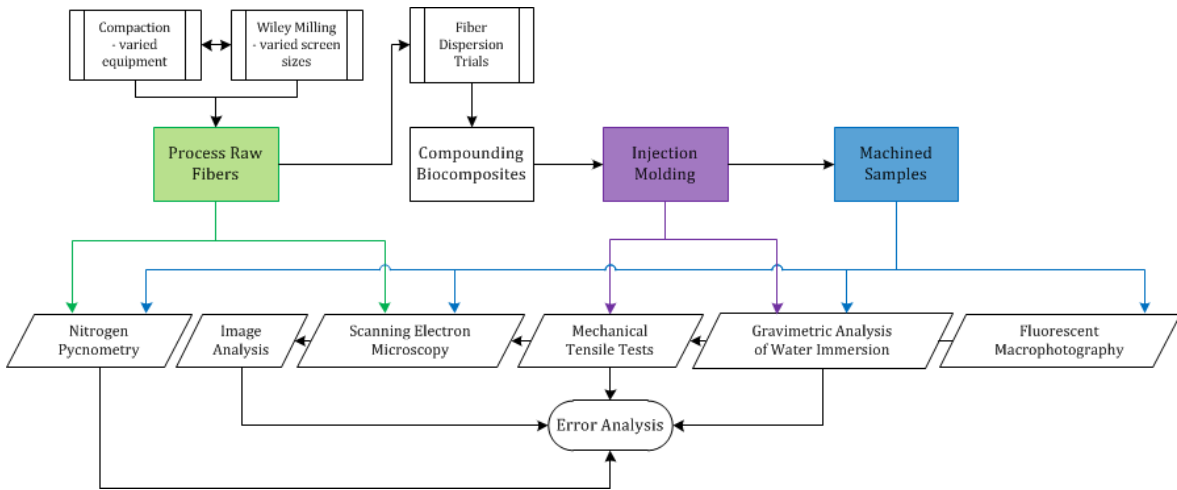


Figure 3.1 Process Flow Diagram of Manufacturing and Analysis Methods

Fiber-matrix compatibilization methods were not included within the work, although commonly reported in literature, for the following reasons: a) studying solely the natural fiber response within the matrix, b) avoid deciphering water absorption response between effect from the compatibilization treatment or natural fiber, c) sufficient literature exists on fiber treatments with certain natural fibers and with the work completed herein could be applied to this literature to provide additional insight into water absorption.

#### 3.1 MANUFACTURING METHODS

✓	Processing	Structure	Property	Performance
---	------------	-----------	----------	-------------

The manufacturing process spans the complexity of combining two dissimilar raw materials, fiber and matrix, to create a biocomposite specimen for further characterization and testing. The manufacturing methods were chosen based on utilization of commercially available and accepted equipment for mass scale production.

The manufacturing process required preprocessing of the fiber, compounding raw materials together, forming (molding) specimens, and post processing machining for specific test requirements. Each processing stage was optimized to produce well distributed and dispersed fibers throughout the matrix for consistent properties and performance. The consistent and repeatable results obtained confirm that the processes were sufficiently optimized.

### 3.1.1 RAW MATERIALS

Polyethylene was selected as the matrix material due to its' commercial relevance and low water permeability (i.e. control for studying fibers in a matrix). The matrix materials were sourced from two suppliers: 1) Low density polyethylene (LDPE) Grade AT418 donated from AT Plastics (Edmonton, Alberta, Canada), and 2) High density polyethylene (HDPE) DMDA 8920 donated from Dow Chemicals (Prentiss, Alberta, Canada). All polyethylene was supplied in the form of pellets.

Milled fiber form was selected to separate the fibers from their raw form into more individualized fibers to increase the surface area of fiber to exploit the maximum properties of the fiber. Hemp fiber was donated by Hemp Technologies (Halesworth, Suffolk, UK). The hemp had been long line decorticated, 10 mm chopped and hammer-milled with a 1mm x 10mm screen. Visually, the bast hemp fiber was free of hurd or other contaminants as seen in Figure 3.2. Aspen Kraft, herein called wood pulp, was donated by Daishowa-Marubeni International (Peace River, Alberta Canada). The wood pulp (Aspen Kraft) had been cross cut from 81cm by 81cm sheets into 2cm by 2cm pieces and disc milled. Fiber morphology of both fiber types are shown in Figure 3.2. The original fiber form before milling has been referenced as fiber feed stock. The fiber length and radius distribution were not characterized.

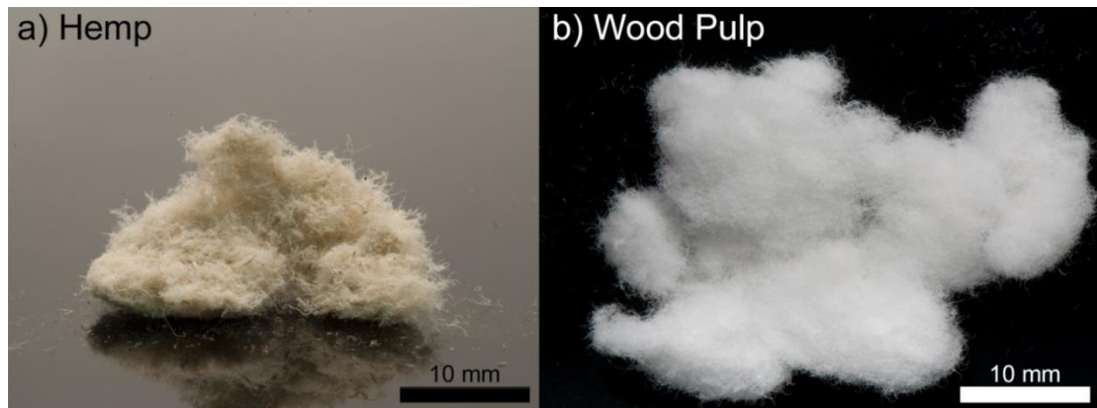


Figure 3.2 As received (milled) fiber condition a) Hemp and b) Wood Pulp.

### 3.1.2 RAW FIBER PROCESSING

The natural fibers as received were unable to be fed into an extruder by a gravity step feeder. Milled fibers are intrinsically light and mechanically intertwined which cause an inconsistent feed rate with gravity type feeders. A constant feed rate is critical to achieve fiber distribution. To overcome this challenge, a series of pelletization trials were conducted to assess the fiber feed rate and fiber dispersion in the melt.

Pelletization was selected as the fiber processing method due to the ability to compact the fibers for consistent feed rates as well as to increase bulk density for gravity fed hoppers. A series of trials were conducted to achieve a loose pellet to enable fiber dispersion as well as be able to feed both fiber types with varying amounts of moisture content. The initial moisture content as well as the method of moisture addition (steam or poured water) was varied and assessed as shown in Figure 3.3. The optimal pelletization process used an Amandus Kahl 33-390 Mill with pre-dried fiber at 90°C until moisture content measured less than 2.5% by Ohaus MB25 Moisture Analyzer, as shown in Figure 3.3. The fiber was pre-dried to limit the fibers binding together by hydrogen bond when under pressure. The pelletized fiber morphology is shown in Figure 3.4.



Figure 3.3 Equipment involved with natural fiber pelletization from left to right: Ohaus Moisture Analyzer[1], Amandus Kahl Die Face Mill with Rollers, and Wiley Mill.

The pelletization process singularly solved the feed rate issue, but not the issue of fiber dispersion within the melt. Before production compounding, a trial was conducted on the extruder which visually assessed the extent of fiber dispersion within the polymer melt. The trial consisted of pellets Wiley milled with different screen sizes to disrupt the pellet structure and enable the fiber dispersion within the melt. The optimal process to achieve both a consistent feed rate and adequate dispersion was pelletization followed by Wiley mill without a screen.



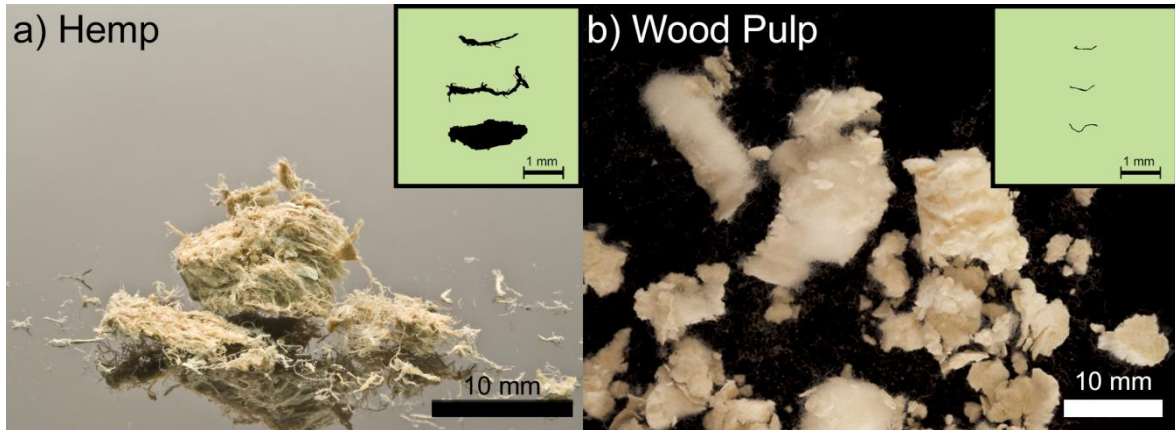


Figure 3.4 Pelletized fiber condition a) Hemp and b) Wood Pulp along with a range of individual fiber bundle silhouettes (obtained from bright field transmitted optical light microscopy) in the top right. Image modified from [2].

### 3.1.3 COMPOUNDING OF BIOCOMPOSITES

Extrusion was selected as the compounding process as it is widely commercially adopted, possesses a high mass throughput, and can be a highly controllable process. Extruders are highly adaptable pieces of equipment used for different thermoplastics and composites. A Thermo Scientific twin screw co-rotating extruder Haake Rheomix PTW 24/40 with a Thermo Scientific at-face pelletizer, shown in Figure 3.5 and Figure 3.6, were used to manufacture all biocomposites studied herein. The at-face pelletizer was selected as the method to cool the hot extrudate over a cold water bath to avoid the introduction of water into the material. A vacuum port was added at the end of the mixing section to draw water vapour out of the biocomposite melt to reduce likelihood of pores in the biocomposite. For specific extrusion parameters of each material variation manufactured, see Appendix A.

Three fractions of each fiber type were compounded with each matrix for a total of 12 biocomposite variations as shown in Figure 3.7. Each variation was named based on the type of matrix, type of fiber and target weight fraction of fiber as displayed in equation 3.1 and Table 3.1. Target weight fractions were 15 wt%, 30 wt% and 45 wt%. The weight fraction of fiber was controlled by the mass rate into the extruder. Both plastic and fiber feeders were calibrated before and after each manufactured batch to ensure steady state processing conditions. Feeder calibration methodology and example calibration are provided in Appendix A. Mass flow of material into the extruder did not equal the mass flow out of the extruder as fiber was observed when cleaning the extruder after each batch was produced. The actual manufactured fiber weight and volume fraction was evaluated by gas pycnometry,

detailed in section 3.2.1. The determined fiber volume fractions are provided in Table 4.1 and 4.2 in brackets. A minimum of 7 kilograms of each material was produced.

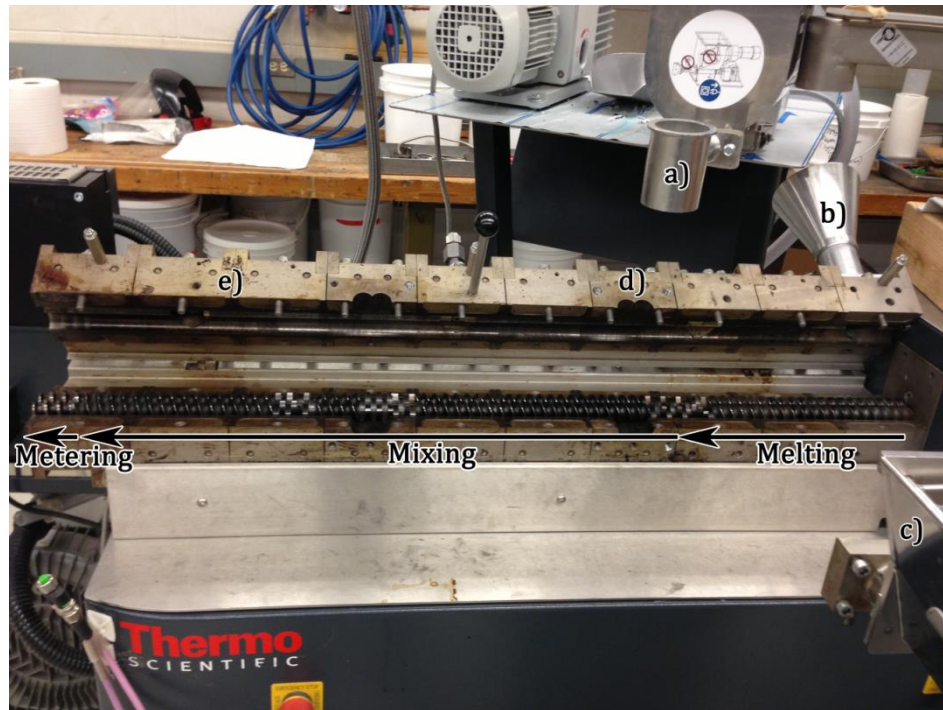


Figure 3.5 Thermo Scientific Twin Screw Extruder a) thermoplastic feeder, b) thermoplastic feeder port, c) natural fiber feeder, d) natural fiber feed port and e) vacuum port location.

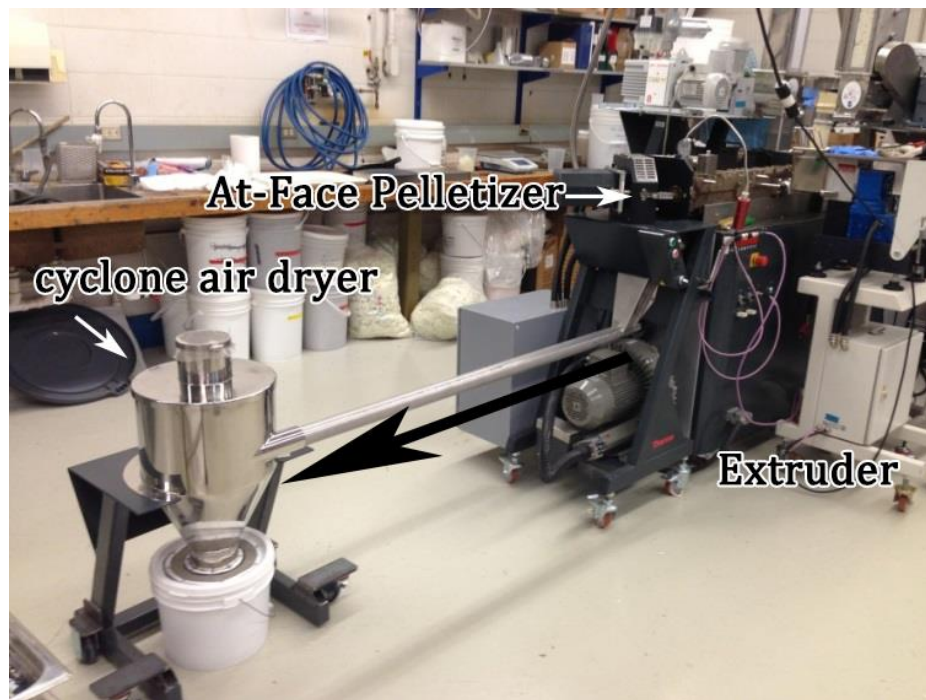


Figure 3.6 Air cooling apparatus after extrusion compounding.

The name convention for the biocomposite materials were:

$$\mathbf{XYZZ} \quad (3.1)$$

Where,

**X** = Matrix Type, L = LDPE and H = HDPE

**Y** = Fiber Type, H = Hemp fiber and W = Wood Pulp

**ZZ** = Target weight fraction of fiber, low = 15, medium = 30 and high = 45

Table 3.1: Name and symbology convention for manufactured biocomposites

		Target Weight Fraction of Fibers (Plastic Fiber wt%)					
		Low Density Polyethylene (LDPE) ◊			High Density Polyethylene (HDPE) ◈		
Fiber Type	Hemp Fiber	LH15 ◊	LH30 ◊	LH45 ◊	HH15 ◈	HH30 ◈	HH45 ◈
	Wood Pulp	LW15 ○	LW30 ○	LW45 ○	HW15 ●	HW30 ●	HW45 ●

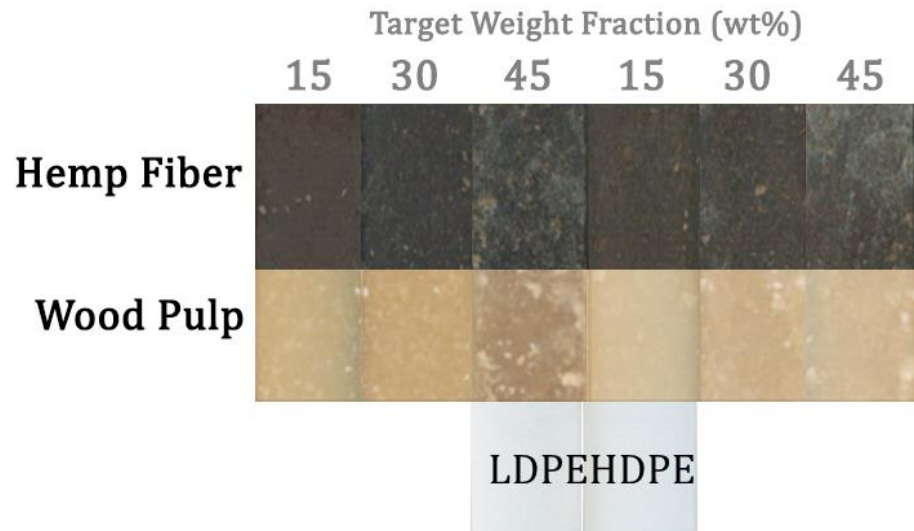


Figure 3.7 Twelve variations of hemp fiber and wood pulp reinforced polyethylene biocomposites displayed in the same arrangement as Table 3.1. The left three columns are LDPE and the right three columns are HDPE variations.

### 3.1.4 INJECTION MOLDING

A BOY 22A injection molding machine was used to manufacture tensile, flexural and izod specimens as per standards ASTM D638-10 Type 1, ASTM D790-10 and ISO 294-1, respectively, as shown in Figure 3.8. Specimen thickness ranged between 3.05mm and 3.2mm due to plastic shrinkage from varied matrix content. The parameters of injection molding the specimens differentiated from one material variation to the next due to the amount of fiber fill and fiber type influencing the rheological melt properties. A successful injection molding run was determined when the specimens were fully packed, no flashing was observed on specimens, no warpage was evident due to shrinkage, and the shot weight remained consistent throughout the batch. Time, temperature and pressure parameters used to achieve successful shots on the BOY 22A as per ISO 294-1[3] were determined using industry guidelines [4] and are listed in Appendix A. Important trends observed include: increase in back pressure in screw filling phase due to pellet properties, increase in transition pressure due to interfacial shear and fiber break up.

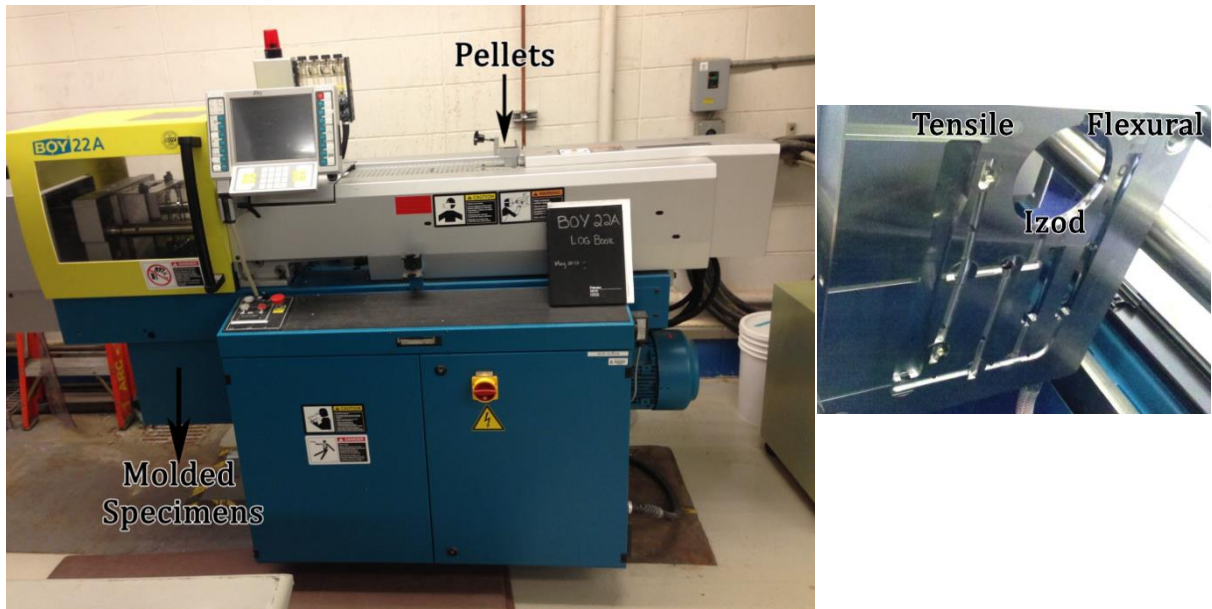


Figure 3.8 Left: BOY 22A Injection molder Right: Mold cavity with all three specimen types manufactured in one injection molded shot.

### 3.1.5 MACHINED SAMPLES

Different forms of specimens were further processed to provide insight into effect of water on the biocomposite system for as molded and interior cut surfaces

#### 3.1.5.1 X-Y Izod Sample Preparation

Cartesian coordinates were “scored” onto the molded surface of an izod specimen by a razor blade to observe fibers on the “as molded” surface as a function of immersion time. The cross hairs provided a reference to locate the same fiber type in the imaging field, described in section 3.2.5.1.

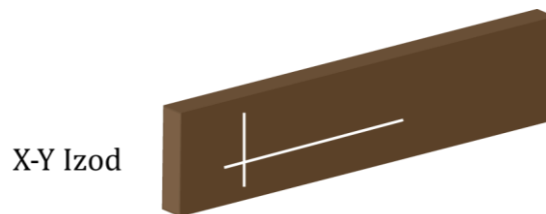


Figure 3.9 X-Y Izod Specimen Type showing fiducial markings (white lines) used for referencing locations in SEM characterization.

#### 3.1.5.2 Sample Preparation: Edge Preparation

Flexural bars were cut with a table saw to remove the “as molded” edge(s). A jig was manufactured to ensure that the total removed volume was within a 1mm tolerance for each material variation. A variety of types of cuts were tested to assess the impact of both the ratio of differences in the ratio of surface area to volume as well as differences machined surfaces relative to injection molding orientation, as illustrated in Figure 3.10.

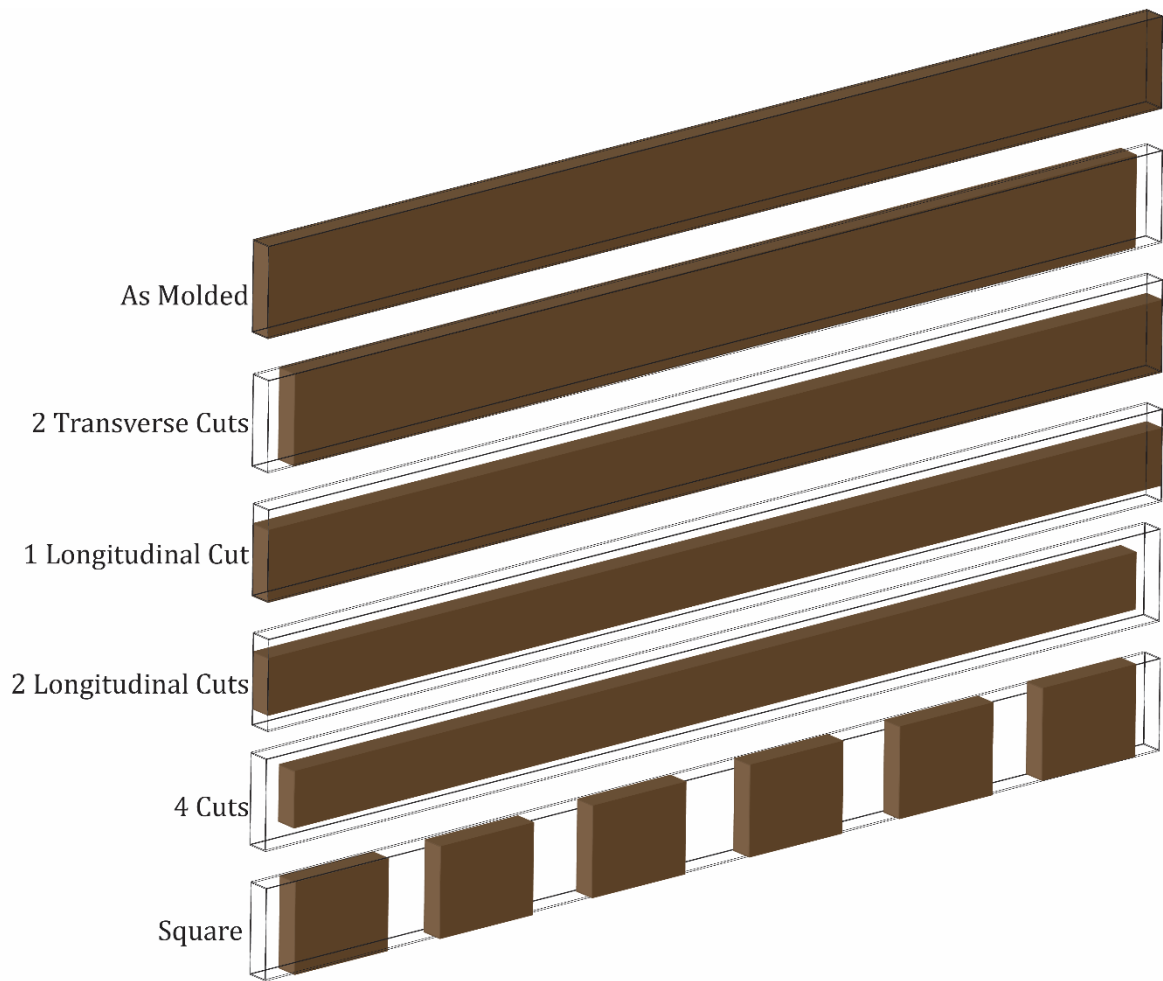


Figure 3.10 Cut edge(s) specimen types.

### 3.2 EVALUATION OF MATERIALS

Processing	✓	Structure	✓	Property	✓	Performance
------------	---	-----------	---	----------	---	-------------

This section details the methods used to characterize the biocomposite materials structure, properties, and performance. A summary of each test method as well as the corresponding information is outlined in Table 3.2.

Table 3.2: Design of Experiments Overview

Test Name	Specimen Type	Property (unit)	Information	
Nitrogen Pycnometry	Fibers	Fiber Density $\rho_{\text{fiber}} \text{ (g/cm}^3\text{)}$	- density of fibers	
	Square	Matrix Density $\rho_{\text{matrix}} \text{ (g/cm}^3\text{)}$	- reference of injection molded matrix density	
		Composite Density $\rho_{\text{biocomposite}} \text{ (g/cm}^3\text{)}$	- for determination of volume fraction fiber manufactured	
Water Immersion - Gravimetric Analysis	Tensile (As Molded)	Percent Mass Gain (%)	Impact of: <ul style="list-style-type: none"> <li>- rate of absorption</li> <li>- maximum of water absorbed</li> <li>- matrix type</li> <li>- fiber type</li> <li>- fiber volume fraction</li> <li>- surface accessible fiber</li> <li>- surface area to volume ratio</li> </ul>	
	Flexural (As Molded)			
	2 Transverse Cut			
	1 Longitudinal Cut	Volume of H <sub>2</sub> O Absorption (cm <sup>3</sup> )		
	2 Longitudinal Cut			
	4 Side Cut			
	Square			
Fluorescent Macrophotography	Square	Relative amount of water absorbed	- visualize location of water absorption and the rate of absorption at the surface	
Mechanical Tensile Test	Tensile	Modulus, E (GPa)	Relationship for each property relative to: <ul style="list-style-type: none"> <li>- fiber type</li> <li>- matrix type</li> <li>- fiber volume fraction</li> <li>- absorbed water</li> <li>- property retention after immersion</li> </ul>	
		Yield Tensile Strength, $\sigma_{\text{YS}}$ (MPa)		
		Ultimate Tensile Strength, $\sigma_{\text{UTS}}$ (MPa)		
		Elongation at Break (%)		
		Toughness (J)		
Scanning Electron Microscopy	1 Longitudinal Cut	Area fiber fraction $A_f \text{ (%)}$	Determine of surface fiber fraction (BS-SEM) on: <ul style="list-style-type: none"> <li>- molded</li> <li>- molded perimeter</li> <li>- longitudinal cut</li> <li>- transverse cut</li> </ul>	
	Square			
	X-Y Izod	Fiber loss, qualitative		- fiber morphology as a function of immersion time on molded surfaces (BS & SE-SEM)
	Tensile	Fraction modes, qualitative		- insight into fracture mode (SE-SEM)

The statistical uncertainty for both the measurements and calculated properties are presented in Appendix B.

### 3.2.1 GAS PYCNOMETRY

Density is a necessary material property to convert weight fraction of a constituent material to a volume fraction, which can subsequently be correlated to material performance. Gas pycnometry was selected to determine density of the manufactured biocomposite ( $\rho_c$ ), fibers ( $\rho_f$ ) and matrix ( $\rho_m$ ) due to iterative measurements, precise results [5], a controlled non-reactive test environment, and a relatively large sample volume (12.2cm<sup>3</sup>). Gas pycnometry is a technique based on the principle of gas displacement from the ideal gas law, equation 3.2. The amount of volume of displaced gas is used to calculate the volume of an object of a known mass, equation 3.3. The density of the sample was calculated, as per equation 3.4, from the measured mass of the sample after from the volume determined in equation 3.3.

$$PV = nRT \quad (3.2)$$

$$V_{sample} = V_c \frac{V_R}{1 - P_1/P_2} \quad (3.3)$$

$$\rho_{sample} = \frac{m_{sample}}{V_{sample}} \quad (3.4)$$

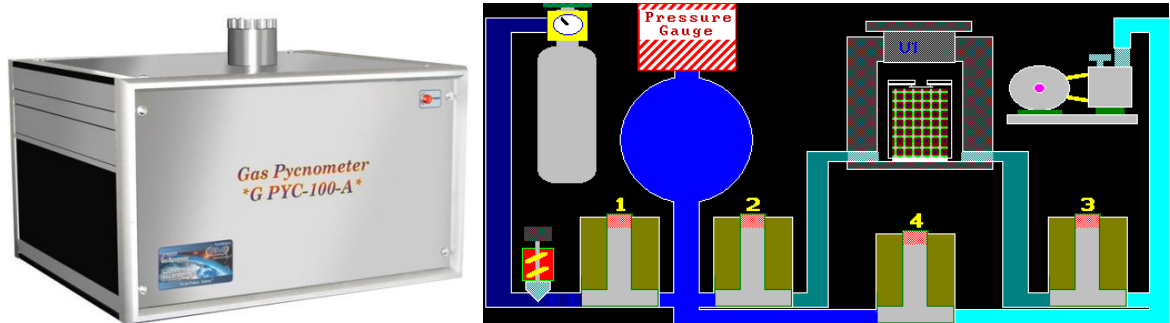


Figure 3.11 Gas Pycnometer [6] (left) and Schematic of Pycnometer Chambers (right).

A PMI Gas Pycnometer Model: PYC – G100A-1, shown in Figure 3.11, was used for all measurements with 99.998% pure Nitrogen gas from Praxair Edmonton, AB. Nitrogen was selected as the inert gas over helium as Helium is known to adsorb onto cellulosic materials and some polymeric surfaces [7]. The pycnometer was modified with an internal fan to dissipate thermal heat produced by internal electrical circuits to ensure the volume chambers operated isothermally. Before testing, the pycnometer was calibrated with a NIST standard, SRM1827b Lead Silica Glass Mass Density Standard [8], to verify the internal volume of the



reference chamber and a study was conducted to ensure volume of specimens met the equipment range, see Appendix A4

Each test comprises 30 iterative measurements. For each test, the sample chamber underwent five cycles of vacuum purge and dry nitrogen sweep before data acquisition to drive residual moisture out of the test specimens. Adhered moisture causes unstable measurements with the mass and volume changing with evaporating moisture. Volumes were measured when the pressure reached 0 psi and 10psi with dry nitrogen. A vacuum of  $10^{-5}$  mTorr ( $-10^{-10}$  mmHg) was achieved each pressure cycle by a Pfeifer Turbo Vacuum, Model TSH071E. A calibrated four-point scale, Denver Instrument PI-124, was used to weigh the sample inside the chamber after the test, where the test specimens were considered dry. The criterion for test acceptance was based on whether the data was normally distributed about the mean and the standard deviation from 30 measurements was less than  $0.002\text{g}/\text{cm}^3$ .



Figure 3.12 Sample chamber filled with square biocomposite specimens

### **3.2.1.1 Fiber Density Assessment**

The natural fibers were assessed in fiber forms: a) as-received, b) pelletized, c) pelletized with subsequent Wiley milled with no screen and d) freezer milled. The fibers were cooled down by liquid nitrogen inside a SPEX6700 Freezer Mill, illustrated in Figure 3.13, to pulverize the fiber into a fine powder for assessment of cell wall density. Truong [5] recommends measurement of fiber density by gas pycnometry for accurate and repeatable results.



Figure 3.13 Freezer Mill (left) and sample tube with rod (right).

### 3.2.2 WATER IMMERSION – GRAVIMETRIC MEASUREMENTS

Gravimetric measurements were selected based on their extensive use in the literature [2, 9-11] to measure water absorption including standards ASTM D570 [12] and ISO 62 Method 1[13]. The method employs a bulk measurement of weight gain or loss which provides insight into rates, magnitudes and characteristics of water movement in time.

Consideration was given to seal the specimen edges around the perimeter to simplify modelling the water absorption data. However, the difficulties associated with selection of a sealant for polyethylene and control in mass of the sealant during application to ensure a repeatable result proved more detrimental than immersion of a manufactured part with 6 surfaces exposed to the environment.

#### 3.2.2.1. Atmospheric Water Immersion

Specimens were dried for a minimum of 48 hours at 65°C under -20 mmHg until the weight remained constant. Specimens were placed in a reverse osmosis water bath at 23 ± 0.5°C, as illustrated in Figure 3.14 At the designated time intervals; each specimen was removed from the water, excess surface water wiped off with paper towel and weighed three times each before the specimen was re-submerged. Measurements were taken on a Sartorius LA 3105 four-point balance with 0.1 mg resolution. All data reported represents the average and standard deviation at each time interval. Water absorption was calculated as shown in equation 3.5.

$$M_t = \frac{w_t - w_i}{w_i} \times 100 \quad (3.5)$$

where  $M_t$  is the percentage weight gain of the specimen at the given time interval,  $w_i$  is the initial weight of the specimen after drying, and  $w_t$  is the weight of the specimen at the given time interval. The number of samples per specimen type is illustrated in Table 3.3.

Table 3.3: Water Immersion Number of Replicates per Specimen Type

Specimen Type	Number of Replicates
Tensile	7
As-molded	3
2 Transversal Cuts	3
1 Longitudinal Cut	3
2 Longitudinal Cuts	3
4 Cuts	3
Square	5

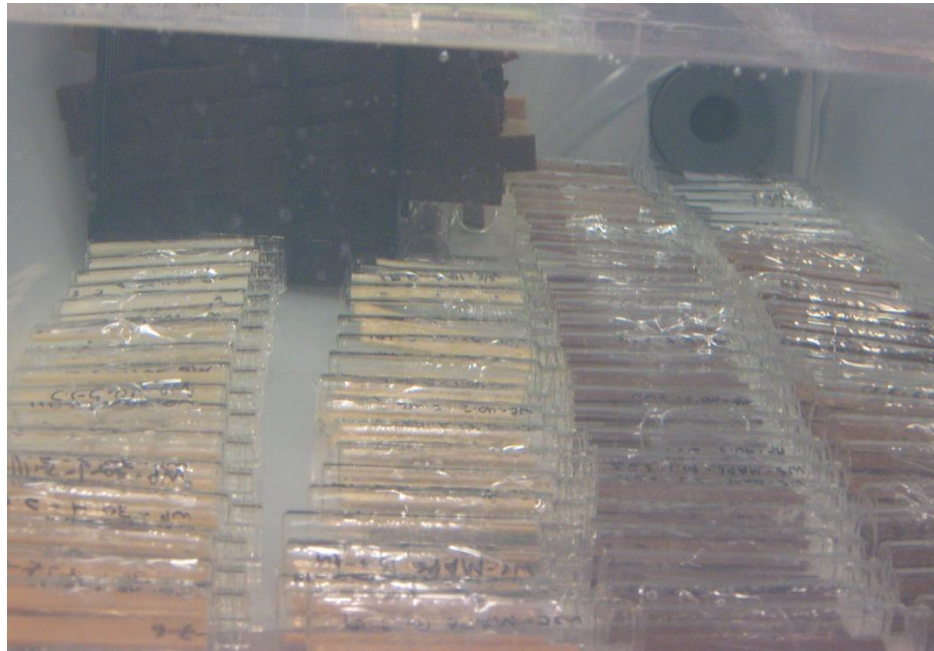


Figure 3.14 Water bath for tensile immersion specimens (at back right) and as molded flexural specimens. Specimens were stacked vertically (tensile) or placed inside glass vials (flexural, square, etc) to reduce area not in direct contact with the water immersion environment while ensuring the specimen remains submerged.

### 3.2.2.2. Pressurized Water Immersion

An aluminum pressure vessel chamber was filled with distilled water. The pressure was applied by a nitrogen tank. Four flexural as molded specimens of both HDPE and HDPE filled with 30% volume fraction of hemp fiber (HH45) were placed inside the chamber fully submerged. The specimens were removed for measurement as per 3.2.2.1 at hourly increments of 1, 4, 24, 48, 72 and 168 hours.

### 3.2.3 MECHANICAL TENSILE TESTS

Monotonic tensile tests were conducted as per ASTM D638 [14] at a strain rate of 5 mm/min using an Instron 4032C load frame with a 1 kN load cell [2]. Strain measurements were obtained from a clip-on extensometer, for strains up to 8% strain, and the cross-head displacement thereafter. The tensile modulus was calculated by Bluehill2 software[15]. The Bluehill2 software divided the data on the strain axis into six equal regions between the first data point and either the maximum load point or the tensile stress yield point. The algorithm determines modulus as the region with the greatest slope by calculation using a least square fit algorithm. Percent elongation (%El) was determined as the strain reading at break. Toughness was assessed from the area under the stress strain curve, which is not a typical test method to determine toughness. Therefore, the toughness results are a general representation of the materials ability to absorb energy. Only results from specimens which failed within the gauge length were utilized for the results.

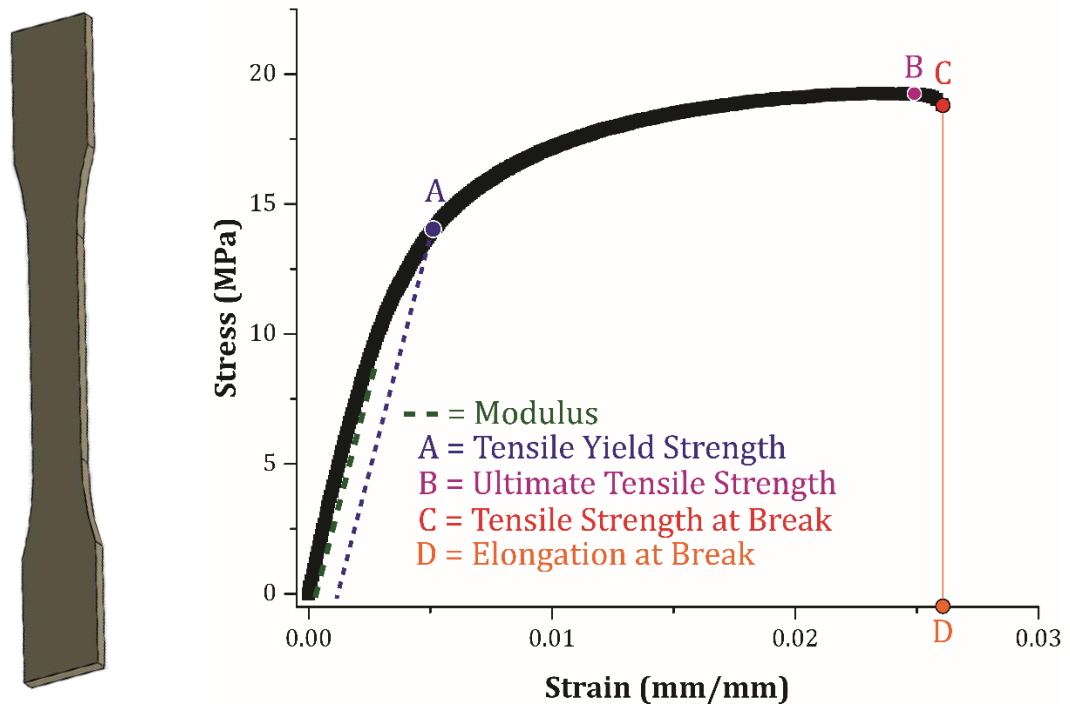


Figure 3.15 Schematic of Tensile Specimen (left) and typical stress strain curve for fiber filled biocomposite (right). Stress Strain curve is representative curve from HH45 prior to water immersion.

#### 3.2.3.1 Design of Experiments

Seven specimens were tested at each water immersion interval detailed in Table 3.4. Specimens were removed from the water bath at designated times, and were tested within 3

minutes of removal to minimize water loss. Each specimen's dimensions were measured with a Mitutoyo 500 Series Digimatic Caliper and was weighed in accordance with section 3.2.2 before being loaded into the mechanical tester.

Table 3.4: Tensile Specimen Water Immersion Intervals

Reading #	1	2	3	4	5	6	7	8	9
Weeks	0	0.14	1	2	4	8	26.03	39.01	39
Hours	0	24	168	336	672	1344	4373	6553	6552*

\*specimens were dried after elapsed immersion time then tested

### 3.2.3.2 Calculation of Normalized Mechanical Properties

The assessment of normalized mechanical property provides context of the relative change in a specific property relative to the manufactured dried specimen. The normalized property was assessed as shown in equations 3.6 and 3.7 where  $o$  represents the original property without exposure and  $t$  represents the time interval exposed. The normalized property of modulus, strength, ultimate tensile strength, elongation at break and toughness are reviewed in section 4.3. The error bars represent the relative scatter in the data at the interval in time as calculated in equation 3.8.

$$\bar{y} = \frac{\sum_{i=1}^n y_i}{n} \quad (3.6)$$

$$\bar{Y} = \frac{\bar{y}_t}{\bar{y}_o} \times 100 \quad (3.7)$$

$$\% \text{ Error} = \frac{C.I.\bar{y}}{\bar{y}} \quad (3.8)$$

where

$y_i$  = measured property (unit)

$n$  = number of replicate material variation

$\bar{y}$  = average property (unit)

$\bar{Y}$  = normalized property relative to time of exposure (%)

$C.I.\bar{y}$  = Confidence interval, 95%, of sample distribution of a property (unit)

### 3.2.4 FLUORESCENT MACROPHOTOGRAPHY

Fluorescent macrophotography dye was used as an imaging technique to track where the ultra-violet water soluble dye travelled within the biocomposite. A greater intensity of

fluorescent response would indicate a higher concentration of dye. The fluorescent dye was manufactured by Risk Reactor product IFWB-C8 Yellow-Green. A stock solution of 1:1000 fluorescent dye to water was mixed for immersion testing. A unique specimen was submerged for each time interval and fiber content. Dyed specimens were imaged with a Nikon D7000, 17-55 mm f2.8 lens with a long wave ultraviolet light, Spectroline Model B-100 (365 nm).

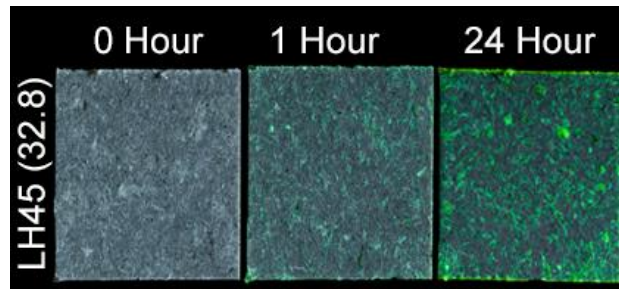


Figure 3.16 LH45(32.8) after immersion in UV water soluble dye. Left to right: 0 hour, 1 hour, and 24 hours.

### 3.2.5 SCANNING ELECTRON MICROSCOPY

#### 3.2.5.1 Secondary Electron Imaging Mode

Secondary electron imaging was selected to investigate the fracture surface topography for insight into fracture mode as well as fiber arrangement. For example, in Figure 3.17, the hemp fiber illustrates a brittle fracture failure mode while the surrounding low density polyethylene displays plasticity surrounding the fiber. Scanning electron micrographs were taken with a JOEL 6301F field emission scanning electron microscope under high vacuum. The specimens were coated with gold using a Nanotech SEM Prep 2 DC sputter coater.

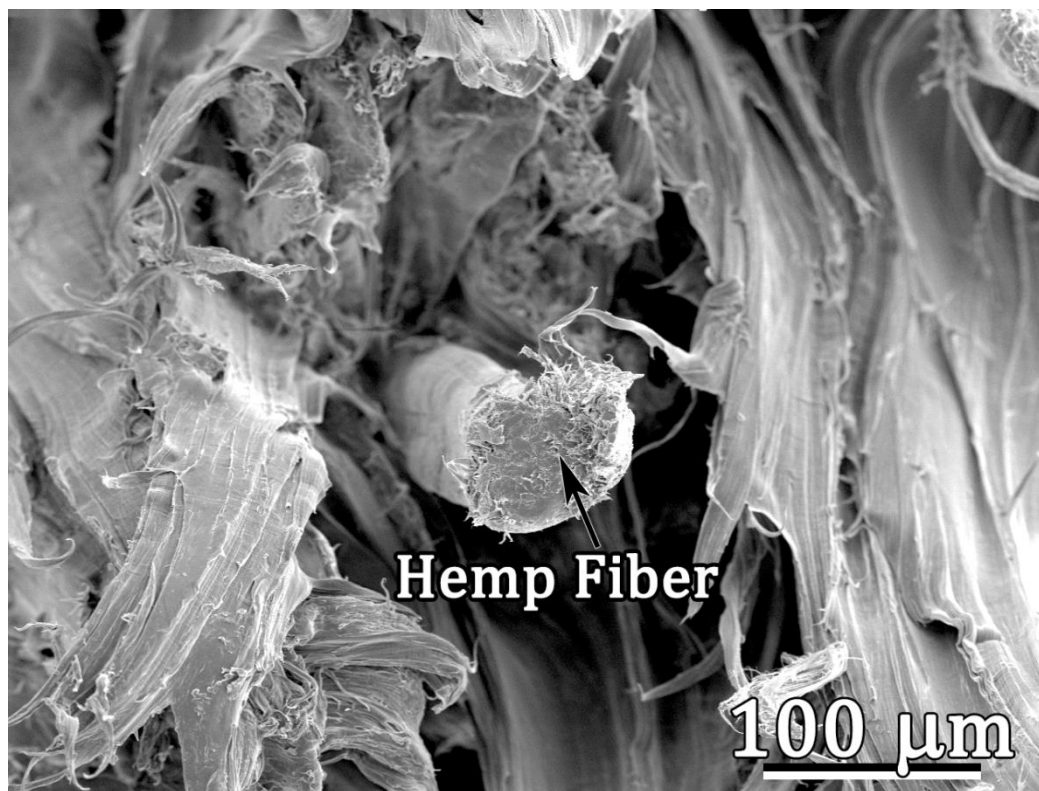


Figure 3.17 Fracture Surface of LH15(9.4) without exposure to water immersion.

### 3.2.5.2 Back Scattered Electron Imaging Mode

Back scattered (BSE) electron imaging mode provides contrast via atomic number differences. BSE was used to image the natural fibers within the matrix to determine the surface area fraction of the biocomposites. The BSE technique has not been reported before for biocomposite fiber spatial imaging. Micrographs were taken on uncoated samples with a Zeiss EVO MA 15 with LaB<sub>6</sub> filament at 25 kV accelerating voltage in variable pressure mode. Molded and cut surfaces were imaged to measure the surface area fraction of fiber, SA<sub>f</sub>(%). Example micrographs are shown in Figure 3.18. Methodology used to calculate area fraction of fibers by image analysis is detailed in Section 3.2.6.

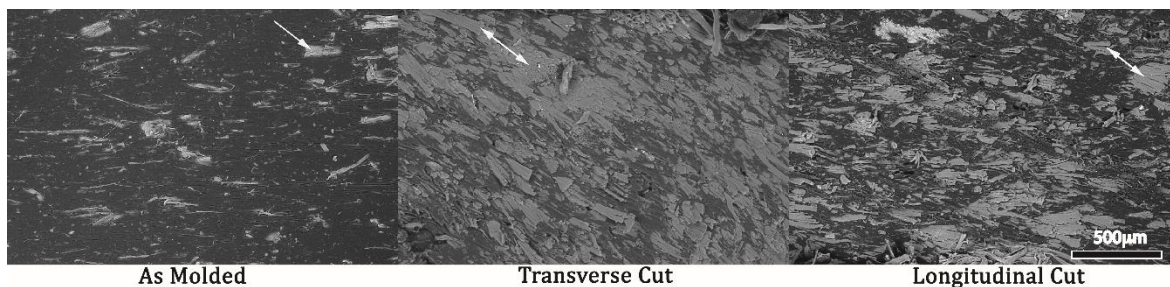


Figure 3.18 Representative BS SEM Images of 30wt% Hemp filled HDPE at each surface. Light grey regions are hemp fibers, as indicated by white arrows

The same operator was utilized to minimize drastic differences in the brightness and contrast between micrographs due to change in surface type and material variation. Differences in contrast and brightness arose due to the difference in chemical composition of hemp fiber and wood pulp hence scattering the electrons differently causing varying profiles of grey scale from one material variation to another which could impact the image analysis conducted on the micrographs, explained in section 3.2.6.

### 3.2.5.3 Combination Back Scattered & Secondary Electron Imaging

A combination of electron imaging modes was utilized to locate the natural fiber on the surface as well as observe changes in sample topography for X-Y Izod specimens. The electron signals were combined from 80% backscattered with 20% secondary electron. Micrographs were taken on uncoated samples with a Zeiss EVO MA 15 at 25 kV accelerating voltage in 55 kPa vacuum with a probe current of 175 pA.

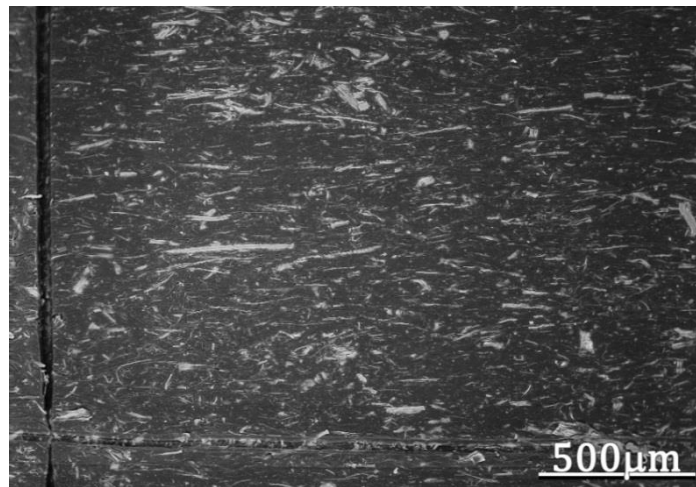


Figure 3.19 Field of View on HH45(36.4) XY Izod Specimen. Notice the fiducial lines at left and bottom.

### 3.2.6 IMAGE ANALYSIS – AREA FIBER FRACTION

To determine fiber fractions present at the biocomposite surfaces BS SEM images were used. Four surface types: as molded, as molded perimeter, transverse cut, longitudinal cut, illustrated in Figure 3.20 were imaged and analyzed. A minimum of 10 micrographs were used for the assessment of surface accessible fiber area fraction.



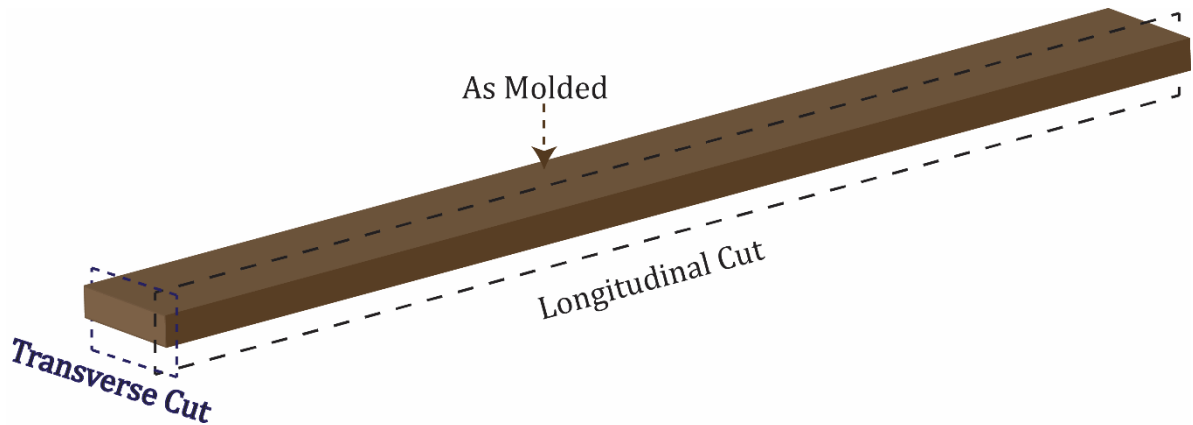


Figure 3.20 Schematic of location of cut surfaces

In the BS-SEM micrographs, the lighter pixels represent heavier elements, fibrous portion of the biocomposite, and the darker pixels represent the matrix, as shown in Figure 3.18. The gray scale value for both the fiber and matrix differs from image to image as seen in Figure A.2. Therefore the setting of the thresholds is of utmost importance in differentiating fiber and matrix to produce a binary image. The ratio of measured black pixels,  $P_B$ , and white pixels,  $P_W$ , are used to calculate the surface accessible fiber area fraction,  $A_f$ , as shown in equation 3.9.

$$\text{Area Fraction, } A_f = \frac{P_W}{P_B + P_W} \quad (3.9)$$

ImageJ, an open source image processing software by Fiji, was used to apply a standard threshold algorithm to each image [16]. Assessments of 16 different algorithms, presets in Fiji, were applied to various images with different fiber fill fraction, type of cut surface and type of fiber. An example of each algorithm is shown in the montage of HH30 As molded surface in Figure 3.21.

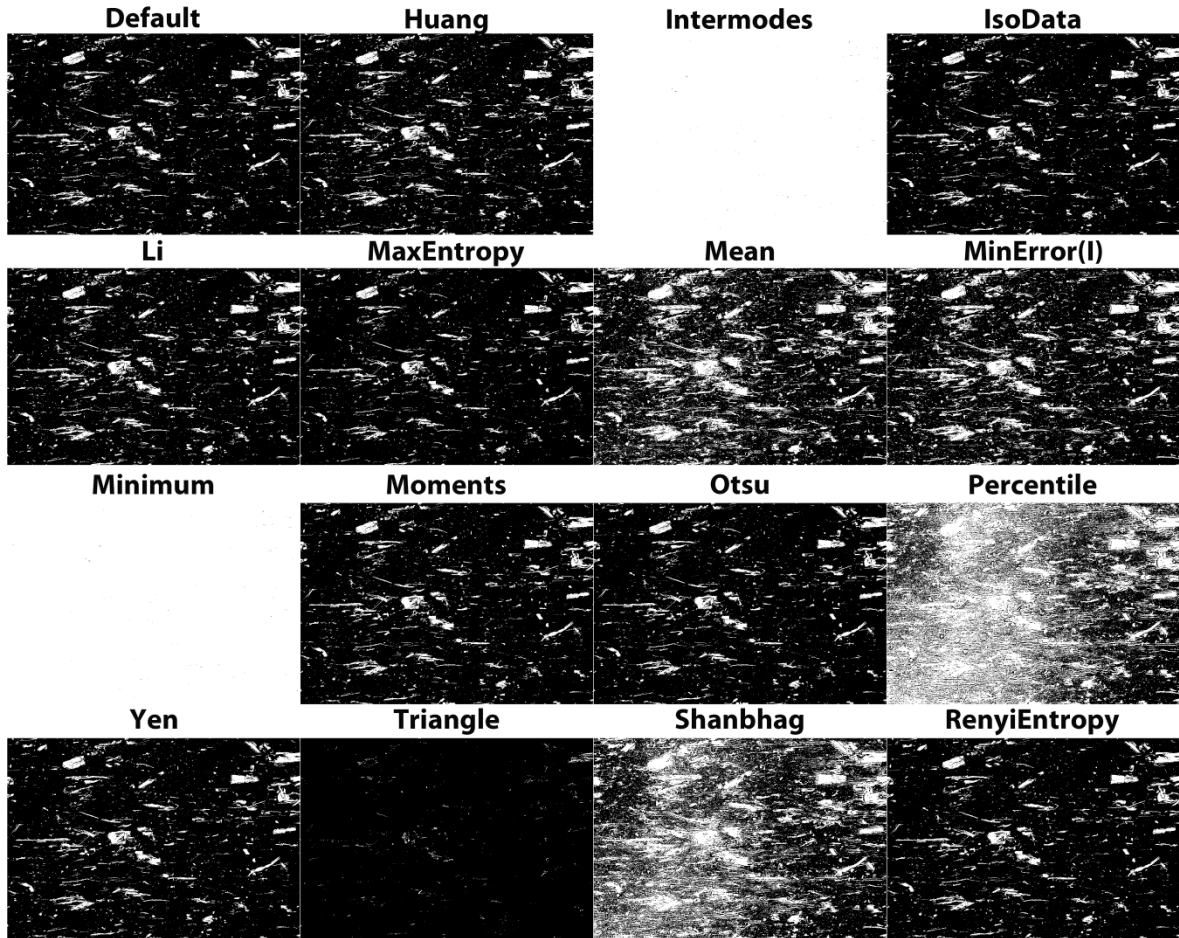


Figure 3.21 Montage of Auto Threshold settings on the As Molded surface of 30wt% hemp filled HDPE. All algorithm results were compared and the “IsoData” algorithm was determined to give the most consistent and reliable results distinguishing between the difference of fiber and matrix for all biocomposite variations. The IsoData algorithm is based on an iterative approach to provide an optimum threshold for distinguishing between an object and the background of an image containing different average levels of gray levels published by Ridler & Calvard in 1978 [17]. The algorithm works by “dividing the image into object and background by taking an initial threshold, then the averages of the pixels at or below the threshold and pixels above are computed. The averages of those two values are computed, the threshold is incremented and the process is repeated until the threshold is larger than the composite average” [18]. As shown in equation 3.10.

$$\text{Threshold} = \frac{(\text{Average Background} + \text{Average Objects})}{2} \quad (3.10)$$

All processed images were double checked to ensure the algorithm did not give a null result. A comparison of the original back scattered SEM micrograph and the IsoData threshold is

illustrated in Figure 3.22. The surface accessible fiber area fraction values are reported with a 95% confidence interval to  $\geq \pm 2.0\%$  area fraction using a student t distribution test.

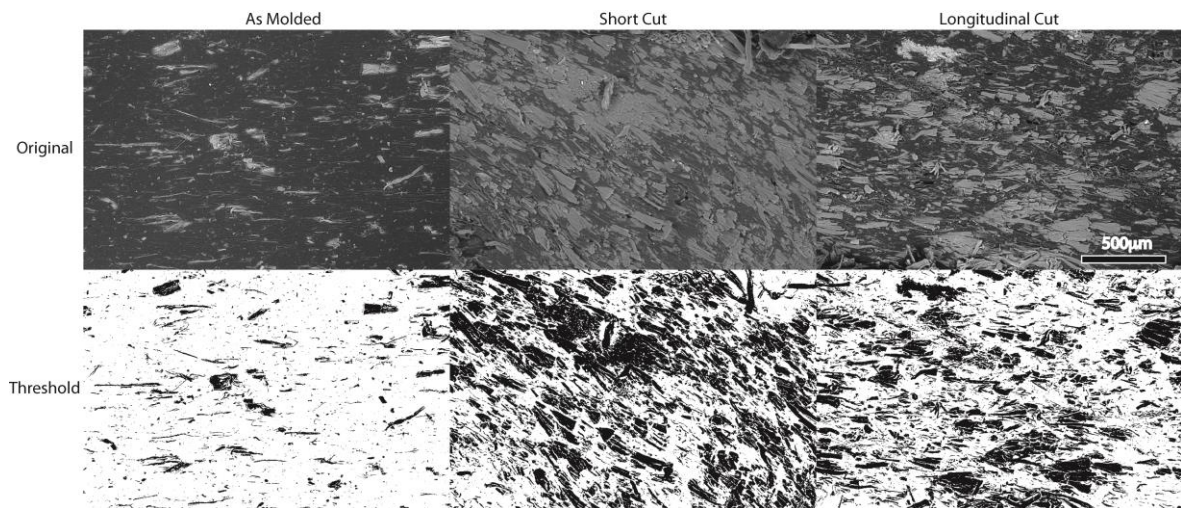


Figure 3.22 Comparison of backscattered and the corresponding IsoData thresholded micrograph at each surface for 30 wt% hemp filled HDPE.

To validate the measurement of the algorithm a micrograph of 250µm glass silica beads were imaged on carbon black tape and analyzed with the IsoData algorithm, shown in Figure 3.23. The percent area of beads was calculated based on each sphere's diameter; with the assumption that each bead is a perfect sphere. The IsoData algorithm detected 15 beads with an area fraction of 29.2%. The difference between the manual calculation and the IsoData algorithm was less than 2% and therefore was determined to be an acceptable method.

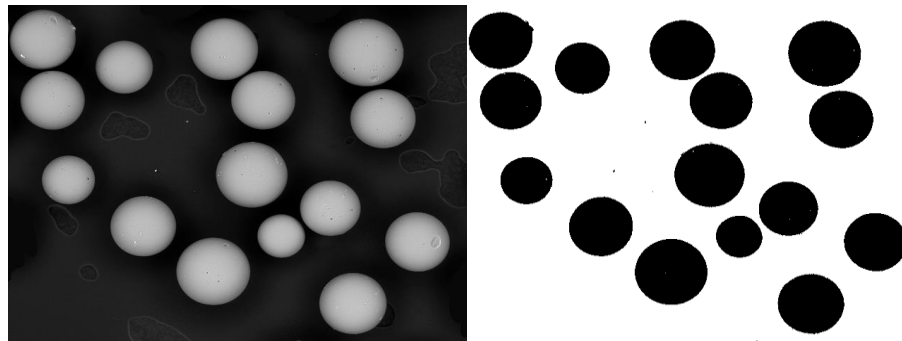


Figure 3.23 (Left) Backscattered micrograph of glass silica beads and (right) IsoData thresholded imaged.

### 3.2.7 NATURAL FIBER WATER CONTENT

Hemp fiber and wood pulp were exposed to a high humidity environment to determine the maximum water content near immersion conditions at 97.3% relative humidity. Three glass containers were weighed and filled with fiber for each fiber type. The containers were placed inside the glass vacuum chamber, see Figure 3.24, where the natural fibers were exposed to 97.3 %RH at 25°C from a super saturated salt solution of potassium sulfate[19] for 336 hours (2 weeks). The concentration of potassium sulfate solution was 12 g/100ml. After exposure to the high humidity environment, the glass containers with natural fibers were vacuum dried for 48 hours at 55°C to determine the ultimate dried fiber weight. The percent water absorbed was calculated as shown in equation 3.11.

$$M_t = \frac{w_{@336 \text{ hours } 97\% \text{ RH}} - w_{\text{vacuum dried}}}{w_{\text{vacuum dried}}} \times 100 \quad (3.11)$$



Figure 3.24 Glass vacuum chamber where salt solution filled the bottom of the container to produce a high humidity environment of 97.3%. Image from [20].

## 3.2 REFERENCES

1. Ohaus. *MB25 Moisture Analyzer*. 2010 [2015/04/25]; Available from: <http://mea.ohaus.com/mea/en/home/products/product-families/MB25-EU.aspx>.
2. Robertson, N.L.M., J.A. Nychka, K. Alemaskin, and J.D. Wolodko, *Mechanical performance and moisture absorption of various natural fiber reinforced thermoplastic composites*. *Journal of Applied Polymer Science*, 2013. **130**(2): pp. 969-980.
3. ISO, *294-1 Plastics - Injection moulding of test specimens of thermoplastic materials - , in Part 1: General principles, and moulding of multipurpose and bar test specimens* 2000. p. 20.
4. Tobin, W.J., *Scientific Injection Molding: The Qualifications, Startups, and Tryouts of Injection Molds*. Fourth Edition ed2010: WJT Associates LLC.
5. Truong, M., W. Zhong, S. Boyko, and M. Alcock, *A comparative study on natural fibre density measurement*. *Journal of the Textile Institute*, 2009. **100**(6): pp. 525-529.
6. PMI. *Gas Pycnometer*. 2009; Available from: <http://www.pmiapp.com/products/productPages/gasPycnometer.html>.
7. Lowell, S., J.E. Shields, M.A. Thomas, and M. Thommes, *Density Measurement, in Characterization of Porous Solids and Powders: Surface Area, Pore Size & Density*, B. Scarlett, Editor 2004, Kluwer Academic Publishers: Boston. p. 347.
8. Technology, N.I.o.S.a., *SRM 1827b - Lead Silica Glass Mass Density Standard*.
9. Adhikary, K.B., S. Pang, and M.P. Staiger, *Long-term moisture absorption and thickness swelling behaviour of recycled thermoplastics reinforced with Pinus radiata sawdust*. *Chemical Engineering Journal*, 2008. **142**(2): pp. 190-198.
10. Tajvidi, M. and A. Takemura, *Recycled Natural Fiber Polypropylene Composites: Water Absorption/Desorption Kinetics and Dimensional Stability*. *Journal of Polymers and the Environment*, 2010. **18**(4): pp. 500-509.
11. Wang, W., M. Sain, and P.A. Cooper, *Study of moisture absorption in natural fiber plastic composites*. *Composites Science and Technology*, 2006. **66**(3-4): pp. 379-86.
12. ASTM, *D570: Standard Test Method for Water Absorption of Plastics*, 1998 (Reapproved 2010). p. 4.
13. ISO, *62 - Plastics: Determination of water absorption*, 2008. p. 22.
14. ASTM, *D638: Standard Test Method for Tensile Properties of Plastics*, 2010. p. 16.
15. *Bluehill 2 Calculations Reference: Reference Manual - Software*, 2012, Instron. pp. 1-224.
16. Schindelin, J., I. Arganda-Carreras, E. Frise, V. Kaynig, M. Longair, T. Pietzsch, S. Preibisch, C. Rueden, S. Saalfeld, B. Schmid, J.-Y. Tinevez, D.J. White, V. Hartenstein, K. Eliceiri, P. Tomancak, and A. Cardona, *Fiji: an open-source platform for biological-image analysis*. *Nat Meth*, 2012. **9**(7): pp. 676-682.
17. Komuriah, A., N.S. Kumar, and B.D. Prasad, *Chemical Composition of Natural Fibers and its Influence on their Mechanical Properties*. *Mechanics of Composite Materials*, 2014. **50**(3): pp. 359-376.
18. Krasowska, K., J. Brzeska, M. Rutkowska, H. Janik, M.S. Sreekala, K. Goda, and T. Sabu, *Environmental Degradation of Ramie Fibre Reinforced Biocomposites*. *Polish Journal of Environmental Studies*, 2010. **19**(5): pp. 937-945.
19. *Equilibrium Relative Humidity Saturated Salt Solutions*. 2013; Available from: [www.omega.ca/temperature/Z/pdf/z103.pdf](http://www.omega.ca/temperature/Z/pdf/z103.pdf).

20. Scientific, C.-P. *Pyrex 3120-250 Brand 3120 dessicator, 250 mm*. [cited 2017 2017-03-23]; Available from: <https://www.coleparmer.com/i/pyrex-3120-250-brand-3120-dessicator-250-mm/3454923>.

## 4. IMPACT OF WATER ON MECHANICAL PROPERTIES

A time series investigation of moisture absorption was conducted to quantify the correlation between water absorption and the corresponding mechanical properties. Fiber content was assessed for each biocomposite variation to evaluate the contribution of the matrix and fiber. The manufactured volume fraction of fiber was determined from nitrogen pycnometry to model the mechanical properties of biocomposites. Mechanical properties, such as tensile modulus, tensile yield strength, ultimate tensile strength, elongation at break and toughness were examined. This chapter evaluates the impact of water immersion on the mechanical properties as a function of time and fiber volume fraction.

### 4.1 DETERMINATION OF VOLUME FRACTION

For all composites, the relative content of reinforcement within the matrix determines the properties and performance of the material. Relative content can be categorized by either weight fraction or volume fraction. Weight fraction is mainly utilized in the manufacturing process due to the ease of measurement; volume fraction is utilized in the analysis of numerous material properties and performance since it is the volume occupied by the constituent materials that contribute to the properties of the biocomposite [1-4]. In literature, however, it is common to analyze the performance with respect to weight fraction due to the complexity of accurately determination of volume fraction. Herein, gas pycnometry, section 2.2.1, was utilized to determine fiber volume fraction and verify the manufactured composition. Volume fraction of fiber was calculated from experimental determination of fiber, matrix, and composite density shown in Equations 4.1 to 4.5. For all equations  $v$  denotes volume ( $cm^3$ ),  $V$  denotes volume fraction (%),  $w$  denotes weight (g),  $W$  denotes weight fraction (%),  $\rho$  denotes mass density ( $g/cm^3$ ), subscript  $c$  for composite, subscript  $m$  for matrix, and subscript  $f$  for fiber.

$$\text{Composite density:} \quad \rho_c = \rho_f V_f + \rho_m V_m \quad (4.1)$$

$$\text{Assumption}^1: \quad V_f + V_m = 1 \quad (4.2)$$

$$\text{Rearrangement:} \quad V_m = 1 - V_f \quad (4.3)$$

---

<sup>1</sup> All volume occupied within the biocomposite is occupied by the native structure of the virgin materials (fiber and matrix) without the introduction of manufacturing flaws.

Substitute Equation 4.3 into Equation 4.1 to give Equation 4.4.

$$\rho_c = \rho_f V_f + \rho_m (1 - V_f) \quad (4.4)$$

Solve for volume fraction of fiber:

$$V_f = \frac{\rho_c - \rho_m}{\rho_f - \rho_m} \quad (4.5)$$

To assess the difference between target weight fraction and the actual manufactured weight fraction, volume fraction of fiber was converted to weight fraction as shown by the derivation from Equation 4.6 to 4.11. Discrepancies between weight fractions are attributed to fiber loss during processing and inaccuracies in feed rate control.

$$W_f = \frac{w_f}{w_c} \quad (4.6)$$

Where,

$$w_f = \rho_f v_f \quad \text{and} \quad w_c = \rho_c v_c \quad (4.7) \text{ and } (4.8)$$

Substitute in:

$$W_f = \frac{\rho_f v_f}{\rho_c v_c} \quad (4.9)$$

Since

$$\frac{v_f}{v_c} = V_f \quad (4.10)$$

$$W_f = \frac{\rho_f}{\rho_c} V_f \quad (4.11)$$

The pore volume fraction<sup>2</sup> was assumed to be zero due to:

- A) Manufacturing precautions were taken to prevent the formation of pores by vacuum pressure applied in the extrusion melt to remove evaporated water from the fibers.
- B) Morphology indicative of pores were not found in any of the fracture surface SEM micrographs.
- C) An assumption of a pore volume fraction other than zero would result in a higher calculated fiber volume fraction; since a pore occupies volume but has no mass. The assumption of zero pore volume fraction results in a conservative assessment of fiber volume fraction where the contribution of the natural fibers to the mechanical properties would not be overestimated.

---

<sup>2</sup> A standard method to determine the pore volume fraction for biocomposites does not exist. Pores are likely to be formed from the evaporation of absorbed water on the high surface area of fiber.



For the above reasons, the absence of pore volume fraction is deemed a reasonable assumption for calculation of fiber volume fraction, as it underestimates fiber volume fraction if pores do exist within the material.

#### 4.1.1 EVALUATION OF POLYETHYLENE DENSITY

The density of both matrix materials, HDPE and LDPE, were assessed in the final manufactured state (as-molded) and compared to the densities specified in the technical data sheet illustrated in Figure 4.1. The suppliers determined density by two other methods: 1) LDPE by a proprietary test method and 2) HDPE by ASTM D792 (a liquid displacement method).

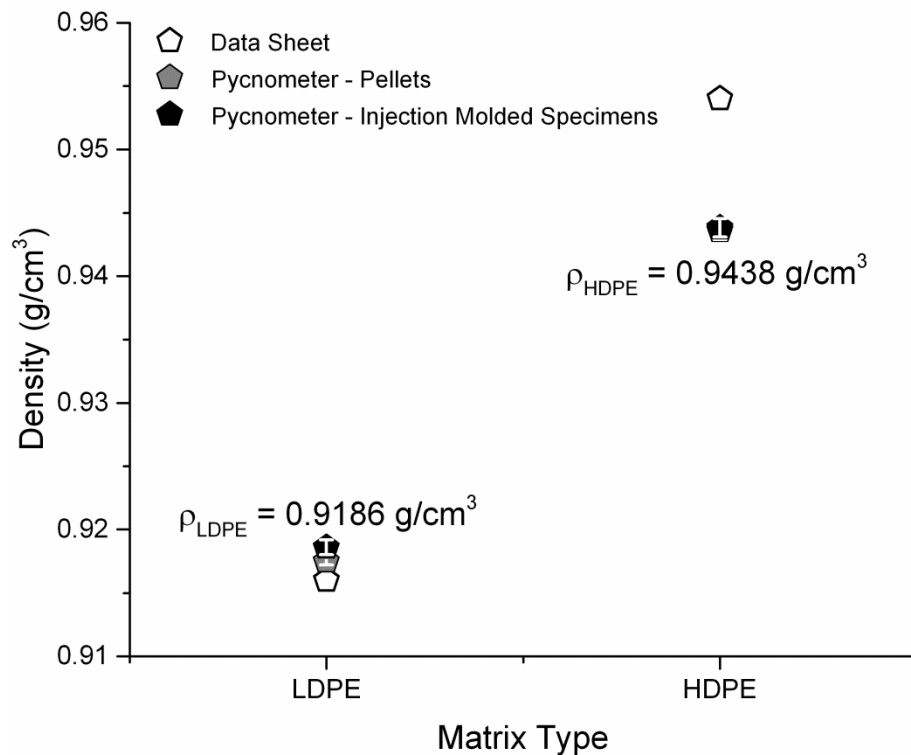


Figure 4.1 Comparison of LDPE and HDPE as molded density determined by nitrogen pycnometry (filled) versus density provided on the technical data sheet (unfilled). The error bars represented a 99% confidence interval based on a proven normal distribution.

The differences in the measured density of both LDPE and HDPE, Figure 4.1, highlights the necessity to compare measured density values determined by the same method and same sample type. Differences in densities between the pellets and injection molded specimens may be attributed to thermal processing where residual solvent evaporates or a change in crystallinity from a different cooling rate. Therefore, in this study, the final processed state,

injection molded sample type, was selected as the chosen condition from which to select density values to eliminate inconsistencies between manufacturing processes and evaluation methods.

#### 4.1.2 EVALUATION OF FIBER DENSITIES

Fiber density is dependent on fiber type and fiber form. Fiber density of both wood pulp and hemp fiber were assessed at each processing stage to evaluate changes in fiber density caused by processing, illustrated in Figure 4.2. The fiber densities at each processing stage were compared to freezer milled type as a control of the maximum amount of exposed close pore volume of a fiber and to maximize the surface area of fiber for measurement purposes. The average fiber density reported for each processing method within the fiber type were determined to be statistically different (wood pulp  $p_{\max}=0.0003$  and hemp fiber  $p_{\max}=1.5E-6$  for 99% confidence interval, where  $p$  represents probability) by ANOVA and student t test, except wood pulp variations cross cut, pelletized and pelletized-Wiley milled.

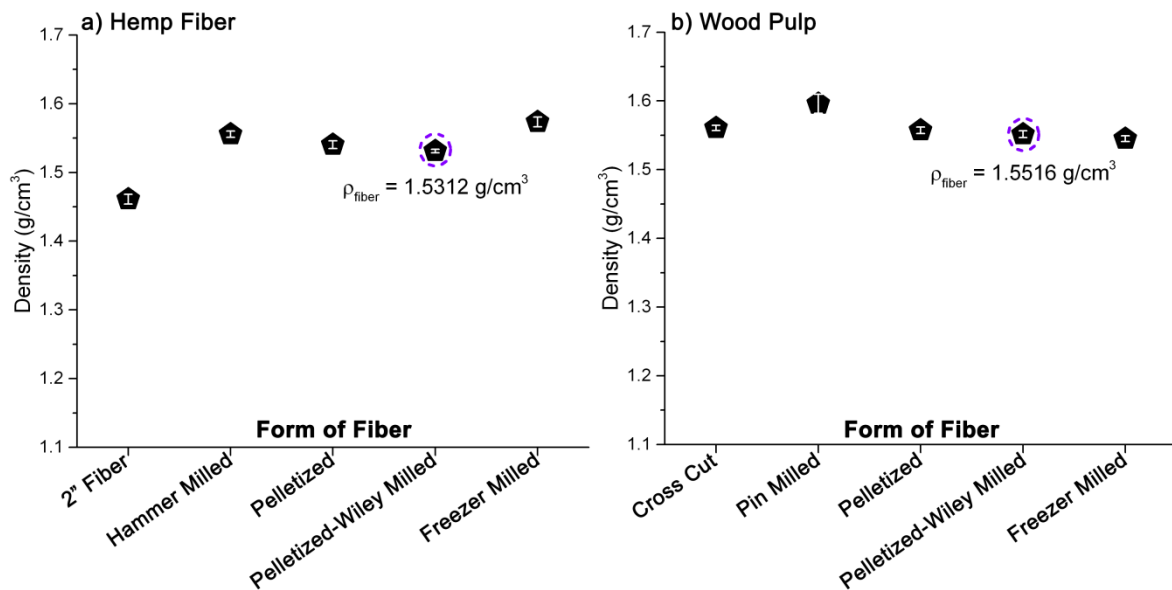


Figure 4.2 Comparison of mass density for Hemp fiber (left) and Wood Pulp (right) after different processing methods. Hemp exhibits higher variability to fiber preparation method than wood pulp as the magnitude of scatter between fiber forms is greater for hemp. The error bars represent a 99% confidence interval around the mean based on a proven normal distribution.

For both fiber types, the first milling process increased the fiber density by decreasing the closed pore volume within the fiber hence increasing the surface area of the fiber exposed to the nitrogen pycnometry gas. The pelletization process decreased fiber density as air became

entrapped within the fiber arrangement in the pellet during compaction. The additional processing stage of wiley milling the pelletized fiber resulted in a minimal change in fiber density, for both fiber types. Pelletized-wiley milled fiber was the form of fiber fed into the extruder, circled in Figure 4.2, and therefore was used to calculate the volume fraction of fiber. For hemp fiber, the freezer mill process resulted in the highest fiber density. The processing of hemp fiber significantly altered its structure by mechanically breaking down the lumen structure and exposing the inner cell walls of the lumen, as shown in Figure 4.3. The structural change observed for the hemp fiber with mechanical processing directly impacts the fiber density. Hemp fiber displayed a range of density from 1.4611 – 1.5735 g/cm<sup>3</sup> (difference of 0.1124) dependent on the fiber processing method. Therefore, fiber density is directly related to the selected processing method.

Since wood pulp had previously undergone significant mechanical and chemical treatments from the pulping process, minimal changes in density (max difference of 0.052 g/cm<sup>3</sup>) were observed with fiber processing. The change in density of wood pulp is attributable to bulk fiber arrangement rather than a change in fiber structure as seen with hemp. The freezer milled density represents the cell wall density of hemp. The form of a fiber type has a significant impact on the density. For wood pulp, the pin milled form exhibits the highest density because fibers are individually exposed to the nitrogen pycnometry with minimal fiber compaction compared to the spacing after the paper making process. The method of fiber processing impacts the closed porosity within the structure of the natural fiber, the lumen space.

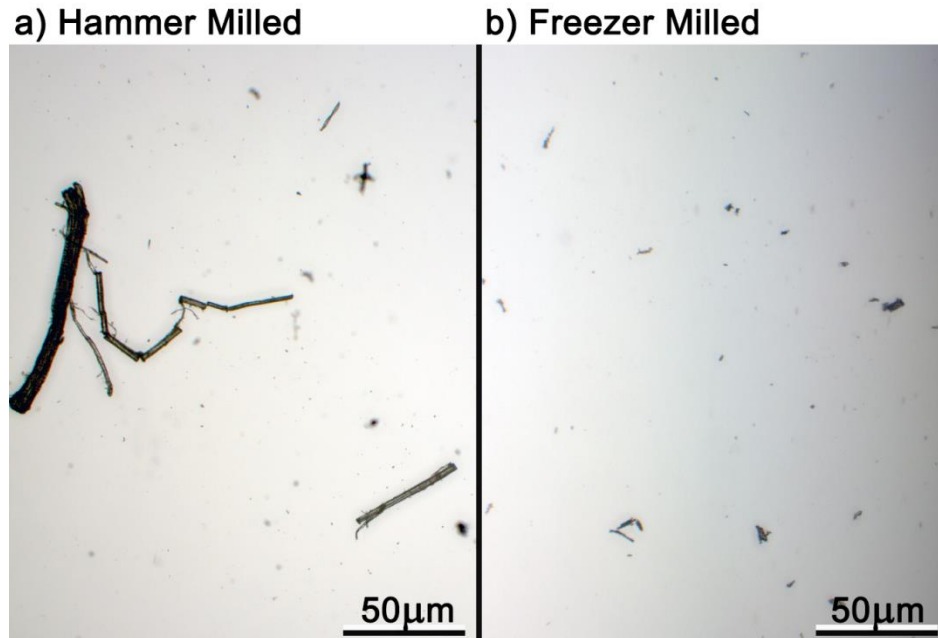


Figure 4.3 Transmitted bright field optical light microscope micrographs of hemp fiber processed by a) hammer milling and b) freezer milling methods. Freezer milling has reduced both fiber size and shape to maximize exposure of fiber closed pore volume.

The density of fiber is lowest when sampled in its natural state. Throughout processing the closed pore volume within the fiber is exposed to the pycnometry gas and density increases. Due to the effects of fiber processing on fiber density (such as fibers with internal closed porosity) caution should be exercised when utilizing natural fiber density values from literature. It is paramount that the fiber form and fiber density is well characterized *in the manufactured composite* rather than from raw materials to reduce the propagation of errors in fiber volume fraction. Variations in fiber density have also been known to arise from crop variety, seed density, soil quality, fertilization, field location, climate and time of harvest [5].

#### 4.1.3 *BIOCOMPOSITE EVALUATION*

Composite material properties are typically estimated by rule of mixtures based on fiber volume fraction. The biocomposite density was assessed on multiple square type specimens by nitrogen pycnometry to determine fiber volume fraction. Both the calculated actual manufactured fiber weight fraction and fiber volume fraction are displayed in Table 4.1 for hemp and Table 4.2 for wood pulp as calculated with equations 4.5 and 4.7. Due to the importance of density to determine volume fraction of fiber a 99% confidence interval was calculated and graphically represented. The comparative standard deviation and 95% confidence interval are reported for reference.

Table 4.1 Hemp filled Biocomposite Densities from Square Specimens

	Hemp Fiber					
	LDPE			HDPE		
Target Fiber Fraction (wt%)	15	30	45	15	30	45
Actual Fiber Fraction (wt%)	10.8	27.7	36.5	20.2	31.6	40.9
<b>Actual Manufactured (vol%)*</b>	<b>6.6</b>	<b>18.5</b>	<b>25.6</b>	<b>13.5</b>	<b>22.1</b>	<b>29.9</b>
Average Biocomposite Density (g/cm <sup>3</sup> )	0.9590	1.0319	1.0754	1.0232	1.0739	1.1197
St. Dev. Biocomposite Density (g/cm <sup>3</sup> )	0.0012	0.0011	0.0014	0.0013	0.0011	0.0014
Confidence Interval 95%	0.000433	0.000419	0.000506	0.000489	0.000415	0.000535
Confidence Interval 99%	0.000583	0.000565	0.000682	0.00066	0.000560	0.000721

\* Calculated by Equation 4.5

Table 4.2 Wood Pulp filled Biocomposite Densities from Square Specimens

	Wood Pulp					
	LDPE			HDPE		
Target Fiber Fraction (wt%)	15	30	45	15	30	45
Actual Fiber Fraction (wt%)	16.6	28.1	39.4	14.0	25.3	33.9
<b>Actual Manufactured (vol%)*</b>	<b>10.5</b>	<b>18.7</b>	<b>27.8</b>	<b>9.0</b>	<b>17.1</b>	<b>23.8</b>
Average Biocomposite Density (g/cm <sup>3</sup> )	0.9851	1.0373	1.0946	0.9986	1.0477	1.0885
St. Dev. Biocomposite Density (g/cm <sup>3</sup> )	0.0008	0.0011	0.0009	0.0014	0.0011	0.0011
Confidence Interval 95%	0.00028	0.00040	0.00034	0.00053	0.00042	0.00043
Confidence Interval 99%	0.00038	0.00055	0.00046	0.00071	0.00057	0.00058

\* Calculated by Equation 4.5

Frequently in the literature, the target manufactured weight fraction fiber is assumed to be the actual weight fraction fiber produced in the final product [6-14]. The merit of this common assumption was challenged as the fiber content must be validated due to the potential for inaccuracies and material loss during manufacturing. In this study, such an assumption was found to be invalid as verified by fiber fraction determination via nitrogen pycnometry. The actual manufactured weight fraction was typically less than the target weight fraction as shown in Figure 4.4. The difference in fiber content is potentially attributed to fiber mass loss and inconsistent feed rates during the manufacturing process. These results demonstrate the importance of assessing the final biocomposite product rather than the control fiber fraction mass input, as values may differ from the targets, particularly at the high fiber content.

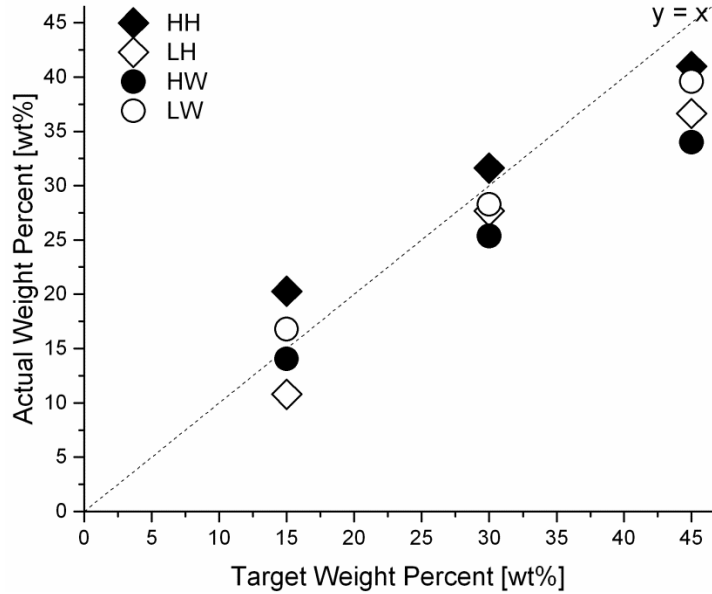


Figure 4.4 Comparison of manufactured target weight percent to actual weight percent, relative to the 1:1 relationship shown by  $y=x$ . The actual weight percent fiber frequently does not match the targeted fiber content, especially as the fiber content increases.

Throughout the work, the specimens are referred to by the intended weight fraction, low medium and high fiber content represented as 15, 30 and 45 target weight fraction respectively. A summary of the material designations are shown in Table 4.3 with the experimentally determined volume fraction of fiber in brackets, as determined by equation 4.11.

Table 4.3 Name designation for manufactured biocomposites

		Target Weight Fraction of Fibers					
		(Label Designation: polymer type, fiber type, target wt% (actual vol%))					
		Low Density Polyethylene (LDPE)			High Density Polyethylene (HDPE)		
Fiber	Hemp	LH15 (6.6)	LH30 (18.5)	LH45 (25.6)	HH15 (13.5)	HH30 (22.1)	HH45 (29.9)
	Wood Pulp	LW15 (10.5)	LW30 (18.7)	LW45 (27.8)	HW15 (9.0)	HW30 (17.1)	HW45 (23.8)

Comparison of material properties must be conducted on a manufactured volume fraction of fiber basis rather than by the targeted weight fraction due to the large distribution of fiber volume fractions at each targeted amount as shown in Figure 4.5. Relative trends within the data are relevant without the use of fiber volume fraction. However, for comparison between

fiber and matrix types or analysis of properties, fiber volume fraction is required. For materials manufactured within this study, direct comparisons are permitted between LW30, LH30 and HW30 as well as between HH30 and HW45 since these variations possess approximately the same volume fraction of fiber.

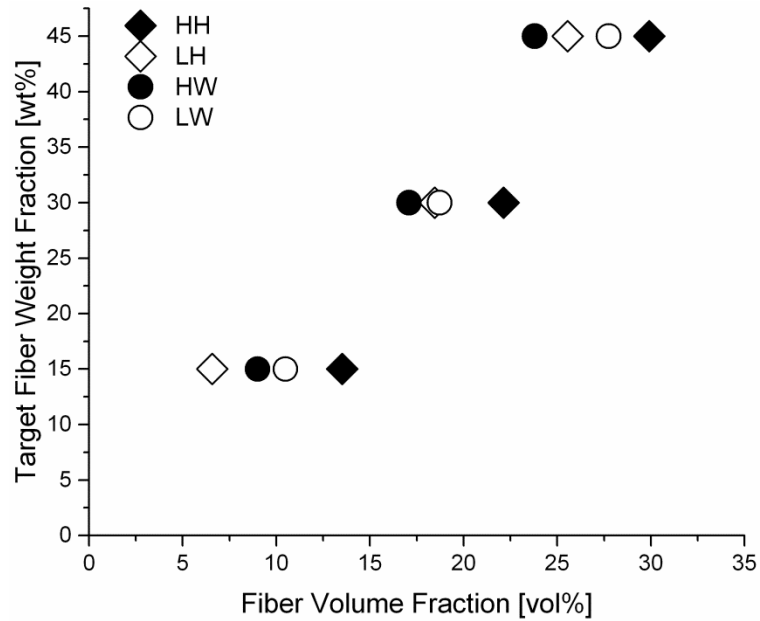


Figure 4.5 Distribution of fiber volume fraction at each targeted fiber weight fraction from manufacturing.

## 4.2 WATER ABSORPTION OF TENSILE SPECIMENS

Traditionally, water absorbed in biocomposites results in a reduction of mechanical properties [8, 15]. Before the mechanical properties are assessed, a basic understanding of the water absorption trends first must be understood. The water absorption of all material variations are presented in Figure 4.6. As commonly known from the literature, a general increase in fiber content leads to an increase of water absorbed at each time interval; what has not been observed in literature is a decrease in water absorption at very long times for certain fiber types and loading.

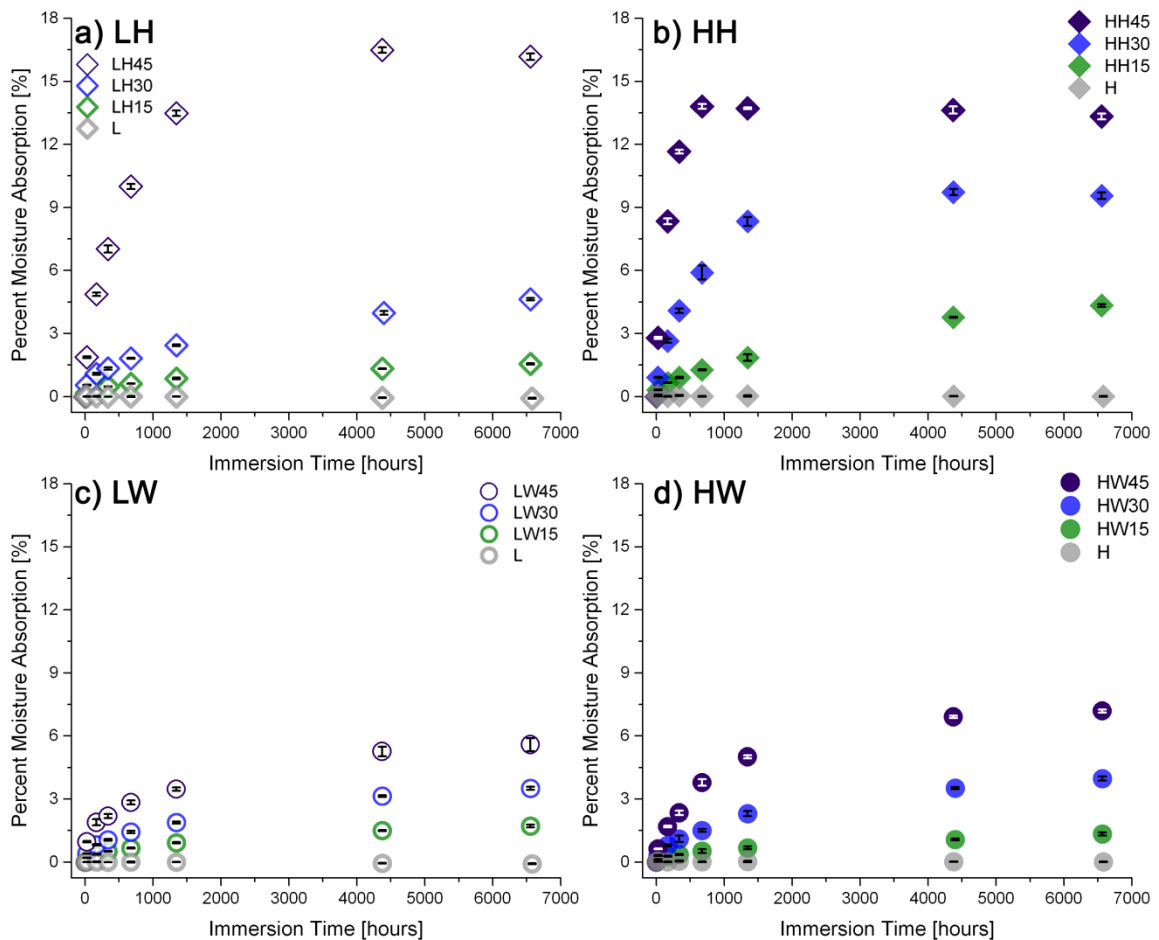


Figure 4.6 Average moisture absorption as a function of time, hemp reinforced biocomposites (diamond) and wood pulp reinforced biocomposites (circle) tensile specimens. The colors designate the relative amount of fiber content, none (control) = grey, target 15 wt% low= green, target 30 wt% medium = blue and target 45 wt% high = purple.

Hemp reinforced biocomposite variations absorbed a greater percentage of water compared to wood pulp reinforced biocomposites. Biocomposites with high hemp fiber content resulted



in a plateau of maximum water absorbed, with a subsequent small decay. Wood pulp variations absorbed similar quantities of water at comparative rates and magnitudes; the same is not true for hemp fiber reinforced variations. HH variations show a similar incremental amount for water absorption with increased immersion time and fiber content unlike LH45 which demonstrates a significant jump in quantity of water absorbed.

The final percent water absorbed (at 6,552 hours) was compared between both fiber types and matrices, relative to verified fiber volume fraction, illustrated in Figure 4.7. Biocomposites reinforced with hemp fiber have a greater ability to absorb water than those with wood pulp, especially at medium to high volume fractions where the fiber dominates the water absorption magnitude. An increase in hemp fiber volume fraction results in a linear correlation with mass gain for HDPE but not LDPE. For LDPE, the increase in percent mass gain shows a more exponential relationship with hemp fiber volume fraction and percent mass gain. However, an increase in wood pulp volume fraction has a linear correlation with mass gain in both polyethylene matrices.

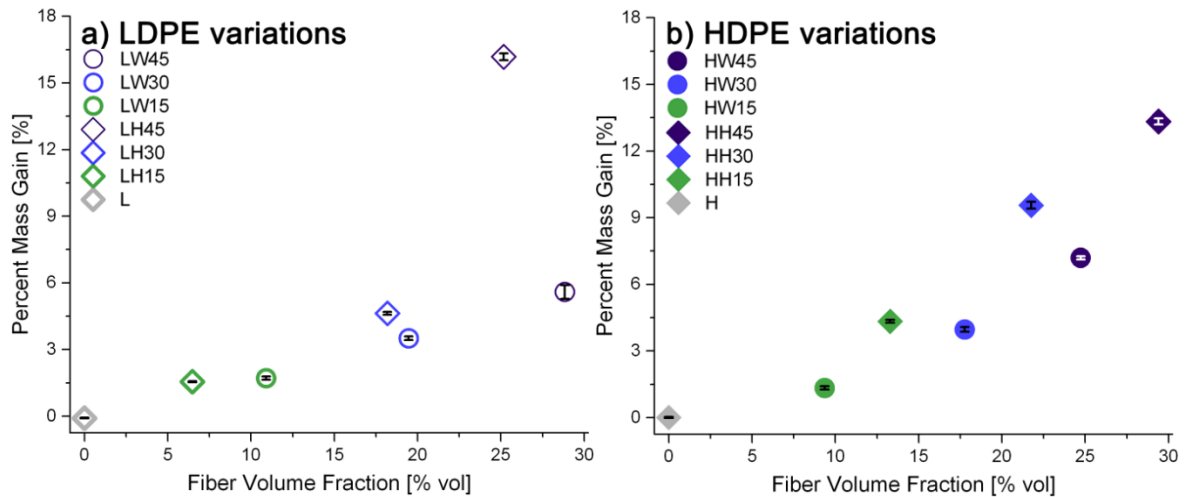


Figure 4.7 Magnitude of water absorbed after 6552 hours immersion comparison between hemp fiber (diamond) and wood pulp (circle) in a) LDPE matrix and b) HDPE matrix. The colors designate the relative amount of fiber content, none (control) = grey, target 15 wt% low= green, target 30 wt% medium = blue and target 45 wt% high = purple.

Further assessment of biocomposite water absorption characteristics along with a predictive model are detailed in Chapter 5 Phenomenon, Mechanism and Predictive Water Absorption Model in Biocomposites.

### **4.3 MECHANICAL PROPERTIES**

Water absorption in biocomposites has been demonstrated to reduce mechanical properties [8, 15]. However, few studies have investigated the change in properties over a “long” period of time (i.e. >100 hours) to characterize property loss, especially of polyethylene based biocomposites. In order to study the impact of water absorption on mechanical properties, baseline properties of the biocomposite were established. Representative tensile stress-strain curves are presented to demonstrate how each material variation performed. Properties such as tensile modulus, tensile yield strength at 2% and ultimate tensile strength are compared to establish both average mechanical properties as well as to compare those properties between matrices, fiber types and fiber content.

The work herein clearly demonstrates that the long term effects of water absorption on mechanical properties and the need to develop a predictive long term water absorption model.

#### *4.3.1 REPRESENTATIVE ENGINEERING STRESS-STRAIN CURVES*

The overall mechanical performance can be visually quantified by stress strain curves. A general representation of the engineering stress-strain data for both polyethylene types is illustrated in Figure 4.8. Overall, LDPE demonstrates lower tensile yield strength, ultimate tensile strength, modulus and ductility compared to HDPE. At the designated strain rate, none of the HDPE specimens fractured, rather all experienced cold draw necking within the gauge length. The lower properties of LDPE explicitly showcase the reinforcement properties of natural fibers.

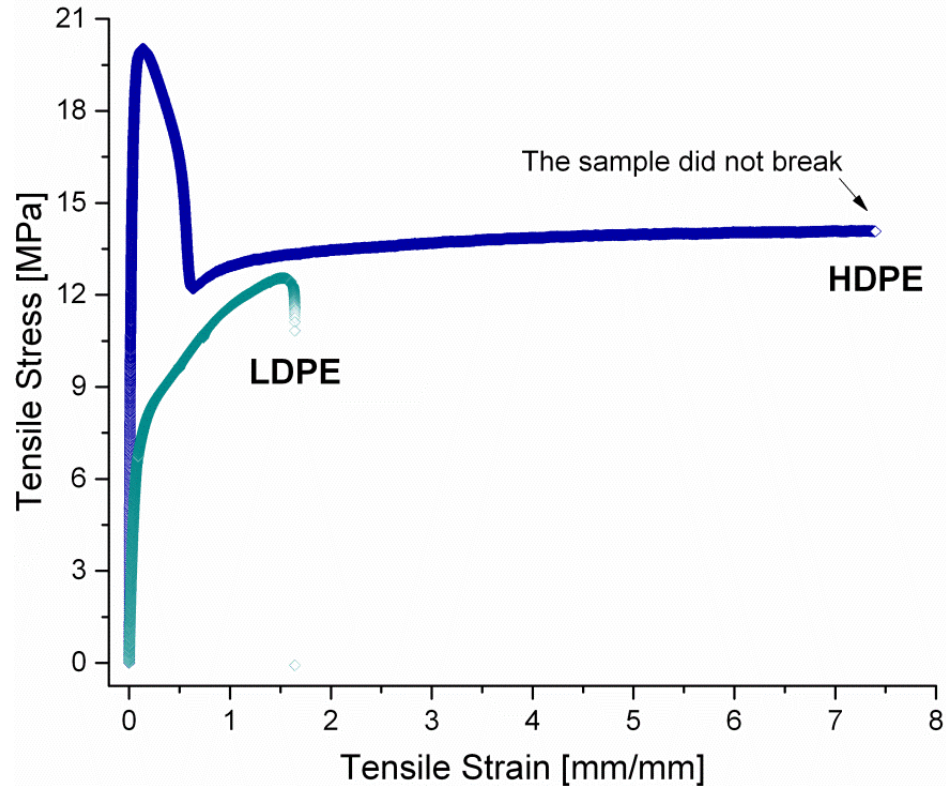


Figure 4.8 Representative stress versus strain curve for both HDPE and LDPE. HDPE demonstrates a greater tensile strength and ultimate tensile strength after which the specimen necks due to chain alignment at low strain rates where by the specimen does not break unlike LDPE which fractured.

From the representative biocomposite samples (the stress strain curves shown in Figure 4.9 and Figure 4.10), an increase in fiber content resulted in both an increase in modulus and strength. However, the addition of natural fibers also reduced the ductility of the material. At low fiber fraction, wood pulp decreased ductility more than hemp fiber. However, at higher fiber fraction where significant reinforcement was observed, hemp fiber was more detrimental to biocomposite ductility than wood pulp. Overall, LDPE reinforced with either hemp fiber or wood pulp demonstrate greater ductility than HDPE variations; opposite of the properties without fiber reinforcement (as can be seen in Figure 4.8). The matrix deformation mode should be considered when selecting a biocomposite for an application.

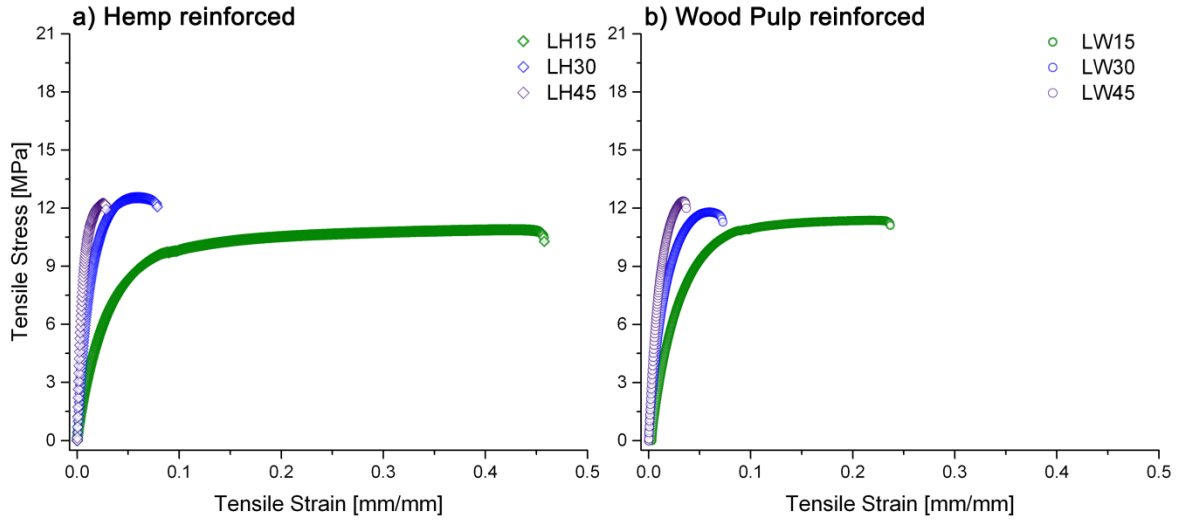


Figure 4.9 Representative engineering stress versus strain curves for low density polyethylene biocomposites a) hemp fiber and b) wood pulp reinforced. Increase in fiber content leads to an increase in tensile modulus and strength at the expense of loss of ductility.

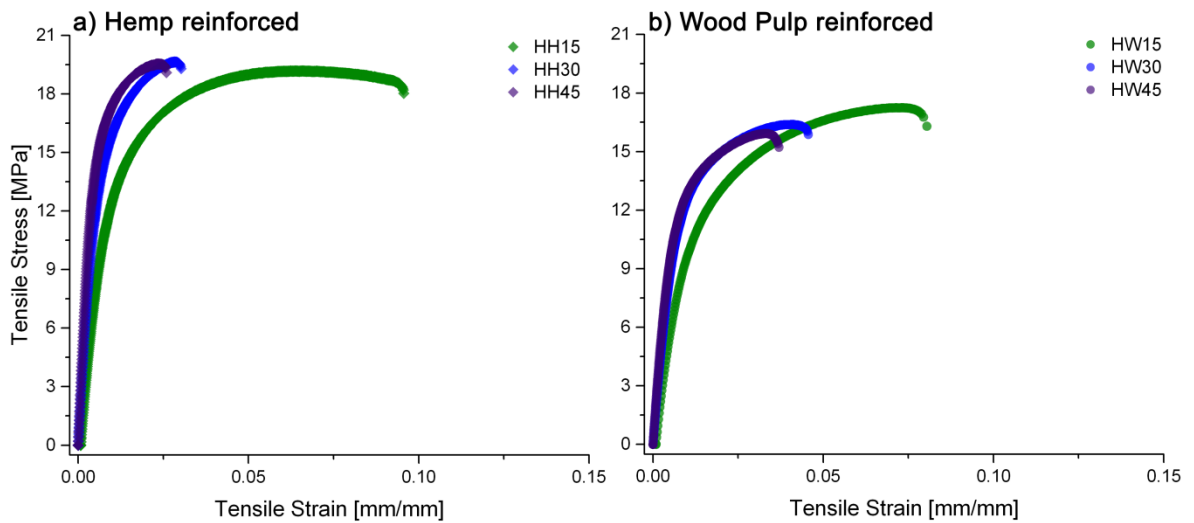


Figure 4.10 Representative engineering stress versus strain curves for high density polyethylene biocomposites a) hemp fiber and b) wood pulp reinforced. The change in fiber content from low to medium results in an increase in elastic modulus but with a decrease in ductility.

The overall ductility was compromised with the addition of natural fibers, most significantly observed for HDPE variations. Although general comparisons can be made with stress strain curves, all quantifiable comparisons of properties shall be assessed with respect to volume fraction of fiber.

### 4.3.2 MODULUS

An increase in fiber volume fraction resulted in an increase in modulus for all LDPE and HDPE biocomposite variations as illustrated in Figure 4.11. Incremental increases in wood pulp resulted in a proportional increase in elastic modulus, whereas, the addition of hemp fiber had an exponential effect on the modulus. Overall hemp fiber types contributed to a greater increase in biocomposite elastic modulus due to higher fiber elastic modulus than wood pulp. For all material volume fractions, the fibers' elastic modulus dominated the interaction between fiber and matrix by synergistically adding to the overall composite properties. The addition of natural fiber reinforcement had a greater effect in the matrix with a lower elastic modulus due to the difference in individual properties. This phenomenon was demonstrated even more pronouncedly in yield strength and ultimate strength.

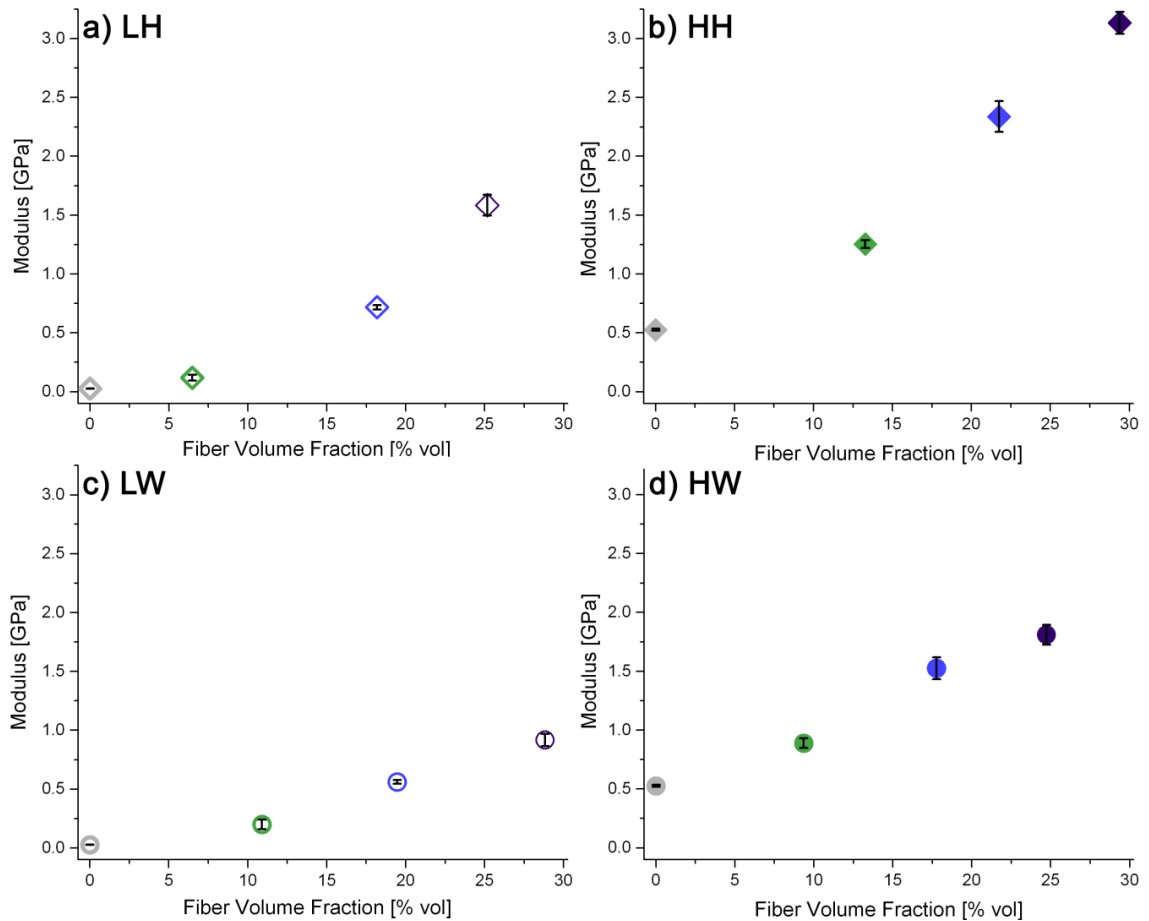


Figure 4.11 Tensile Modulus as a function of fiber volume fraction for LDPE (unfilled symbols) and HDPE (filled symbols). Increase fiber content translates into an increase in tensile modulus. The colors designate the relative amount of fiber content as reported.

### 4.3.2.1 Impact of Water Absorption on Modulus

Normalized tensile modulus demonstrates an exponential decay as a function of immersion time as illustrated in Figure 4.12. The extent of the decay is dependent on fiber type and fiber fraction. Hemp fiber in both LDPE and HDPE experienced a minimum normalized modulus at approximately 22% even though the two variations differ by 4 vol % of fiber. Wood pulp reinforced variations did not demonstrate a uniform minimum rather continued to experience a loss in modulus even after 6552 hours.

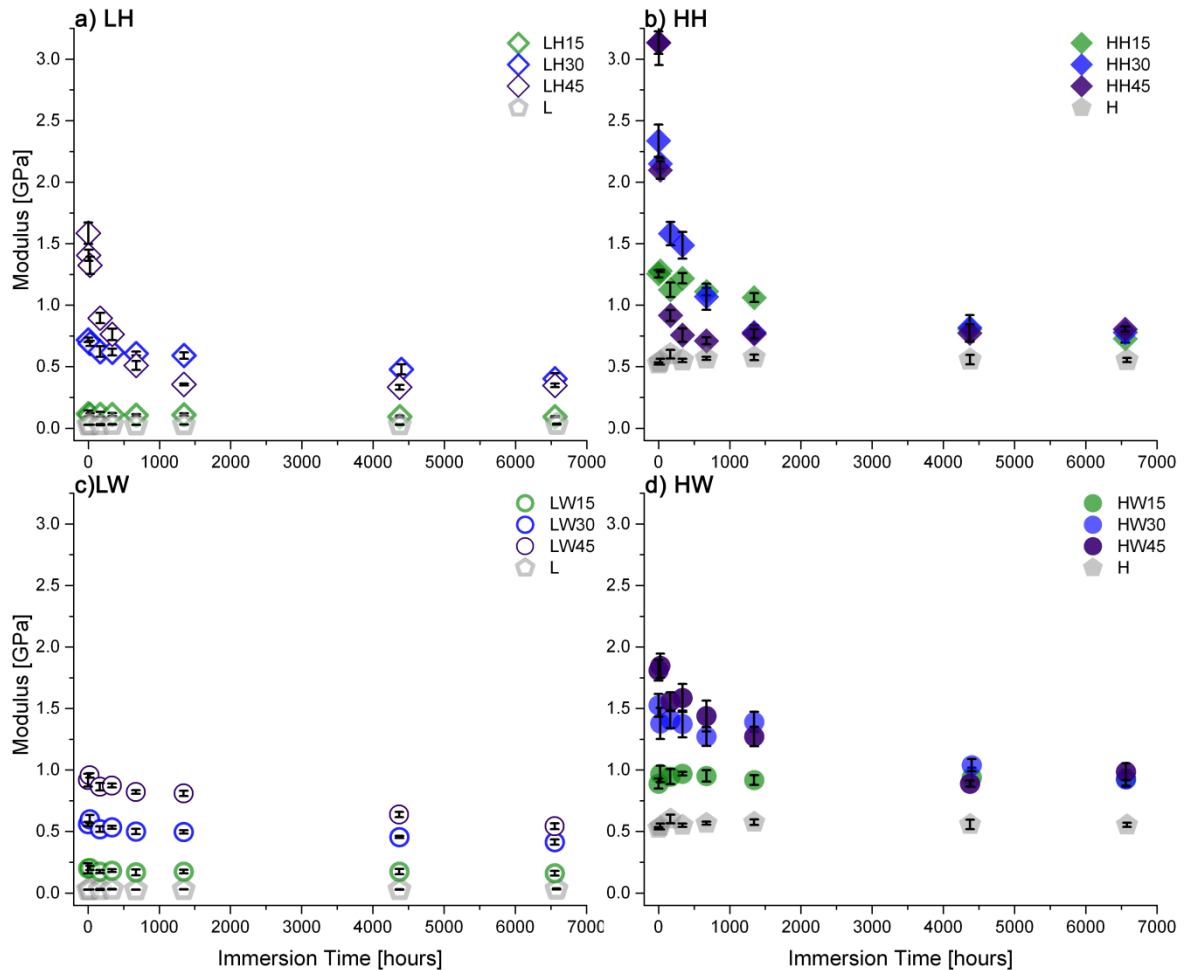


Figure 4.12 Tensile modulus as a function of water immersion time for all material variations. Observed continued decline after 168 hours immersion in modulus. The colors designate the relative amount of fiber content, none (control) = grey, target 15 wt% low= green, target 30 wt% medium = blue and target 45 wt% high = purple.

The longer a material was immersed in water the more water became absorbed within its structure as illustrated in Figure 4.6. Modulus of LDPE and HDPE did not change with increased immersion time, and neither matrix absorbed quantifiable amounts of water seen

in Figure 4.6 and Figure 4.13. The mass gain was attributed to water absorbed by the natural fiber which negatively impacted the fibers ability to resist load [12].

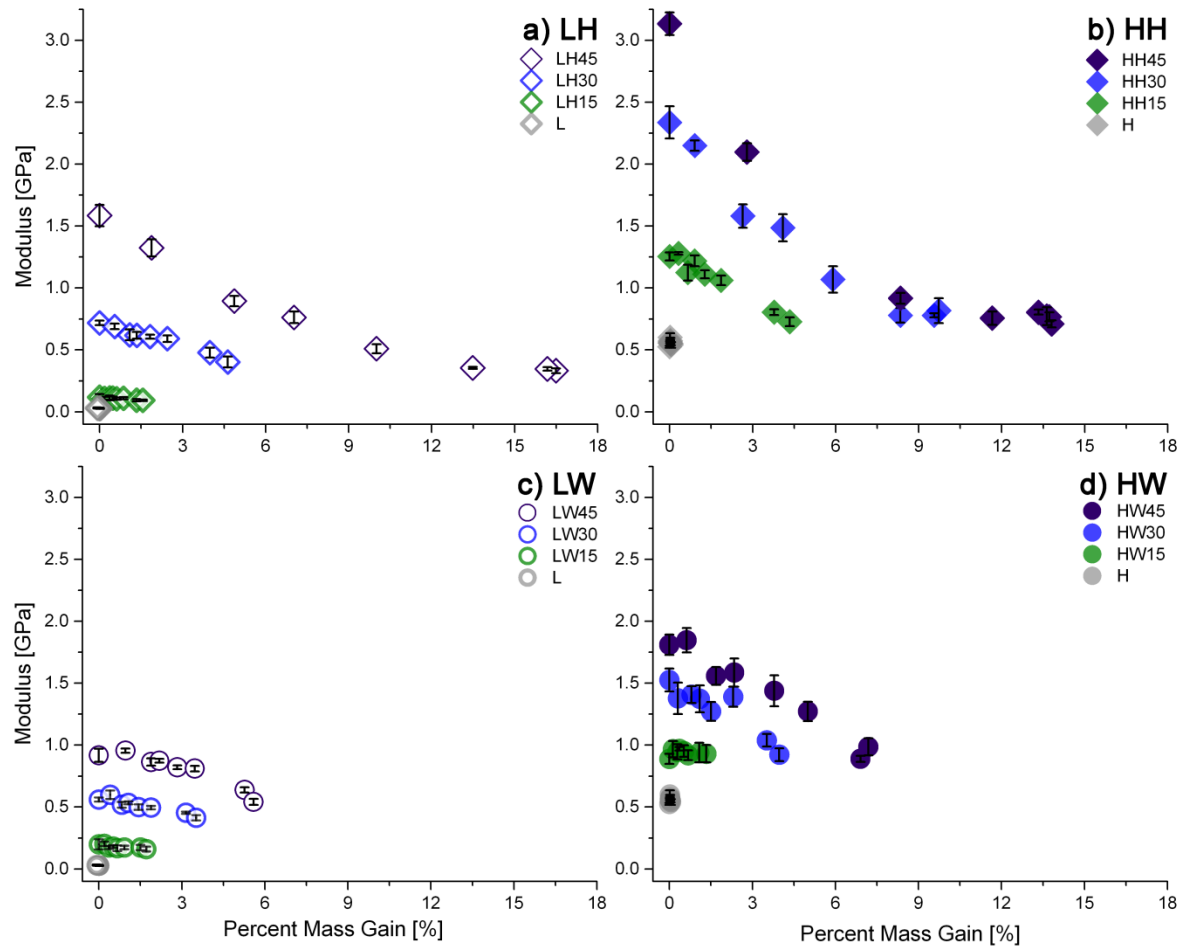


Figure 4.13 Tensile modulus versus absorbed water for all material variations. Increased mass gain led to decreased modulus, to varying degrees, in all biocomposite formulations. The colors designate the relative amount of fiber content, none (control) = grey, target 15 wt% low= green, target 30 wt% medium = blue and target 45 wt% high = purple.

For all durations of water immersion, the biocomposites variations demonstrated a greater modulus than the virgin matrix material. Therefore, even though the biocomposite has absorbed water, the natural fibers contribute to a greater specimen modulus compared to the virgin material. The effect of fiber contribution is more evident in LDPE matrix, since HDPE possess higher modulus than LDPE.

All biocomposite material variations experienced a near linear decrease in modulus with an increase in water absorbed with the exception of HH45 and LH45 which experience plateaus after 12% water absorbed, as illustrated in Figure 4.13. Hemp fiber in both LDPE and HDPE experienced a minimum normalized modulus at approximately 22% even though the

two variations differ by 4 vol % of fiber. Wood pulp reinforced variations did not demonstrate a uniform minimum rather continued to experience a loss in modulus with increased absorbed water. The magnitude in the change of modulus was correlated with the fiber content of the material variations. Hemp fiber reinforced biocomposites showed a greater change in tensile modulus than wood pulp reinforced specimens in Figure 4.13. The hemp fiber reinforced HDPE biocomposites (HH) experienced the greatest change in modulus with water absorption.

#### 4.3.2.2 Normalized Modulus

A universal correlation has been discovered between the change in normalized modulus, calculated by equation 3.7, relative to the percentage of water absorbed independent of matrix type and fiber type at all volume fractions. The exponential decay for normalized tensile modulus and percent mass gain is illustrated in Figure 4.14 with the mathematical equation to model the behaviour provided in Equation 4.8. Regression analysis yielded an R<sup>2</sup> equal to 0.96.

$$\% \text{ Normalized Tensile Modulus} = 100e^{-0.1048 * \text{Percent Mass Gain}} \quad (4.12)$$

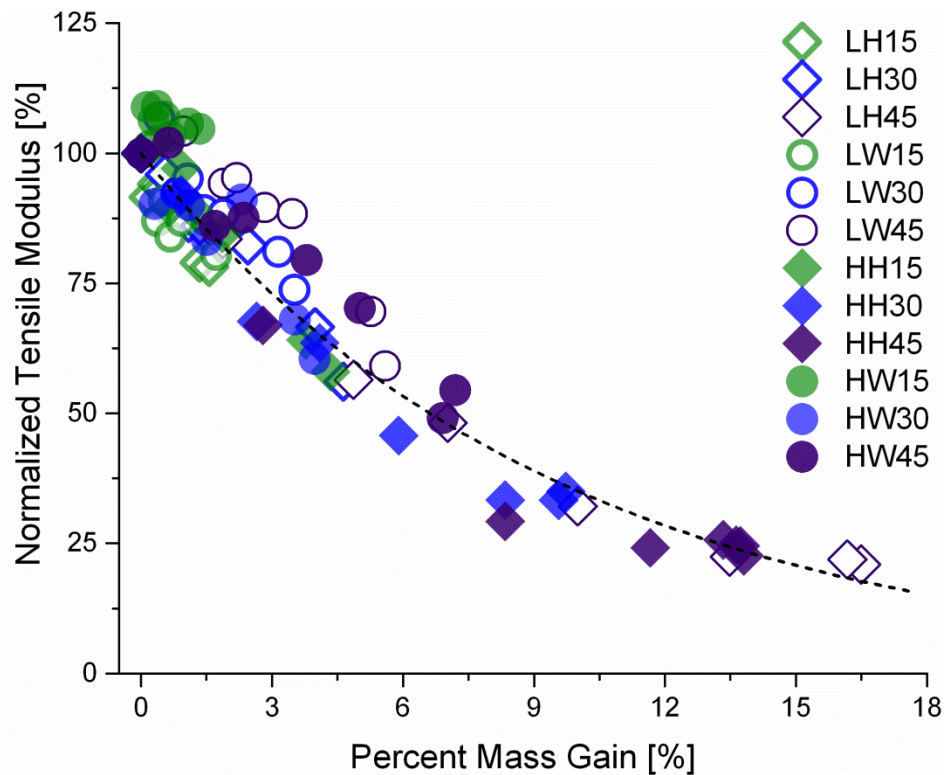


Figure 4.14 Exponential decay, Equation 4.8 (dashed line), of normalized tensile modulus and percent mass gain of water for all biocomposite variations



A limit is observed at approximately 23% normalized tensile modulus in Figure 4.14. This limit is evidence that there is a limit to the extent of degradation of mechanical modulus of natural fibers. At this limit, the moduli of the biocomposite variations are still greater than the virgin polymer modulus/biocomposite dry modulus. Properties of the biocomposite greater than the virgin material provides evidence that even with absorbed water, the natural fibers provide some level of reinforcement to the polymer for both HDPE and LDPE.

Another limit of maximum degradation of modulus is observed for HH30 (blue filled diamond) at approximately 33% tensile modulus in Figure 4.14. Although the limits are similar, they are not identical because the proportion of natural fibers within the biocomposite which experience water absorption is lower for HH30 than HH45. It is only the proportion of natural fibers exposed to water which degrade. It is proposed that the maximum degradation observed for modulus is fiber content dependent since the extent of the fibers accessible to water is a function of fiber content, for further explanation reference section 5.1.1.

Further research is required into the degradation of short natural fiber mechanical properties in an immersion environment for biocomposite applications.

#### 4.3.2.3 Back Calculated Fiber Modulus

The back calculated (or “in-situ”) fiber modulus was calculated to determine the effect of water exposure on the intrinsic fiber properties over time. This in-situ property was calculated using the “Rule of Mixtures” as described in equations 4.13 to 4.15.

$$E_c = E_f V_f + E_m V_m \quad (4.13)$$

Substitute Equation 4.3 for  $V_m$

$$E_c = E_f V_f + E_m (1 - V_f) \quad (4.14)$$

Rearrange equation 4.14 to solve for fiber modulus,  $E_f$ .

$$E_f = \frac{E_c - E_m}{V_f} + E_m \quad (4.15)$$

The back calculated fiber modulus for all material variations is shown in Figure 4.15 for both dry (0 hours) and water immersion (6552 hours) conditions. The back calculated fiber modulus was found to be affected by the matrix type, as there was a smaller change observed in the hemp and wood pulp modulus for LDPE compared to HDPE. Hemp demonstrates a

greater fiber modulus than wood pulp in HDPE at each given fiber content. Uniform fiber modulus was not observed for LH and HH material variations, as an increase in fiber modulus was seen with increased fiber content. Therefore it is likely that fiber molding orientation impacts the in situ fiber modulus. As more fiber content is added the more aligned the fibers become in the mold. For wood pulp in a dry state a relatively uniform fiber modulus was observed.

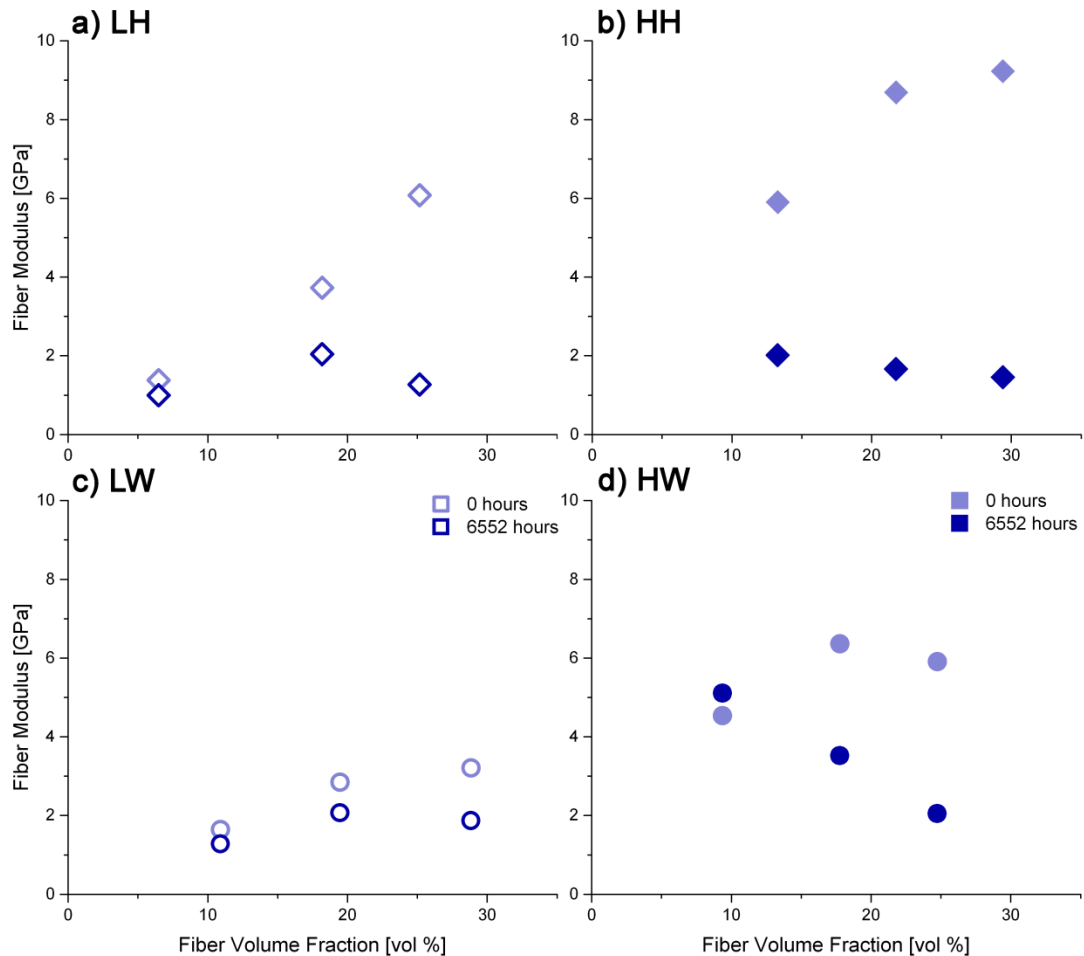


Figure 4.15 The average load carrying capability of the natural fibers by volume fraction of fiber at time 0 (light blue) and after 6552 hours (dark blue) for all material variations. For all variations except HW15, exposure time in an immersion environment resulted in a decrease in in situ fiber modulus.

For high fiber contents, the in situ fiber modulus after exposure to water was distinctly lower than the dry condition. Hemp fiber experienced a greater drop in fiber modulus than wood pulp.

### 4.3.3 YIELD STRENGTH

The addition of natural fiber resulted in a slight increase in properties for all biocomposite variations except for wood pulp reinforced HDPE (HW), as shown in Figure 4.16. The reinforcement effect of natural fibers was more predominant in LDPE due to the LDPE's lower tensile yield strength. However, additional strength provided from the natural fiber plateaus at a specific volume fraction of fiber for both hemp and wood pulp fiber types. For hemp fiber, the maximum reinforcement effect was experienced at fiber loading fraction of 18 vol% in LDPE and 20 vol% in HDPE. With respect to wood pulp in HDPE, the addition of fiber did not change the tensile yield strength at any given fiber volume fraction. Therefore the tensile yield strength of wood pulp is approximately equal to tensile yield strength of HDPE.

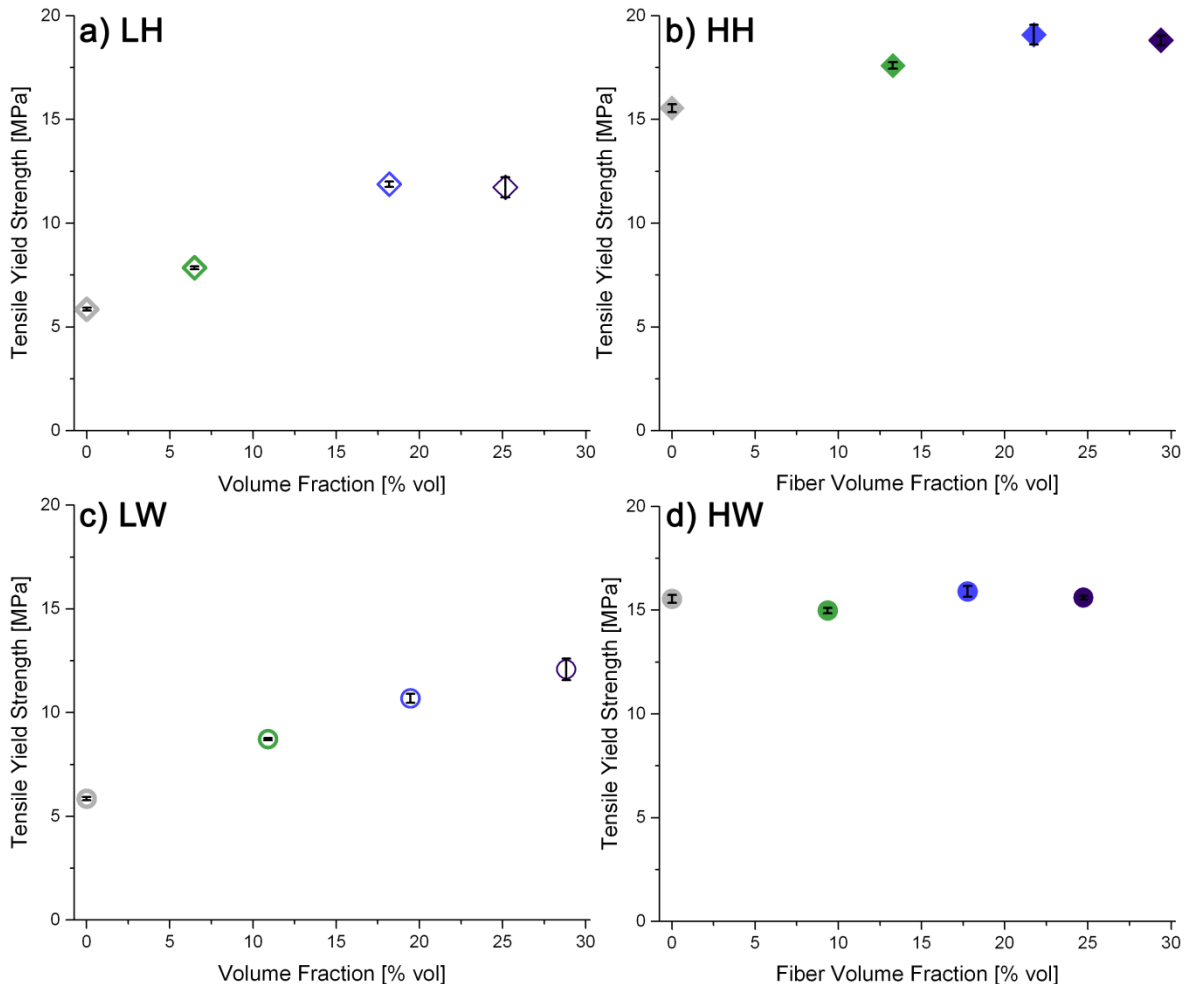


Figure 4.16 Tensile yield strength as a function of fiber volume fraction for LDPE (unfilled symbols) and HDPE (filled symbols). Natural fibers provide additional strength to the biocomposite for all variations except wood pulp reinforced in high density polyethylene, HW.

### 4.3.3.1 Impact of Water Absorption on Yield Strength

All material variations, except HW15, experienced an exponential decay with increased immersion time as shown in Figure 4.17. The greater the fiber content the more severe the loss in normalized tensile yield strength was observed. Not only was the loss in property more severe with increase fiber content but also the rate of decline. For example, HH45 and HH30 after 6552 hours approximately lost the same relative magnitude in tensile yield strength however the higher content biocomposite, HH45 took a reduced amount of time to reach its minimum.

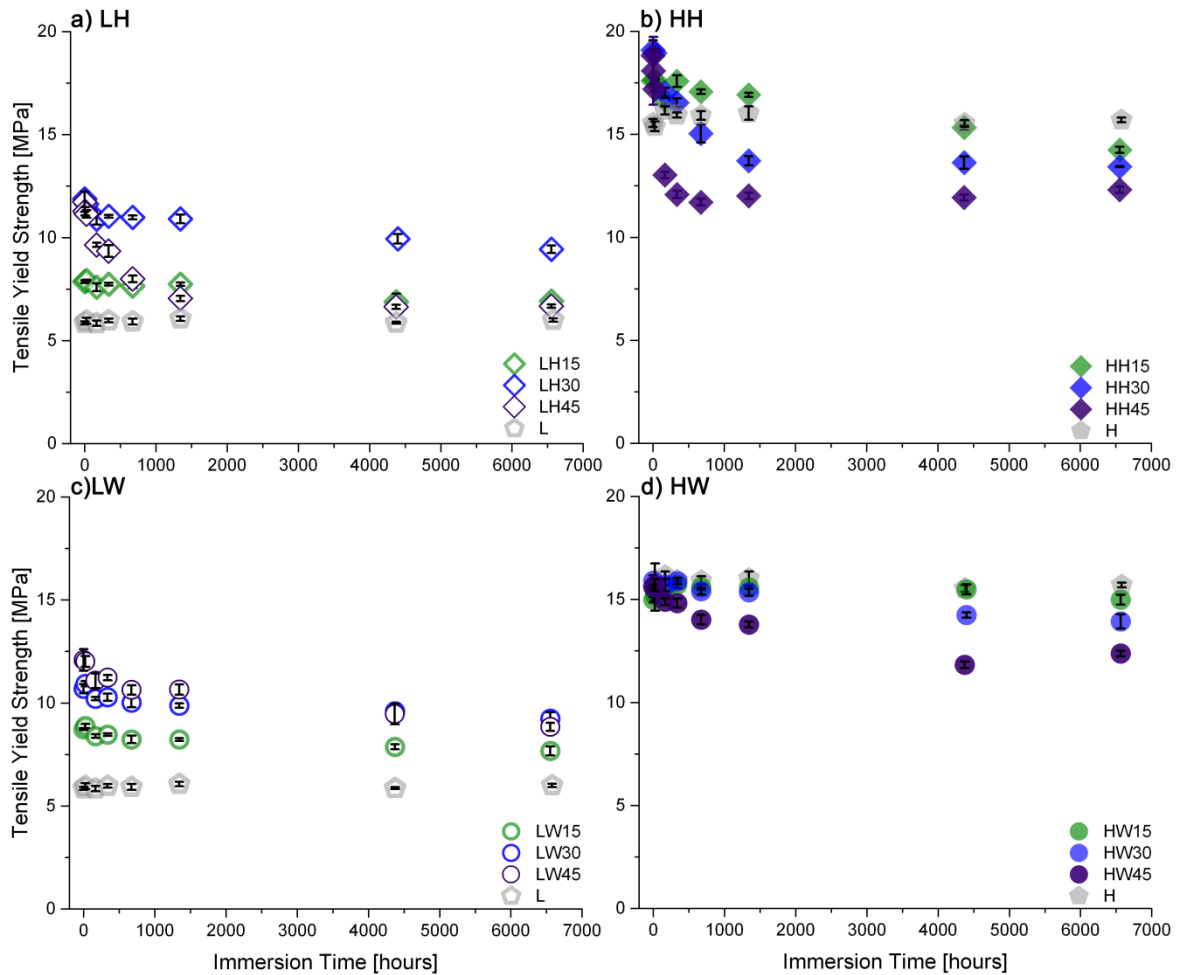


Figure 4.17 Yield strength as a function of water immersion time for all material variations. Tensile yield strength declines with immersion time.

A linear universal correlation has been discovered between the change in yield tensile strength relative to the percentage of water absorbed. For all biocomposite variations, an increase in water absorbed resulted in degradation of tensile yield strength. The more the

natural fiber contributed to the tensile yield strength, the more drastic the effect absorbed water degraded the strength. Therefore, the magnitude of decrease in yield strength is related to the loss of fiber yield strength caused from water absorption (amount of moisture absorbed and the volume fraction of fibers). Water absorption is linearly related to mechanical property degradation. For LDPE, the tensile yield strength doesn't degrade below the virgin polymer for both wood pulp and hemp fiber. However, for HDPE variations, the biocomposite tensile yield strength decreases below virgin polymer HDPE with a minimal amount of water absorbed. This trend is attributed to the initial minor contribution of natural fibers to overall biocomposite strength.

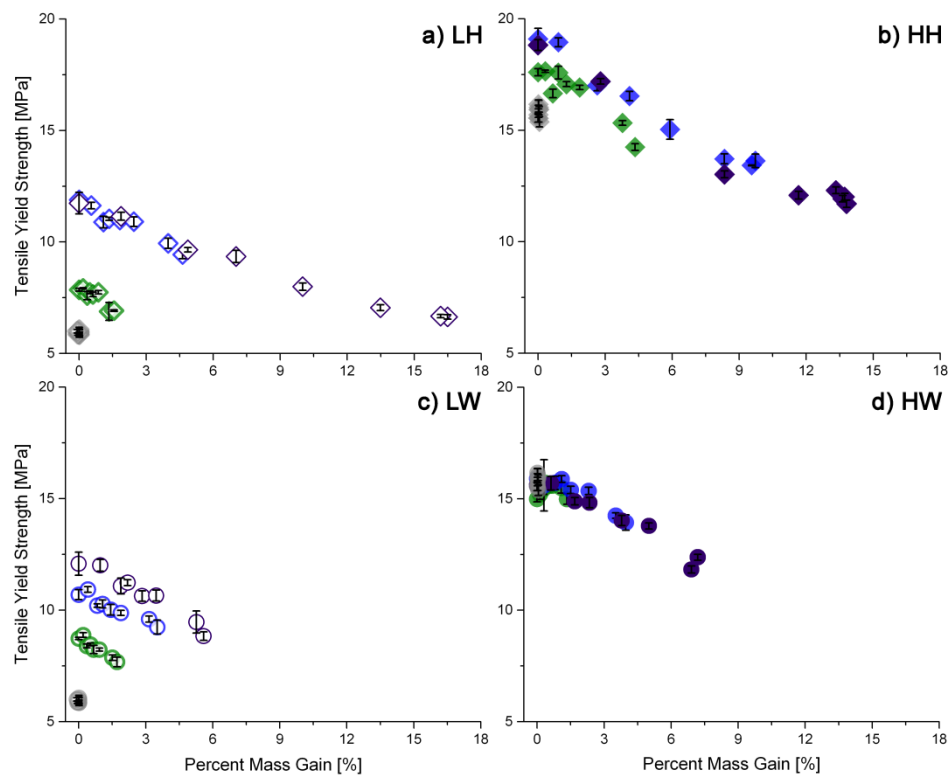


Figure 4.18 Tensile yield strength versus percent water absorbed for all material variations. Tensile yield strength decreases as the percent mass gain of water increases. The colors designate the relative amount of fiber content, none (control) = grey, target 15 wt% low= green, target 30 wt% medium = blue and target 45 wt% high = purple.

### 4.3.3.2 Normalized Yield Strength

To assess the relative change in tensile yield strength due to water absorption the normalized tensile yield strength were calculated by equation 3.7, and graphically represented in Figure 4.19. The degradation of each biocomposite variation collapses onto a linear relationship defined in Equation 4.9. Therefore, no matter the fiber content the properties change linearly with exposure to water immersion compared to its original state.

$$\% \text{ Normalized Tensile Yield Strength} = 100 - \text{Percent Mass Gain} * 3.06 (\pm 0.04) \quad (4.16)$$

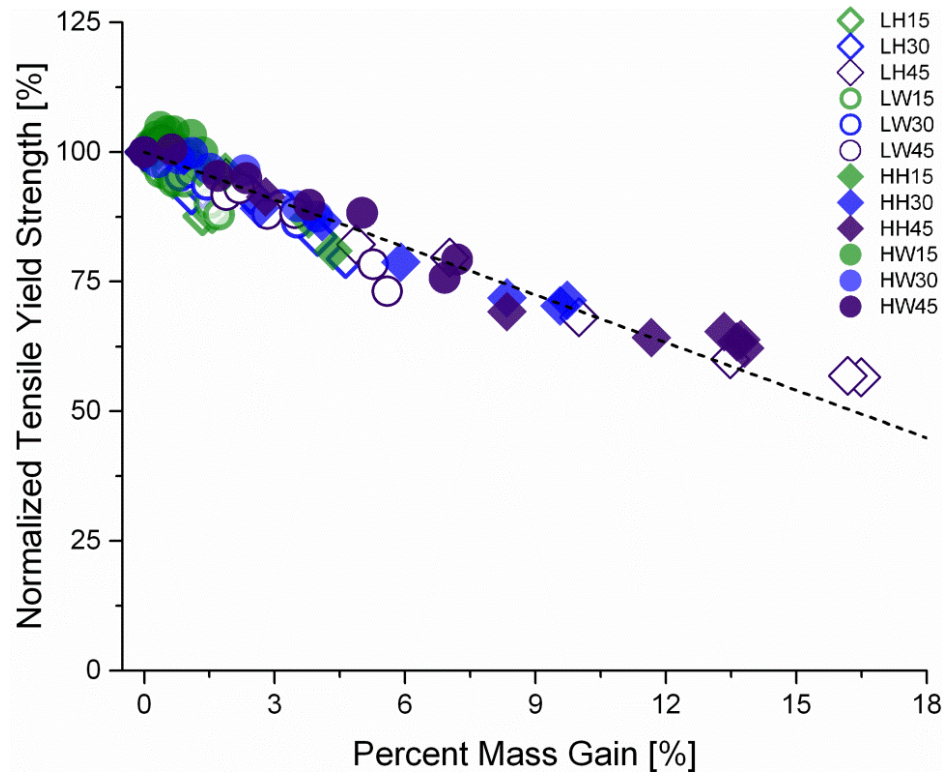


Figure 4.19 Linear relationship, Equation 4.9 (dashed line), of normalized tensile yield strength and percent mass gain of water for all biocomposite variations. The colors designate the relative amount of fiber content, none (control) = grey, target 15 wt% low= green, target 30 wt% medium = blue and target 45 wt% high = purple.

#### 4.3.4 ULTIMATE TENSILE STRENGTH

The addition of natural fibers did not contribute to an increase in biocomposite ultimate tensile strength (UTS), as seen in Figure 4.20. In some cases, HW variation, the addition of natural fibers decreased the biocomposites' ultimate tensile strength. The lack of additive reinforcement may be due to a poor interface to transfer the load from the matrix to the fiber or decreased fiber in situ properties due to fiber orientation, distribution and dispersion.

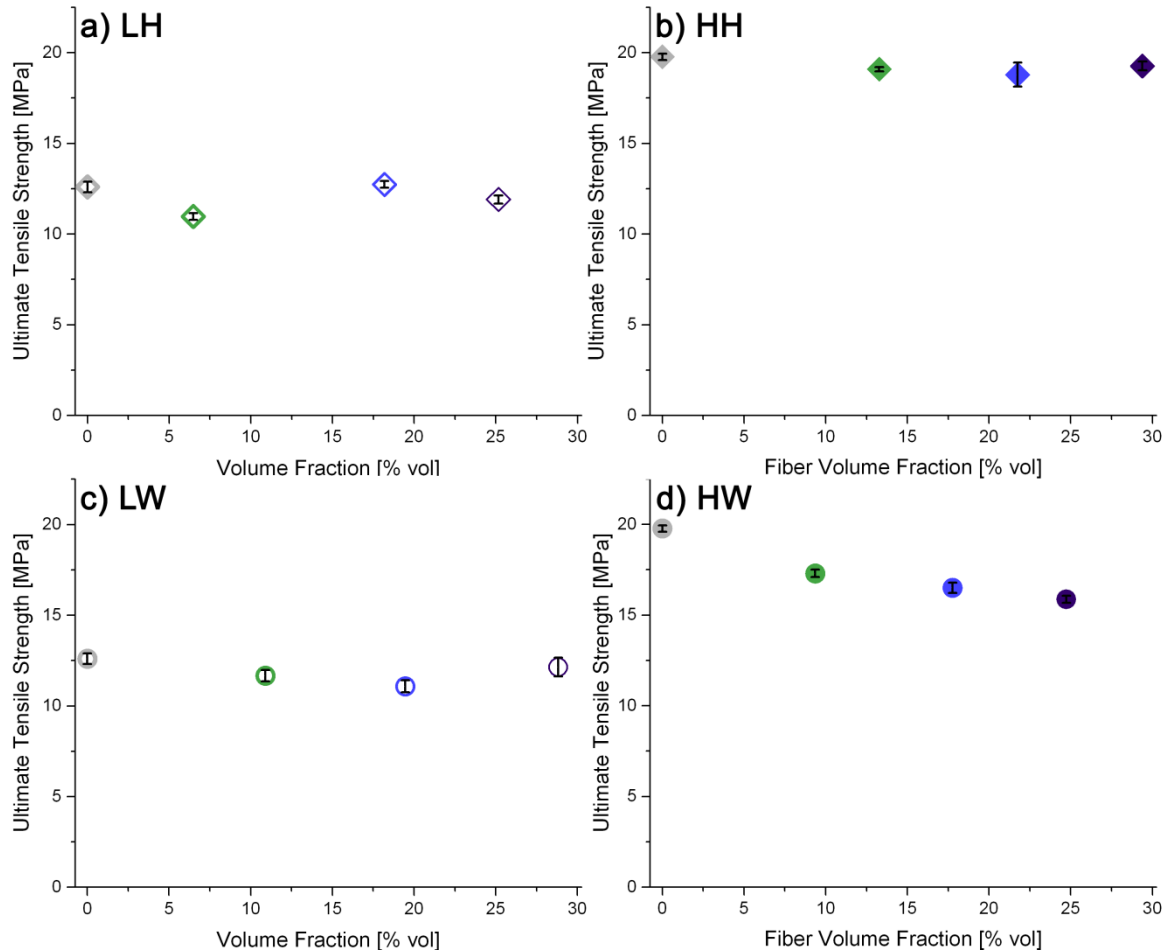


Figure 4.20 Ultimate tensile strength as a function of fiber volume fraction for LDPE (unfilled symbols) and HDPE (filled symbols). No increase observed in UTS with the addition of natural fibers. The colors designate the relative amount of fiber content, none (control) = grey, target 15 wt% low= green, target 30 wt% medium = blue and target 45 wt% high = purple.

##### 4.3.4.1 Impact of Water Absorption on Ultimate Tensile Strength

Hemp fiber reinforced biocomposites compared to wood pulp reinforced biocomposites experienced a greater decline in both ultimate tensile strength and yield strength with immersion time. The effect of immersion time on ultimate tensile strength was dependent on

both matrix and fiber content as shown in Figure 4.21. LW variations barely experienced a decline, and an increase in ultimate tensile strength was observed for LW30. For LDPE variations, only the highest fiber contents demonstrated a loss in ultimate tensile strength. A decline in ultimate tensile strength was observed for all HDPE variations with the exception of HW15. The greatest decrease in UTS was observed for the highest fiber fraction for both hemp fiber and wood pulp.

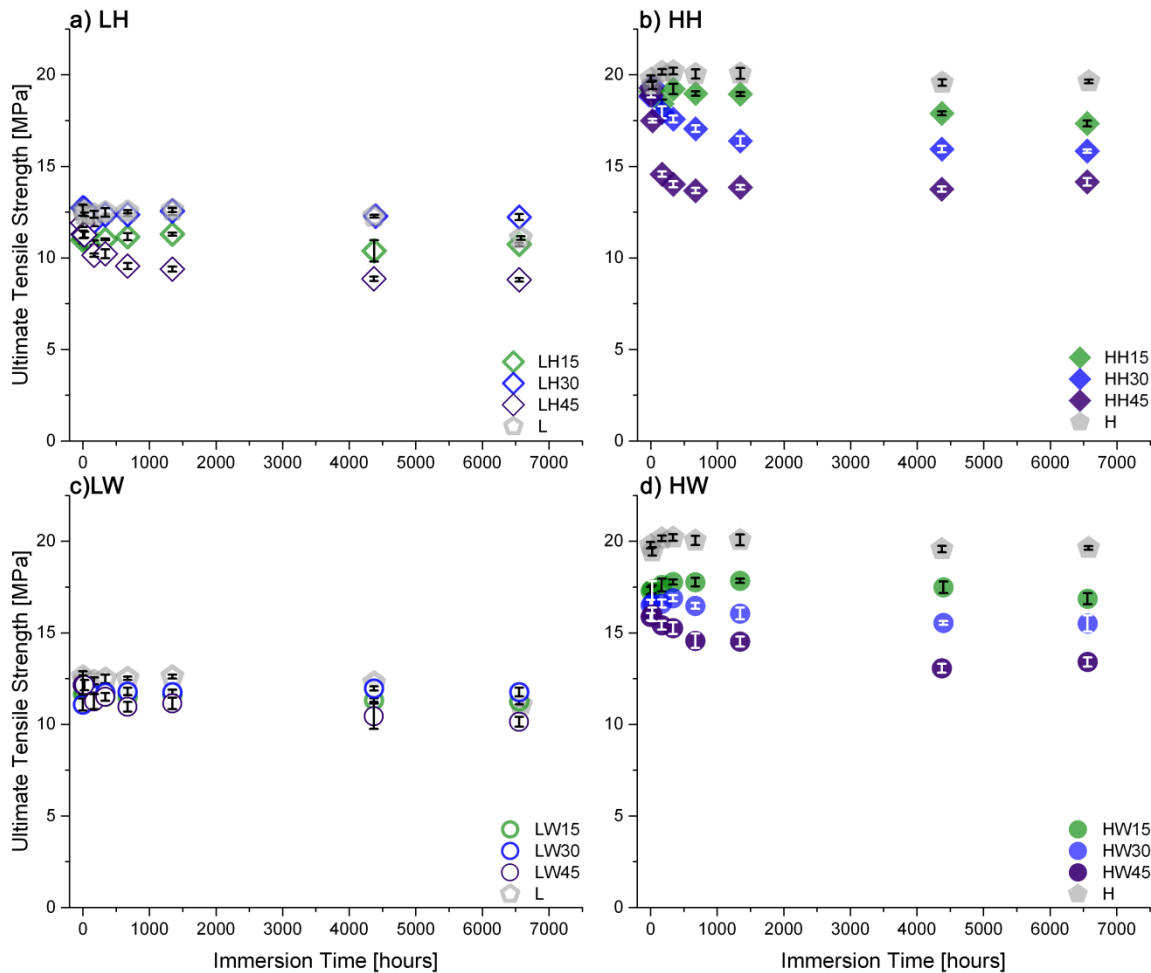


Figure 4.21 Ultimate tensile strength as a function of water immersion time for all material variations. Continued decline of ultimate tensile strength after 168 hours immersed. The colors designate the relative amount of fiber content, none (control) = grey, target 15 wt% low= green, target 30 wt% medium = blue and target 45 wt% high = purple.

The virgin matrix materials, LDPE and HDPE, do not absorb water and therefore the duration of immersion does not impact ultimate tensile strength. The extent of biocomposite property degradation approximates the contribution from only the matrix since the matrix's properties do not degrade with exposure to an immersion environment. Both virgin materials



demonstrate superior ultimate tensile strength (UTS) properties compared to their respective reinforced biocomposites. Since HDPE possess a greater ultimate tensile strength than LDPE, the magnitude of property loss with water absorbed in the natural fibers was greater for these specimens, as seen in Figure 4.22. The decline in UTS has been attributed to both inferior properties of the natural fiber, as well as a decrease in the natural fibers ultimate tensile strength due to absorbed water.

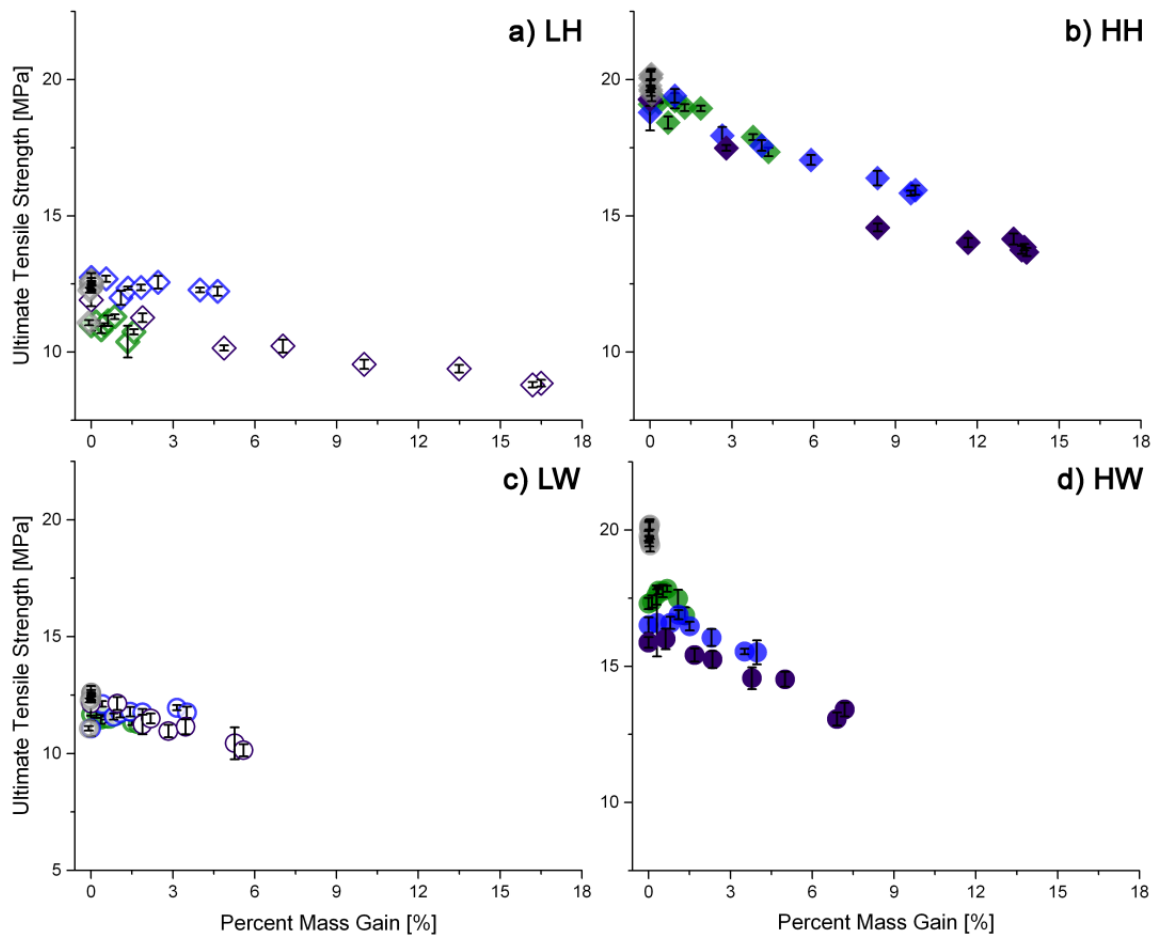


Figure 4.22 Ultimate tensile strength versus percent water absorbed for all material variations a) hemp reinforced LDPE, b) hemp reinforced HDPE, c) wood pulp reinforced LDPE and d) wood pulp reinforced HDPE. Ultimate tensile strength decreases as the percent mass gain of water increases to a greater extent for HDPE based biocomposites than LDPE based. The colors designate the relative amount of fiber content, none (control) = grey, target 15 wt% low= green, target 30 wt% medium = blue and target 45 wt% high = purple.

For LH45 and HH45, the reinforcement contributions from the natural fiber to the biocomposites' ultimate tensile strength are lost after long immersion. The loss additional strength provides evidence that the water absorbed has impacted the majority of natural fibers present within the biocomposite. For HW variations the materials properties are so

much less than the contribution of the matrix only, therefore the addition of natural fibers actually hinders the polymers ability to withstand load, therefore the areas of fiber inclusion act as stress concentrators and therefore decrease the ultimate tensile strength to values significantly less than the matrix material.

#### 4.3.4.2 Normalized Ultimate Tensile Strength

With respect to UTS, fiber had a negligible impact on additional strength since the virgin polymer demonstrated greater properties. Therefore, the impact of water absorption of the fiber is less prevalent than tensile strength and modulus since the matrix material was the predominant contributor. Although the magnitude of degradation is dependent on the magnitude of the virgin materials strength, the normalized decrease in properties is proportional as seen in Figure 4.23. The normalized UTS was calculated by equation 3.7.

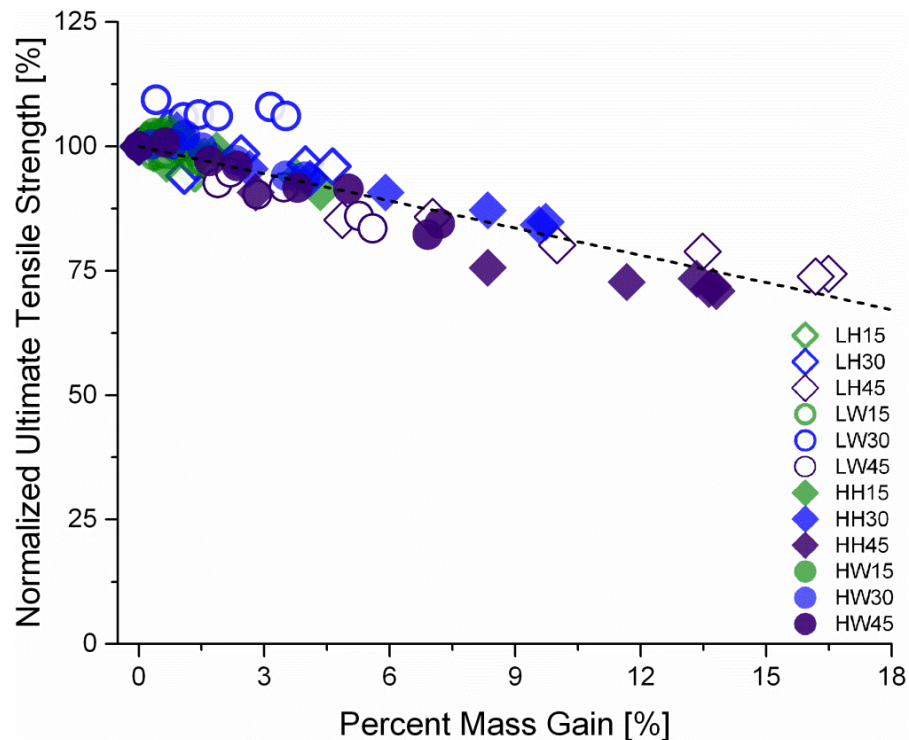


Figure 4.23 Linear relationship, Equation 4.10 (dashed line), of normalized ultimate tensile strength and percent mass gain of water for all biocomposite variations. The colors designate the relative amount of fiber content, none (control) = grey, target 15 wt% low= green, target 30 wt% medium = blue and target 45 wt% high = purple.

The normalized ultimate tensile strength for each biocomposite collapses onto a generic linear correlation of degradation, Equation 4.10. The equation models how the proportional properties degrade with water absorption to a 95% confidence interval.

$$\% \text{ Normalized UTS} = 100 - \text{Percent Mass Gain} * 1.82 (\pm 0.08) \quad (4.17)$$

#### 4.3.5 *ELONGATION AT BREAK & TOUGHNESS*<sup>3</sup>

Elongation at break and toughness are indicative of a materials capability to resist change in shape without crack formation measured by relative change in dimensions, and total energy absorbed up to failure, respectively [16]. Both factors are indicators for either a ductile or brittle dominated fracture mode. Elongation at break was measured directly from the stress-strain responses while toughness (or strain energy) was defined as the area under the stress-strain curve.

For all biocomposite variations an increase in fiber volume fraction resulted in a decrease in both elongation at break. Figure 4.24, and toughness, Figure 4.25. Virgin HDPE did not fracture at the selected stain rate within the load frame extension unlike LDPE which eventually failed in a ductile manner, see section 4.5.3 fracture morphology. The drastic change from virgin polymer to fiber reinforced biocomposite filled fractions for both elongation at break and toughness demonstrate that the addition of natural fiber caused the material to transition from a ductile failure mode to brittle failure mode with natural fibers present. The effect of natural fiber on both elongation at break and toughness is more pronounced for HDPE than LDPE.

---

<sup>3</sup> Toughness values were assessed from the area under the stress strain curve, which is not typically the test method utilized to report toughness. Therefore, the results are a general representation of how toughness changes with increased fiber volume fraction and immersion time.

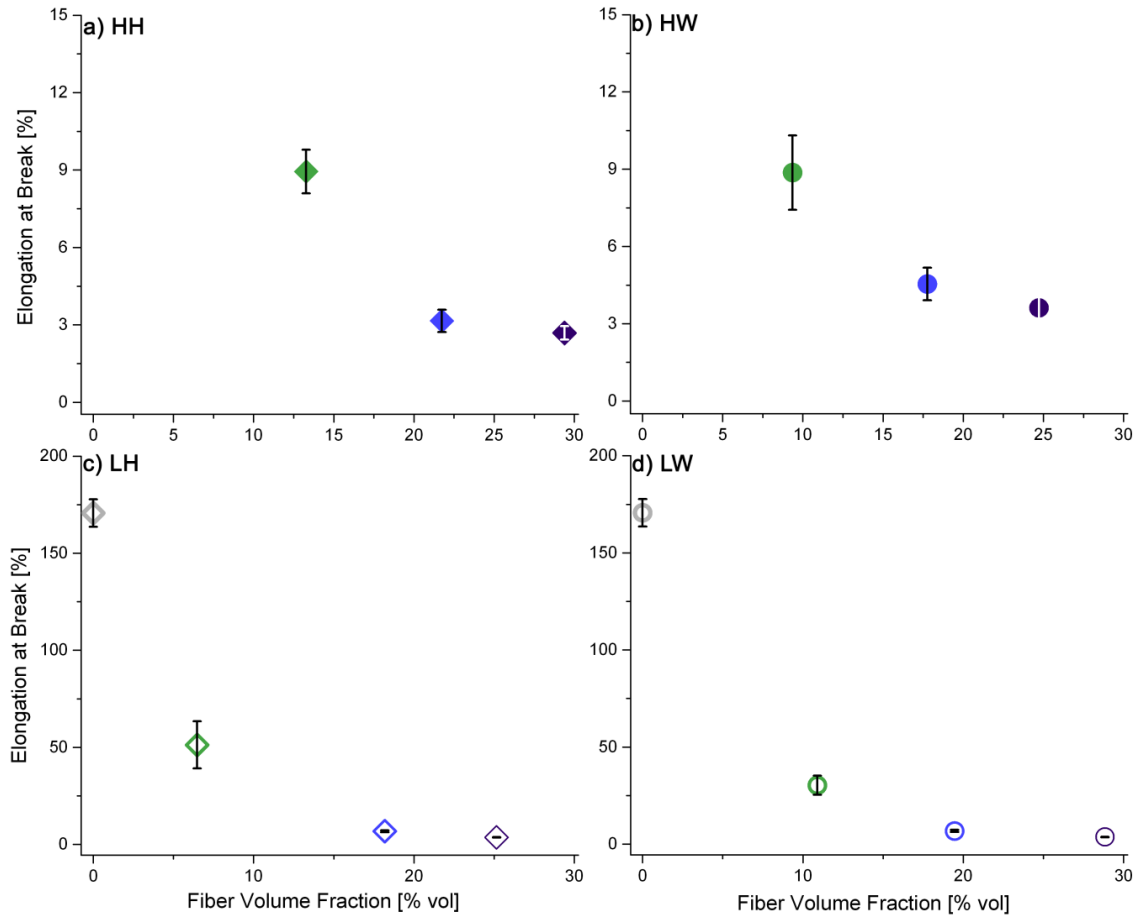


Figure 4.24 Elongation at break as a function of fiber volume fraction for LDPE (unfilled symbols) and HDPE (filled symbols). Increased fiber content results in a decrease in ductility represented by elongation at break. The colors designate the relative amount of fiber content, none (control) = grey, target 15 wt% low= green, target 30 wt% medium = blue and target 45 wt% high = purple.

Although toughness is not typically determined from the area under the tensile stress strain curve, it does provide a measure of the materials' general ability to absorb energy. The addition of natural fibers yielded a decrease in toughness. HDPE experienced the greatest change in toughness with the addition of either of natural fiber types. The relative quantity of fiber had minimal impact on toughness, rather just the addition of fiber decreased the material toughness.

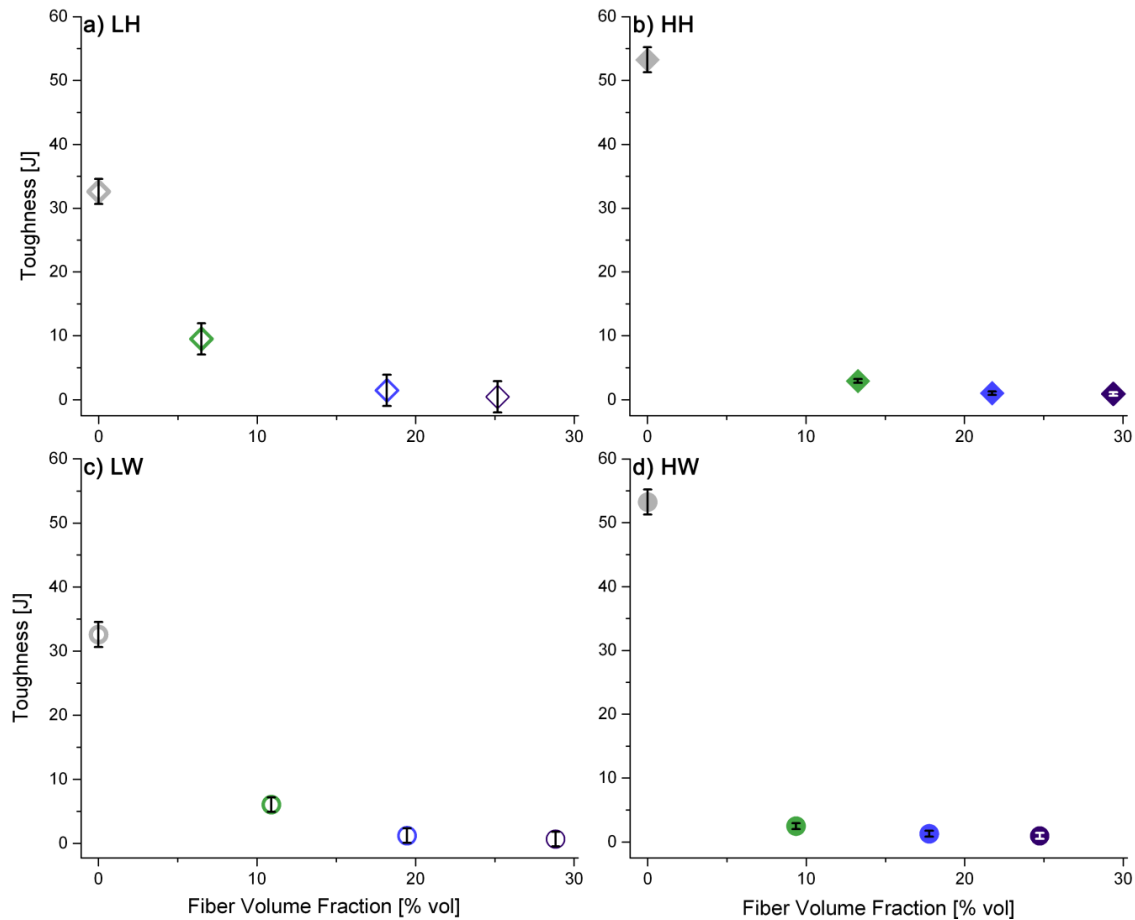


Figure 4.25 Toughness as a function of fiber volume fraction for LDPE (unfilled symbols) and HDPE (filled symbols). The addition of natural fibers results in a sharp decrease in tensile toughness. The colors designate the relative amount of fiber content, none (control) = grey, target 15 wt% low = green, target 30 wt% medium = blue and target 45 wt% high = purple.

It is recommended that another test method Izod [17], Charpy [18] or Tensile Impact Resistance [19] be utilized to assess impact resistance as a measure of material toughness. Typically, indications of material toughness of biocomposites are difficult to assess due to the heterogeneity and structure of the material. Data typically obtained with the above mentioned test methods result in similar data scatter [6]. Therefore, the results within this section are indicative of global changes in toughness.

#### 4.3.5.1 Impact of Water Absorption on Elongation at Break & Toughness

For the previously explored mechanical properties, modulus, tensile yield strength, and ultimate tensile strength, the water immersion did not affect the virgin materials properties. Only for LDPE, a slight decrease in elongation after 6552 hours immersed as observed in Figure 4.26. A corresponding increase in toughness of LDPE was not observed. Both

elongation at break and toughness demonstrate significant scatter in the data. Due to the natural scatter in data, both properties have been assessed concurrently to draw conclusions about the materials' response to water absorption. The same analysis for HDPE cannot be conducted between elongation at break and toughness since the virgin specimens did not break at the designated strain rate and maximum elongation limited by the testing equipment. For the same reason, the toughness to failure could also not be compared for HDPE.

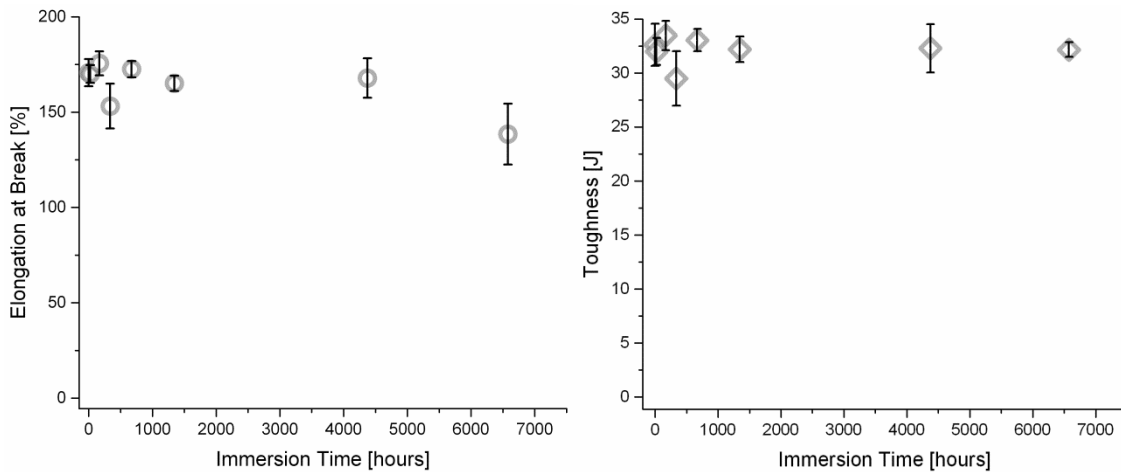


Figure 4.26 Elongation at break (left) and Toughness (right) of LDPE as a function of immersion time. No observed trends were observed for LDPE in either elongation at break or toughness due to the scatter in the data. HDPE results are not reported as the virgin material did not fracture.

Natural fiber reinforced biocomposites showed a minimal change in ductility after exposure to water immersion environment as shown from both elongation at break and toughness as shown in Figure 4.27 and Figure 4.29.

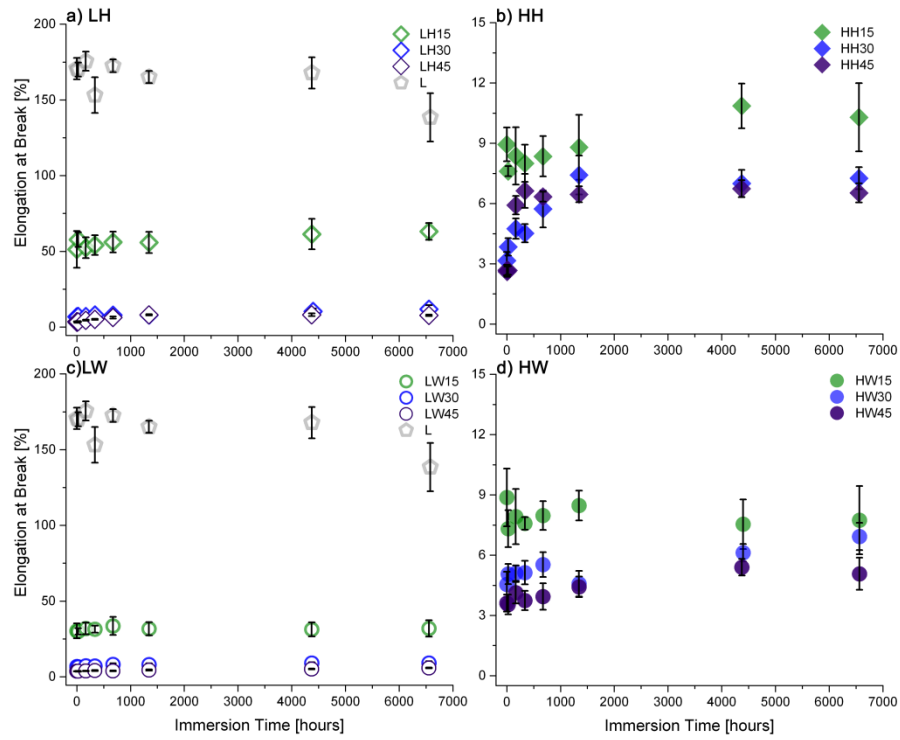


Figure 4.27 Elongation at break as a function of water immersion time for all material variations. Duration of immersion does not alter the elongation at break.

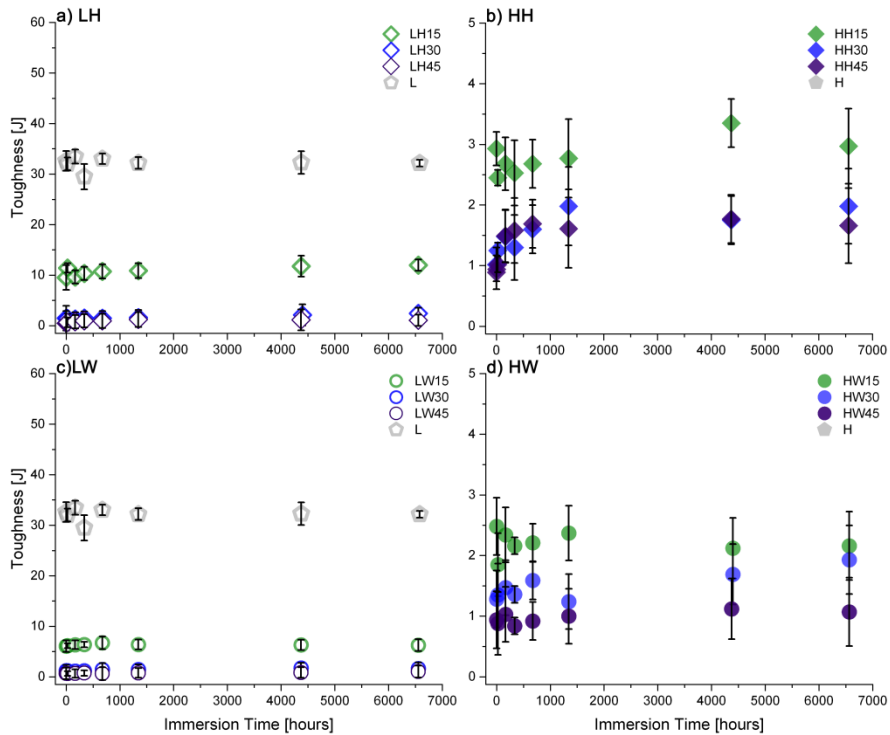


Figure 4.28 Toughness as a function of water immersion time for all material variations. Duration of immersion does not alter the biocomposite toughness.

HDPE biocomposites demonstrated a slight increase in elongation at break with an increased water absorbed as shown in Figure 4.29. The increase in ductility was more evident in hemp fiber than wood pulp. Negligible changes in toughness were observed between natural fiber types within each matrix type as well as between HDPE and LDPE as shown in Figure 4.30.

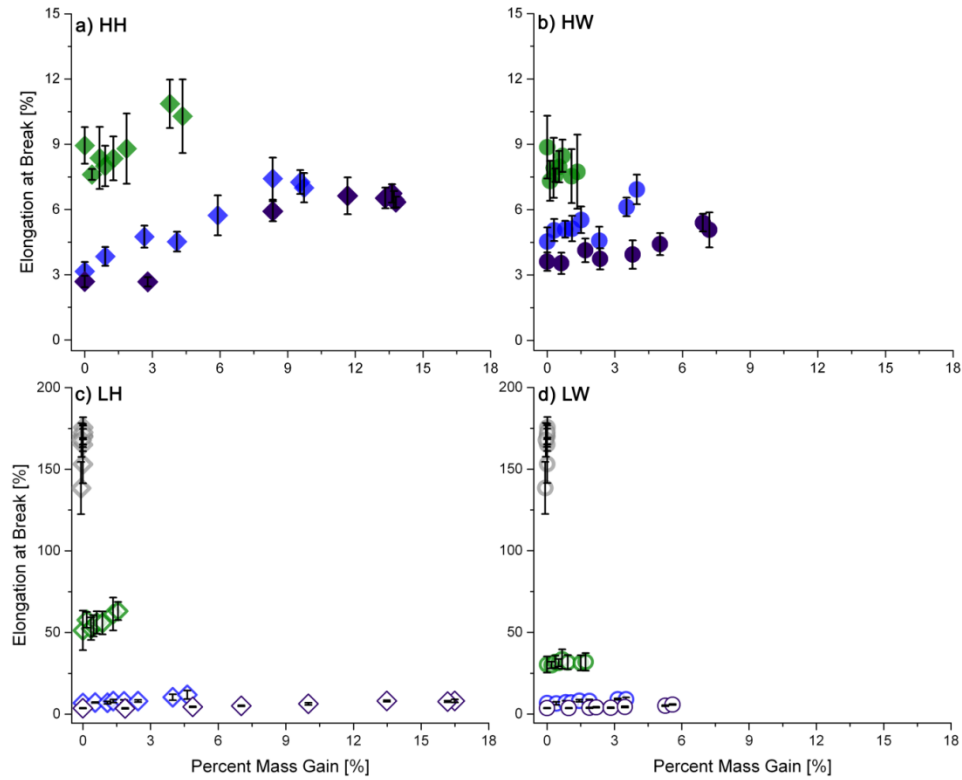


Figure 4.29 Percent water absorbed versus elongation at break for all material variations. A slight increase in elongation at break was observed for medium (blue) and high (purple) fiber contents in HDPE; otherwise no trend is observed.



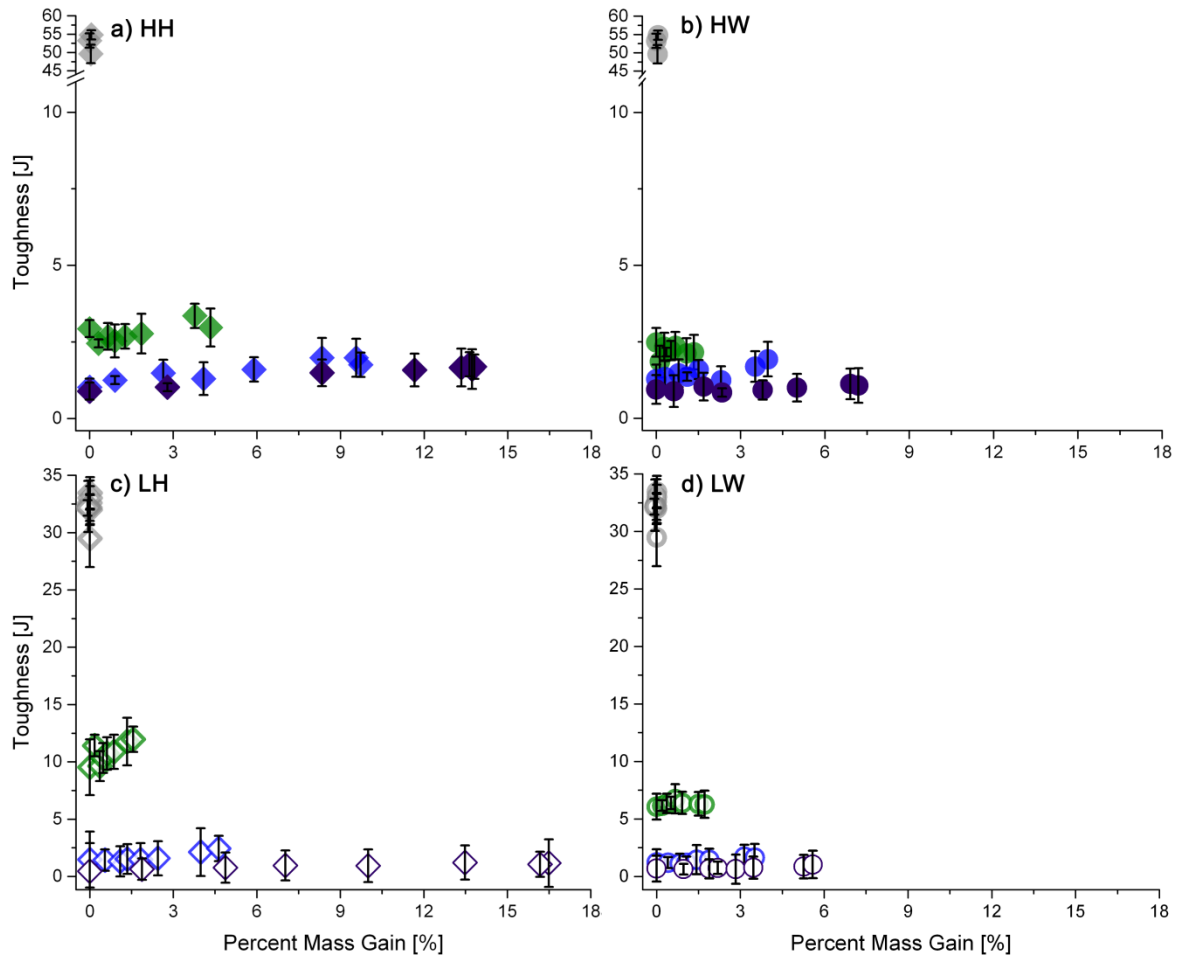


Figure 4.30 Toughness of each material variation with respect to water absorbed. No observed change in biocomposite tensile toughness with water immersion. The colors designate the relative amount of fiber content, none (control) = grey, target 15 wt% low= green, target 30 wt% medium = blue and target 45 wt% high = purple.

### 4.3.5.2 Normalized Elongation at Break and Toughness

The normalized properties were calculated by equation 3.7. A general increase in ductility via normalized elongation at break was observed with an increase in water absorption for all fiber reinforced biocomposites shown in Figure 4.31. The magnitude of elongation at break is dominated by polymer matrix properties and is hindered by the addition of natural fibers. Therefore, as the natural fibers absorb water, the biocomposite gains ductility as outlined in Equation 4.11 (at 95% confidence interval).

$$\% \text{ Normalized Elongation at Break} = 100 + \text{Percent Mass Gain} * 9.47 (\pm 0.26) \quad (4.18)$$

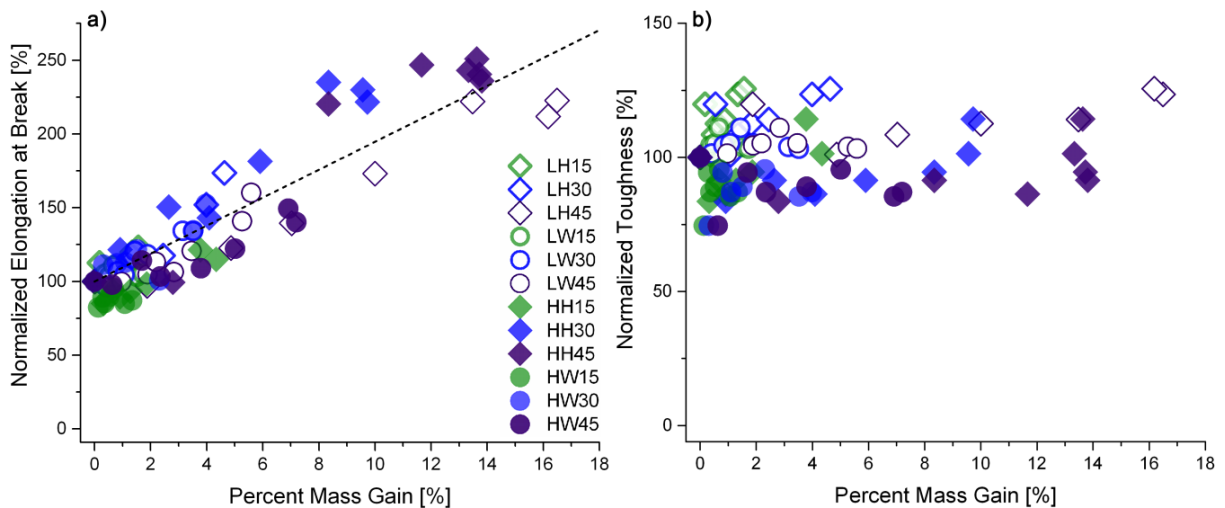


Figure 4.31 Normalized elongation at break relative to percent mass gain from water immersion, with Equation 4.11 graphed (dashed line). Linear increase in ductility with absorbed water without an observed increase in toughness. The colors designate the relative amount of fiber content, none (control) = grey, target 15 wt% low= green, target 30 wt% medium = blue and target 45 wt% high = purple where filled are HDPE variations and unfilled are LDPE.

Biocomposite toughness was not affected by water absorbed within the material, as shown in Figure 4.31. Generally, the HDPE variations showed a decline from the control (no immersion sample) compared to LDPE which demonstrated a slight increase in toughness with water absorbed. Therefore, no mathematical model relationships were developed.

## **4.4 REVERSIBILITY OF MECHANICAL DEGRADATION**

The extent of reversible versus irreversible loss in mechanical properties caused by water absorption for design purposes is explored in this section. Specimens immersed for 6552 hours, maximum immersion exposure, were dried for up to one week and mechanically tested to assess the materials' ability to reverse the effects of water absorption. The assessment of mechanical properties in a dried state after prolonged water immersion determines if losses in mechanical properties are recoverable or whether permanent damage has occurred.

### *4.4.1 MODULUS LOSS*

For tensile modulus, the virgin matrix materials for both LDPE and HDPE demonstrated slight mass loss with approximate full recovery of tensile modulus. No substantial difference was observed between how the fibers respond in LDPE versus HDPE. With respect to fiber type, wood pulp experienced less permanent degradation in modulus than hemp fiber reinforced biocomposites. A possible theory to explain the difference in response is chemical components, such as hemicellulose and extractives, in hemp fiber were hydrolyzed during immersion resulting in permanent degradation in the fiber modulus. Since wood pulp has been chemically refined by the pulping process to be cellulose, the same extent of degradation was not observed. Both fibers experienced a loss in modulus due to surface fiber loss during water immersion as explained in section 5.3. For all variations the magnitude of permanent degradation of modulus increased with increasing fiber volume fraction.

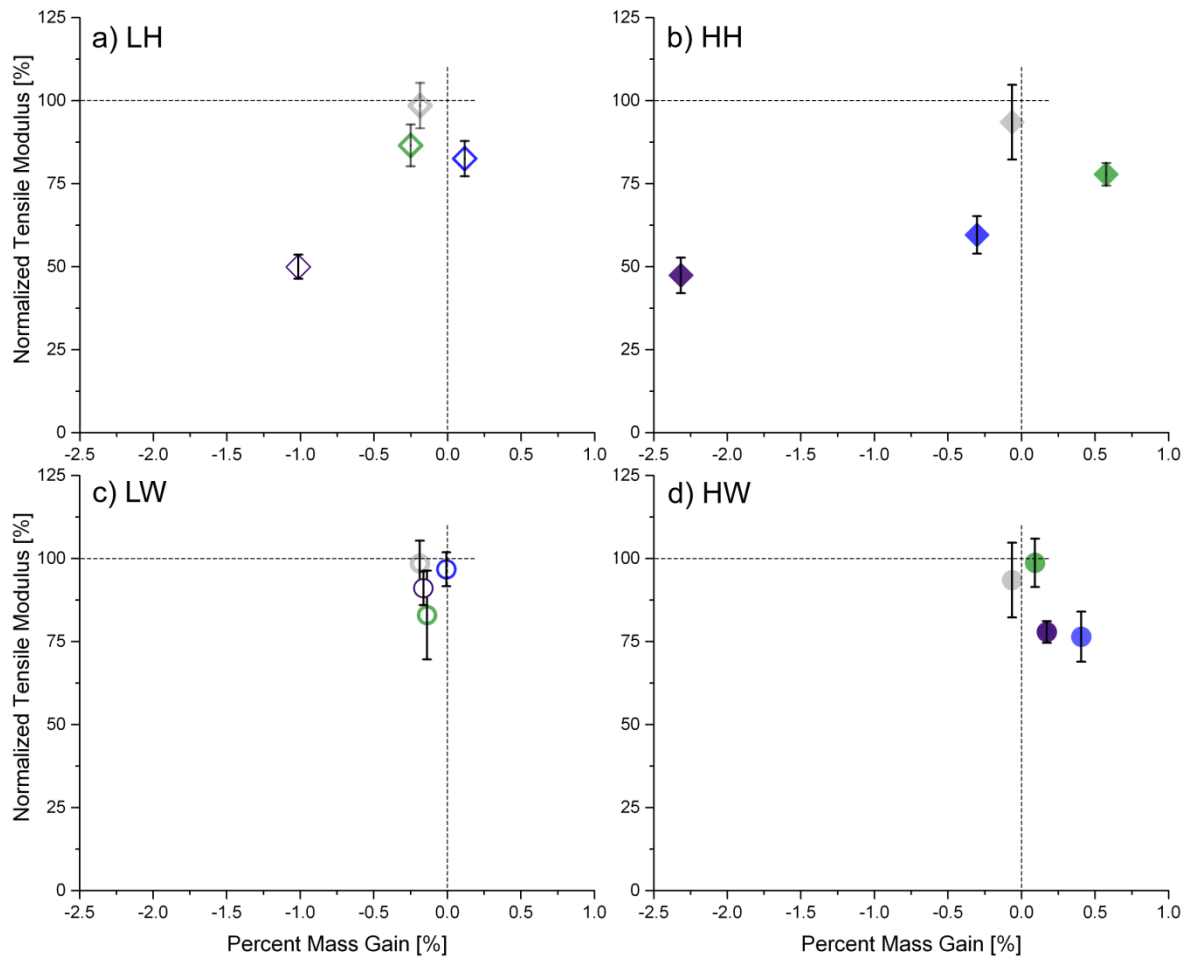


Figure 4.32 Normalized tensile modulus of specimens dried after 6552 hours of immersion, where grey is virgin, blue represents 15 wt%, green represents 30 wt% and purple represents 45 wt%. Permanent degradation in tensile modulus after prolonged immersion correlated with an observed mass loss. The colors designate the relative amount of fiber content, none (control) = grey, target 15 wt% low = green, target 30 wt% medium = blue and target 45 wt% high = purple.

#### 4.4.2 TENSILE YIELD STRENGTH LOSS

The permanent degradation was not as significant for yield strength compared to tensile modulus. For wood pulp, there was negligible degradation of tensile strength as the properties for all fiber fractions exhibited almost complete recovery to their original state post-drying. In the case of hemp fiber, a pronounced effect was observed at high fiber fraction with increased mass loss. Therefore, the degradation of property can be correlated to mass loss of the biocomposite.

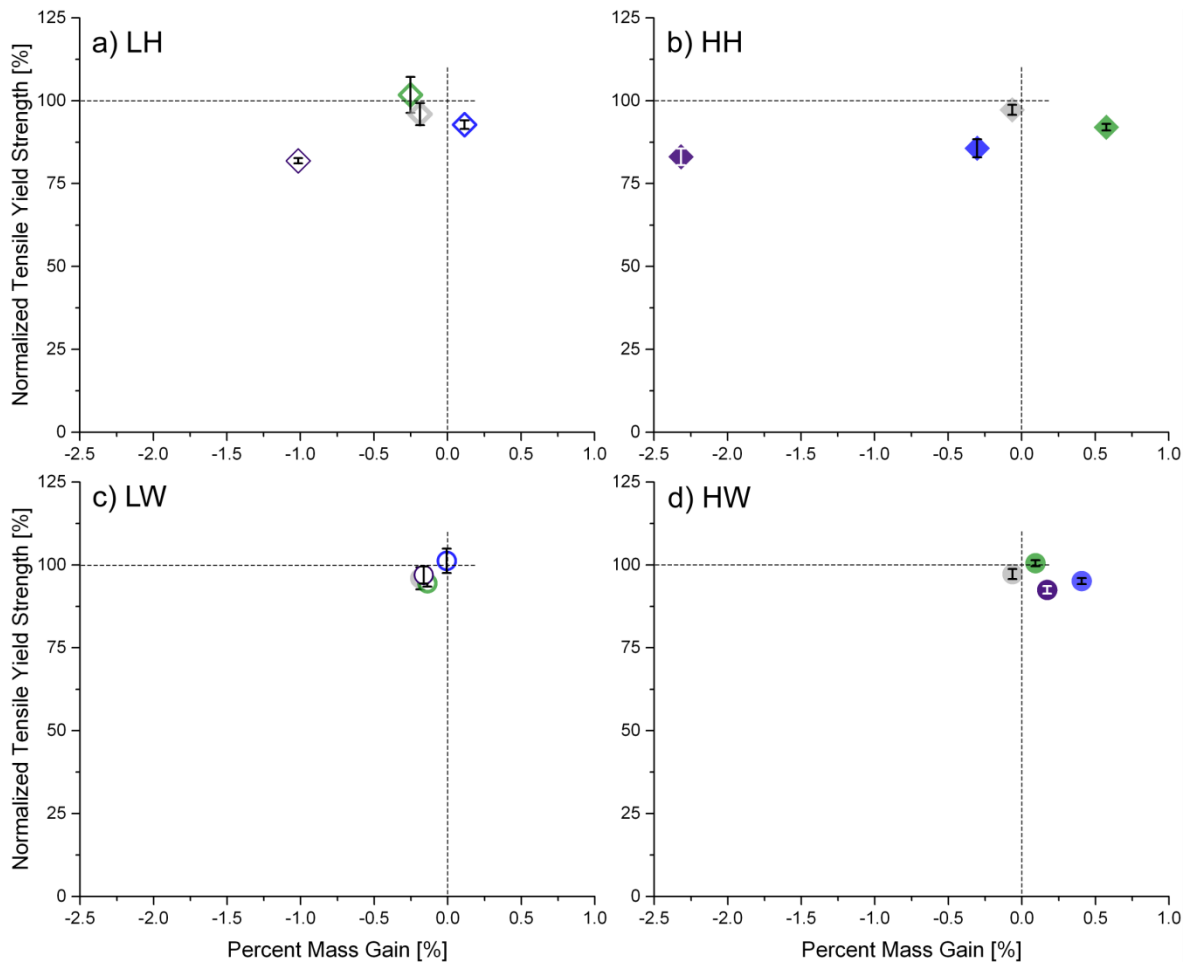


Figure 4.33 Normalized tensile yield strength of specimens dried after 6552 hours of immersion, where grey is virgin, blue represents 15 wt%, green represents 30 wt% and purple represents 45 wt%. Permanent degradation observed in tensile yield strength for hemp fiber reinforced specimens. The colors designate the relative amount of fiber content, none (control) = grey, target 15 wt% low = green, target 30 wt% medium = blue and target 45 wt% high = purple.

#### 4.4.3 ULTIMATE TENSILE STRENGTH LOSS

Absorbed water had minimal impact on biocomposite ultimate tensile strength properties. Therefore, the recovery of loss in ultimate tensile strength were also minimal. The exceptions were two high hemp fiber content variations, LH45 and HH45 which experienced a noticeable permanent loss of ultimate tensile strength. The inability to recover original dry properties of the biocomposite is attributed to the fiber mass loss experienced after 6552 hours of immersion.

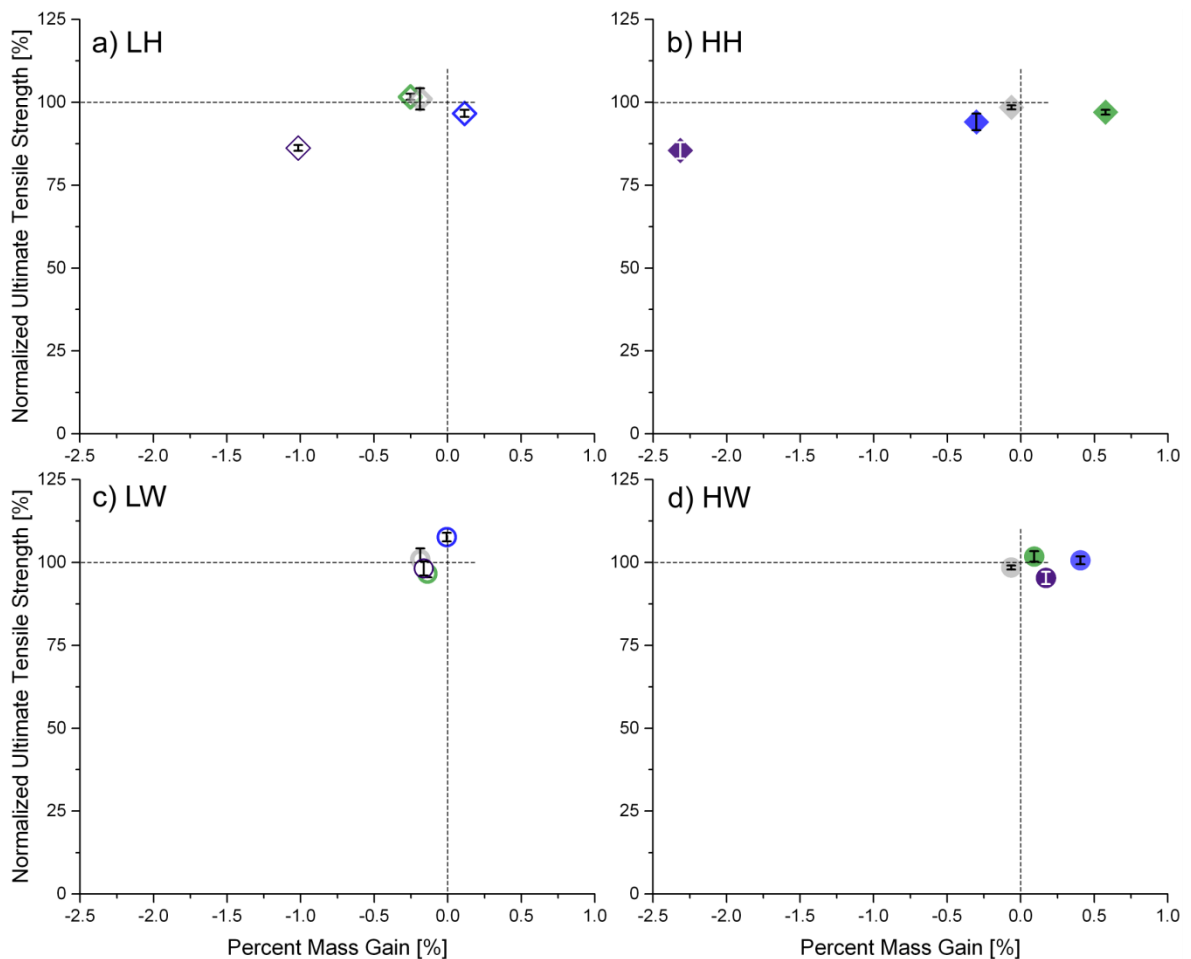


Figure 4.34 Normalized ultimate tensile strength of specimens dried after 6552 hours of immersion, where grey is virgin, blue represents 15 wt%, green represents 30 wt% and purple represents 45 wt%.

Permanent degradation in the ultimate tensile strength for hemp fiber reinforced specimens is observed; no significant change for wood pulp reinforced specimens is observed. The colors designate the relative amount of fiber content, none (control) = grey, target 15 wt% low= green, target 30 wt% medium = blue and target 45 wt% high = purple.

#### 4.4.4 ELONGATION AT BREAK & TOUGHNESS LOSS

The ductility of all immersed and re-dried biocomposites increased compared to the original specimens, independent of any mass change. LDPE type biocomposites more readily recovered ductility as it is more matrix dependent since the matrix can deform around the natural fibers more easily compared to HDPE type biocomposites. Wood pulp fibers experienced a less significant change than hemp fiber variations.

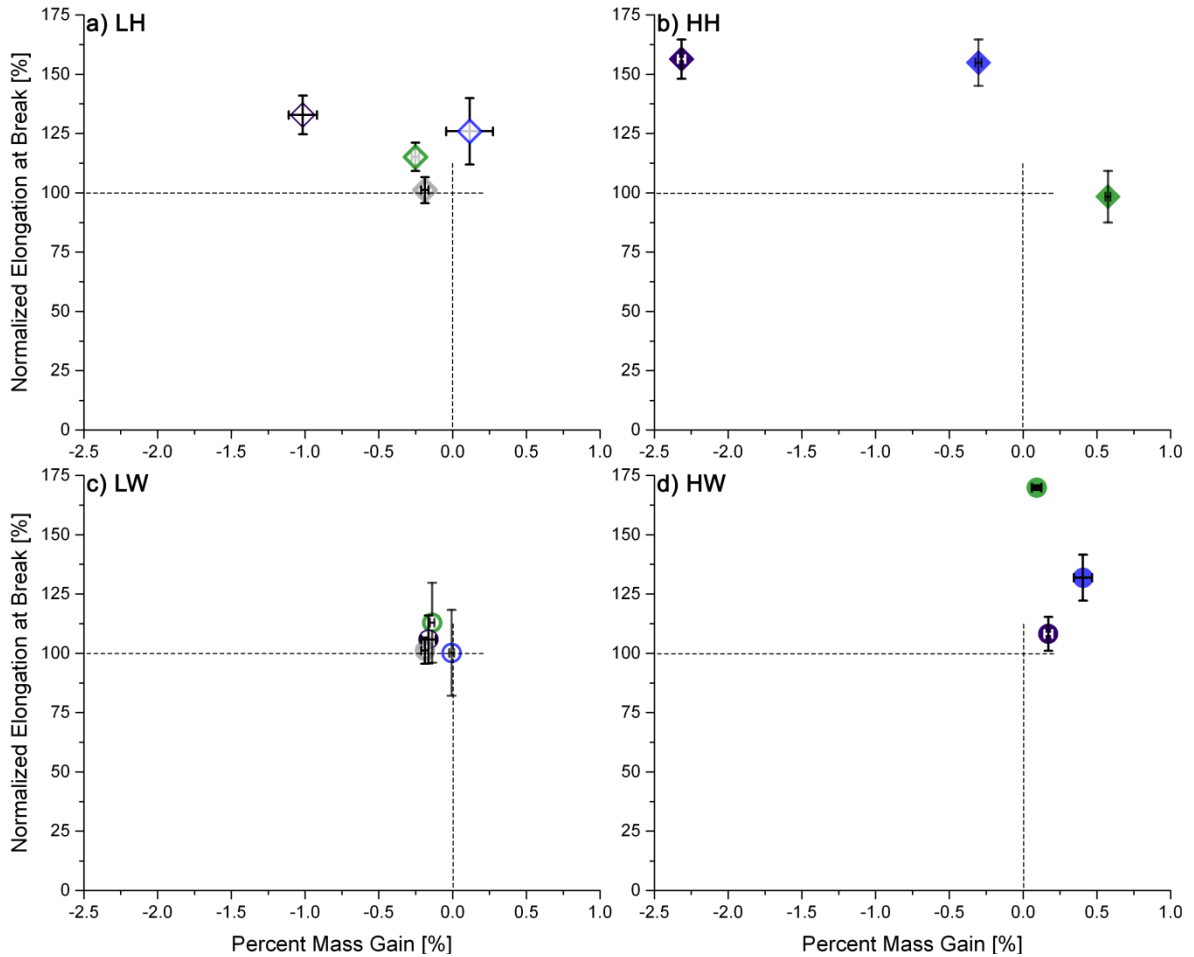


Figure 4.35 Normalized elongation at break of specimens dried after 6552 hours of immersion, where grey is virgin, blue represents 15 wt%, green represents 30 wt% and purple represents 45 wt%. Water immersion environment resulted in increased ductility. The colors designate the relative amount of fiber content, none (control) = grey, target 15 wt% low = green, target 30 wt% medium = blue and target 45 wt% high = purple.

The toughness of all biocomposites rebounded well after prolonged water immersion. The wood pulp reinforced biocomposites had little to no differences, whereas the hemp fiber reinforced materials showed some variation, especially the higher hemp fiber fraction materials as these specimens experienced mass loss compared to the other material variations.

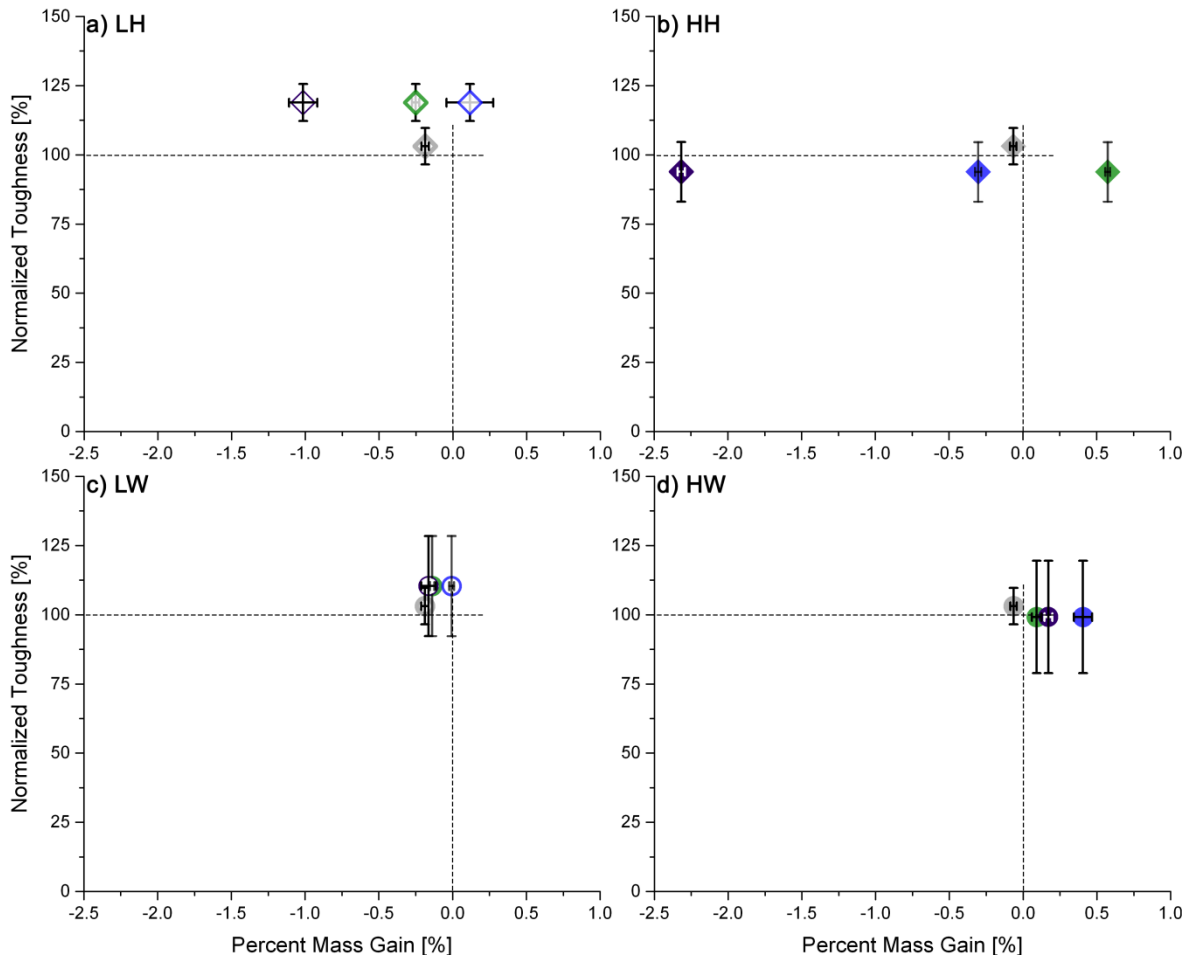


Figure 4.36 Normalized toughness of specimens dried after 6552 hours of immersion, where grey is virgin, blue represents 15 wt%, green represents 30 wt% and purple represents 45 wt%. Negligible changes in toughness observed with the exception of LH variations which gained additional toughness. The colors designate the relative amount of fiber content, none (control) = grey, target 15 wt% low = green, target 30 wt% medium = blue and target 45 wt% high = purple.

The variation in mass loss due to water absorption for wood pulp reinforced specimens was minimal as were the changes to both the tensile toughness and elongation at break. Overall both toughness and elongation at break demonstrated an increase in ductility for composites immersed for 6552 hours then re-dried.



## 4.5 FRACTURE MODE ASSESSMENT

Investigation of the fracture surface provides insight into the physical processes involved when the material is damaged and fails [1]. Observations reveal information such as failure mode (ductile or brittle), direction of failure, and potentially the composition of constituents at the fracture surface. Composite materials, however, pose some difficulty with distinguishing each constituent and their interactions in the failure process. Biocomposites are even more complicated to assess due to the natural variation in fiber length and diameter, along with the random orientation from injection molding. Each matrix and natural fiber has been thoroughly studied, and representative images of fracture surfaces are displayed in Figure 4.37, Figure 4.38 and Figure 4.39.

### 4.5.1 POLYMER

Virgin LDPE and HDPE mechanical properties are unaffected by water immersion. Since virgin HDPE did not fail in tension at the controlled strain rate, a comparison between the two polymer fracture surfaces was conducted on low fiber fill fraction before immersion, as shown in Figure 4.37. HDPE illustrates both smooth bundles of polymer strands, as well as a dimpled surface due to failed attempts to form chain alignment under stress. Whereas LDPE illustrates long wave like morphology from the polymer recoiling from the fracture. LDPE displays greater ductility than HDPE due to the wavy polymer strands indicating elastic recoil from plastic deformation in Figure 4.37. Therefore, the presence of natural fibers within HDPE disrupts the preferred method of deformation under stress causing a brittle fracture mode around a fiber and a ductile fracture mode when chain alignment is not disrupted.

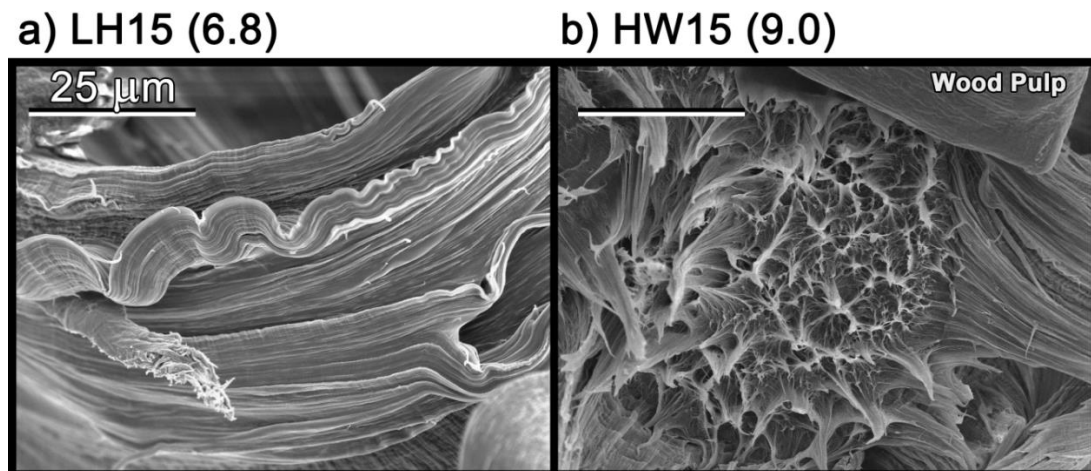


Figure 4.37 Ductile fracture surface for both a) LDPE and b) HDPE near a reinforcing fiber.

Polyethylene is intrinsically ductile at room temperature; therefore the fracture mode is ductile with chain alignment to a shear tearing of the material. The fracture mode transitions to a more brittle response when the natural fibers disrupt the matrices ability to elastically deform, as shown in b of Figure 4.37.

#### *4.5.2 FIBER*

The fracture mode of fibers within the biocomposites were investigated before and after water immersion as well as dried after maximum immersion, Figure 4.38. In contrast, a slight change in fiber failure mode is observed. Water absorption changes the fibers' failure mode from ductile, flat cleavage surface, to a ductile mode with fiber bundles pulled out from the bulk of the material. The effect is more pronounced with hemp fiber. For hemp, some of the ductile fracture mode is retained even after the specimen is dried. This evidence indicates that there is a change in hemp fiber properties after water immersion. These conclusions are also supported by the mechanical properties.

Images displayed in Figure 4.38 were taken within the bulk of the material and therefore depict how the interior fibers are changing; a more extreme change could have been seen at the fibers closer to the perimeter of the fracture cross section. Also, due to the extensive fiber processing it is possible that the fiber fracture mode illustrated is at the end of the fiber and has exposed the damage from the fiber processing rather than the fracture mode from mechanical testing.

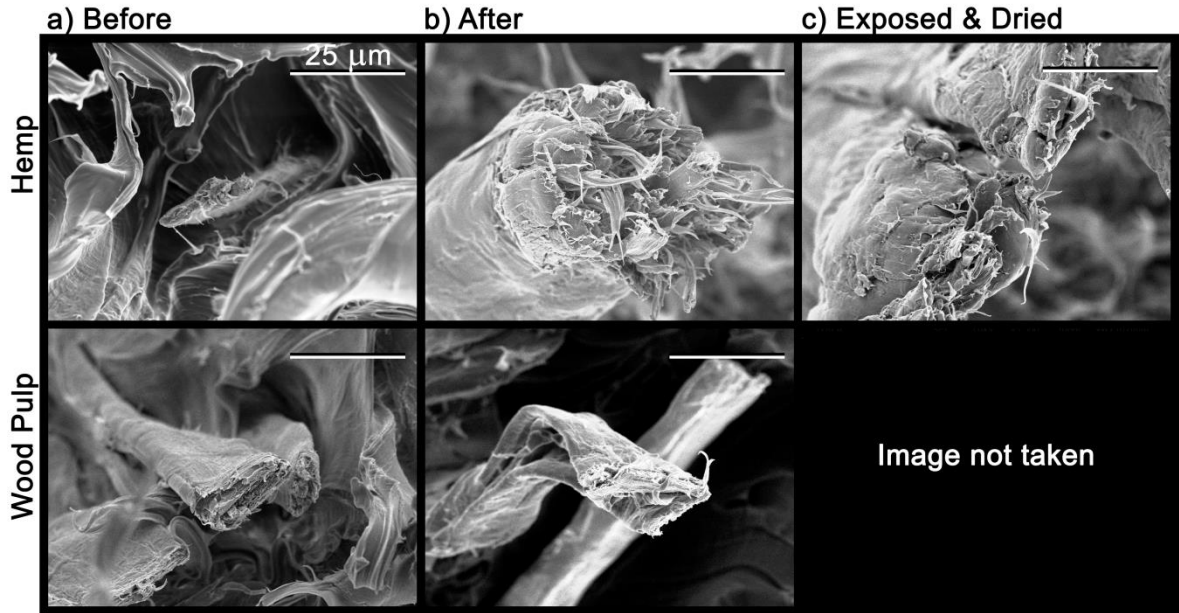


Figure 4.38 Fiber fracture surfaces at different stages with regards to water immersion a) before exposure, b) after exposure c) exposed and dried.

#### 4.5.3 *BIOCOMPOSITE*

A macro view of the biocomposite fracture surface in LDPE was investigated and displayed in Figure 4.39. The lowest fiber fill fraction was selected for this analysis to aid in the visual differentiation between natural fibers within the polyethylene matrix. LDPE fractures in a ductile mode based on the wavy ripple and ridge morphology as a result of recoiled fibril features after fracture. After one month of water exposure, LDPE demonstrated increased ductility with additional ductile strands attached to the ductile fracture surface. This ductile fracture mode of LDPE is also prevalent within the biocomposite structure and was retained after exposure to water immersion.

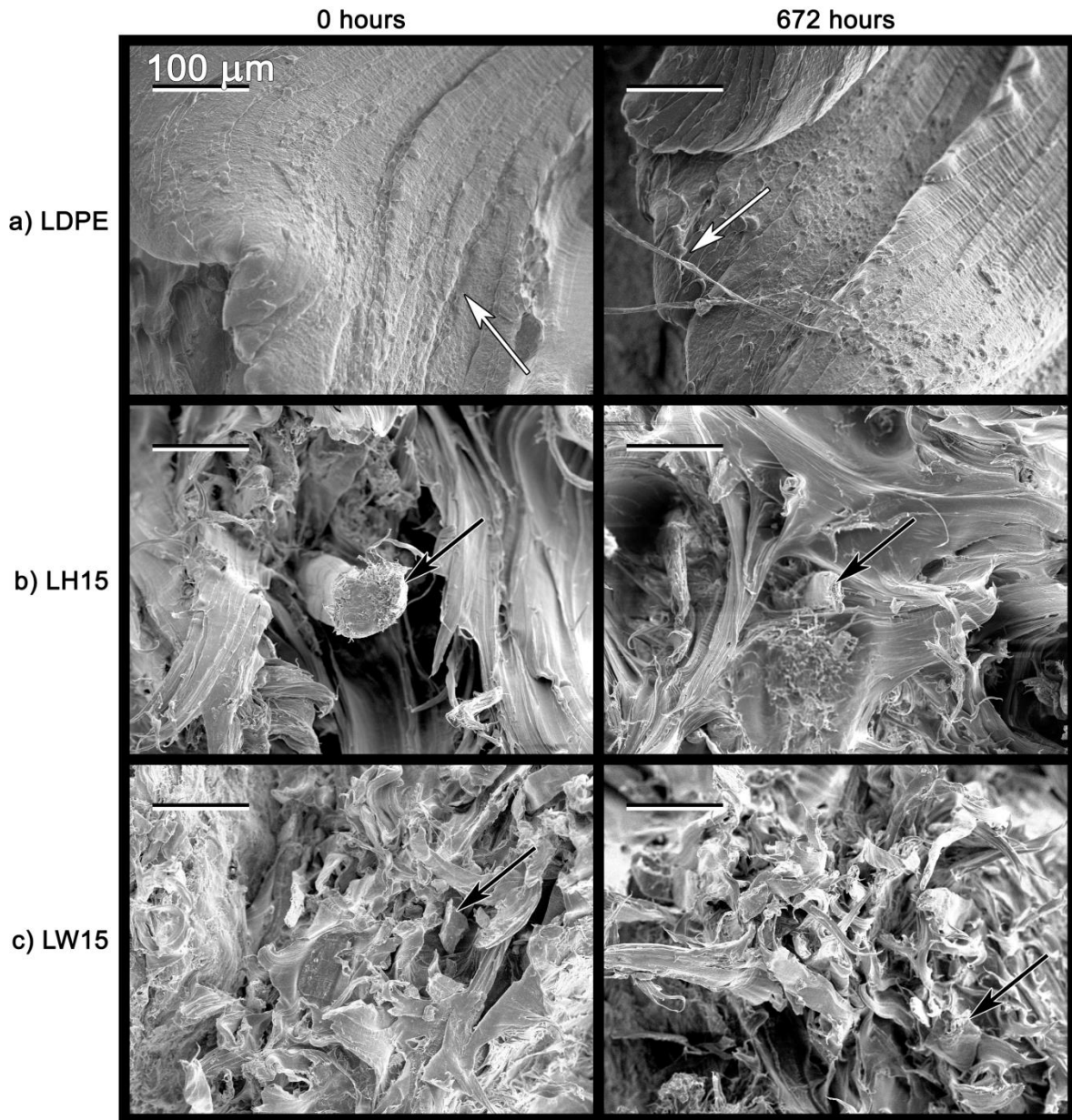


Figure 4.39 Fracture surface at 0 hours and 672 hours of immersion for a) LDPE, b) LH15 and c) LW15 where the white arrows identify the matrix and the black point to the natural fiber. LDPE changes from ductile to brittle with addition of natural fiber, however, when immersed in water, LDPE plasticizes as shown by smoother ductile surfaces elongated in multiple directions compared to the rough fibril surfaces observed when dry.

Micrographs of hemp fiber reinforced LDPE prior to immersion (Figure 4.39) showed evidence of clean brittle fracture of the fiber. After one month of water immersion, the same fracture mode cannot be observed rather the hemp fiber fracture morphology was wavy as a result of tearing due to increased ductility from the immersion environment. Wood pulp

experienced the same change in fiber fracture morphology as hemp, although to a lesser extent.

Both the mechanical results and the micrograph analysis support the conclusion that the natural fiber response transitions from a brittle mode of fracture to a more ductile mode of fracture after exposure to moisture. The micrograph of the fracture surfaces support the trend that increased water absorption decreases the natural fibers' ability to resist load and therefore a shift in fiber fracture mode is observed from brittle to more ductile.

## 4.6 SUMMARY

### **Determination of Volume Fraction**

The assumption that the targeted weight fraction of fiber is equivalent to the actual manufactured fraction was challenged. The fiber content in the manufactured biocomposites differed from the targets amount. Nitrogen gas pycnometry has proven to be an accurate and precise non-destructive technique to assess fiber [20], matrix and biocomposite density. The densities were then used as a means to verify the manufactured weight and volume fraction of fiber. To eliminate variation in measurement caused by variations in manufacturing processes, the final injection molded samples were used to determine matrix and biocomposite densities.

Fiber density was assessed as an extent of fiber processing to determine the possible change in fiber density during the manufacturing process. Mixing and forming processed have been shown to reduce fiber dimensions. Freezer milled was used as the worst case scenario to expose the maximum closed pore volume to the nitrogen gas in the pycnometer. The difference between freezer milled, fine fiber structure and the fiber form feed into the extruder was minimal compared to the difference between raw feedstock fiber and freezer milled. Fiber density is dependent on the form of fiber and therefore literature values are suggested to be used as an approximation rather than an accurate value. Furthermore, depending on the magnitude in difference between densities of fibers, comparison between fiber types may be misleading.

These results suggest that fiber content verification of all manufactured biocomposites should be completed for comparable results within the same study as well as for usability between studies.

### **Water Absorption of Tensile Specimens**

From initial analyses of water absorption of tensile specimens, hemp-fiber-reinforced biocomposites were able to absorb more water than wood-pulp-reinforced composites. For all material variations, an increase in fiber volume fraction and immersion time corresponds to an increase in absorbed water. Material variations with higher hemp fiber contents absorbed water to a maximum and underwent a small drop. The wood pulp variations all absorbed similar quantities at comparative rates and magnitudes; the same is not true for

hemp fiber reinforced variations. Ultimately, a greater fiber volume and a longer immersion time corresponded to increased water absorption for all biocomposite variations.

### **Mechanical Properties**

The addition of fiber types, wood pulp and hemp fiber, resulted in increased modulus and strength with a correspondent decrease in elongation at break and toughness. The reinforcement effects of the natural fibers were more pronounced in LDPE than HDPE, due to the lower modulus and strength of LDPE. The same trends with the addition of fiber were observed for HDPE albeit to a lesser extent.

The mechanical properties of the biocomposites degrade with exposure to a water immersion environment. A relationship definitive relationship between the degraded mechanical property and immersion time does not exist. However there is a clearly defined relationship between the percentage of a normalized mechanical property and the percentage of water absorbed with the exception of toughness. All of the biocomposite variations collapse onto the same relationship for each property, as shown in Figure 4.40. Mechanical strength, yield and ultimate, degrade linearly with absorbed water whereas the ductility increases linearly. Tensile modulus degrades exponentially with increased absorbed water. Therefore, **the extent of mechanical degradation due to water absorption is based on both the original mechanical property and the relative amount of water absorbed.** The predictive degradation equations 4.7 to 4.10 graphed in Figure 4.40 are re-written:

$$\% \text{ Normalized Tensile Modulus} = 100e^{-0.1048 * \text{Percent Mass Gain}} \quad (4.7)$$

$$\% \text{ Normalized Tensile Yield Strength} = 100 - \text{Percent Mass Gain} * 3.06 (\pm 0.04) \quad (4.8)$$

$$\% \text{ Normalized Ultimate Tensile Strength} = 100 - \text{Percent Mass Gain} * 1.82 (\pm 0.08) \quad (4.9)$$

$$\% \text{ Normalized Elongation at Break} = 100 + \text{Percent Mass Gain} * 9.47 (\pm 0.26) \quad (4.10)$$

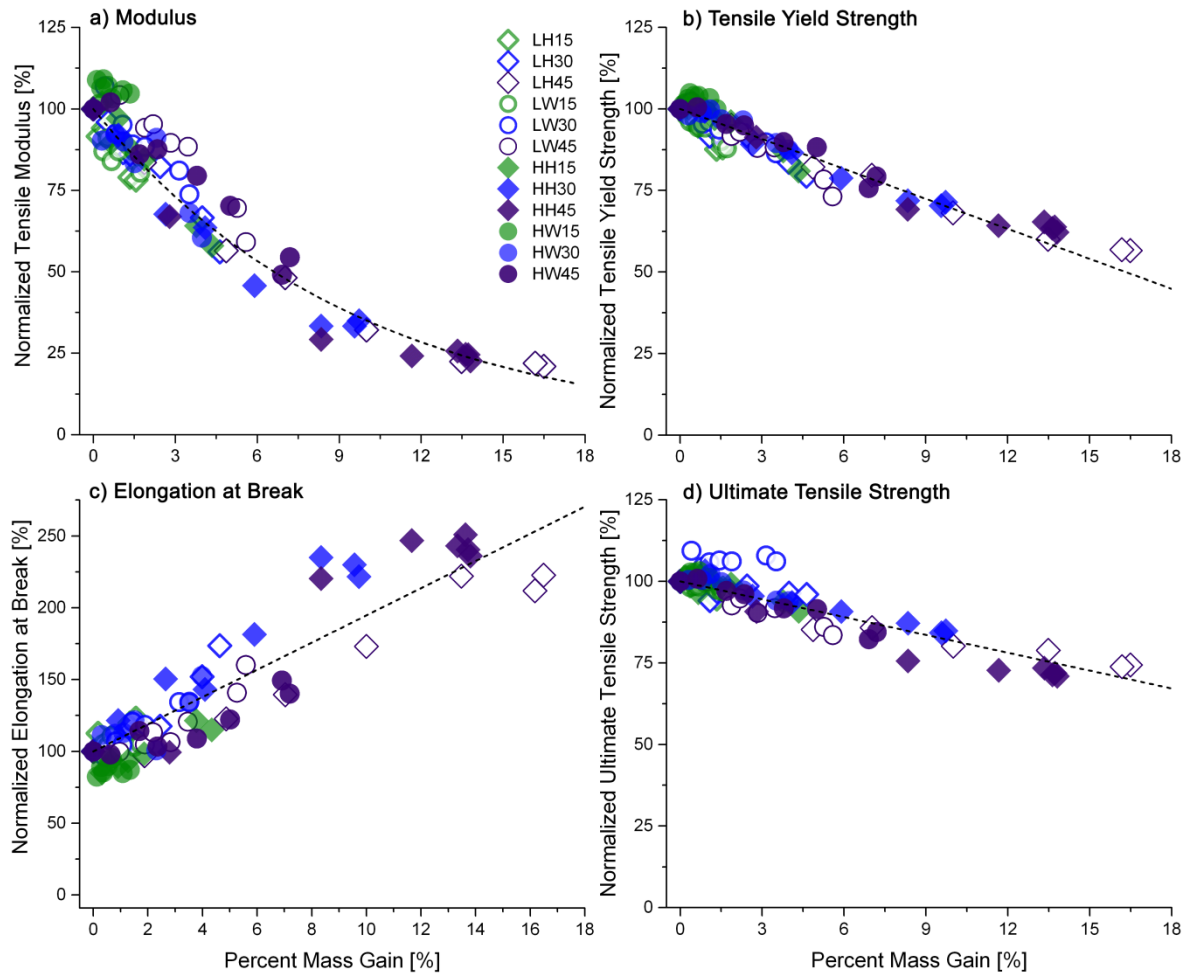


Figure 4.40 Overview of all the normalized mechanical properties as a function of water absorbed, a) Modulus, b) yield tensile strength c) elongation at break and d) ultimate tensile strength. The degradation of mechanical properties are dependent on the water absorbed within the specimen for all material variations.

### **Reversibility of Mechanical Degradation**

Permanent damage to biocomposite materials was caused by long-term exposure to water immersive environments. Minor differences in recovery of each property was observed between variations. A correlation exists between the extent of mass loss after immersion and irreversible loss of properties. Wood pulp variations underwent less modulus degradation than hemp-fiber-reinforced samples. A reasonable explanation is since wood pulp has already been chemically treated and purified compared to hemp fiber which still has extractive water soluble components. Further work should be conducted to assess the relationship with loss of property and mass loss of the biocomposite.



### **Fracture Mode**

The addition of natural fibers reduces biocomposites' ductility due to the disruption in the polymer network of the matrix. The micrographs illustrated how the matrix material deforms around the natural fibers.

The fracture morphology of the biocomposites before and after water immersion illustrates the transition of fracture mode of the natural fiber from brittle to ductile. Therefore the water absorbed by the biocomposite disrupts the natural fibers structure and therefore its failure mode.

### **Impact**

Empirical equations were developed to predict the extent of the change in modulus, yield strength, ultimate strength and elongation at break relative to the percent magnitude of water absorbed into the material. The relationships developed for each property were independent of both matrix and fiber type, as all the biocomposite variations collapsed onto the same relationship.

Currently, predictive water absorption models only predict the first 100 hours immersed. Significant changes in mechanical properties are observed after the 100 hours as illustrated in Figure 4.12, Figure 4.17, Figure 4.21 and Figure 4.27. Since the prediction in loss of mechanical properties has been directly attributed to the quantity of water absorbed, as shown in Figure 4.40 a model must predict quantity of water absorbed. A long term water absorption predictive model has been developed in Chapter 5 to enable designers to predict mechanical properties.

## REFERENCES

1. Greenhalgh, E. and M. Hiley, *Fractography of polymer composites: current status and future issues*, in *13th European Conference on Composite Materials* 2008.
2. Agarwal, B.D., L.J. Broutman & Chandrashekhara K., ed. *Analysis and Performance of Fiber Composites*. 3rd ed. 2006, John Wiley & Sons Inc: New Jersey. 562.
3. Rothon, R.N., *Particulate-filled Polymer Composites* 2003: Rapra Technology Limited.
4. John Bootle, Frank Burzesi, and L. Fiorini, *Design Guidelines*, in *ASM Handbook: Composites* 2001, ASM International. p. 1201.
5. Dicker, M.P.M., P.F. Duckworth, A.B. Baker, G. Francois, M.K. Hazzard, and P.M. Weaver, *Green composites: A review of material attributes and complementary applications*. *Composites Part A: Applied Science and Manufacturing*, 2014. **56**: pp. 280-289.
6. Robertson, N.L.M., J.A. Nychka, K. Alemaskin, and J.D. Wolodko, *Mechanical performance and moisture absorption of various natural fiber reinforced thermoplastic composites*. *Journal of Applied Polymer Science*, 2013. **130**(2): pp. 969-980.
7. Joseph, P.V., M.S. Rabello, L.H.C. Mattoso, K. Joseph, and S. Thomas, *Environmental effects on the degradation behaviour of sisal fibre reinforced polypropylene composites*. *Composites Science and Technology*, 2002. **62**(10): pp. 1357-1372.
8. Arbeláiz, A., B. Fernández, J.A. Ramos, A. Retegi, R. Llano-Ponte, and I. Mondragon, *Mechanical properties of short flax fibre bundle/polypropylene composites: Influence of matrix/fibre modification, fibre content, water uptake and recycling*. *Composites Science and Technology*, 2005. **65**(10): pp. 1582-1592.
9. Beg, M.D.H. and K.L. Pickering, *Mechanical performance of Kraft fibre reinforced polypropylene composites: Influence of fibre length, fibre beating and hygrothermal ageing*. *Composites Part A: Applied Science and Manufacturing*, 2008. **39**(11): pp. 1748-1755.
10. Lin, Q.F., X.D. Zhou, and G. Dai, *Effect of hydrothermal environment on moisture absorption and mechanical properties of wood flour-filled polypropylene composites*. *Journal of Applied Polymer Science*, 2002. **85**(14): pp. 2824-2832.
11. Kittikorn, T., E. Stromberg, M. Ek, and S. Karlsson, *Comparison of Water Uptake as Function of Surface Modification of Empty Fruit Bunch Oil Palm Fibres in PP Biocomposites*. *Bioresources*, 2013. **8**(2): pp. 2998-3016.
12. Stamboulis, A., C.A. Baillie, S.K. Garkhail, H.G.H. Van Melick, and T. Peijs, *Environmental Durability of Flax Fibres and their Composites based on Polypropylene Matrix*. *Applied Composite Materials*, 2000(7): pp. 273-294.
13. Adhikary, K.B., S. Pang, and M.P. Staiger, *Long-term moisture absorption and thickness swelling behaviour of recycled thermoplastics reinforced with Pinus radiata sawdust*. *Chemical Engineering Journal*, 2008. **142**(2): pp. 190-198.
14. Le Duigou, A., A. Bourmaud, P. Davies, and C. Baley, *Long term immersion in natural seawater of Flax/PLA biocomposite*. *Ocean Engineering*, 2014. **90**: pp. 140-148.
15. Espert, A., F. Vilaplana, and S. Karlsson, *Comparison of water absorption in natural cellulosic fibres from wood and one-year crops in polypropylene composites and its influence on their mechanical properties*. *Composites Part A: Applied Science and Manufacturing*, 2004. **35**(11): pp. 1267-1276.
16. *Elongation at Break*. 2016 [cited 2016 July 3, 2017]; Available from: <http://www.ensinger-online.com/en/technical-information/properties-of-plastics/mechanical-properties/elongation-at-break/>.
17. ISO, *180 - Plastics - Determination of Izod impact strength*, 2013. p. 10.

18. ISO, *179-1 Plastics - Determination of Charpy impact properties*, 2010. p. 28.
19. ISO, *8256 - Plastics - Determination of Tensile-Impact Strength*, 2004. p. 22.
20. Truong, M., W. Zhong, S. Boyko, and M. Alcock, *A comparative study on natural fibre density measurement*. *Journal of the Textile Institute*, 2009. **100**(6): pp. 525-529.

## 5. PHENOMENON, MECHANISM AND PREDICTIVE WATER ABSORPTION MODEL IN BIOCOMPOSITES

As examined in Chapter 4, absorbed water has a detrimental impact on biocomposite mechanical properties. The time dependent water absorption was examined to determine a predictive absorption model. Motivation for investigation is borne from the fact that current models do not account for long term water absorption as demonstrated in section 2. A multitude of experimental techniques were used to identify critical absorption factors and quantify their impact on long term water absorption. A new mathematical model of water absorption is proposed for a variety of biocomposites. The proposed model predicts water absorption behaviour from all material variations and specimen types analyzed in this work. The predicted model parameters are dependent on three parameters: 1) fiber volume fraction, 2) fraction of surface accessible fiber surface area, and 3) initial diffusion coefficient. The new mathematical model fits the data extremely well with  $R^2_{\text{DOF}}$  ranging from 0.96 to 1.00 due to the addition of an additional new term to account for fiber loss upon immersion.

## 5.1 VISUAL CHARACTERIZATION OF BIOCOMPOSITES

Factors that influence the biocomposite response to water immersion which had been identified by UV Macrophotography and Scanning Electron Microscopy (SEM) techniques were used to assess the location of absorbed water, the location of fiber within the matrix, respectively. The UV water soluble dye acted as a visual marker for tracing the location of absorbed water as shown in Figure 5.1. The UV dye was absorbed into the natural fibers accessible at the biocomposite surface (i.e., fibers intersecting the specimen surface and open to the immersion environment). Factors affecting absorption include: 1) matrix type, 2) fiber content, 3) fiber dispersion, 4) fiber distribution and 5) flux of UV dye as a function of time. The absence of fluorescence within LDPE confirms the conclusion in section 5.1.1 that water absorption is fiber dependent.

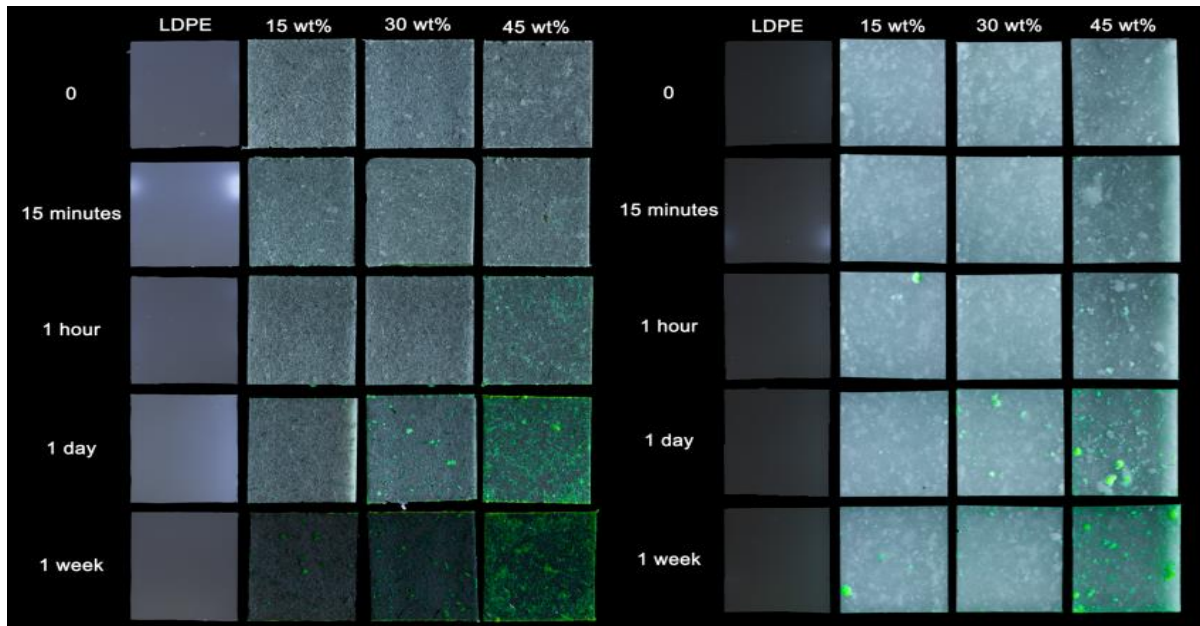


Figure 5.1 Time series of immersed UV dyed hemp (left) and wood pulp (right) filled low density polyethylene square specimens. The green dyed regions correspond only with fibers intersecting the surface of the specimen and the intensity increases with immersion time.

The fluorescent intensity, therefore quantity of dye, increases as a function of time for natural fibers exposed at the surface of the biocomposite. The UV dye illustrates how the flux of water into the biocomposite is controlled by natural fibers present at the surface. Higher volume fractions of fibers within the biocomposites correlate to higher amounts of dye uptake. Therefore, the initial stage of water absorption is controlled by the quantity of natural fibers

present at the surface. The quantity of the fiber available on the surface must be quantified to obtain a flux of water through the surface area, see section 5.3.1.

On closer examination of 1 week immersed UV dye specimens, illustrated in Figure 5.2, the quantity of fluorescent fibers at the surface with absorbed UV dye is not directly proportional to the known fiber volume fraction as far as the eye can judge. An indepth investigation conducted in section 5.3.1 confirms the disconnect between the fiber volume fraction and surface accessible fiber.

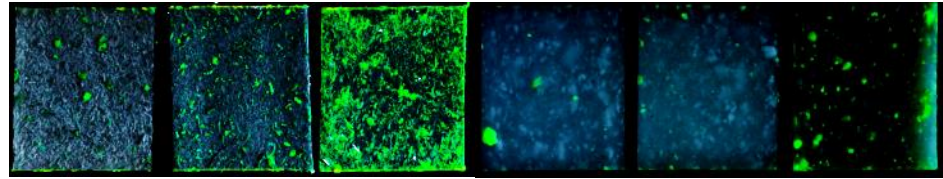


Figure 5.2 LH series (left) and LW series (right) after UV Dye Immersion of 1 week.

The difference in fiber content exposed at the surface compared to the bulk material was investigated by cross sectional micrographs of LH30 and LH45, as shown in Figure 5.3. The fiber fraction is not uniform from the as molded surface inward to the bulk of the biocomposite, left to right as illustrated in Figure 5.3; a gradient exists. A thin film of polyethylene has been identified on the molded surface, commonly referred to as the “skin”. The skin effect occurred due to two phase flow, molten plastic and particle reinforcement, in the mold cavity. The molten thermoplastic cooled on the mold surface while the remainder of the cavity was filled with the bulk of the material when it was injection molded. The ability of the molten plastic to flow and cool at the mold surface decreases with increased fiber fraction. Therefore, at increased fiber fractions, the difference between the surface and bulk material is decreased.

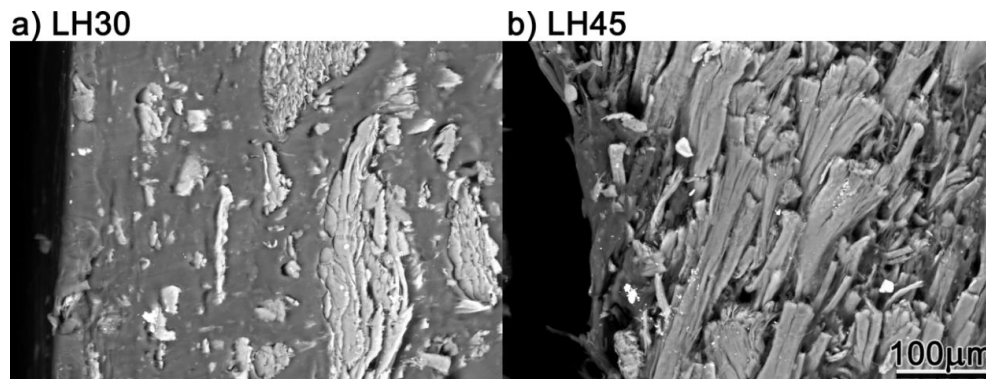


Figure 5.3 Back scattered cross sectional assessment of fiber distribution from as molded surface, left, into the bulk biocomposite, right for a) LH30 and b) LH45. Note the increasing gradient in fiber concentration going from left to right in each image; the width of the fiber gradient is much smaller for LH45 (b) than LH30 (a)

Micrographs, Figure 5.2 - Figure 5.4, support the conclusion that the manufactured biocomposites are not homogenous isotropic materials but rather have two distinct structural morphologies: 1) at the surface of the biocomposite, and 2) the bulk of the material. A fiber concentration gradient exists in the transition from one structural morphology, as-molded surface, to the bulk of the material which is dependent on fiber volume fraction. The assumption of biocomposites with 100% random orientation and isotropic properties is proven incorrect. Future work is suggested to model fiber orientation to predict the percentage of fibers on the surface and quantify “fiberflow” within various thermoplastic systems.

### 5.1.1 ASSESSMENT OF SURFACE AREA PERCENT FIBER

Different surface configurations were assessed to determine the quantity of natural fibers present on the surface of the biocomposite; the location where water flux initiates. The four surface configurations are 1) as-molded (top surface), 2) as-molded perimeter, 3) transverse cut and 4) longitudinal cut as shown in Figure 5.4a. Three of the four surface types in Figure 5.4b demonstrate the difference in exposed surface fiber content by fluorescence. The transverse and longitudinal cut surfaces have more exposed surface fibers than the as molded surface.

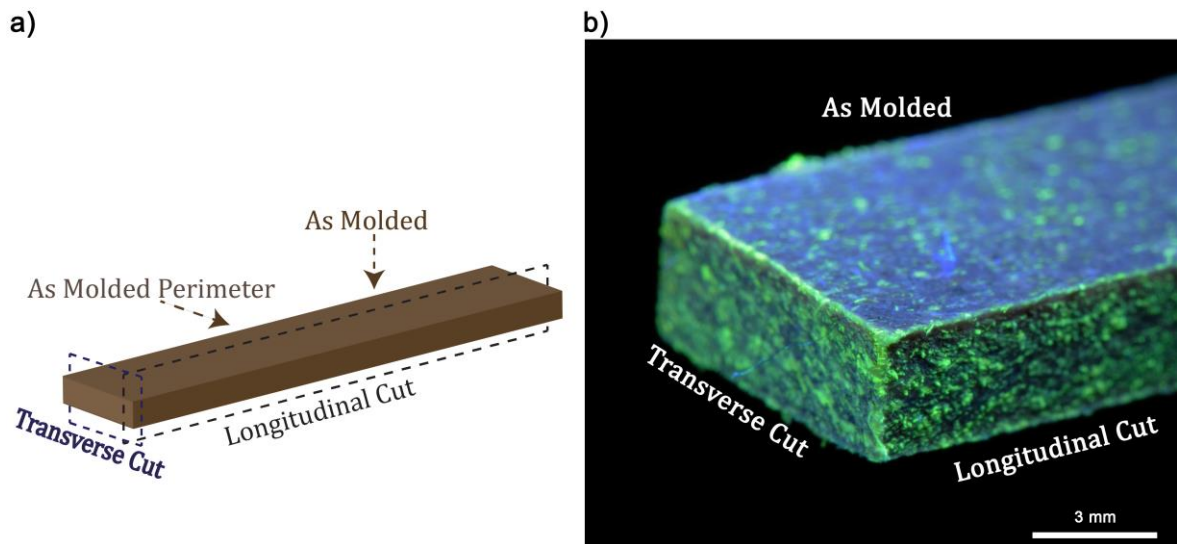


Figure 5.4 a) Schematic of the four types of surfaces: as-molded, as-molded perimeter, transverse and longitudinal cut. b) Green fluorescence maps the higher concentration of natural fibers on the cut surfaces relative to the molded of LH45 after 1 week immersion.

Image analysis was performed on BS-SEM images of each surface type as molded, as-molded-perimeter, transverse cut and longitudinal cut as per section 3.2.5.2 and 3.2.6 to determine

percentage of surface accessible fiber for all biocomposite variations. For all biocomposite variations illustrated in Figure 5.5 the machined surfaces (transverse and longitudinal) display a greater percentage of fiber compared to the as molded surfaces which is consistent with Figure 5.4. Typically, the longitudinal cut surface had the highest content of surface exposed fibers, however the amount was dependent on the material composition. Transverse cut surface displayed the highest variability in percentage of fiber. It is theorized that this variability is due to fiber pull out or excess fiber remaining as the saw blade was not sharp enough to capture a cross section but rather resulted in the fibers being pulled out of the sample since the saw blade travelled perpendicular to the mold flow direction. All image analysis results are tabulated in Appendix F1.

A noticeable difference exists between as molded and as molded perimeter surface types. The difference between the surface types has been attributed to the difference in melt flow index(MFI) of LDPE compared to HDPE. LDPE variations display an insignificant difference between “as molded” and “as molded perimeter” surface, due to the ability of the polymer resin to evenly cover the mold surface at low fiber fractions. However, HDPE variations displayed a noticeable difference which suggests HDPE did not cover the mold surface to the same extent. Since LDPE has a higher melt flow index than HDPE, it explains the little variation at low fiber contents. At high fiber contents, the as molded perimeter has displayed high surface accessible fiber percentage with the exception of LW. In conjunction with fiber content, melt flow index (MFI) should be a consideration for mold design with respect to surface fiber accessibility.



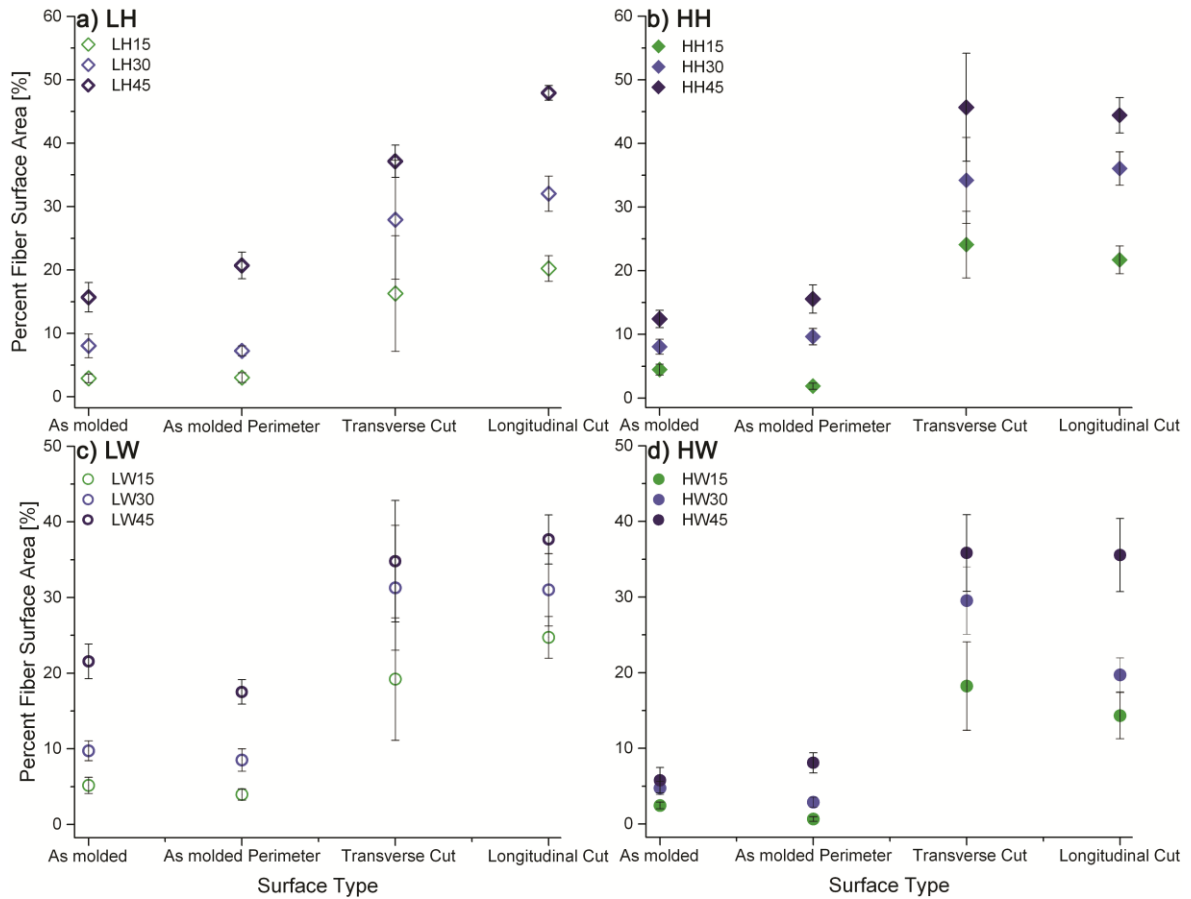


Figure 5.5: Overview of the surface types and the corresponding accessible fiber on the biocomposite surface of variations: a) LH, b) HH, c) LW and d) HW. As-molded surfaces have less accessible fiber content which intersects the biocomposite surface.

From the accessible fiber percentage determined for each surface type, the overall specimen surface area fraction of fiber was calculated for each variation and specimen geometry; reference Appendix A2. Three noticeable groupings of percent surface area fiber occur, as shown in Figure 5.6, at each fiber content. The group with this highest percentage of exposed natural fiber includes specimen geometries 4 cut and 2 longitudinal cut. The minimum percentage of exposed fiber comprised of specimen geometries as-molded flexural, 2 transverse cut and tensile. The percentage of fiber at the surface increases with increased proportion of cut surfaces to molded surfaces, as explained from the clusters of surface area fraction.

The accessible surface area of fiber linearly correlates with the volume fraction of fiber. The percentage of accessible fiber at the surface is typically *less* than the bulk volume fraction of fiber; demonstrated with the data shown underneath the 1:1 guideline in Figure 5.6. For

LDPE biocomposites the fiber surface area fraction is nearly linearly proportional to the fiber volume fraction for 4 cut and 2 longitudinal cut specimen geometries. However, linear proportionality was not the case for HDPE reinforced specimens, as the percentage of exposed fibers lags in the amount relative to the volume fraction of fiber. LDPE has a lower melt flow index (MFI) which allowed for increased fiber movement within the melt that resulted in a reduced natural fiber density gradient from surface to bulk. Although LDPE biocomposites contained a lower fiber volume fraction, the effective surface accessible fiber content on the surface was greater than HDPE biocomposites. The magnitude of water absorption of LDPE was also greater as shown in section 5.2.2 and 0. Therefore, the effective fiber content of the biocomposites is based on the surface accessible fiber fraction.

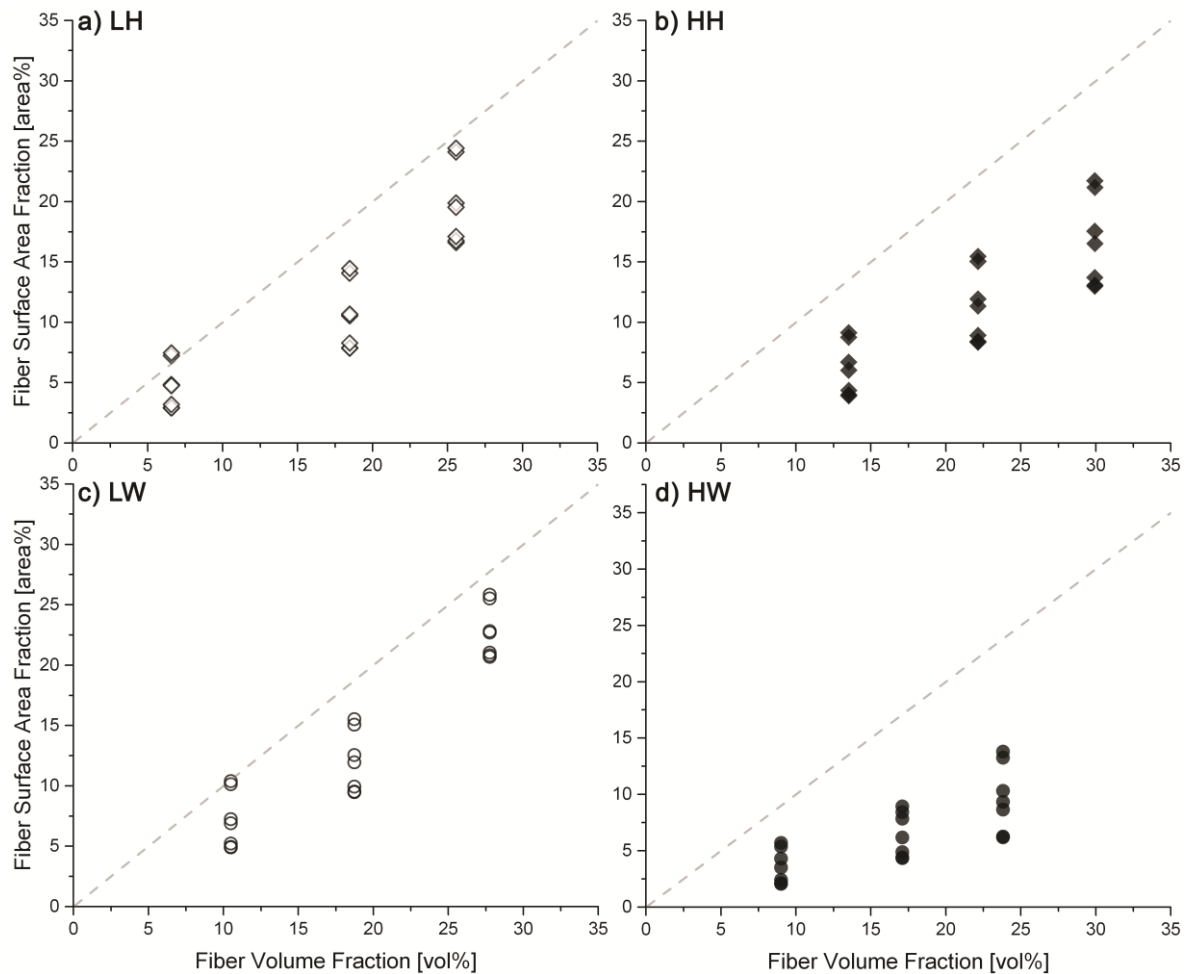


Figure 5.6 Relationship between fiber volume fraction and calculated percentage of fiber surface area with specimen geometries for all material variations; x = y dashed gray guideline for reference.

The natural fiber distribution gradient is clearly illustrated in Figure 5.7 as the results from both longitudinal and transverse cut surfaces are compared relative to the molded surface. The differential between the cut surface and the as molded surface (y-axis) decreases with increasing volume fraction to near homogenous material, with the exception of HW45. Conversely, the effect of additional machined surfaces decreases at high fiber contents since the effect of the “skin” diminishes.

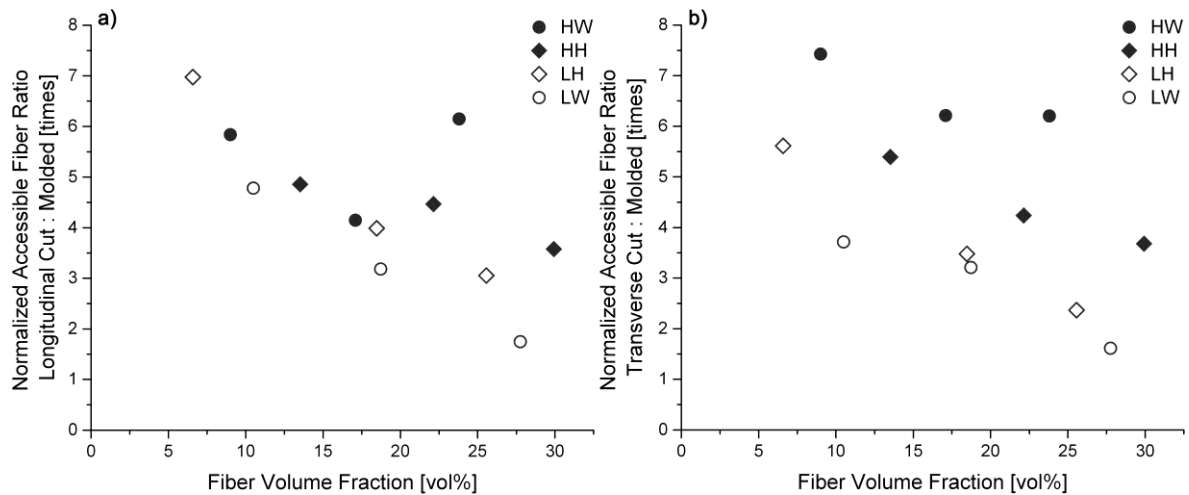


Figure 5.7 Surface area of fiber, normalized longitudinal cut relative to molded surface (a) and normalized transverse cut relative to molded surface (b). Notice as the fiber volume fraction increases, the surface area of accessible fiber approaches a homogenous material with the same ratio of fibers on the longitudinal(left) and transverse (right) relative to the molded surface, represented with a near 1:1 ratio.

An example of the effect of a machine cut surface relative to a molded specimen is given in Figure 5.8. The additional fibers influence the rate of absorption, magnitude of water absorbed and the biocomposites long term response. Therefore, the surface accessible fiber content is a critical factor in water absorption for both short term and long term immersion.

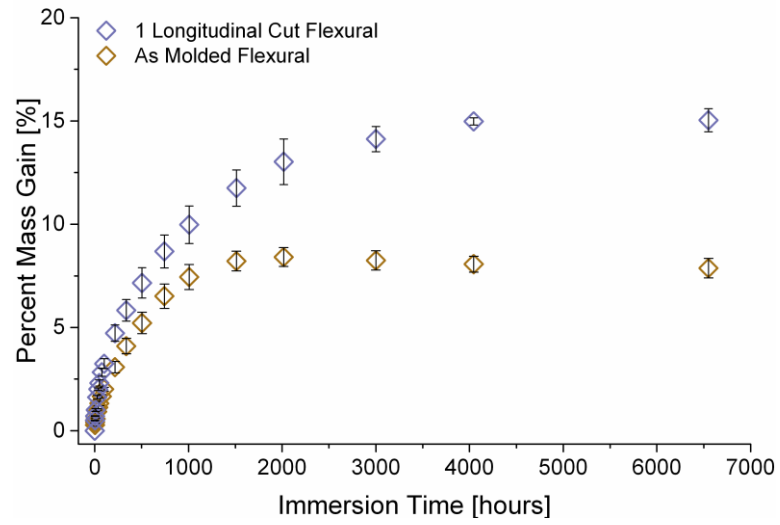


Figure 5.8 Effect of one longitudinal cut on the absorption profile of HH30. By sectioning the specimen, a 2-fold increase in maximum mass gain was observed for this material combination.

## 5.2 COMPREHENSIVE WATER ABSORPTION CURVES

A comprehensive data set of 12 biocomposite material compositions, detailed in Table 4.3, and 7 specimen geometries, illustrated in Figure 3.10 and Figure 3.14 were tested with controls for a total of 98 absorption curves. The duration of immersion was over 4000 hours (24 weeks) *longer* than the majority of studies with specimens immersed up to 9000 hours (53.5 weeks) to examine long term behaviour. The array of biocomposite composition and specimen types allow for conclusions to be drawn between matrix material, fiber types, fiber content and specimen geometry. The extensive material variations, specimen geometries and duration of immersion are unique aspects of the data.

The water absorption curves for each material variation and specimen type are displayed in with respect to virgin matrix control, Figure 5.9, hemp fiber reinforced, Figure 5.10 and wood pulp reinforced biocomposites Figure 5.11.

### 5.2.1 MATRIX

The water absorbed for both matrix types is negligible for all specimen geometries, with the average absorbed water of -0.03% for HDPE and -0.04 % for LDPE. The scatter in data shown in Figure 5.9 is attributed with measurement error caused by static charge build up from drying the specimens. Due to differences in dielectric properties of high and low density polyethylene, the drying process had a larger impact on the HDPE samples. The impact appears magnified as a slight change in mass results in a greater percentage change since the matrices are less dense than the biocomposite materials.

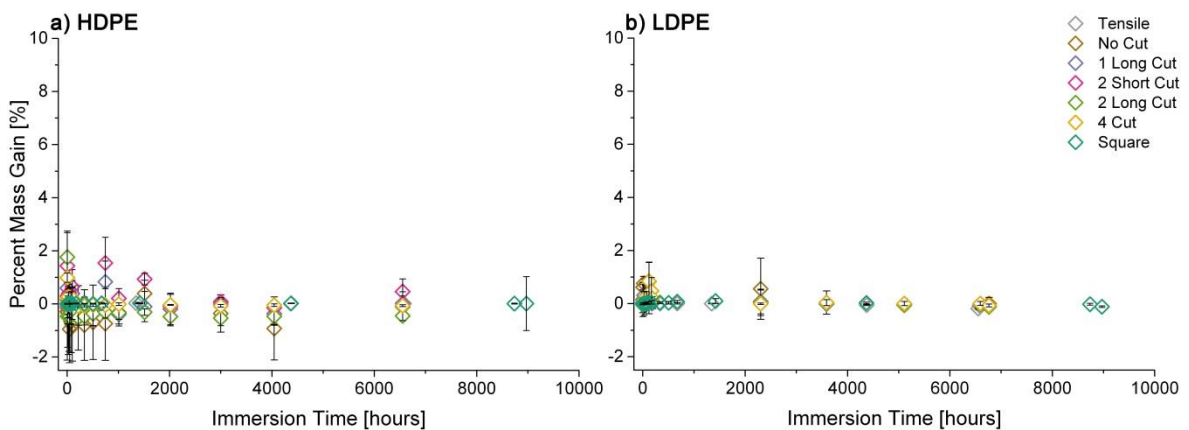


Figure 5.9 Water Absorption of control matrix materials: a) HDPE (left) and b) LDPE (right) up to 9000 hours immersion time.

### 5.2.2 HEMP REINFORCED BIOCOMPOSITES

The general response of the absorption curve is impacted by matrix type, and fiber content. Hemp reinforced biocomposites absorb water as the duration of immersion time increases as shown in Figure 5.10. An increase in fiber content results in an increase in both the magnitude and rate of water absorbed. A direct comparison cannot be made between LH and HH variations because of the different experimental volume fraction of fibers at each targeted fraction, reference for volume fraction of fiber Table 4.1.

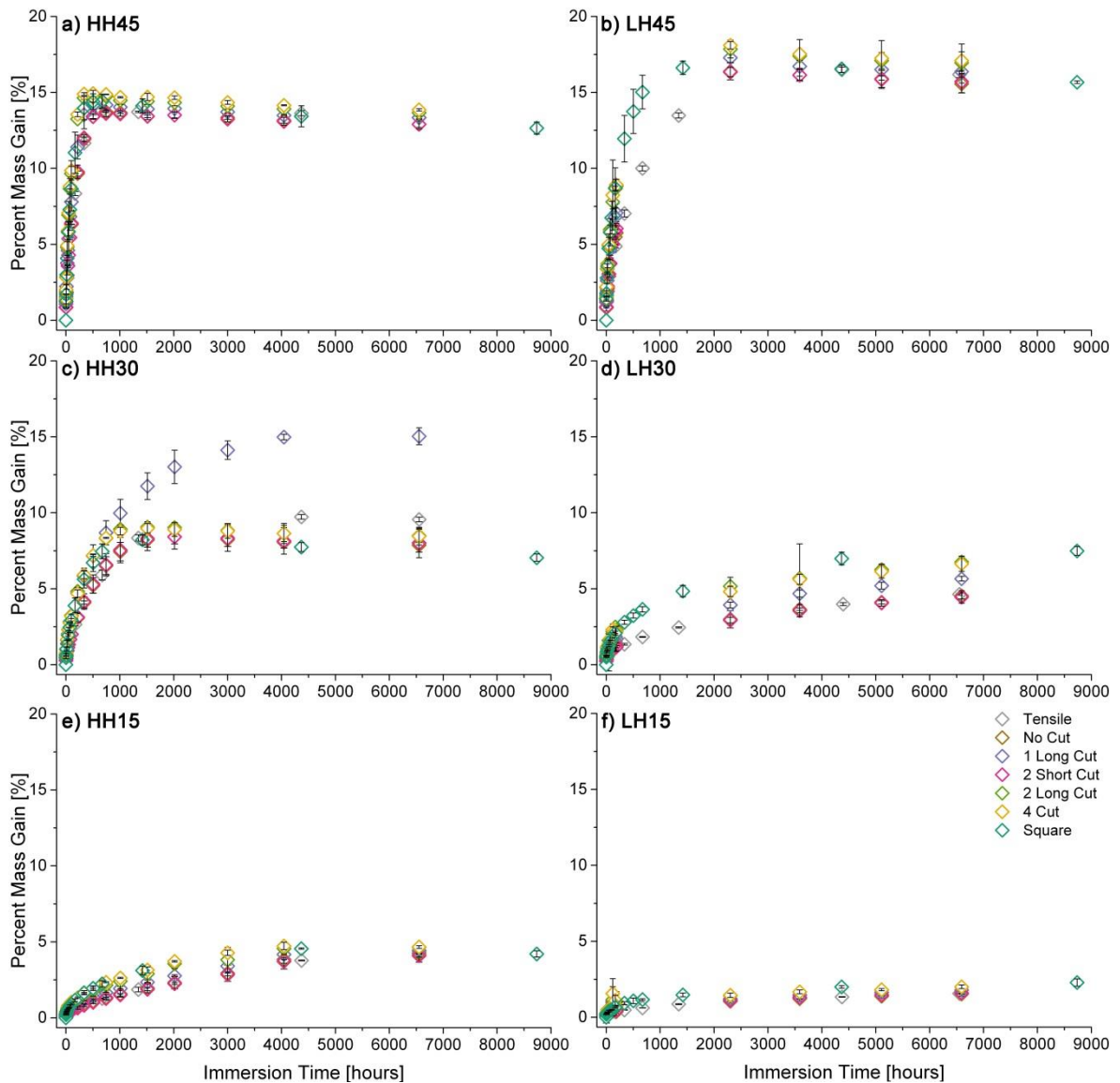


Figure 5.10 Water Absorption of hemp fiber reinforced biocomposites for both HDPE (left) and LDPE (right) arranged from high fiber fill fractions (top) to lower fill fractions (bottom) up to 9000 hours immersion time. Higher volume fractions of fibers result in higher rates of water absorption and larger magnitudes of total water absorption.

The impact of specimen geometry was minimal at low fiber variations due to a small amount of fiber exposed to immersion environment. An increase in fiber content results in an increase in both quantity and rate of water ingress. The greater the number of cut surfaces resulted in more water being absorbed. The difference between specimen types becomes more noticeable as the fiber content increases. It is hypothesized that there is little to no difference at the greatest fiber content, due to the theoretical maximum water uptake, see section 5.4.3.

### *5.2.3 WOOD PULP REINFORCED BIOCOMPOSITES*

The water absorption curves for wood pulp reinforced HDPE and LDPE biocomposites are illustrated in Figure 5.11. The quantity of water absorbed increases with increasing fiber content. The magnitude of water absorbed for wood pulp (absorbed water from 1.2-7.5%) is significantly less than hemp fiber (absorbed water from 1.5-18.1%) observed in Figure 5.10. For wood pulp reinforced biocomposites, variation in specimen geometries demonstrated a less distinct change in absorption than hemp fiber with increased number of cut surfaces due to a lower magnitude of water absorbed. Increase cut surfaces did result in an increase in water absorption. The water absorption responses for wood pulp biocomposites are independent of matrix type.

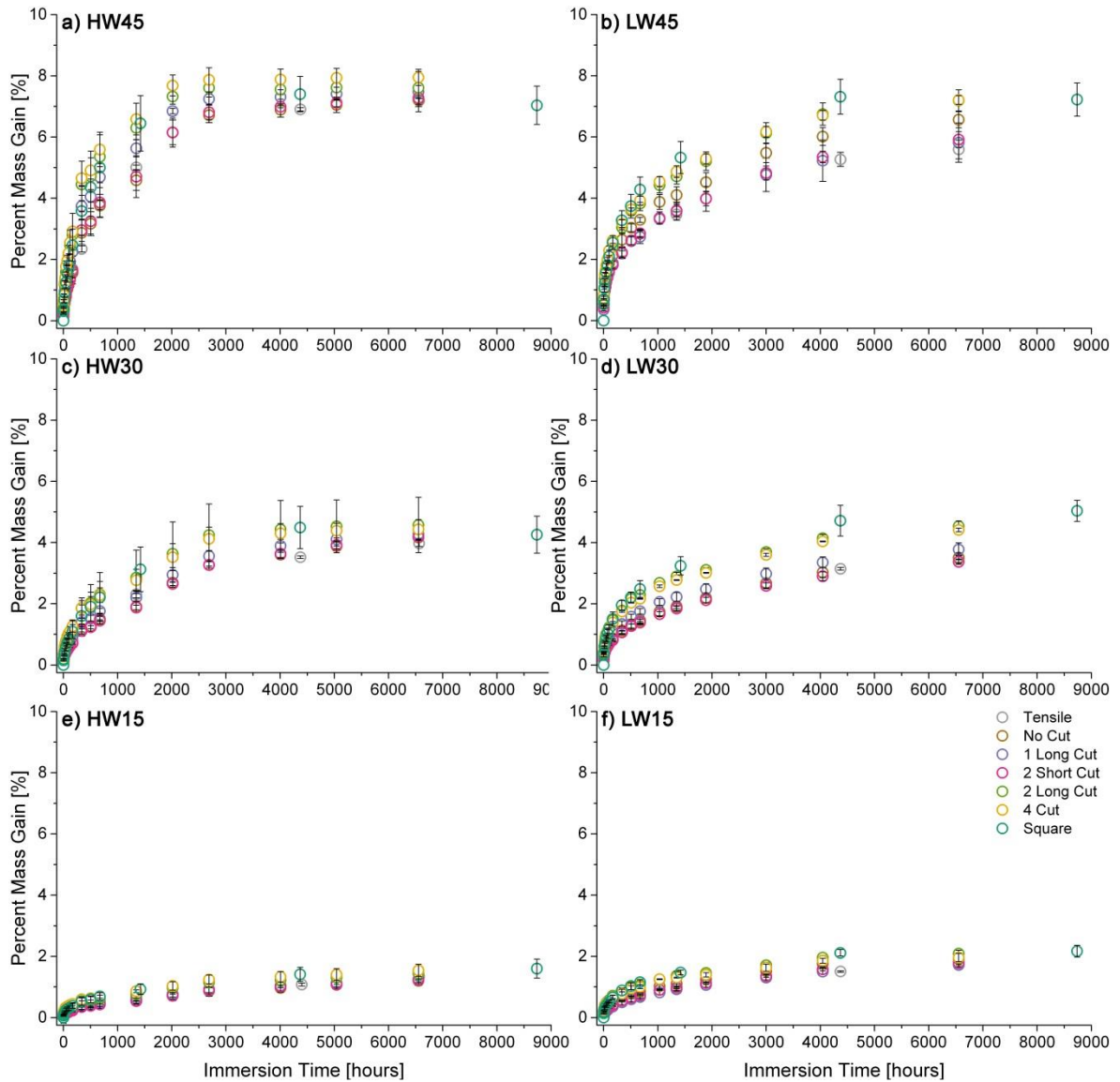


Figure 5.11 Wood Pulp reinforced biocomposites with (left) LDPE and (right) HDPE arranged from high fiber fill fractions (top) to lower fill fractions (bottom). As for hemp (Figure 5.10) higher water absorption is associated with higher volume fractions of wood pulp fibers.

#### 5.2.4 FIBER VOLUME FRACTION & MAXIMUM WATER ABSORPTION

For both fiber types, an increase in fiber volume fraction resulted in an increase in maximum amount of water absorbed, as shown in Figure 5.12. Wood pulp fiber types demonstrate a linear increase in maximum water absorbed with fiber volume fraction. The response of hemp fiber was dependent on matrix type. Hemp reinforced HDPE (HH) also showed a linear increase whereas hemp reinforced LDPE (LH) demonstrated a parabolic increase in



maximum water absorbed. The difference in response of LH suggests the importance of fiber connectivity within the injection molded material structure which increases as fiber contents are increased. Since, LH variations contain lower fiber contents than HH, it is inferred that the difference in material structure was caused during the manufacturing process from the difference in melt flow indexes (MFI). At each volume fraction, hemp demonstrated a greater range of water absorbed due to specimen geometry. HDPE variations displayed a smaller range of water absorbed compared to LDPE based biocomposites.

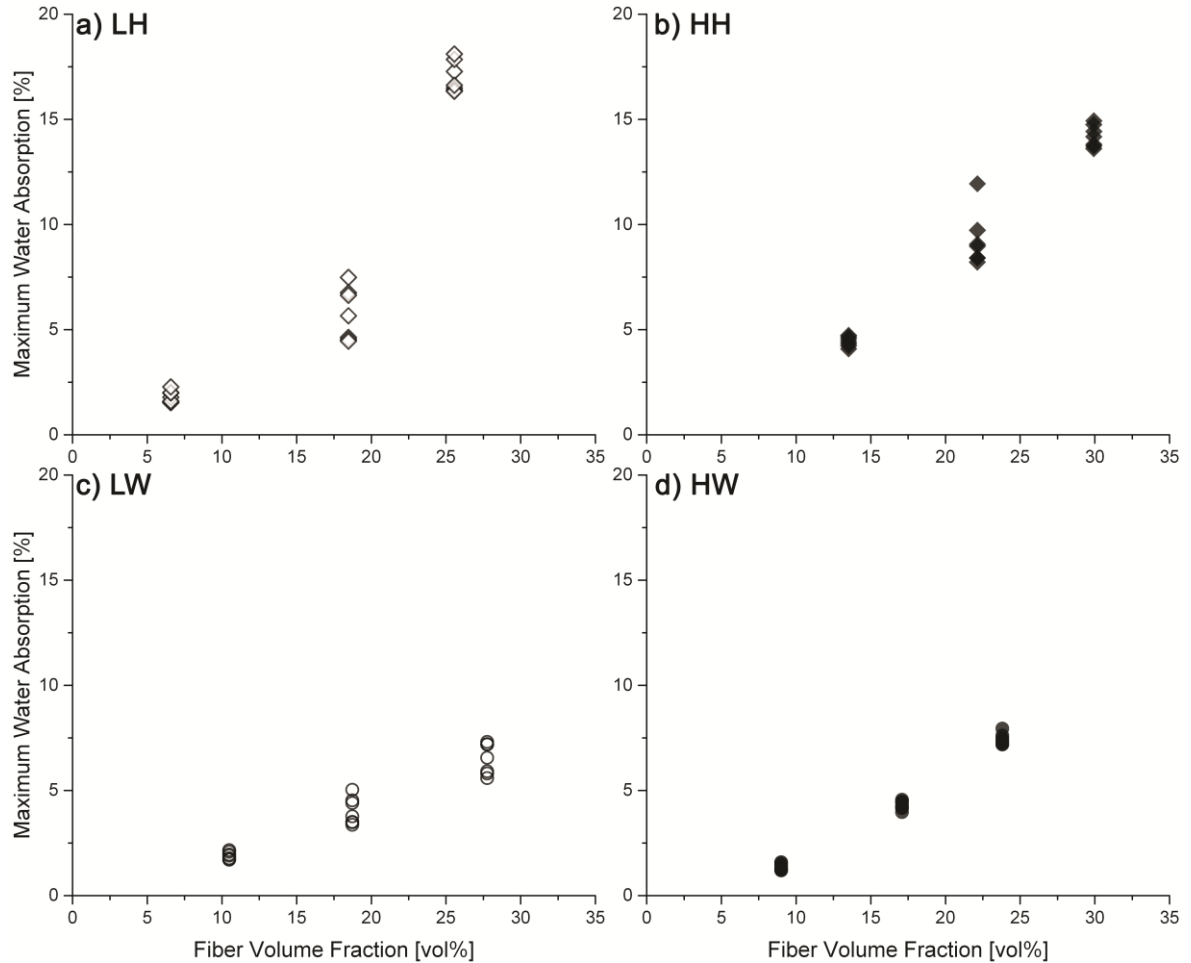


Figure 5.12 Maximum magnitude of water absorbed during 6552 hours of immersion for all specimens as a function of fiber volume fraction. Hemp fiber reinforced biocomposites absorb a greater amount of water than wood pulp variations and the maximum amount absorbed increases linearly with fiber volume fraction with the exception of LH45.

### 5.2.5 OVERVIEW OF WATER ABSORPTION OF FIBER REINFORCED BIOCOMPOSITES

An increase in fiber content for both hemp fiber and wood pulp reinforced biocomposites resulted in an increased rate of absorption and quantity of water absorbed. The differences in water absorption for the various geometries are noticeably discerned as the fiber content increases, with the exception of HH45 and LH45. The duration required to observe negligible further mass gains varied based on fiber type, fiber content and specimen geometry. The time required to reach equilibrium is a unique aspect of the data, where most studies assume equilibrium has been reached at 120 hours independent of specimen geometry. Even for HW15 a minimum immersion time *greater* than 3500 hours was required to establish a negligible change in specimen mass.

### 5.3 REVERSIBILITY OF WATER ABSORPTION – DRYING

From chapter 4, water absorption was shown to cause irreversible mechanical damage. The permanent decrease in mechanical properties was associated with mass loss (from fiber degradation). The biocomposite variations were investigated by both the assessment of changes in surface morphology after immersion and the magnitude of mass loss experienced for 65 specimen<sup>1</sup> variations.

#### 5.3.1 SURFACE FIBER DEGRADATION

Each fiber and matrix combination at the highest fiber content was assessed by BS-SEM to investigate if any physical effects were noticed after immersion. The same location on the specimen surface was imaged prior to immersion, 1 week (168 hours) and 5 weeks (850 hours) after water immersion, shown in Figure 5.13 for HH45. The natural fiber began to degrade after 168 hours (1 week). After 5 weeks immersed the natural fibers disappeared from the biocomposite surface. This phenomenon, loss of surface accessible fiber, occurred for both natural fiber types in both matrices as illustrated in Figure 5.14. The majority of the natural fibers disappeared from the surface after 5 weeks immersion. The plausible mechanisms for fiber loss include dissolution, microbial attack, dislodging from physical experimental handling (rare), or a combination of mechanisms.

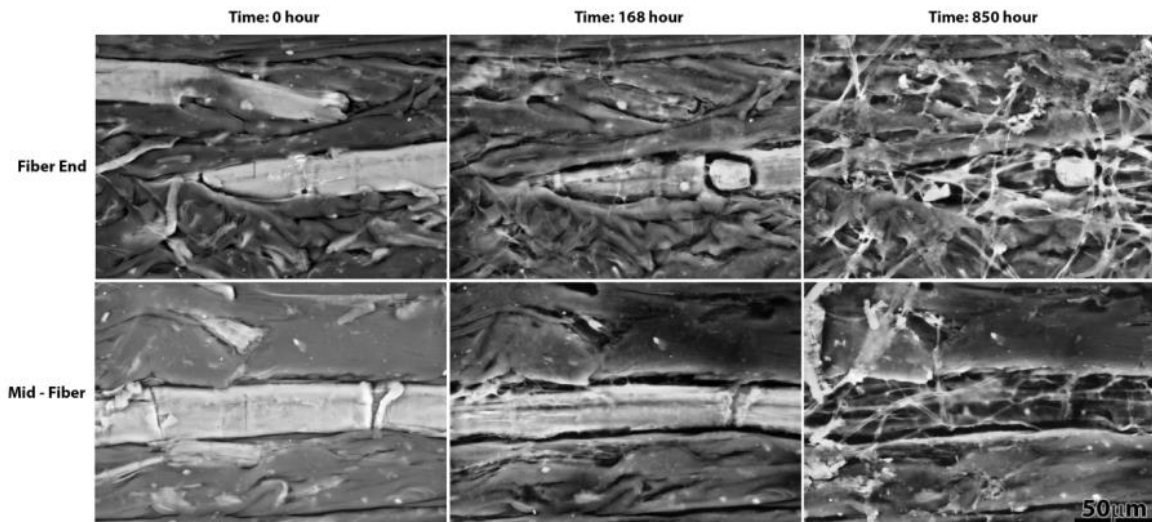


Figure 5.13 Two locations of hemp fiber present on an as-molded surface within high density polyethylene (HH45), imaged as a function of increasing time (left to right). The fiber degraded, and disappeared from the surface as a function of increase in immersion time.

<sup>1</sup> HW cut geometry specimens, 19 of 84 biocomposite variations, were accidentally destroyed from an error in experimental handling. Therefore the data was not obtained.

Removal from experimental handling is not supported by the micrographs since an EDX spectrum was obtained on the fiber which resulted in a cubic structure etched in the fiber shown in the 168 hour fiber end micrograph, (Figure 5.13). The lack of change in the cubic structure after 4 weeks of immersion supports that the fiber was not affected from the intense electron sampling was removed but the burned fiber remained embedded in the matrix.

The stringy spider like white line morphology present at 850 hours in Figure 5.14, suggests a mechanism of microorganism/fungal attack of surface accessible hemp fibers across the general biocomposite surface, which is not a localized phenomenon. The absence of these morphological indicators for wood pulp reinforced biocomposites suggests this phenomenon occurs to a lesser extent and/or at a slower rate which cannot be confirmed by the micrographs. However, since the fibers are not present after the same amount of immersion time, a dissolution mechanism in addition to microbial attack is likely; the gradual nature of fiber loss in Figure 5.13 supports a combination of both dissolution and microbial attack mechanisms.

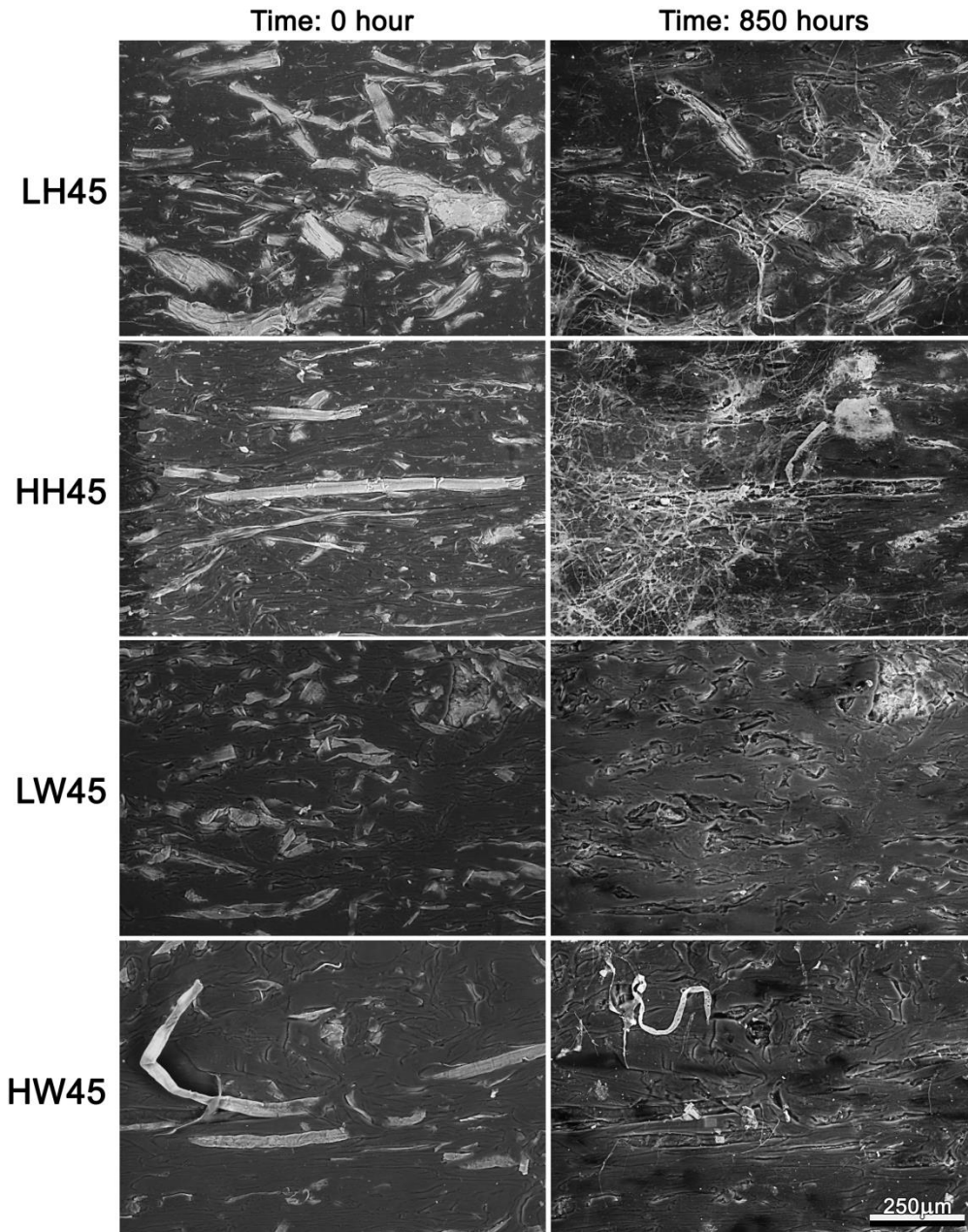


Figure 5.14 BS-SEM micrographs of high fiber fraction biocomposites surface morphology prior to and after 5 weeks of water immersion to demonstrate the loss of surface accessible fiber. Extent of fiber loss for all material variations due to water immersion.

### 5.3.2 GRAVIMETRIC QUANTIFICATION OF FIBER LOSS

The relative amount of fiber loss was quantified as the difference between the mass of specimen prior to immersion and the specimens' dried mass after maximum immersion, as shown in equation 5.1. The results are reported in terms of percent dried mass. A negative result means the specimen lost mass, predominately attributed to fiber loss as shown in

Figure 5.13 and Figure 5.14. Whereas, a positive result indicates that the specimen either retained moisture or accumulated biomass from biological attack; drying was conducted after the longest immersion duration for only one week as detailed in section 3.2.2. The relative percent dried mass, given in Equation 5.1, was not monitored as a function of drying time to determine the effective drying time required to reach negligible change of each material variation. Therefore, the calculated dried masses are not conclusive rather partial measures during the drying process. However, the metric does provide a relative measure to illustrate the extent of the magnitude of mass loss.

$$\text{Percent Dried Mass} = \frac{m_{final} - m_{initial}}{m_{initial}} \times 100 \quad (5.1)$$

LDPE based biocomposites demonstrated a lower magnitude of fiber loss than HDPE as shown in **Figure 5.15**. It is hypothesized that LDPE's lower stiffness and higher malleability allowed for the fibers to swell from absorbed water alleviating internal stresses which reduced the number of fibers lost.

The relative mass loss for both hemp fiber and wood pulp are illustrated in Figure 5.16. Both fiber reinforcement types experienced quantifiable mass loss, attributed to loss of fiber. As fiber volume fraction increased a subsequent increase in specimen mass loss occurred. The magnitude of mass loss for wood pulp was less significant than hemp fiber, which is supported by the visual evidence in Figure 5.14. For both matrices, an increase in volume fraction of fiber resulted in an increase in the mass loss. Therefore, both the gravimetric measurements and surface morphological assessment corroborate that mass loss is attributed to fiber loss.

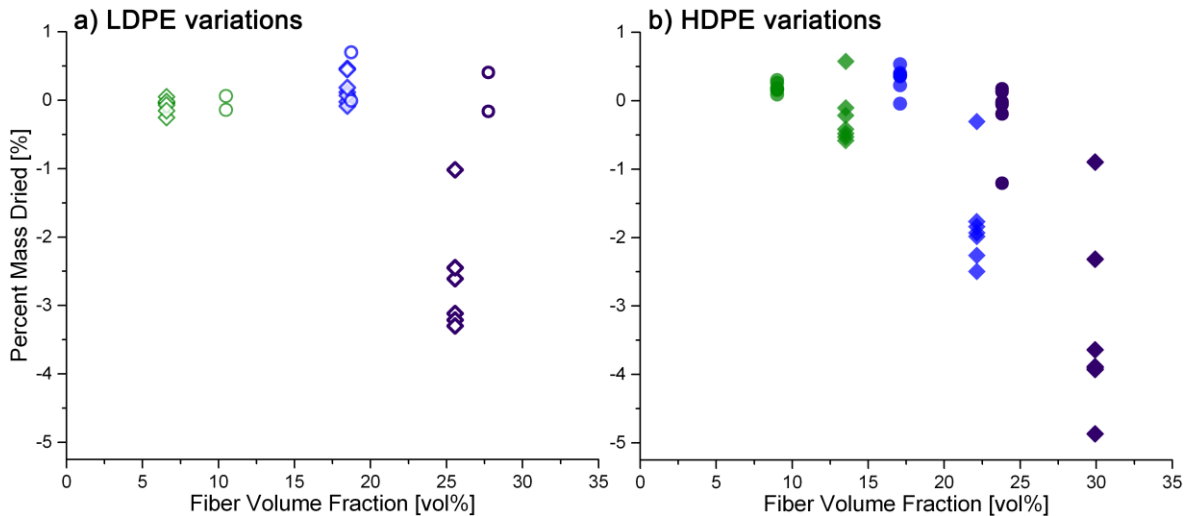


Figure 5.15 Comparison of LDPE and HDPE percent dried mass after 6552 hours immersion based on fiber volume fraction for hemp (diamond) and wood pulp (circle).

Since the fiber loss occurs from the surface, there must be sufficient quantity of surface area fiber for the fiber loss to impact the overall water absorption. From Figure 5.16 for both fiber types an increase in fiber surface area to volume ratio within each fiber fraction results in a slight increase in mass loss observed. The impact of fiber loss on the overall water absorption decreases as the specimen thickness increases due to reduction in ratio of surface area fiber to volume of the specimen.

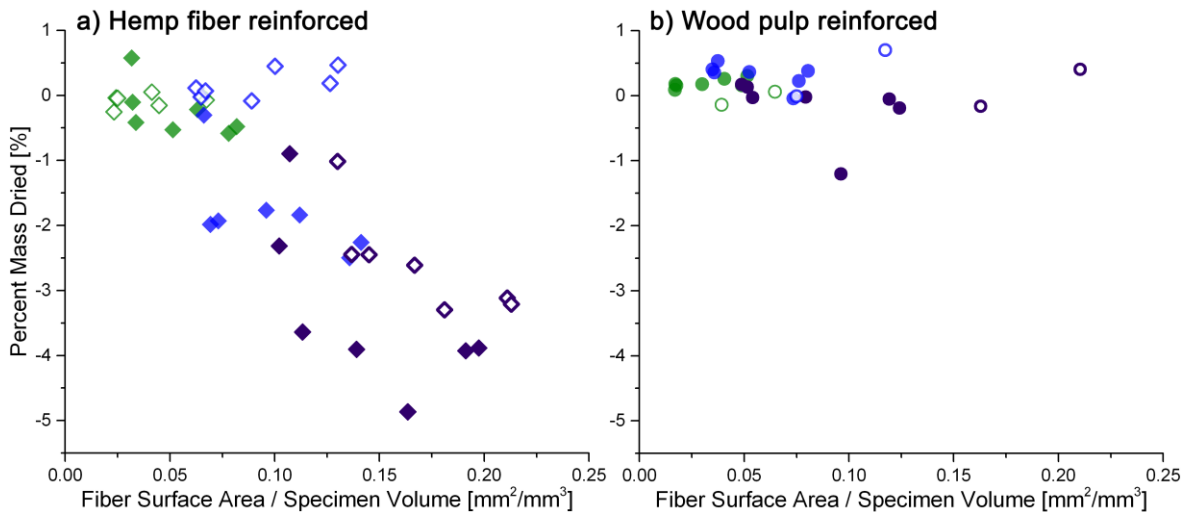


Figure 5.16 Comparison of percent dried mass after 6552 hours immersion a) hemp and b) wood pulp reinforced biocomposites HDPE (filled) and LDPE (unfilled) based on ratio of accessible fiber surface area to specimen volume. Wood pulp biocomposites did not endure appreciable mass loss as did hemp fiber, the latter which is inversely proportional to the ratio of accessible fiber area to specimen volume.

The extent of fiber degradation diminishes through the thickness as the specimens' surface accessible fiber decreases. The surface accessible fiber area of the specimen may or may not

be connected through thickness of the specimen. The extent of fiber degradation to the fibers directly underneath the surface is unknown. Many fibers are “land locked” or “partially land locked” by the matrix within the biocomposite, as illustrated in Figure 5.17, yet some exhibit connectivity.

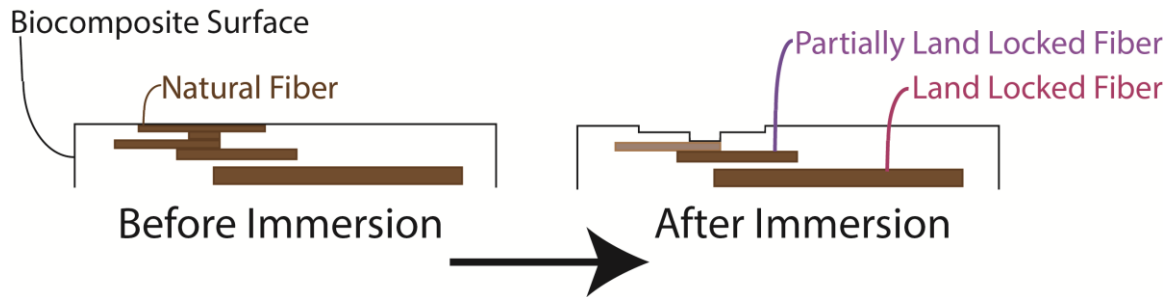


Figure 5.17 Cross sectional illustration of natural fiber dissolution from the surface to the bulk material. Interconnection of natural fibers to the surface; it remains unknown and therefore so does the depth of interconnected fiber loss.

However, it is speculated that if the fiber volume fraction is high enough to obtain fiber connectivity through thickness that with sufficient time all the fiber would degrade to leave only the matrix material. For thermoplastic moldable biocomposite commercial formulations, it is unlikely that through thickness fiber connectivity would occur due to the difficulties associated with processing high fiber volume fraction biocomposites. For applications with degradable matrices, this biocomposite material architecture may be desirable for providing layered - layered exposure to the environment. However LH45 demonstrates this interconnectivity of fibers through thickness, and is discussed in section 5.4.3.



## 5.4 ANALYSIS OF CURRENT WATER ABSORPTION MODELS

The validity of existing water absorption mechanisms and models were tested against experimental data collected to assess water movement within biocomposites. Representative absorption curves were selected to represent the three long term water absorption specimen responses observed in Figure 5.9, Figure 5.10, and Figure 5.11. The three generic material responses are illustrated in Figure 5.18; the three material responses have been classified by the biocomposites long term response: a) continued gradual increase (maroon), b) established steady state (navy), c) inevitable gradual decay (purple).

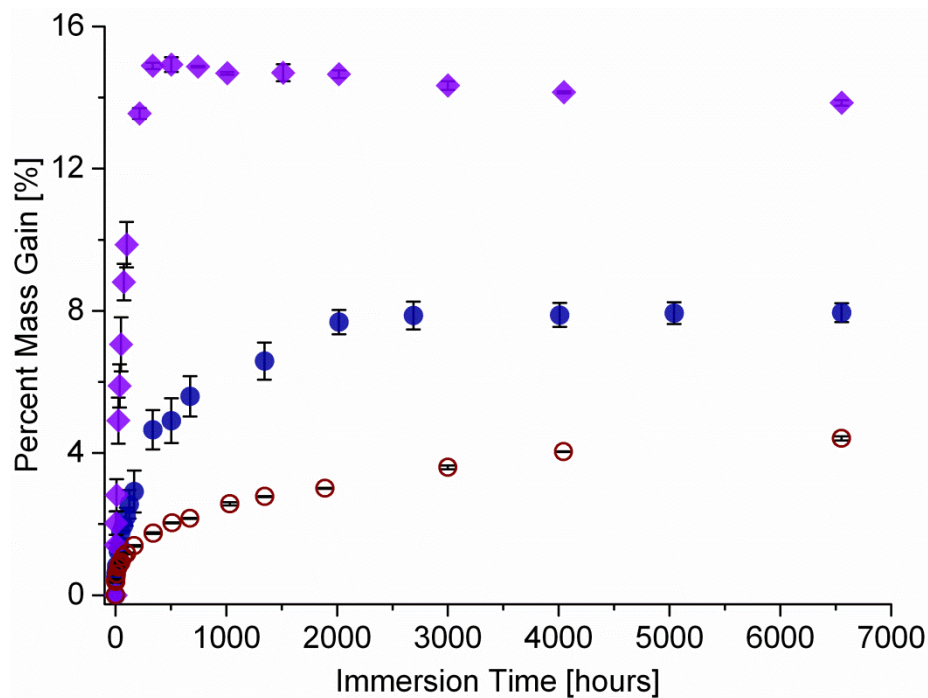


Figure 5.18 Representative water absorption curves isolated from HH45 (purple diamond filled), HW45 (blue circle filled) and LW30 (maroon circle unfilled) all 4 cut specimen type.

Table 5.1: Characteristic curves classification of the type of diffusion cases, reported in terms of  $n$ ,  $k$  and maximum content of water absorbed for 4 cut geometries assessed up to 100 hours.

Biocomposite	$n$	$k$ ( $10^{-3}s^2$ )	$M_{\infty}$ (%)
LW30	0.362	2.329	4.41
HW45	0.403	1.622	7.95
HH45	0.509	0.992	14.93

### 5.4.1 TRANSPORT OF WATER BY PRESSURE

Sar and other authors have established the significant effect of external pressure on the kinetics of moisture diffusion in polymers due to internal stress states caused by the coefficient of moisture expansion[1]. A plausible method to increase mass transport rates is the addition of pressure onto a material to push the water into the material. HH45 was selected to undergo a pressure dependency test on mass gain due to its high fiber content to illustrate the biggest effect in the smallest time frame. In order to identify mechanisms associated with two pressure conditions: 1 bar and 50 bar. The comparative water absorption curve under both conditions is illustrated in Figure 5.19.

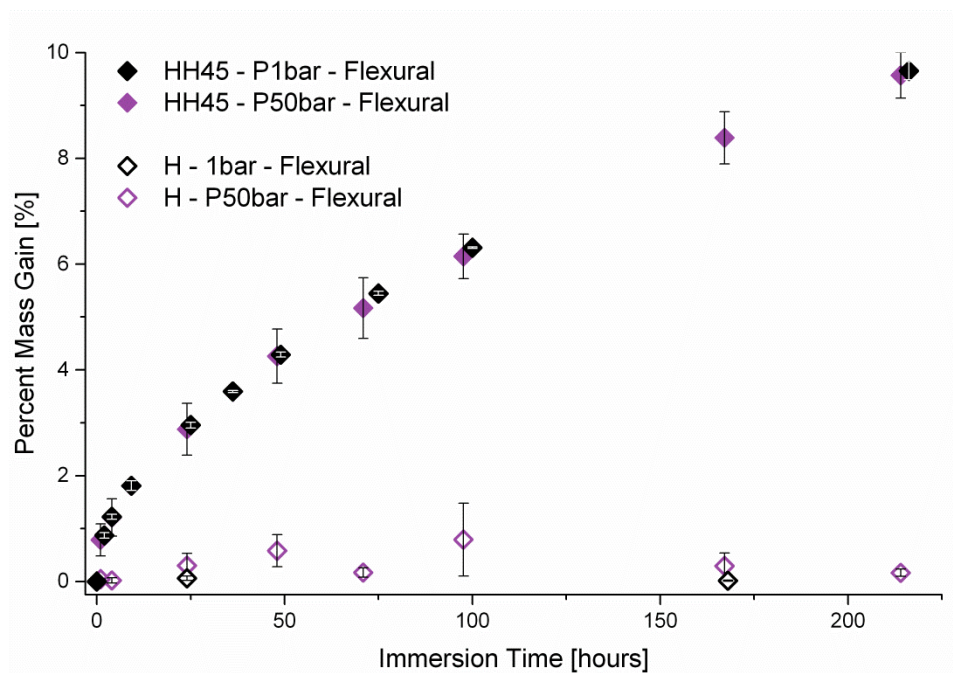


Figure 5.19 Water Absorption of HH45 Flexural specimen type with both 50bar and 1 bar of pressure, negligible difference observed.

The addition of 50 bar (5,000 kPa) pressure had no effect on the characteristic sorption curve in terms of magnitude or rate. Due to the insignificance of pressure on the specimens' water absorption, "bulk flow" of water through the fiber or fiber-matrix interface was eliminated as a plausible water absorption mechanism. Also other mass transport mechanisms influenced by pressure, such as the multi-physics model approach to anomalous diffusion [2] were also eliminated as feasible mechanisms and models.

## 5.4.2 DIFFUSION

Molecular diffusion, described as Fickian diffusion, is based on molecular movement of a species through another species. The three selected characteristic curves in Figure 5.18 were used to assess the applicability of known Fickian moisture absorption models to model the long term phenomenon. For a full representation of all of the specimens, reference Appendix E – Assessment of fit between varying models.

### 5.4.2.1 Fickian Diffusion

According to ISO 62 [3] first order Fickian diffusion occurs within the first 100 hours for plastic. A widely accepted method cited in literature is to plot the absorption against the square root of time for a simplified approximation. First order Fickian diffusion accurately models the absorption curves of biocomposite specimens within the first 100 hours of immersion, as seen in Figure 5.20. Therefore, Fickian diffusion is a valid model for immersion times ranging from 0 – 100 hours for biocomposite specimens.

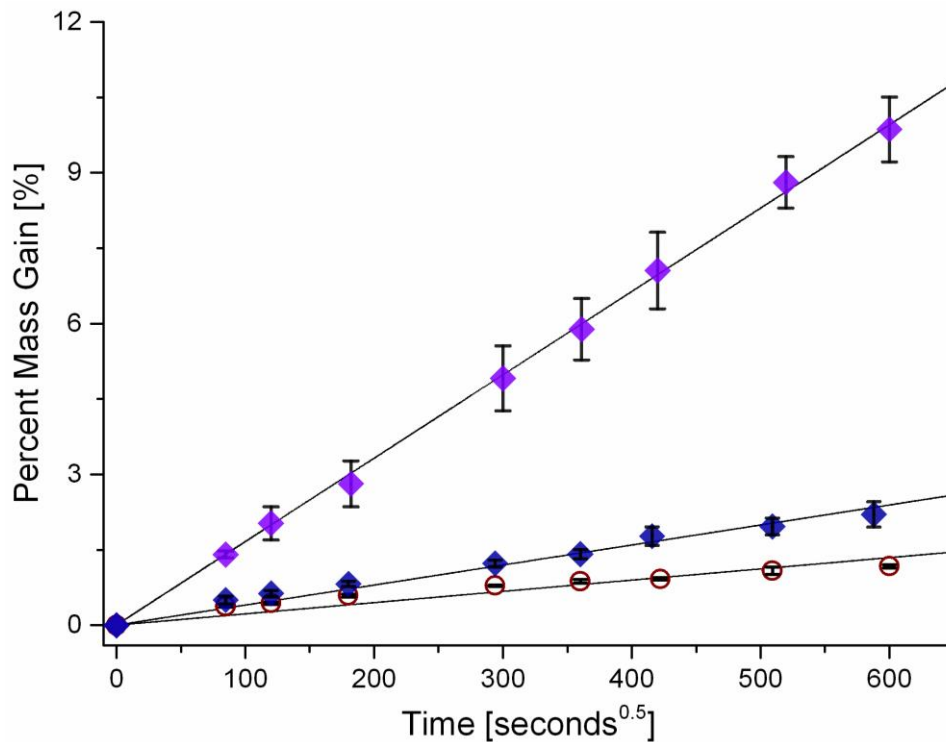


Figure 5.20 Fickian Diffusion for characteristics curves after 100 hours immersed adequately represents absorption in short immersion times.

Analysis of the calculated Fickian diffusion coefficient demonstrates that there is an undeniable trend which validates Fickian absorption mechanisms as a viable option for modeling water absorption.

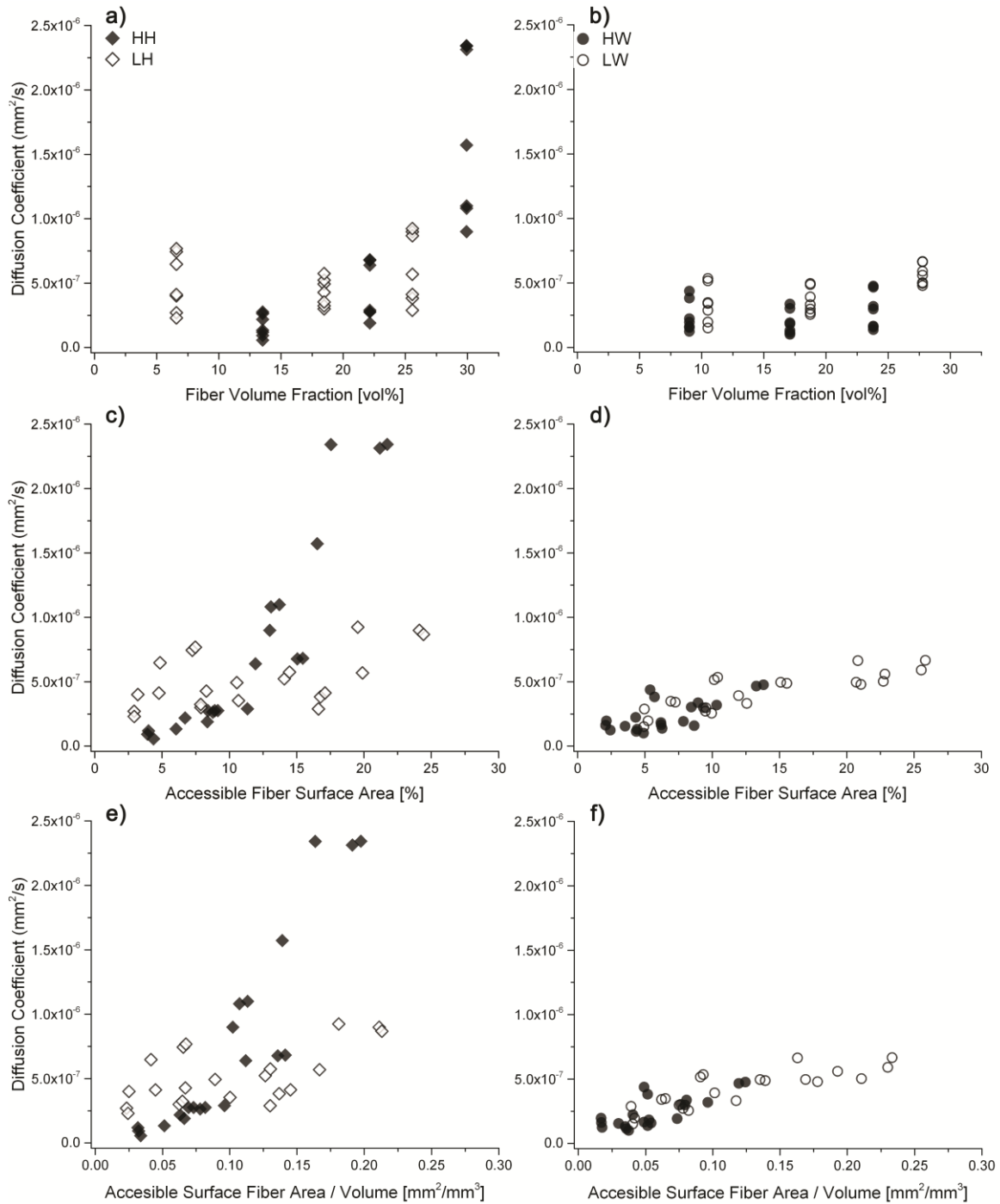


Figure 5.21 Fickian Diffusion coefficient displayed as a function of fiber volume fraction (a & b), percent fiber surface area (c & d), and accessible fiber area per volume (e & f) for hemp fiber variations (left) and wood pulp variations (right) for all specimen types except tensile bars. Linear increase in the Diffusion coefficient with an increase in accessible fiber surface area, except for LH45 variations,

The calculated diffusion coefficients of both hemp and wood pulp variations demonstrate a linear relationship with surface accessible fiber fraction, irrespective of fiber type as seen in Figure 5.21. The magnitude of diffusion coefficient is similar for both hemp and wood pulp variations, with the exception of HH45. The difference in values may be attributed to interconnected fibers, hence the mechanism for water ingress differs from the others. Analysis of interconnected fiber network is discussed in section 5.4.3. However, the diffusion coefficient values are all within the same order of magnitude which supports the validity of a diffusion based mechanism for water absorption. Since various fiber surface area fractions and fiber surface area to volume ratios were assessed, there is a range for the diffusion coefficient at each fiber volume fraction. As expected, the difference in matrix materials does not influence the diffusion coefficient, as the determined values are within the same order of magnitude.

Although Fickian diffusion accurately predicts water absorption from 0 – 100 hours, it does not adequately predict the mass gain after the initial exposure, as seen in Figure 5.22. This result was expected as Fick's first law is based on the diffusion of one substance through another (such as water through natural fiber), rather than a system with two phases, one of which is partially interconnected allowing additional absorbed water. Therefore, the simple solution of a first order Fickian diffusion is not sufficient for long term water absorption prediction for short natural fiber reinforced biocomposites as it does not account for continued water absorption nor accounts for quantities of fiber loss.

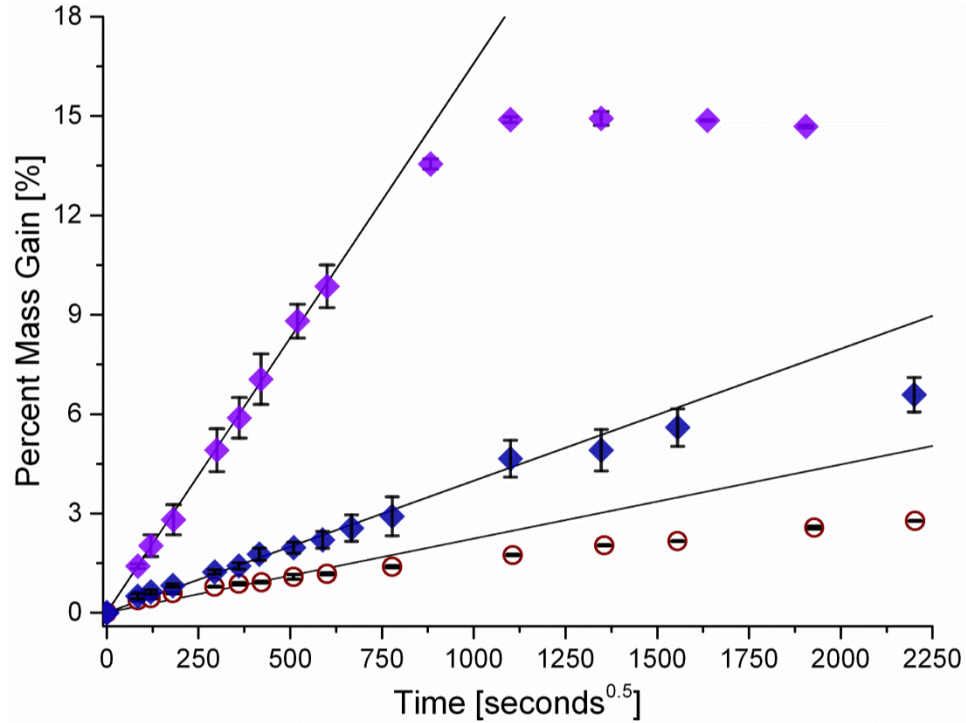


Figure 5.22 Fickian Diffusion for characteristics curves after 9 weeks immersed. Fickian diffusion is unable to predict long term immersion for HH45 (purple diamond filled), HW45 (blue circle filled) and LW30 (maroon circle unfilled) all 4 cut specimen type.

#### 5.4.2.2 Dual Phase Fickian Diffusion Model

Others in literature such as Celino [4] have utilized dual phase Fickian diffusion to capture absorption of water of natural fibers in immersion conditions. Limited differences were found compared to Fickian diffusion. Dual phase Fickian diffusion was assessed for biocomposite water absorption due to description of two phase absorption. Dual Phase Fickian Diffusion adequately fits the majority of the specimen types up until 500-1500 hours consistently, as shown in Figure 5.23. Micrograph in Figure 5.3, and gravimetric data are consistent in the support of two absorption rates. The material is not homogenous with two main structural morphologies: one absorption rate for through the “skin” material structure and another absorption rate through thickness of the bulk material.

However, the dual phase Fickian diffusion model shown in Figure 5.23 does not account for fiber loss, or gradual continued uptake of water past the initial 500 hours for all biocomposite scenarios. Previous research lacked long term data to expose this inconsistency. Therefore, the prolonged effects of water absorption have not been well understood. Due to the

extended duration of immersion data in this study, a modified dual phase absorption model is proposed which builds on the knowledge of molecular diffusion.

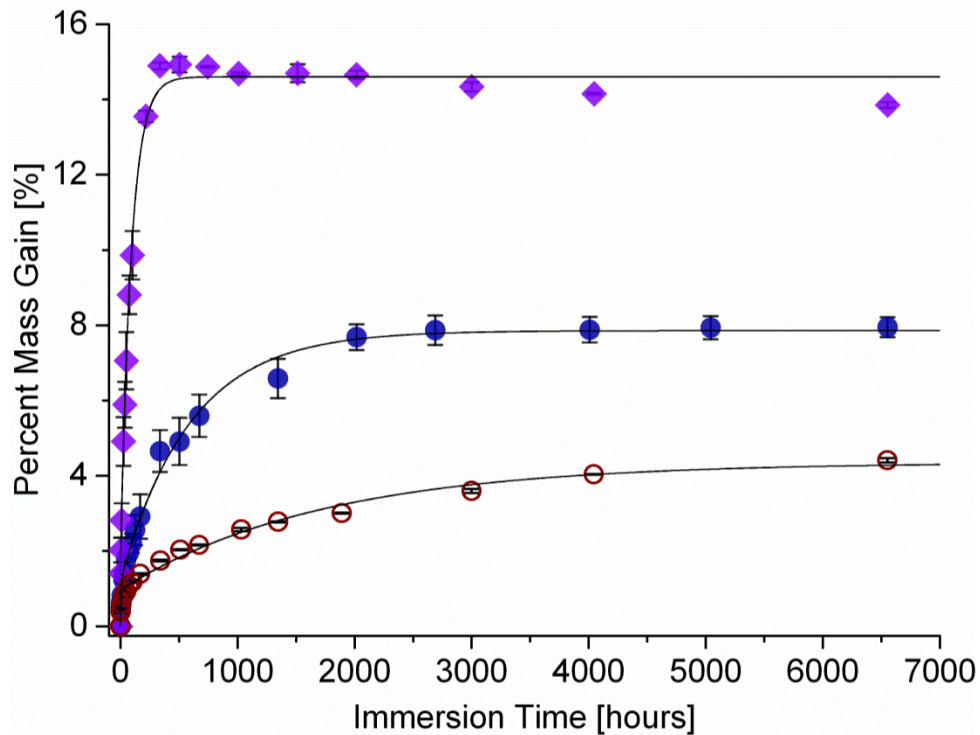


Figure 5.23 Dual Fickian Diffusion curve fit for characteristics curves are unable to capture continued water absorption LW30 (maroon circle unfilled) and HH45 (purple diamond filled) continued decrease.

### 5.4.3 INTERCONNECTIVITY

Permeation is the process of a liquid passing through a secondary phase and is a plausible phenomenon of mass transport in biocomposites if the liquid-transporting materials' structure, fibers are interconnected. The interconnected structure would allow the water to permeate through the biocomposite by pathway of the natural fibers. The extent of interconnectivity of the biocomposite variations was assessed to determine if percolation was a plausible mechanism. The average fiber water content was calculated from experimental absorption values with the assumption that all fibers absorb water if an interconnected structure exists. The calculation for average fiber water content is given in Equation 5.2. The calculated average fiber water content was compared to the potential theoretical maximum water content for each fiber shown in Table 5.2. The water content at 97% relative humidity was determined by the methodology in section 2.2.7. Utilization of the maximum water

content at 97% relative humidity is a valid comparison due to the unknown level of restraint from the matrix on the fiber attributed from fiber swell during water absorption.

$$W.C._{expt'l} = \frac{\text{Percent Average Mass Gain} / 100 * m_{\text{Avg.composite}}}{m_{\text{Avg.composite}} * W_{\text{fiber}}} \quad (5.2)$$

Table 5.2: Maximum Water Content of Natural Fibers

	<b>Water Content of Fiber, <i>W.C.fiber</i> (%)</b>	
	<b>Liquid Immersion</b>	<b>97% Relative Humidity</b>
Hemp	63 %* [4]	35.4 %
Wood Pulp		30.1%

\*denoted as absorption, however this was the maximum water content value prior to desorption

Calculated average experimental water content compares to the maximum water content at 97% RH for the same fiber type is illustrated in Figure 5.24 and Figure 5.25. For wood pulp, interconnectivity is unlikely to exist as the calculated experimental fiber water content is less than the water content experienced at 97% relative humidity. The absence of interconnectivity for wood pulp translates to the fact that the fiber was well distributed throughout the matrix. From visual assessment, the wood pulp fibers were not well dispersed as shown in Figure 5.2 potentially limiting the ability for the fibers to be interconnected. For hemp fiber, variations LH45, HH45 and HH30 demonstrate the potential for an interconnected fiber structure due to an average fiber water content equal to or greater than the fibers content at 97% relative humidity. LH45 has the highest probability of having an interconnected structure due to its highest average fiber water content, as well as the results for the maximum water absorbed demonstrates a parabolic increase rather than a linear increase observed for the other material variations. Additional evidence for an interconnected structure does not exist for HH45 or HH30. It is possible that some of fibers are connected without an interconnected network through thickness. As for the remainder of hemp reinforced specimens, interconnectivity does not exist due to well distributed and dispersed natural fibers within the matrix.



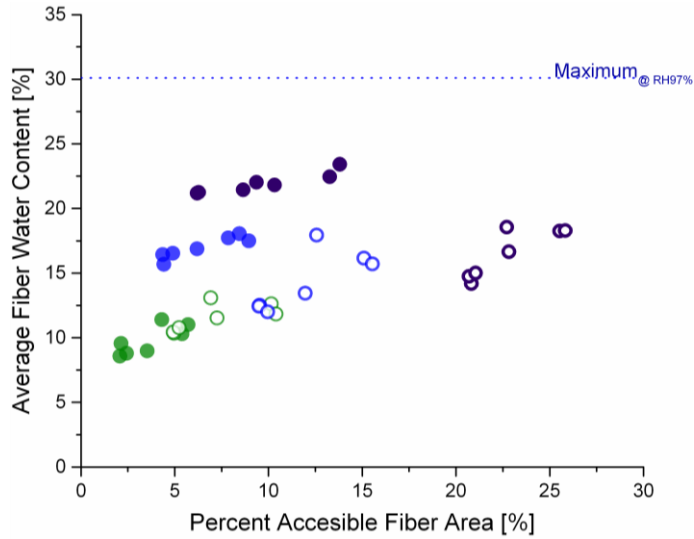


Figure 5.24 Experimentally calculated average fiber water content for wood pulp reinforced biocomposites, HDPE (filled) and LDPE (unfilled), relative to the maximum possible fiber water content in 97% relative humidity (dotted line). HW45 has the highest probability of possessing an interconnected fiber network.

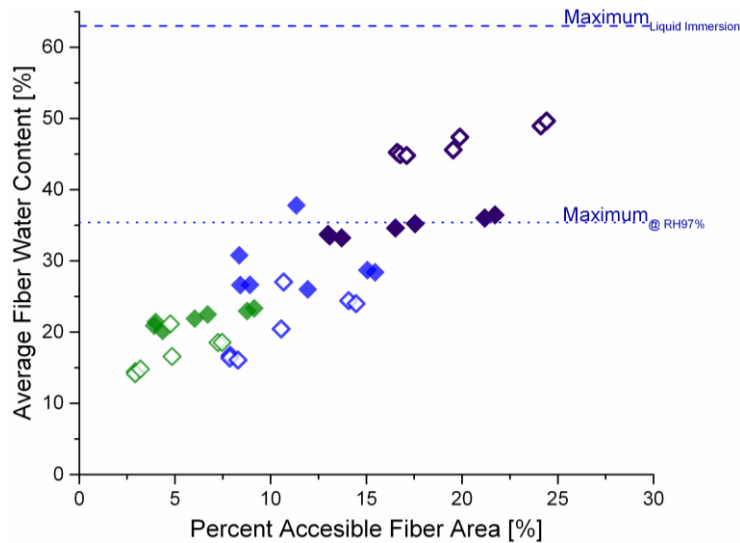


Figure 5.25 Experimentally calculated average fiber water content for hemp fiber reinforced biocomposites, HDPE (filled) and LDPE (unfilled), relative to the maximum possible fiber water content in 97% relative humidity (dotted line) and liquid immersion (dashed). The average fiber water content for LH45, HH45 and HH30 variations demonstrate greater water content than observed at 97.3% relative humidity which may suggest the possibility of an interconnected fiber network.

### 5.4.3.1 Limitation of Florescent Macrophotography

Florescent macrophotography was selected to assess the depth of absorbed water. An LH45 square specimen was sectioned in the width-thickness plane half way along its length as

shown in Figure 5.26 after immersed in UV dye for 1.5 years due to its' likelihood of having an interconnected fiber structure as discussed in the previous section. The resultant cross sectional image was inconclusive for fiber interconnectivity as the dye was not observed throughout the specimen but only around the perimeter. Only fibers in direct contact were able to absorb water, as the white fibers identified did not absorb any UV dye

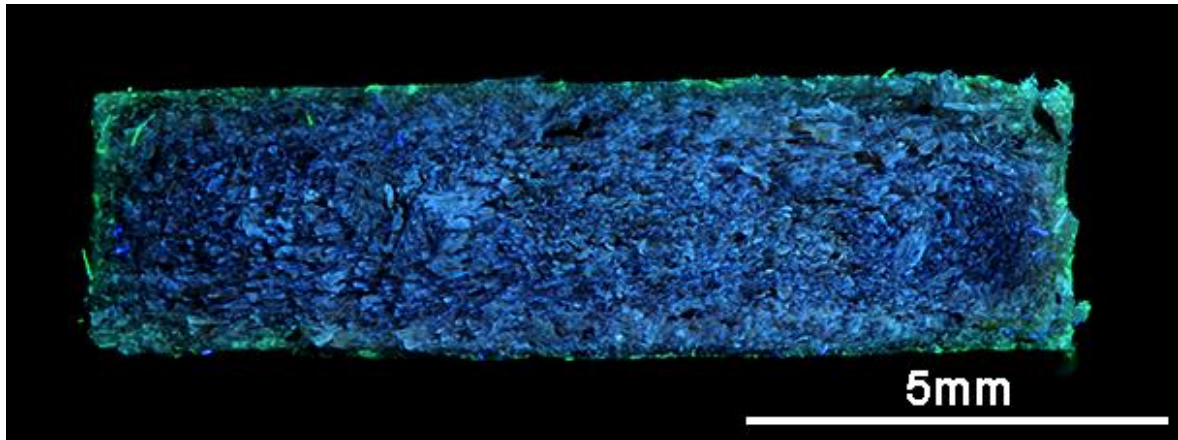


Figure 5.26 Cross sectional view of LH45 square geometry after immersed in UV dye for 13,176 hours (1.5 years), specimen thickness 3.11mm. Minimal dye penetration observed around the perimeter.

The penetration depth of a particle calculated from the diffusion coefficient is provided in equation 5.3 [5-7], where  $\Delta x$  is the depth of absorbed water,  $D$  is the diffusion coefficient, and  $t$  is the duration of time exposed.

$$\Delta x = \sqrt{2 * D * t} \quad (5.3)$$

The calculated depth of absorbed water after 100 hours of immersion, a fraction of the total time immersed, was 1.30mm based on a diffusion coefficient of  $2.34 \times 10^{-6} \text{ mm}^2/\text{s}$ . The estimated maximum depth of dye penetrated after 13,176 hours from Figure 5.26 estimated less than 0.5mm, approximately a third of the 100 hour immersed calculated depth. The difference in molecular size of the Xanthene dye, 250 Angstroms, compared to water, 18 Angstroms, limited the penetration depth due to two reasons:

1. The natural fiber acts as a filter of the dye, as the molecular diameter of dye is greater than the porosity found within the fiber.
2. The interfacial space between the natural fiber and the matrix is smaller than the molecular diameter of the dye.

Immersion in UV dye does not map the location of absorbed water in biocomposites but does demonstrates the size limitation of the contribution of natural fiber and fiber-matrix interface

porosity on water absorption. More advanced mapping the final state of water absorption ingress would provide additional evidence to assess the water absorption. It is recommended to conduct either micro CT or MRI for three-dimensional assessments.

## 5.5 DUAL PHASE DIFFUSION ABSORPTION WITH DECAY MODEL

A proposed model has been developed to account for dual phase diffusion as well as fiber degradation for agri-fiber thermoplastics. The general form of the Dual Phase Diffusion Absorption with Decay model is detailed in Equation 5.3 and was empirically fitted to all 84 biocomposite absorption curves with a  $R^2_{DOF}$  between 0.96 - 1.00. The equation includes initial water absorption and long term water absorption as well as mass decay from fiber loss.

$$\text{Percent Mass Gain} = \underbrace{A*(1-e^{-B*t})}_{\text{Initial Absorption}} + \underbrace{C*(1-e^{-D*t})}_{\text{Long Term Absorption}} - \underbrace{E*(1-e^{-F*t})}_{\text{Fiber Loss}} \quad (5.4)$$

{A} Magnitude of initial water absorbed    {C} Maximum magnitude of water absorbed    {E} Magnitude of fiber dissolution  
 {B} Rate of initial water absorption        {D} Bulk biocomposite diffusion rate        {F} Rate of fiber dissolution

where e = Euler's number (correct to five decimal places 2.71828)

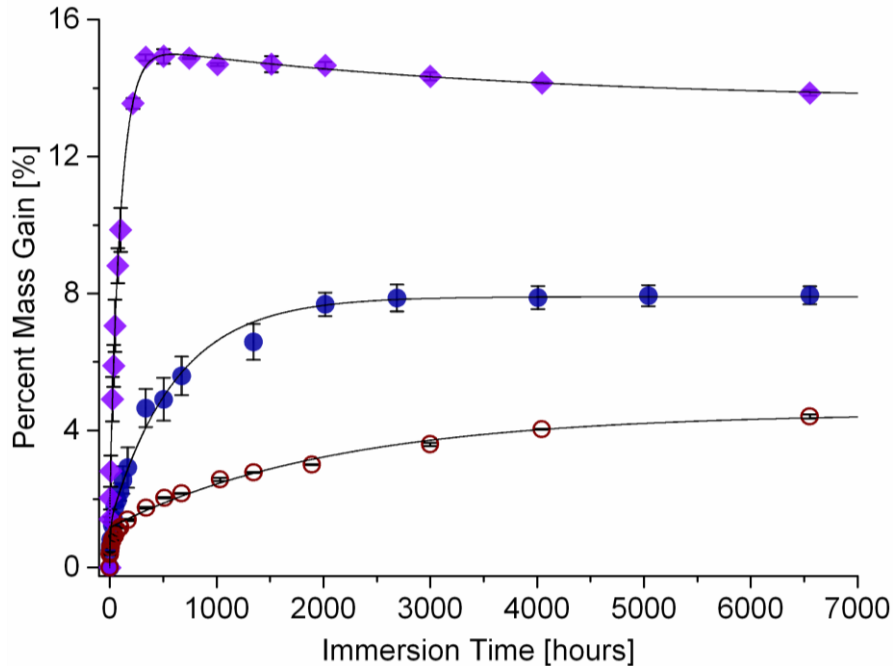


Figure 5.27 Representative water absorption curves isolated from HH45 (purple diamond filled), HW45 (blue circle filled) and LW30 (maroon circle unfilled) all 4 cut specimen type.

The *dual phase diffusion absorption with decay model* for agri-fiber thermoplastics was applied to all the long-term absorption curves in this study and representative curves to demonstrate the empirical fit are shown in Figure 5.27. The model provides the ability to predict both continued gradual increase (LW30 – unfilled maroon circles) as well as dominate absorption followed by decay (HH45 – filled purple diamond). Both these material responses could not be predicted by any other model found in the literature, including the dual phase

diffusion model, as the mass gain and mass loss phenomena occur simultaneously -albeit at different rates due to the different mechanisms.

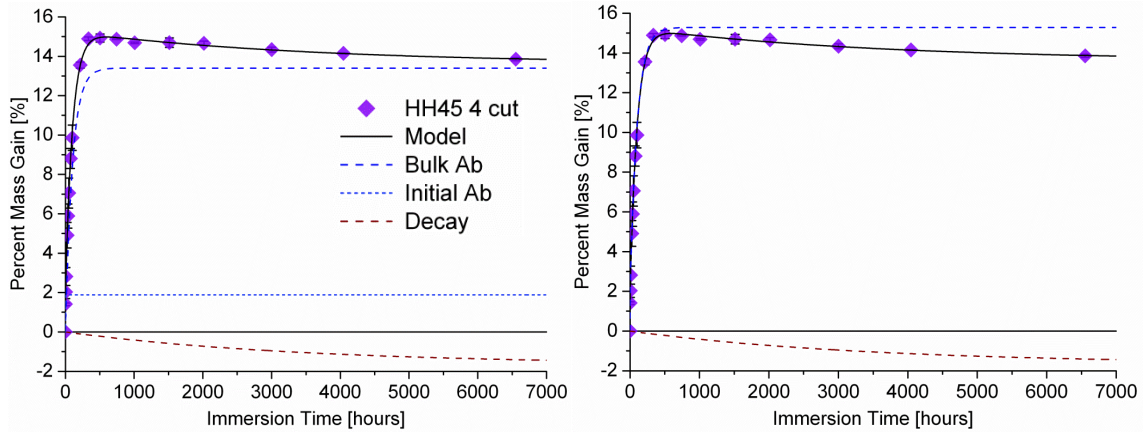


Figure 5.28 Model Dual Phase Absorption and Decay decoupled to show each function separately (left). Each term within the equation has been isolated to illustrate the contribution of decay, as well as the inability of only growth to predict the absorption curve (see Figure 5.28). The initial absorption (blue short dot), occurs nearly instantaneously similar to the Fickian diffusion coefficient. The bulk absorption (blue long dash) models the longer exposure absorption. The combination of both absorption terms allows for the prediction of the maximum water absorbed. The decay function was previously ignored and demonstrates the slow rate of fiber removal. This decay term outlasts the absorption. At a point, the ingress of water is less than the material lost. Although water may continually penetrate, the fiber loss becomes the dominant factor with long term immersion.

The following sections explain how each model parameter represents the phenomenological process throughout water absorption in natural fiber reinforced biocomposites.

### 5.5.1 INITIAL MASS ABSORPTION TERM

The initial water absorption phase is modelled by two parameters A and B. Parameter A represents the magnitude of mass gain during the initial absorption whereas parameter B reflects the rate at which the absorption occurs. The contribution of the term occurs within the first 50 hours of immersion, as shown in Figure 5.29 for each representative curve.

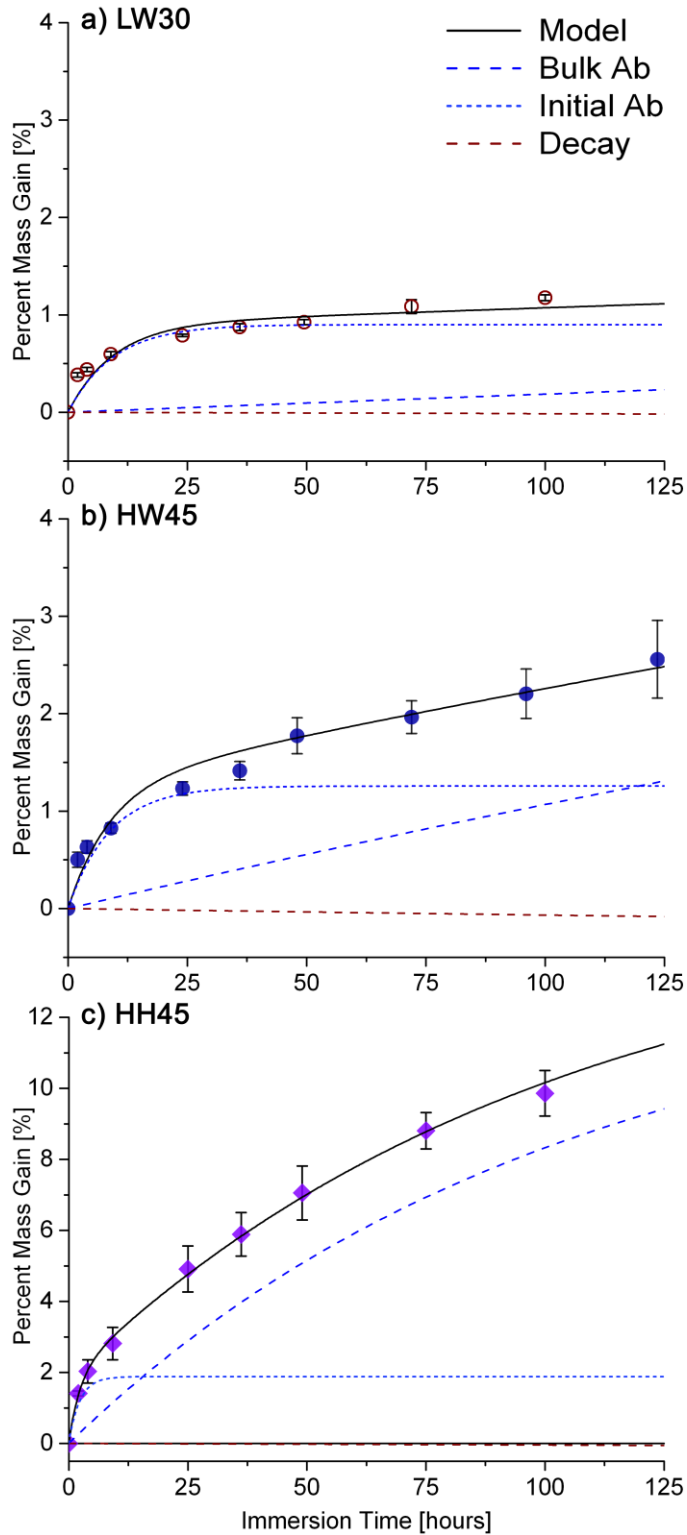


Figure 5.29 Contribution of initial absorption (blue short dash), bulk absorption (blue dash), and fiber decay (red dash) in the first 125 hours of absorption for the three characteristic curves; a) LW30, b) HW45 and c) HH45.

### Parameter A: Initial magnitude of water absorbed

The initial magnitude of water absorbed correlates linearly with the percentage of surface accessible fiber as shown in Figure 5.30. The more surface accessible fiber the greater the driving force of water into the biocomposite. Therefore, the initial flux of water into the biocomposite is controlled by the structure of the biocomposite expressed as the surface accessible fiber ratio. These findings support conclusions drawn from the fluorescent macrophotography work, as the UV dye intensity increased as a result of flux of water into the biocomposite through the natural fiber as evidenced by an increase in dye concentration.

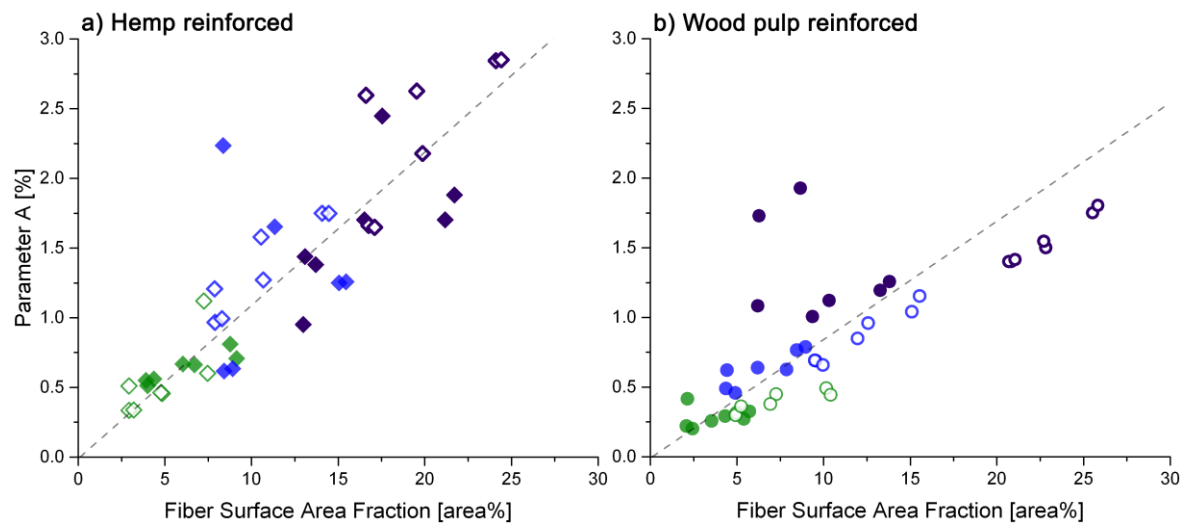


Figure 5.30 Linear dependency of parameter A on the accessible surface area fiber fraction of the biocomposite for a) hemp fiber variations and b) wood pulp variations.

The linear relationship is dependent for fiber type.

For hemp fiber,

$$\text{Parameter A} = 0.11 * \text{Fiber Surface Area Fraction} \quad (5.5)$$

For wood pulp fiber,

$$\text{Parameter A} = 0.085 * \text{Fiber Surface Area Fraction} \quad (5.6)$$

The relative contribution of the initial magnitude of water uptake to the maximum water absorbed is constant for all geometries and fiber contents as shown in Figure 5.31. The initial magnitude of water uptake determined by parameter A is approximately a fifth of the maximum water absorbed; slightly greater for LDPE. The scalability from parameter A to

maximum water absorbed serves as an excellent approximation for the worst absorption case to predict the greatest degradation in mechanical properties expected.

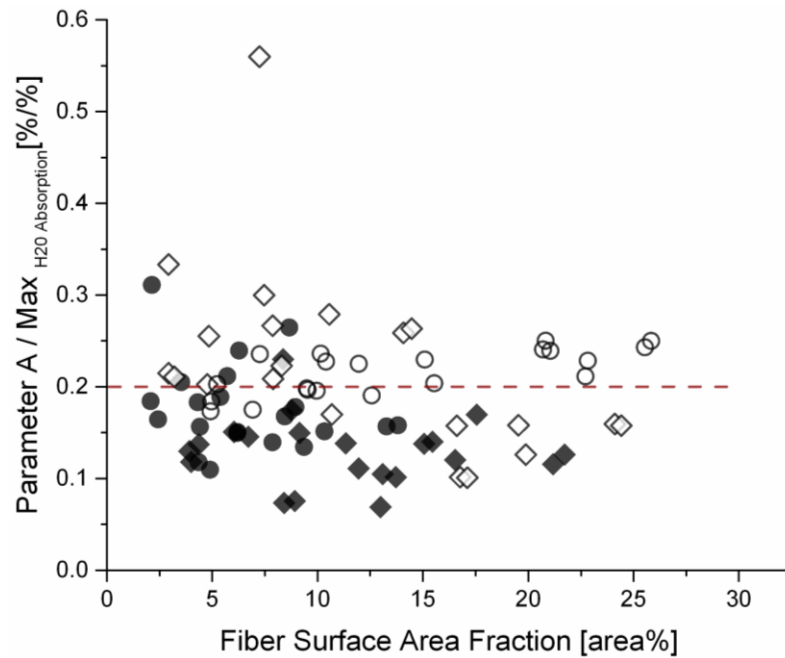


Figure 5.31 Relative contribution of parameter A compared to the maximum water absorbed for all specimen geometries.

**Parameter B:** Initial biocomposite diffusion rate

The initial biocomposite diffusion rate, Parameter B, represents the first 50 hours of immersion. Parameter B displays a positive correlation with both percent of accessible surface fiber fraction in Figure 5.32 and ratio of surface area fiber to biocomposite volume in Figure 5.33. The more fibers present at the surface relative to the volume of the specimen, the higher the flux of water. When the fiber content increases to the point where fiber-fiber connectivity exists (potentially through thickness), as with LH45 (purple open diamonds) a relationship between fiber surface area fraction nor the ratio of accessible surface area fiber to specimen volume is sufficient for parameter B.

The rate of initial absorption, parameter B, relates to the fraction of fibers accessible to immediately absorb water relative to the volume of composite, i.e. it's relative effect on overall mass gain. The structure of the material dictates the rate of absorption independent of fiber or matrix type. Therefore, parameter B is a reflection of the materials structure as described in equation 5.7.



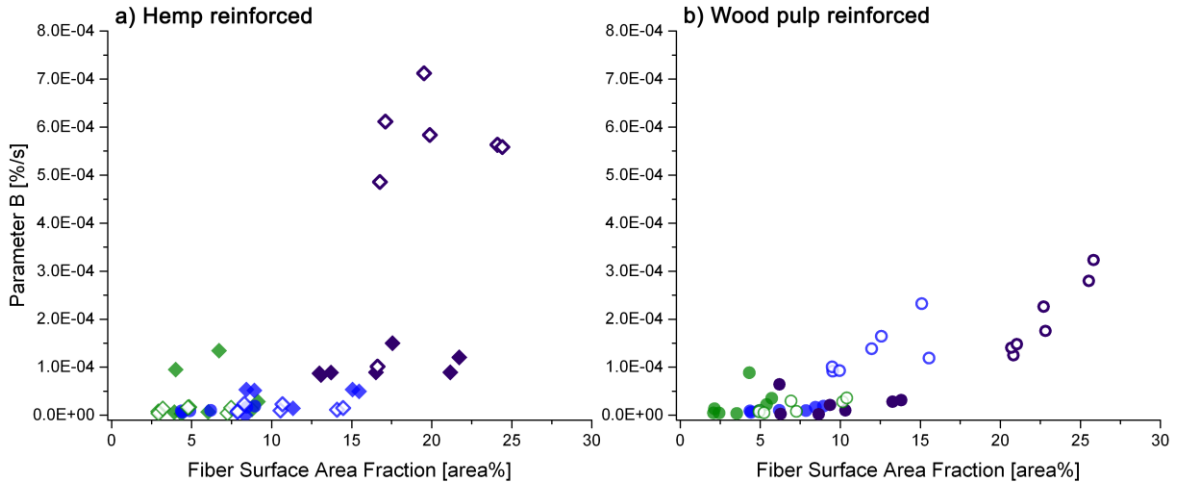


Figure 5.32 Parameter B as a function of accessible surface area fiber fraction for a) hemp fiber variations and b) wood pulp variations for all specimen geometries.

General increase in the initial water absorption rate with an increase in the ratio of surface accessible fiber to biocomposite volume as represented in 5.7 and shown in Figure 5.33.

$$\text{Parameter B} = 5.8186 \text{ E-}06 * e^{17.977 * \text{Accessible Fiber Area} / \text{Volume}} \quad (5.7)$$

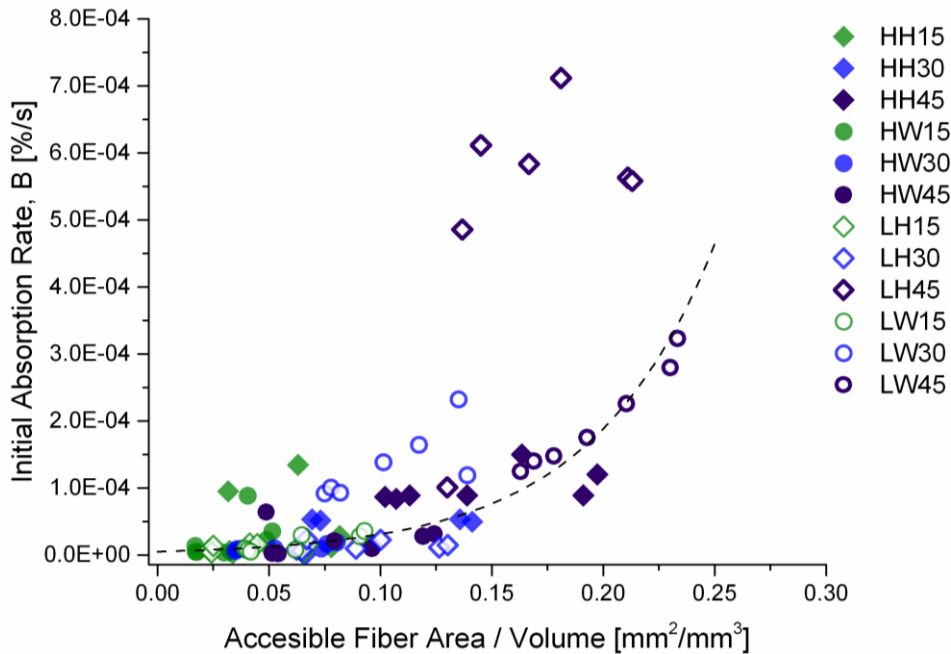


Figure 5.33 The biocomposite initial absorption rate is controlled by the ratio of surface accessible fiber to specimen volume, with the exception of LH45 variations due to suspected interconnected fiber network. Dashed line is a best-fit curve, Eq. 5.7.

### 5.5.2 BULK WATER ABSORPTION MAGNITUDE AND RATE

Long term water absorption is modelled by parameter C (magnitude) and D (rate). The contributions of these two parameters occur over the duration of absorption and are dependent on fiber surface area fraction and correlated to traditional diffusion coefficient.

#### Parameter C: Magnitude of water absorbed over long term immersion

Parameter C reflects the bulk absorption that continuously occurs as the specimen is exposed to the immersion environment. Within the model, *C* predicts the experimental maximum amount of water absorbed with a near 1:1 ratio for all specimen types as illustrated in Figure 5.34. The prediction of maximum water absorbed is significant since it translates into the maximum deterioration of mechanical properties outlined in section 4.6. For designers this prediction of maximum water absorbed allows them to account for worst-case mechanical performance for increased product safety.

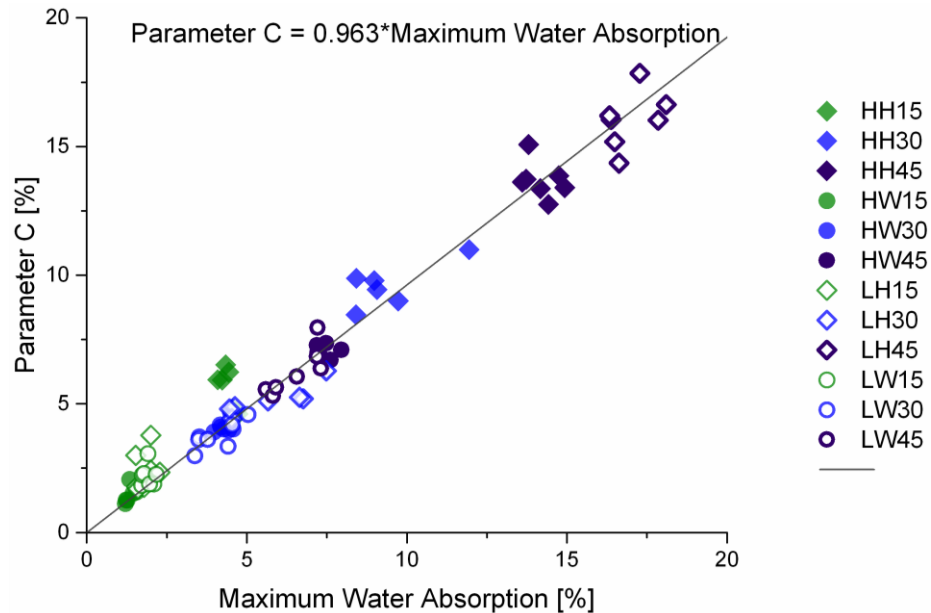


Figure 5.34 Experimental correlation between maximum water absorbed and model parameter C.

Due to the importance of the prediction of maximum water absorption a relationship must be determined relative to material structure or composition to avoid the requirement for long term immersion studies. A linear relationship exists between volume fraction of fiber and maximum water absorbed, except LH45 variations, as shown in Figure 5.35. The higher the fiber volume fraction the greater the maximum amount of water absorbed. Hemp fiber fractions absorb more water than wood pulp and therefore have larger values of *C*.

Parameter C is dependent on the quantity of fiber. For the LH 45 a sharp increase is observed in the amount of water absorbed hypothesized due to interconnectivity of natural fibers providing more capacity within the fibers to absorb and retain water. The effect of interconnectivity for LH45 has also been supported in section 0. The interconnectivity for other biocomposite variations does not seem to exist based on a linear relationship with the amount of water absorbed to the quantity of fiber. Hemp fibers absorb approximately double the magnitude of water as wood pulp. The linear relationship is dependent on fiber type and volume fraction, with the exclusion of fiber interconnectivity is as shown in Figure 5.35, equation 5.8 and 5.9.

For hemp fiber reinforced,

$$\text{Parameter C} = 41.79 * \text{Fiber Volume Fraction} \quad (5.8)$$

For wood pulp reinforced,

$$\text{Parameter C} = 24.61 * \text{Fiber Volume Fraction} \quad (5.9)$$

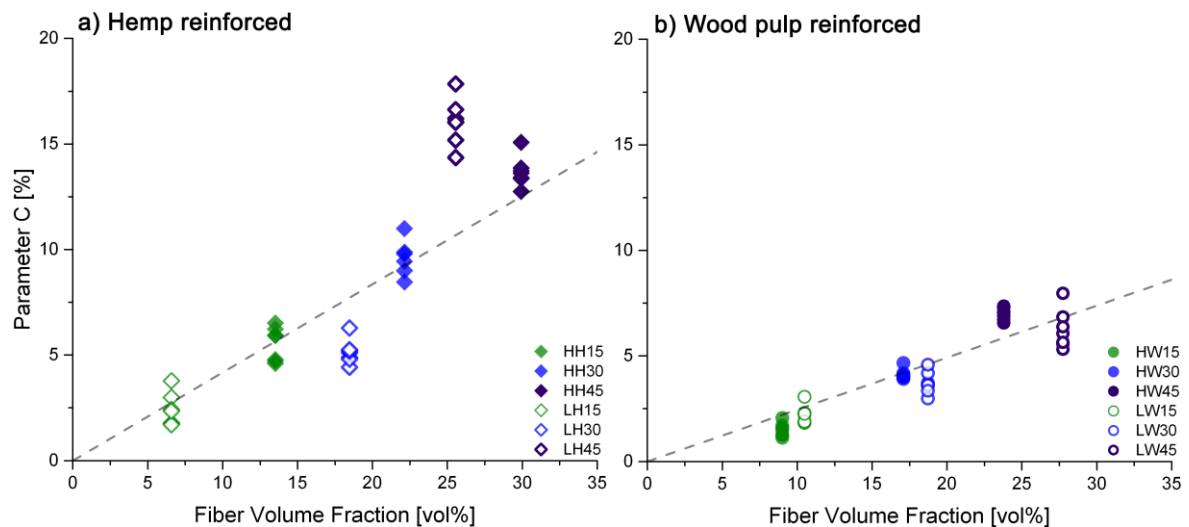


Figure 5.35 Parameter C assessed as a function of fiber volume fraction for a) hemp fiber variations and b) wood pulp variations for all specimen geometries. Dashed lines are best-fit curves as shown in equations 5.8 and 5.9 respectively.

With respect to the physical phenomenon, for water to be absorbed into the bulk of the material, the water must first diffuse through the fibers at the surface which act as a gate into the biocomposite. The maximum water absorption is dependent on the content of fiber available to absorb water such as the ratio of accessible fiber surface area,  $SA_f$  to the volume of specimen available as shown in Figure 5.36 and equation 5.4 and 5.5. The parameter does have some dependence on matrix type without the fiber interconnectivity, as shown in the

top of Figure 5.36. The linear relationship is dependent on fiber type as well as the ratio of surface accessible fiber to volume of specimen.

For hemp fiber reinforced:

$$\text{Parameter C} = 84.6 * \text{Surface Accessible Fiber/Volume Specimen} \quad (5.10)$$

For wood pulp reinforced:

$$\text{Parameter C} = 39.0 * \text{Surface Accessible Fiber/Volume Specimen} \quad (5.11)$$

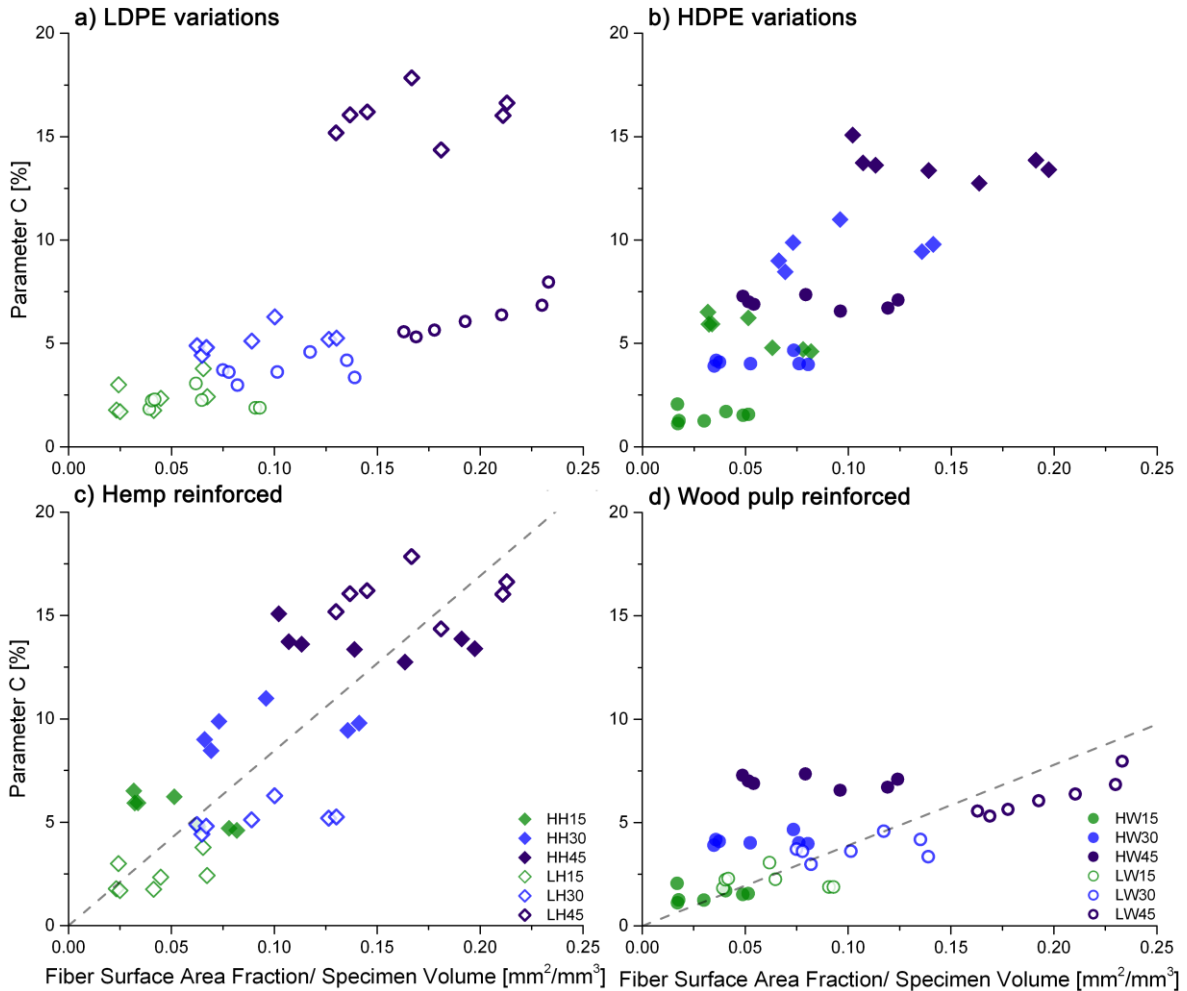


Figure 5.36 Parameter C assessed as a function of ratio of fiber accessible surface area fraction to specimen volume as a function of matrix type a) LDPE b) HDPE as well as a function of fiber type c) hemp variations and d) wood pulp variations. Dashed lines (c and d) are best-fit curves as shown in equations. 5.10 and 5.11 respectively.

The magnitude of maximum water absorption is fiber dependent although there are some influences where the LDPE variations are slightly less than the comparative HDPE variation.

The relationship, relative to the volume of specimen, allows for future assessments with different geometries since fiber connectivity can influence the relationship.

**Parameter D: Bulk Biocomposite Diffusion Rate**

Once the initial water diffuses into the surface fibers, the water continues to diffuse into the bulk material, albeit at a rate slower by two orders of magnitude. Since only the natural fibers absorb water, the bulk diffusion rate is a measure of the rate of diffusion within the fiber as well as between fibers. The bulk biocomposite diffusion rate dominates long term water absorption. The long term diffusion rate is dependent on the fiber type and content. Hemp fiber reinforced biocomposites demonstrate a higher bulk diffusion rate than wood pulp biocomposites as shown in Figure 5.37. For hemp fiber, a near exponential relationship is found between parameter D and fiber volume fraction. Wood pulp variations have an incremental linear correlation of bulk diffusion rate, parameter D, with fiber volume fraction, with the exception of HW45 variations.

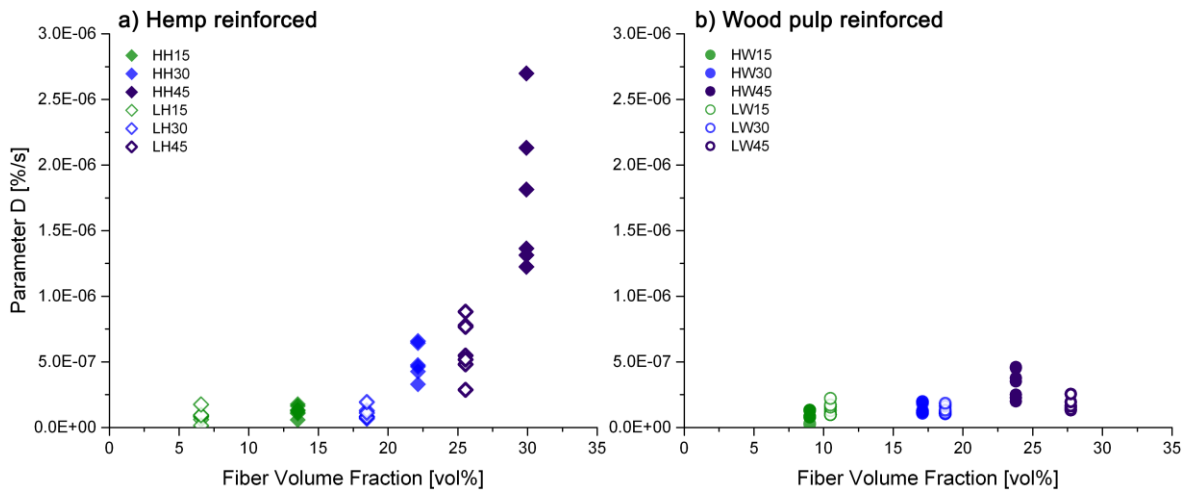


Figure 5.37 Parameter D assessed as a function of fiber volume fraction for a) hemp fiber variations and b) wood pulp variations for all specimen geometries. At higher fiber volume fractions, an exponential relationship reemerges in the bulk diffusion rate, variations HH45, HH30, LH45 and HW45. The difference in response from HH45, HH30, LH45 and HW45 indicates a structural change between the natural fibers within the biocomposite. The addition of fibers increases the capacity for water to be absorbed and increases the likelihood for fiber interconnectivity. It is theorized that incremental increases in bulk diffusion rate relates to the incremental addition of fiber without change to the extent of fiber to fiber interconnectivity. Conversely an exponential relationship between bulk diffusion rate and an increase in fiber fraction like indicates of fiber to fiber interconnectivity. An interconnected network provides additional

pathways for water to absorb and therefore increases the bulk diffusion rate. Hemp fibers have long hair like structures and are more likely than wood pulp to entangle to create interconnected pathways. The size effect of the fiber structure alone may explain the delay in the exponential increase for wood pulp. Fiber to fiber interconnection is the beginning of interconnectivity, where as it is hypothesized through thickness fiber interconnectivity is observed for LH variations.

Fiber volume fraction is not an accurate predictor of bulk absorption rate due to a lack of representation of the structure created from the volume fraction of fibers present. Both fiber surface area fraction and the ratio of fiber surface area fraction to specimen volume were assessed to determine a relationship between material structure and bulk absorption rate. Similar trends are seen in both fiber surface area fraction and ratio between fiber surface area fraction and the volume of the specimen, shown in Figure 5.38. A linear relationship still exists for wood pulp and a near exponential relationship for hemp fiber. While neither property displays a worthwhile correlation, it does support the assertion that at medium (blue) and high (purple) volume fractions fiber to fiber connectivity exists for the ratios examined.

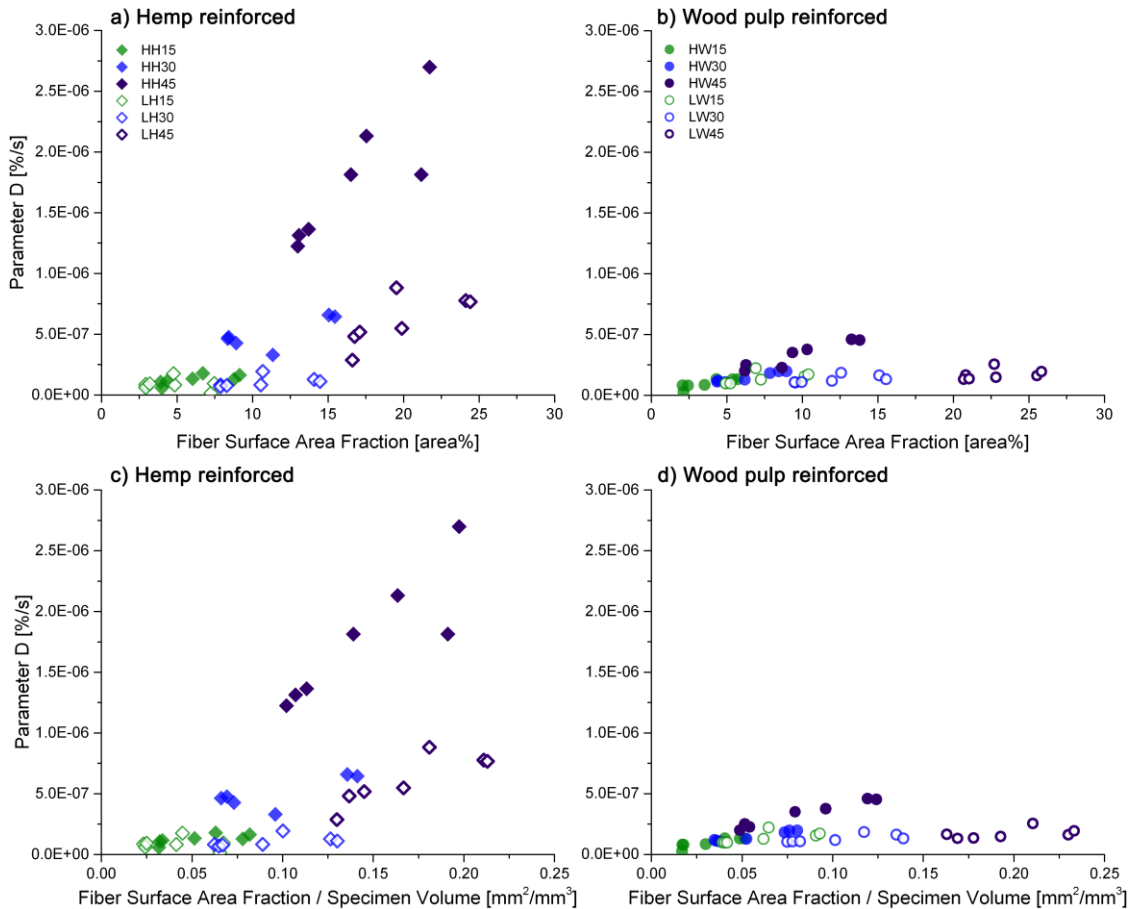


Figure 5.38 Parameter D assessed as a function fiber surface area fraction (a & b) and ratio of fiber accessible surface area fraction to specimen volume (c & d) as a function of fiber type for hemp variations (a & c) and wood pulp variations (b & d).

The diffusion coefficient conveys information about the initial rate of absorption relative to the maximum absorbed water at maximum time. Since it is not practical to obtain experimental long-term absorption rates due to the required immersion duration a correlation factor between parameter D and the diffusion coefficient has been determined for interconnected and distributed fiber structures. As a rule of thumb parameter D nearly has a 1:1 ratio with diffusion coefficient for interconnected structure and a constant bulk diffusion rate for non- connective structures. The relationships based on material structures are:

For interconnected variations: LH45, HH45, HH30 and HW45

$$\text{Parameter D} = 0.9325 * |\text{Diffusion Coefficient (mm}^2/\text{s)}| + 1.2 * 10^{-7} \quad (5.12)$$

For dispersed and distributed variations:

$$\text{Parameter D} = 0.0472 * |\text{Diffusion Coefficient (mm}^2/\text{s)}| + 1.09 * 10^{-7} \quad (5.13)$$

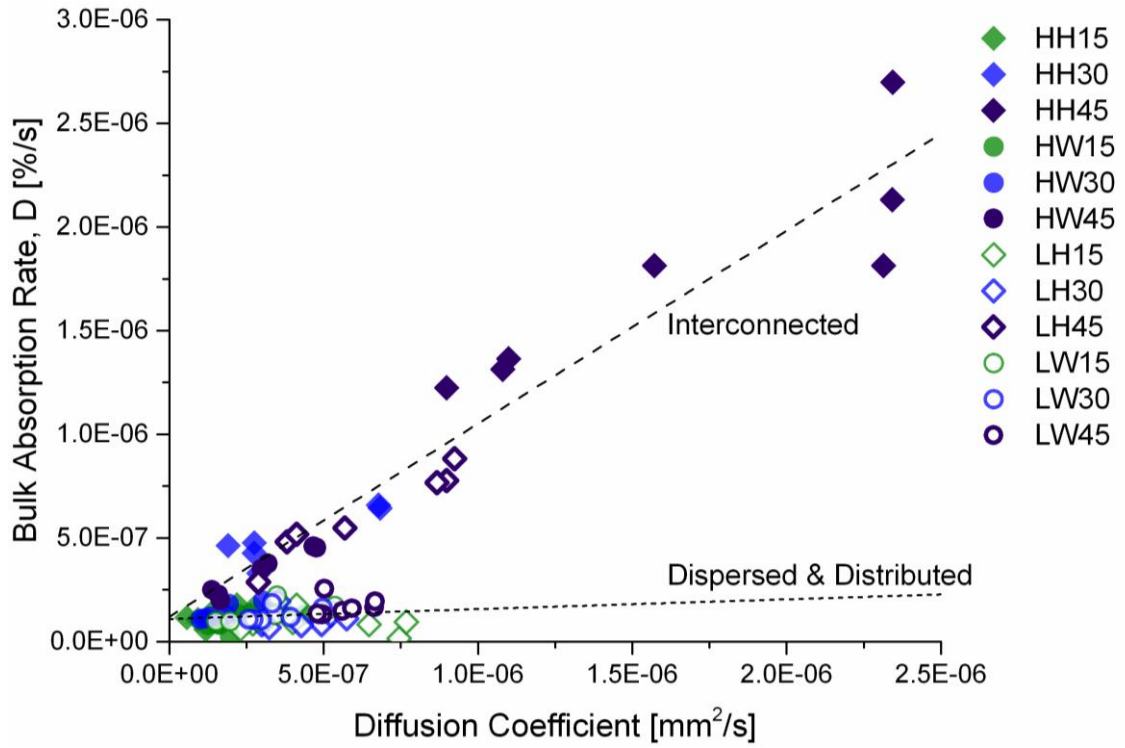


Figure 5.39 Bulk biocomposite absorption rate is dependent on diffusion coefficient of the biocomposite if there is an interconnected structure. Dashed lines: interconnected (Eq. 5.12) and dispersed and distributed (Eq. 5.13).



### 5.5.3 LONG TERM FIBER DECAY

The phenomenon of fiber degradation due to water immersion was discussed in section 0. The surface accessible fibers are degraded by a combination of dissolution and/or biological organism attack, as shown in Figure 5.13, and Figure 5.14. An increase in mass loss was observed in Figure 5.15, as the fiber content increased. Since mass loss occurs at the surface of the specimen, mass loss was dependent on the accessible fiber at the surface of the biocomposite, and is confirmed by the linear relationship between mass loss and fiber surface area fraction in Figure 5.40. The impact of decay is minimal for low fiber fraction biocomposite due to a lower percentage of natural fiber exposed on the specimen surface. LDPE based biocomposites generally lost less natural fibers than HDPE after 1 year of immersion.

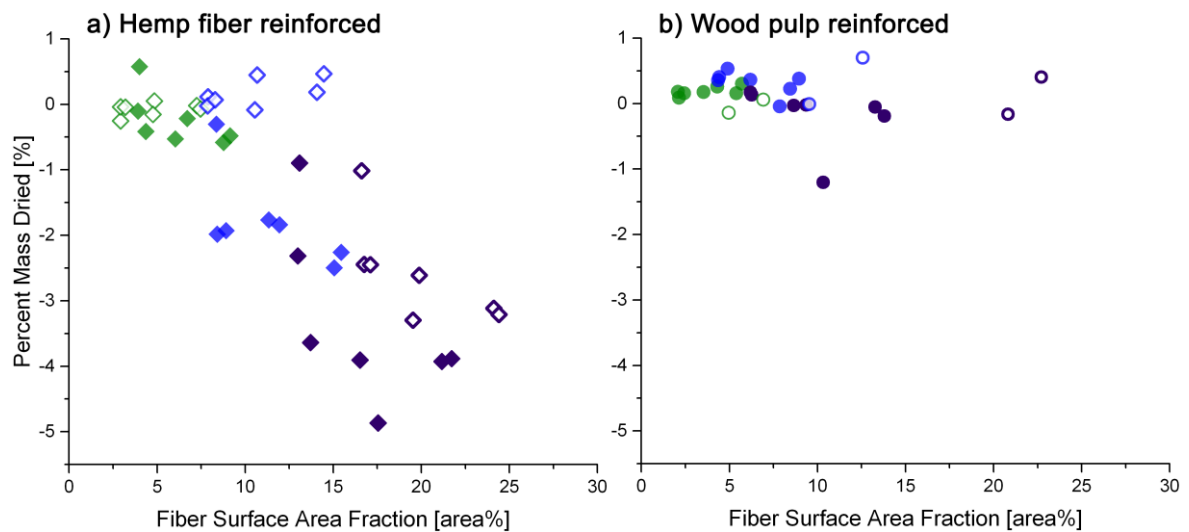


Figure 5.40 Percent mass loss for a) hemp variations and b) wood pulp variations (right) as a function of percent fiber surface area for all specimen geometries. Note: LW cut geometries are not included.

#### Parameter E: Predicted Magnitude of Mass Loss

The magnitude of mass loss due to fiber loss is represented by parameter E within the model, shown in Figure 5.41. Unfortunately, the duration of drying time was insufficient to accurately determine the final dried mass, as discussed in 0 and is demonstrated by the variability between parameter E and percent dried mass. The scattered data centralizes near zero change in mass after immersion and zero parameter E for low fiber content variations. The lower magnitude of the mass loss is correlated with a lower percentage of surface accessible fiber. The greater fiber volume fraction correlates with a larger E parameter, as higher fiber contents increase the likelihood of degradation and removal of the fiber.

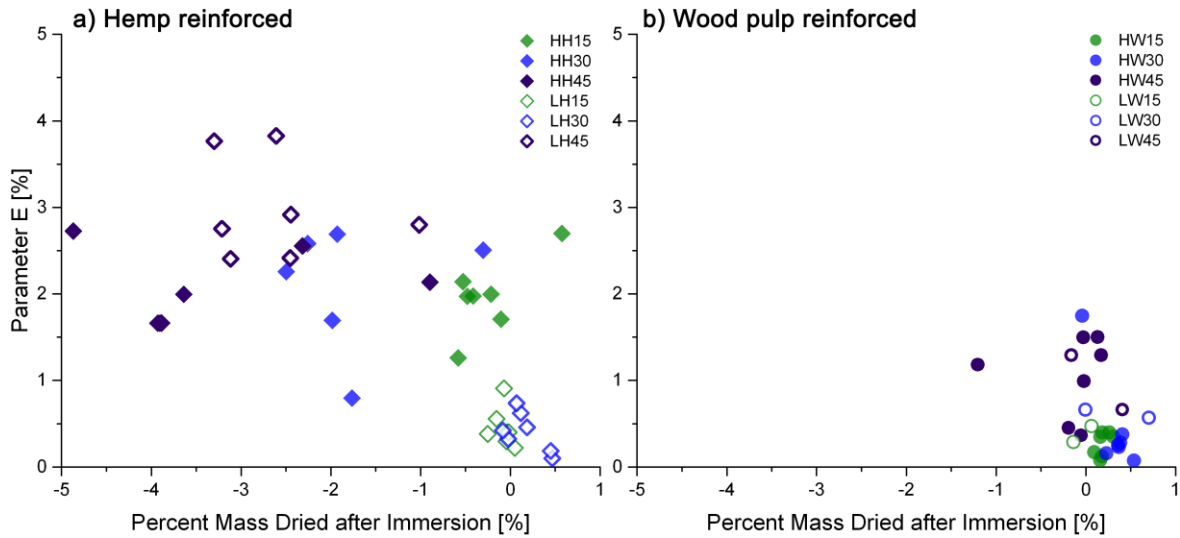


Figure 5.41 Parameter E variables for a) hemp fiber variations and b) wood pulp variations for all specimen geometries.

Wood pulp demonstrates little variation in parameter E since mass loss after immersion was assessed as negligible. The general shape of the absorption curves confirms that significant decay does not occur in wood pulp biocomposites, unlike the decay experienced by hemp fiber variations in Figure 5.10. Hemp experiences more degradation as the fiber is more soluble in water than wood pulp since hemp fiber has not been chemically purified by the pulping process and has a chemical composition of hemicellulose, lignin and extracts. Hemp fiber therefore has a greater ability to dissolve and/or biodegrade. Also, for biocomposites with interconnected fiber networks the mass loss was not only limited to surface fibers. However, since LH45 has been theorized to have through thickness interconnectivity, as referenced in section 0, the variation was not included in the linear analysis but is displayed to illustrate the difference.

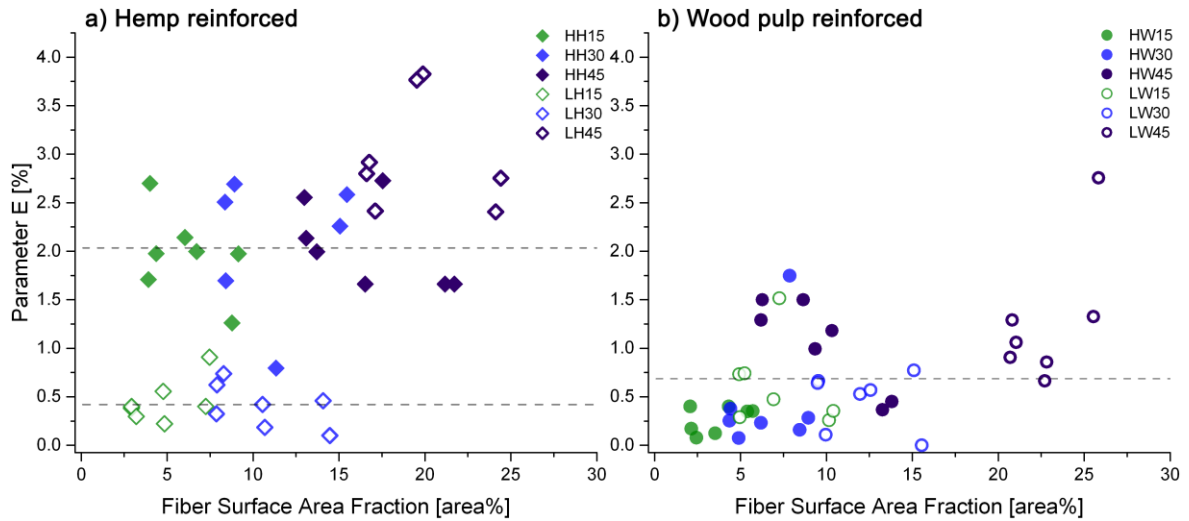


Figure 5.42 Parameter E as a function of accessible surface area fiber fraction for a) hemp fiber variations and b) wood pulp variations for all specimen geometries. Dashed lines: are for equations 5.14, 5.15 and 5.16 for LH, HH and Wood Pulp respectively.

Since mass loss is synonymous with fiber lost from the surface, parameter E plotted relative to fiber surface area fraction is shown in Figure 5.42. As previously determined mass loss occurs at the surface of the specimen and therefore parameter E is graphically compared against fiber surface area fraction. The fiber surface area has little to no effect on parameter E and remains fairly constant for each material variation, other than LH45 which has through thickness fiber connectivity. Therefore, parameter E is dependent on fiber type with the following constants given:

$$LH = 0.65 \quad (5.14)$$

$$HH = 2.75 \quad (5.15)$$

$$\text{Wood Pulp} = 0.69 \quad (5.16)$$

### Parameter F: Predictive Mass Loss Rate of Fiber

Within the model, Parameter F reflects the rate of mass loss of fiber. The rate was difficult to predict since only two points, prior to immersion and after immersion are relative. Therefore, the rate of fiber mass loss was inferred throughout immersion from relative losses in mass in the absorption curve. Reference the future work section for methodologies to predict mass loss of fibers from biocomposites.

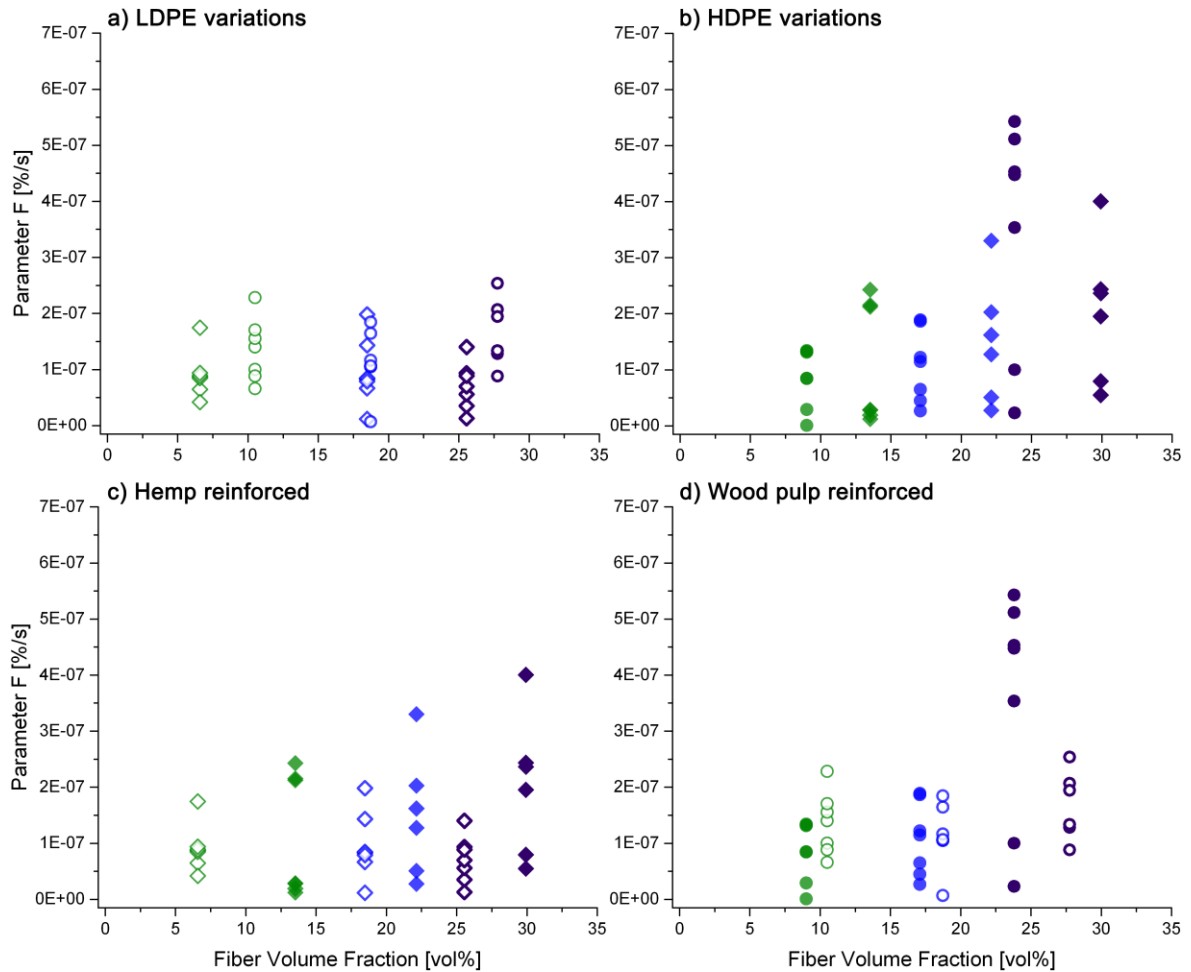


Figure 5.43 Parameter F as a function of fiber volume fraction by both matrix type a) LDPE and b) HDPE as well as by fiber type c) Hemp fiber reinforced and d) Wood pulp reinforced for all specimen geometries.

Parameter F ranges from 2E-8 to 4E-7 %/s, with the exclusion of three data points of HW45 as illustrated in Figure 5.43. An increase in fiber volume fraction results in a greater range of the rate of fiber loss rather an increase in the rate itself for all material variations. The rate of fiber loss is dependent on matrix type. LDPE demonstrated a constant rate of fiber loss of 1.2E-07 %/s, whereas for HDPE demonstrated an increase in fiber loss rate with increase fiber volume fraction for both fiber types. The differences observed support the theory that the lower matrix material modulus better allows for fiber swelling during water immersion.

The ranges observed for parameter F within each fiber volume fraction were not attributed to the accessible fiber fraction, as shown in Figure 5.44. Parameter F is constant for hemp fiber and is independent of fiber surface area fraction. The rate of fiber degradation slightly

increased for hemp reinforced HDPE to  $1.5\text{E-}07$  %/s compared to  $1.2\text{E-}07$  %/s for LH variation. For HW an increase in accessible fiber surface area resulted in an increase rate of fiber loss. The increase in fiber loss rate was attributed the inability of HDPE to deform to allow for fiber swell during absorption, hence large clumps of wood pulp were removed. As the accessible fiber surface area increased, so did the number of locations for this mechanism to take place and hence an increase in rate was observed.

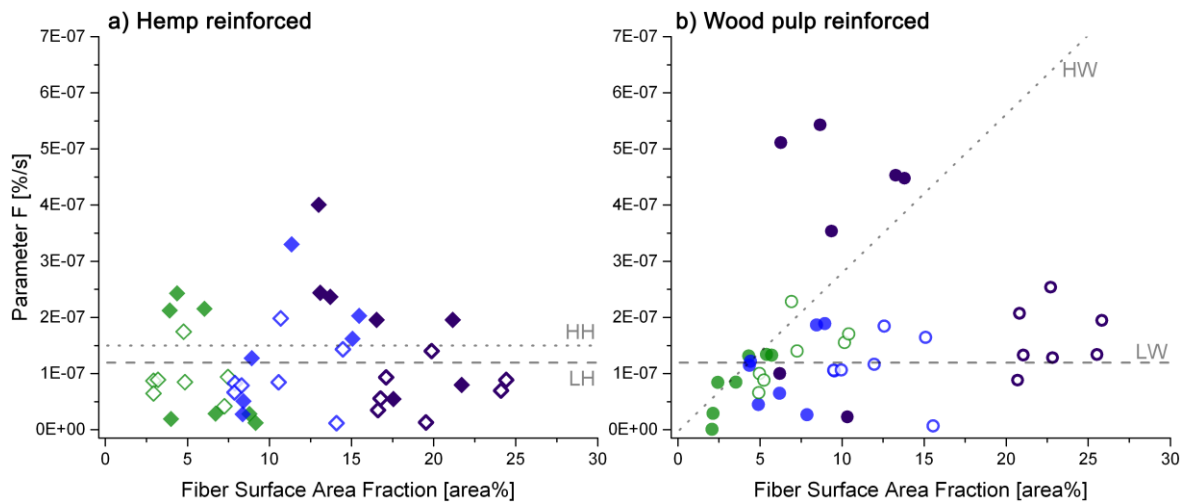


Figure 5.44 Parameter F as a function of accessible surface area fiber fraction for a) hemp fiber variations and b) wood pulp variations for all specimen geometries.

The rate of fiber mass loss is dependent on matrix type, fiber type and fiber surface area fraction and the relationships graphically displayed in Figure 5.44 are given below.

$$\text{LDPE based} \quad \text{Parameter F} = 1.2 \cdot 10^{-7} \quad (5.17)$$

$$\text{HH} \quad \text{Parameter F} = 1.5 \cdot 10^{-7} \quad (5.18)$$

$$\text{HW} \quad \text{Parameter F} = 2.8 \cdot 10^{-7} \cdot \text{Fiber Surface Area Fraction} \quad (5.19)$$

Future work is required to better understand the mechanism of fiber removal. The significance of fiber loss can be attributed to the degraded mechanical properties after immersion.

## 5.6 MODEL FUNCTIONALITY

The applicability of the model is demonstrated when utilized in conjunction with the predictive normalized mechanical properties established in Section 4, equations 4.7 to 4.11. The predicted mass gain would be plugged into each relative equation at the immersion time of interest for the percent of the retained property.

$$\text{Percent Mass Gain} = \underbrace{A*(1-e^{-B*t})}_{\text{Initial Absorption}} + \underbrace{C*(1-e^{-D*t})}_{\text{Long Term Absorption}} - \underbrace{E*(1-e^{-F*t})}_{\text{Fiber Loss}}$$

{A} Magnitude of initial water absorbed    {C} Maximum magnitude of water absorbed    {E} Magnitude of fiber dissolution  
 {B} Rate of initial water absorption        {D} Bulk biocomposite diffusion rate        {F} Rate of fiber dissolution        (5.4)

$$\% \text{ Normalized Tensile Modulus} = 100e^{-0.1048 * \text{Percent Mass Gain}} \quad (4.7)$$

$$\% \text{ Normalized Tensile Yield Strength} = 100 - \text{Percent Mass Gain} * 3.06 (\pm 0.04) \quad (4.8)$$

$$\% \text{ Normalized Ultimate Tensile Strength} = 100 - \text{Percent Mass Gain} * 1.82 (\pm 0.08) \quad (4.9)$$

$$\% \text{ Normalized Elongation at Break} = 100 + \text{Percent Mass Gain} * 9.47 (\pm 0.26) \quad (4.10)$$

### Magnitude { % Mass Gain }

**A =** Hemp fiber                      Parameter A = 0.11 \* Fiber Surface Area Fraction

Wood pulp                              Parameter A = 0.085 \* Fiber Surface Area Fraction

**C =** Hemp fiber                      Parameter C = 41.79 \* Fiber Volume Fraction

Wood pulp                              Parameter C = 24.61 \* Fiber Volume Fraction

OR

Hemp fiber                              Parameter C = 84.6 \* SA Fiber/Volume Specimen

Wood pulp                              Parameter C = 39.0 \* SA Fiber/Volume Specimen

**E =** LH                                      Parameter E = 0.42 (except LH45)

HH                                        Parameter E = 2.03

Wood pulp                              Parameter E = 0.69

**Rate {%/s}**

**B=** All Biocomposites

$$\text{Parameter B} = 5.82 \text{ E-06} * e^{17.977 * \text{Accessible Fiber Area/Volume}} \quad (5.7)$$

**D =** Interconnected

$$\text{Parameter D} = 0.93 * |\text{Diffusion Coefficient (mm}^2/\text{s)}| + 1.2 * 10^{-7} \quad (5.12)$$

Dispersed and Distributed

$$\text{Parameter D} = 0.0472 * |\text{Diffusion Coefficient (mm}^2/\text{s)}| + 1.09 * 10^{-7} \quad (5.13)$$

**F=** LDPE based                      Parameter F =  $1.2 * 10^{-7}$

HH                                      Parameter F =  $1.5 * 10^{-7}$

HW                                      Parameter F =  $2.8 * 10^{-7} * \text{Fiber Surface Area Fraction}$

The advantages of the model include:

1. The ability to assess the initial diffusion coefficient and apply it to determine the other coefficient for initial and long term absorption rates, respectively, parameter F and B.
2. The importance to experimentally determine surface accessible fiber volume fraction as the effective fiber content for water absorption and the importance of fiber volume fraction for mechanical properties.

The limitations of the model are relative to the kinetics, magnitude and mechanism of fiber loss. Fiber loss during immersion was not studied as a function of immersion time. The reasons for the models limitation include:

1. The data which pertains to fiber decay was only assessed after 6552 hours of immersion rather than as a function of immersion time. The mathematical function to predict fiber loss was assumed exponential; analogous to absorption water.
  - o At low fiber fractions, the fiber loss does not have a significant impact on the water absorption. However, it should be determined at what fiber content or surface accessible fiber area does the fiber decay influence gravimetric measurements of water absorption.
2. Only two fiber types were assessed. The fiber decay properties are likely akin to absorption properties (fiber type dependent).

3. A range of melt flow index (MFI) and polyethylene molecular weight distributions should be looked at to be able to decipher if it is the MFI influencing the fiber structure or if it is the molecular weight contribution to the dependency of diffusion coefficient or a combination of both.



## 5.7 CHAPTER SUMMARY

A comprehensive long term, 6552 hours, water immersion study investigated two matrices, (LDPE and HDPE), three fiber contents, four distinct surface area to volume specimen ratios, and four types of manufactured surfaces. The advantage of the large dataset limited common issues found within the literature such as using a consistent manufacturing method and validation of the fiber contents. The following clear trends emerged from the large volume of data:

### Initial absorption

- (1) The initial flux of water absorption increases as a function of surface accessible fiber. The flux was visualized from an increase in UV dye on the surface of specimens and seen as an increase in mass absorbed as a function of immersion time. These findings support the main mechanism of water absorption to be through the natural fiber. The utilization of back scattered SEM was proven to be a useful technique for assessment of accessible fiber ratio on a molded or machined surface.
- (2) Pseudo-Fickian to Fickian diffusion values were established for all biocomposite variations. An increase in fiber content resulted in the specimens'  $n$  value increase to 0.5, Fickian diffusion. These findings support that molecular diffusion is the fundamental process of water absorption.

### Long term absorption

- (3) Long term immersion data was required due to durations required for mass gain to plateau. An inaccurate determination of maximum water absorption impacts the assessment of the mode of diffusion as well as influencing the diffusion coefficient.
- (4) Fiber interconnectivity was proven by both:
  - a) An exponential increase in diffusion coefficient with increase fiber fraction. The exponential increase in diffusion coefficient with increased fiber fraction conveys that not only are the additional fibers absorbing water but also forming pathways to connect an even greater percentage of the fiber content to absorb water.
  - b) The averaged water content per volume fraction of fiber assessed the relative amount of water for each specimen type relative to fiber saturation point in a

high humidity environment. Specimen types at fiber contents with an average water content greater than experienced at high humidity environments were confirmed as having interconnected fiber networks within the material.

- c) The extent of fiber dispersion and distribution from manufacturing techniques has a significant influence on long term immersion due to the potential for interconnectivity.
- (5) Fiber decay was confirmed as a function of immersion time, from both gravimetric data and back scattered SEM analysis of the biocomposite surface. Fiber decay has been mentioned as a mechanism but a predictive model has never incorporated this mechanism. It is theorized that the extent of fiber decay may be dependent on the fiber network where water can wash out soluble compounds through the interconnected pathways.

All of the findings lead to a new model to predict long term water absorption data for natural fiber reinforced polyethylene biocomposites. The model builds from established principles such as Fickian diffusion with the diffusion coefficient assessed as well as expands the work from Wang on the importance of accessible fiber ratio. The proposed model in conjunction with the correlations established in section 4 for degradation of mechanical properties will help aid material designers in the prediction of long term biocomposite properties.

## 5.8 REFERENCES

1. Sar, B.E., S. Freour, P. Davies, and F. Jacquemin, *Coupling moisture diffusion and internal mechanical states in polymers - A thermodynamical approach*. European Journal of Mechanics A/Solids, 2012(36): pp. 38-43.
2. Sar, B., S. Fréour, A. Céline, and F. Jacquemin, *Accounting for differential swelling in the multi-physics modeling of the diffusive behavior of a tubular polymer structure*. Journal of Composite Materials, 2015. **49**(19): pp. 2375-2387.
3. ISO, 62 - *Plastics: Determination of water absorption*, 2008. p. 22.
4. Céline, A., S. Fréour, F. Jacquemin, and P. Casari, *Characterization and modeling of the moisture diffusion behavior of natural fibers*. Journal of Applied Polymer Science, 2013. **130**(1): pp. 297-306.
5. Crank, J. and G.S. Park, *Diffusion in Polymers* 1968: Academic Press. 452.
6. Crank, J., *The Mathematics of Diffusion*. Second ed 1975, Great Britain: Oxford University Press.
7. Jost, W., *Diffusion in Solids, Liquids, Gases*. 3rd ed. PHYSICAL CHEMISTRY: A series of monographs, ed. E. Hutchinson and P.V. Rysselberghe 1960, New York: Academic Press Inc.

## 6. CONCLUSIONS

✓ Processing ✓ Structure ✓ Property ✓ Performance

A comprehensive gravimetric and mechanical dataset were used to evaluate and analyze the impact of long term water immersion on hemp fiber and wood pulp reinforced polyethylene biocomposites. Water absorption was observed for all biocomposite specimens. Absorbed water relative to the specimens' mass correlated with an observed trend in mechanical tensile property degradation. The prediction of absorbed water within a biocomposite can also predict the mechanical performance of the material.

The two fiber types were selected to compare the difference between a chemically refined cellulose fiber (wood pulp) and a mechanically processed agriculturally produced fiber(hemp). Despite differences in chemical composition both fibers had similar densities (1.55 g/cm<sup>3</sup> and 1.53 g/cm<sup>3</sup>) and responded phenomenologically similar with absorbed water. The use of two types of polyethylene, low density and high density, allowed for the investigation of the influence of matrix permeation rates with the same chemical composition and the removal of assumption regarding the interfacial bonds based on chemical differences.

Three fiber contents were studied to determine its impact on both water absorption and mechanical properties over the range of processable volume fractions of fiber by extrusion and injection molding. The determined volume fraction of fiber based on the manufactured specimen, rather than an estimation from the material mass balance during manufacturing is a unique aspect of this study. Different specimen geometries were also assessed to explore both surface area to volume ratios and the effect of machined surfaces to simulate after part finishing. For the same material variation, the act of machining a molded specimen increased the surface accessible natural fiber and therefore increased the water absorbed.

### 6.1 WATER ABSORPTION

Water absorption in polyethylene based biocomposites is dependent on the content of natural fiber, as polyethylene absorbs significantly smaller amounts than natural fibers. Water absorption has typically been modelled over short durations (0-100 hours). Due to the environmental need for sustainable materials long term models in different environmental conditions are required to predict material performance. The proposed “dual phase absorption with decay” model leverages information obtained from short term model into a long term model, represented in equation 5.3.

The model has three terms to present the three stages observed in water immersion environments  
 1) initial absorption 2) long term absorption and 3) fiber loss.

$$\text{Percent Mass Gain} = \underbrace{A*(1-e^{-B*t})}_{\text{Initial Absorption}} + \underbrace{C*(1-e^{-D*t})}_{\text{Long Term Absorption}} - \underbrace{E*(1-e^{-F*t})}_{\text{Fiber Loss}}$$

{A} Magnitude of initial water absorbed    {C} Maximum magnitude of water absorbed    {E} Magnitude of fiber dissolution  
 {B} Rate of initial water absorption        {D} Bulk biocomposite diffusion rate        {F} Rate of fiber dissolution        (6.4)

An overview of all the parameters relative to either magnitude and rate of absorption are summarized in Table 6.1.

Table 6.1 Summary of model parameter as a function of material variation

Magnitude {% Mass Gain}	A	Hemp fiber	= 0.11 * Fiber Surface Area Fraction
		Wood pulp	= 0.085 * Fiber Surface Area Fraction
	C	Hemp fiber	= 41.79 * Fiber Volume Fraction
		Wood pulp	= 24.61 * Fiber Volume Fraction
		OR	
		Hemp fiber	= 84.6 * SA Fiber/Volume Specimen
		Wood pulp	= 39.0 * SA Fiber/Volume Specimen
	E	LH	= 0.42 (except LH45)
		HH	= 2.03
Wood pulp		= 0.69	
Rate {% per second}	B	All	= 5.82 E-06 * e <sup>17.977*Accessible Fiber Area/Volume</sup>
	D	Interconnected	= 0.93 *  Diffusion Coefficient (mm <sup>2</sup> /s) +1.2 * 10 <sup>-7</sup>
		Dispersed & Distributed	= 0.0472 *  Diffusion Coefficient (mm <sup>2</sup> /s) + 1.09 * 10 <sup>-7</sup>
	F	LDPE based	= 1.2 * 10 <sup>-7</sup>
		HH	= 1.5 * 10 <sup>-7</sup>
		HW	= 2.8 * 10 <sup>-7</sup> * Fiber Surface Area Fraction

Water absorption of natural fibers allow for tailored degradation rates. Natural fibers can control the water absorption by the selection of natural fiber type, percent volume fraction of fiber, and the extent of additional surface preparation after molding. The relative fraction of absorbed water is dependent on:

1. Percentage of surface accessible fiber.
2. Volume fraction of fibers connected to the surface accessible fibers.

3. Water capacity of the fibers, based on fiber type (internal structure, chemical composition, closed-pore porosity, etc.)
4. The extent of interfacial bonding, both physical and/or chemical, to restrain the fiber within the biocomposite to limit magnitude of mass loss by mechanical removal from swelling.

The rate at which water ingresses into the material is dependent on:

1. The rate of initial water absorption is dependent on the ratio of surface accessible fiber area to biocomposite volume for all material variations.
2. The rate of bulk water absorption is dependent on the fiber structure within the biocomposite. Interconnected versus dispersed and distributed microstructures have two separate long term absorption rates based on the diffusion coefficient of the biocomposite.
3. The diffusion coefficient is dependent on the percent of surface accessible fiber.
4. Natural fibers' dissolution rate into the aqueous medium.

## 6.2 MECHANICAL PROPERTIES

Overall, the addition of either hemp fiber or wood pulp to both types of polyethylene increased the tensile modulus and tensile yield strength. The addition of hemp and wood pulp fiber had minimal effect on ultimate tensile strength, except for HW variations which experienced a decrease with increased fiber content. Both elongation and toughness decreased with increased natural fiber, due to the brittle nature of the natural fiber. The reinforcement effect was more pronounced in the weaker matrix material, LDPE.

A direct correlation between relative mechanical properties and the percent water absorbed was demonstrated in Chapter 4. The normalized mechanical properties for both hemp fiber and wood pulp deteriorate as a function of percent mass gain of water. The effect of absorbed water was the same for both types of polyethylene. The predictive degradation equations 4.78 to 4.10 are graphed in Figure 6.1.

$$\% \text{ Normalized Tensile Modulus} = 100e^{-0.1048 * \text{Percent Mass Gain}} \quad (4.7)$$

$$\% \text{ Normalized Tensile Yield Strength} = 100 - \text{Percent Mass Gain} * 3.06 (\pm 0.04) \quad (4.8)$$

$$\% \text{ Normalized Ultimate Tensile Strength} = 100 - \text{Percent Mass Gain} * 1.82 (\pm 0.08) \quad (4.9)$$

$$\% \text{ Normalized Elongation at Break} = 100 + \text{Percent Mass Gain} * 9.47 (\pm 0.26) \quad (4.10)$$

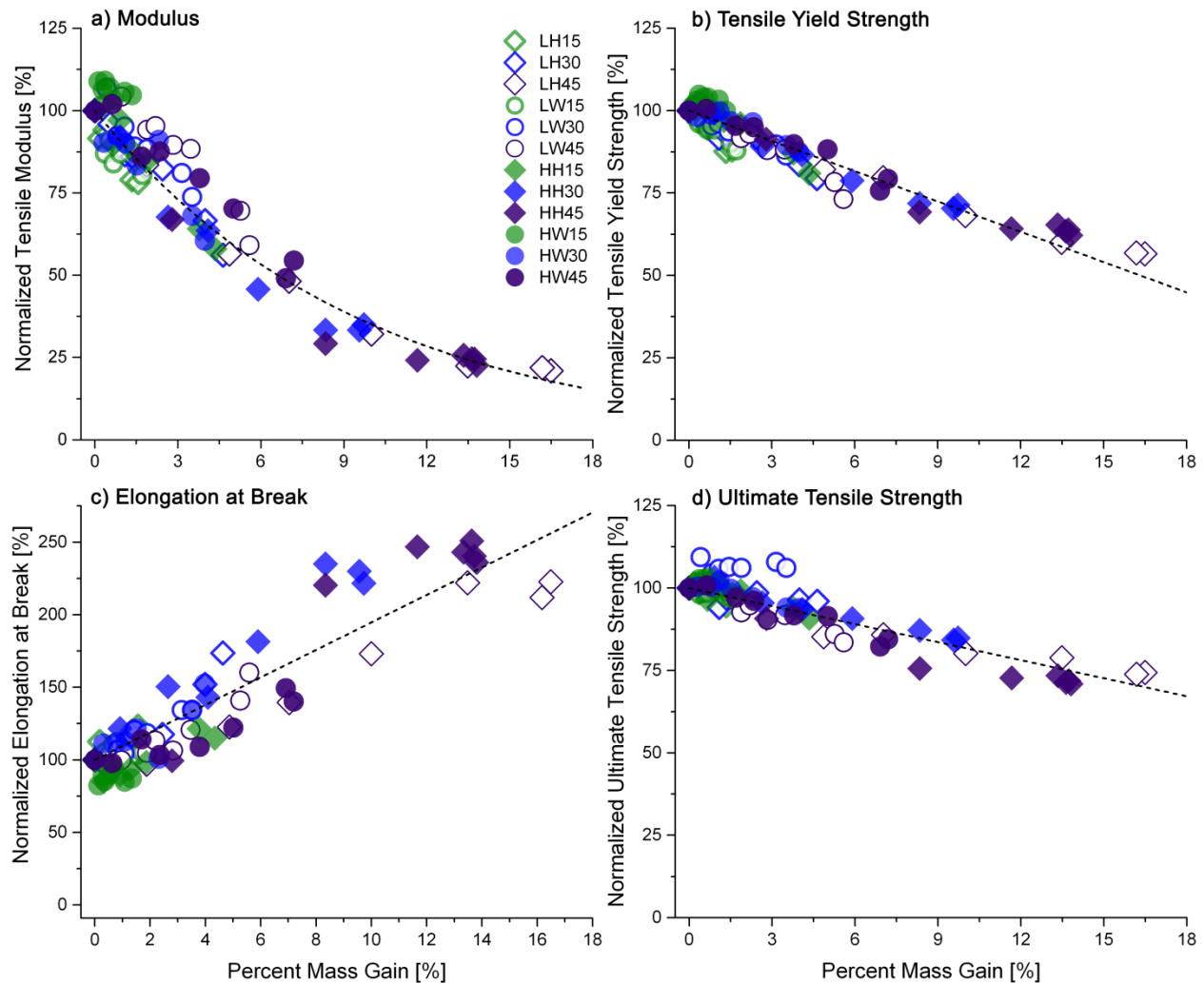


Figure 6.1 Overview of all the normalize mechanical properties as a function of water absorbed, a) Modulus, b) yield tensile strength c) elongation at break and d) ultimate tensile strength. The degradation of mechanical properties are dependent on the water absorbed within the specimen for all material variations. The colors designate the relative amount of fiber content, target 15 wt% low= green, target 30 wt% medium = blue and target 45 wt% high = purple.

The degradation in mechanical properties due to absorbed water, were not fully recovered once the specimens were dried. A permanent loss in modulus was experienced for all biocomposite variations. The higher fiber contents experienced greater permanent modulus loss. With respect to strength, yield and ultimate tensile, wood pulp variations were able to recover unlike higher fiber contents of hemp fiber reinforced biocomposites. Toughness remained nearly unchanged compared to elongation at break which experienced an increase for hemp fiber specimens.

### 6.3 SUMMARY

A predictive methodology was created for engineers to use natural fiber reinforced polyethylene biocomposites with tailored degradation rate in a water immersion environment. Water absorption was the focus to lay the foundation for future work on design of biodegradable materials, since the majority of biodegradation processes require the presence of water. Absorbed water has proven to degrade the mechanical properties of biocomposites. The tensile mechanical properties were shown to degrade as a function of absorbed water. The correlation developed applies to both matrix types and fiber types. Since the prediction of mechanical degradation was dependent on the quantity of water absorbed within the material, a predictive long term water absorption model was developed. The absorption model included the addition of a fiber loss term to dual Fickian diffusion model to account for the loss of material from the surface of the biocomposites. The other parameters in dual Fickian diffusion were linked back to quantifiable material structure parameters such as fiber volume fraction, accessible fiber surface fraction of the surface area fraction of fiber relative to the volume of the specimen. The mechanical correlations and predictive water absorption model used in combination allows for the prediction of both long term water absorption and long term mechanical properties in an immersion environment.

The model has the ability to be applied to other biocomposite systems as long as the inputs are obtained. Inputs of the model include material characterization to determine the fiber volume fraction as well as the accessible surface fiber on the composite and baseline absorption (<100 hours) and mechanical tests of the manufactured biocomposites.

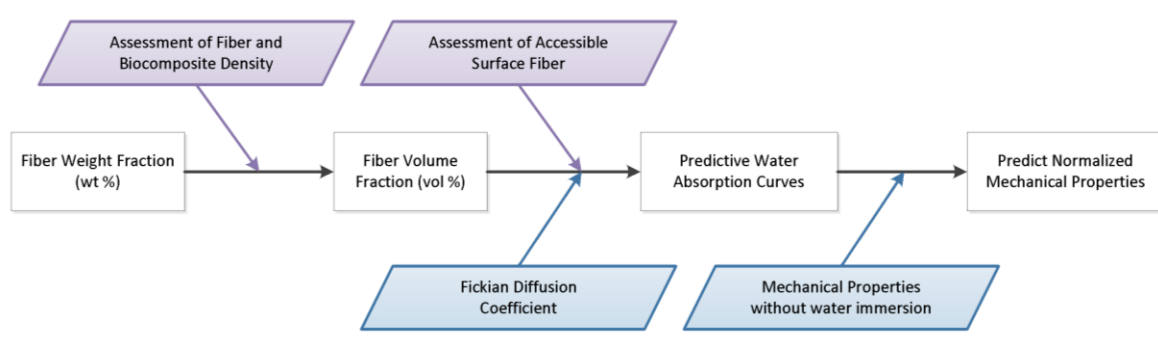


Figure 6.2 Overview of how fiber weight fraction can be translated into predict models of normalized mechanical properties from characterization of the material (purple boxes) and performance (blue boxes) completed within this work.



The predictive methodology allows a range of composites to be tailored for both short term and long term applications. The accomplished research objectives are listed below with reference to the section. The listed contributions of the research are:

1. Comprehensive long term data set of both mechanical properties and water absorption for an array of fiber types as well as fiber contents for future research. (Appendix C and Appendix D)
2. Established the requirement and method to evaluate fiber volume fraction of manufactured biocomposite specimens. (Chapter 4)
  - a. Examination and comparison of processing effects on natural fiber density.
3. Developed constitutive governing mathematical relationships to quantify the degradation of tensile mechanical properties dependent on the quantity of water absorbed from immersion environments. (Chapter 4)
4. Developed a mathematical model to predict kinetics of water absorption of a biocomposite as a function of immersion time to account for matrix type, fiber type, fiber volume fraction, surface accessible fiber, and accessible fiber surface area to specimen volume (Chapter 5)
  - a. Refined the assessment of accessible fiber ratio parameter.
    - i. Developed method to assess surface accessible fiber fraction and highlighted the differences with as molded versus cut surfaces.
  - b. Confirmed diffusion-based water absorption mechanism.
  - c. Natural fiber degradation captured into a long term water absorption model.
  - d. Model correlates short term experimental data into extrapolated long term prediction of water absorption to avoid the requirement for long term studies.

All of these contributions lead to an improved understanding of water ingress and transport in biocomposites. The research *brings designers **one incremental step** closer to the utilization of biocomposites rather than traditional non-degradable non-renewable plastics.*

## 7. FUTURE WORK

While some questions have been answered regarding how biocomposites absorb water and the subsequent degradation of mechanical properties, other questions have been uncovered. Below are areas to be further explored with the field broken down by processing, structure, property, material characterization and performance.

### Processing

1. Determine the impact on mold flow index on the percent accessible fiber on the surface on the specimen by utilizing the same fiber type with a varied MFI values. From the work conducted it is theorized that the higher the MFI at medium to high fiber contents, increases the percentage of the surface covered.

### Structure

2. Determine the impact of material isotropy on the water absorption model.
  - a. Isotropy occurs during injection molding. There is a difference between the outer skin and the inner core of the material. Also for high fill fraction there is a perceived change in fiber fraction as a function of distance from the injection gate
3. Determine a conclusive experimental method to determine fiber distribution and orientation in the specimen as well as fiber interconnectivity. Suggested methods include:
  - a. Deuterium tracing
  - b. Micro computed tomography (microCT) to not only image the fiber distribution, dispersion and fiber orientations but also to validate the assumption of negligible pore content within the fiber structure.
  - c. Magnetic resonance imaging of specimens after immersion for one year. The imaging should provide an image of all natural fibers interconnected after immersion.
  - d. Modelling fiber injection molding flows, and simulations on how the natural fibers loss length after travelling through an screw based machine.

It is suggested that future work be conducted on modelling “fiberflow” within thermoplastic systems to determine fiber orientation to predicted fibers on the surface. The ability to model and predict the natural fiber present at the surface of

the mold would enable mold designers to either tailor the biocomposites susceptibility to environmental attack (mainly water absorption and biological attack to the fibers) through the natural fibers present at the surface.

4. Determine the extent of natural fibers' structure on impact of biocomposite water absorption and its' subsequent influence on mechanical properties.
  - a. Conduct a similar study with other types of natural fibers to assess other natural fiber structures and compare the parameters. Hemp and wood pulp were similar densities and therefore structures, whereas rice husks or wheat straw have different morphological properties and is likely an additional factor to be accounted for when modelling both water absorption and its effect on mechanical properties.

#### Material Characterization

5. Development of a standard method to determine fiber volume fraction for natural fiber thermoplastic biocomposites. Evidence provided for nitrogen pycnometry for this method to determine fiber and biocomposite densities. More fiber and matrices combinations are required to establish this as a standard method to determine fiber volume assessment.

#### Mechanical Property Modelling

6. Micro-mechanical model relating known properties of fibers to the overall biocomposite.
7. Long term viscoelastic property assessment to predict how the material responds after prolonged use for practical application.

#### Moisture Absorption Modelling

8. Moisture absorption as a function of temperature was not conducted a part of this study.
9. Refine the decay function by exploration of fiber loss in different environments as well as with different matrix materials and fiber types.
  - a. Determine the magnitude of mass loss at multiple intermediate steps to validate the model and mechanism predicted

# BIBLIOGRAPHY BY CHAPTER

## INTRODUCTION REFERENCES

1. Andrady, A.L. and M.A. Neal, *Applications and societal benefits of plastics*. Philosophical Transactions of the Royal Society B: Biological Sciences, 2009. **364**(1526): pp. 1977-1984.
2. Zolfagharifard, E. *Watch humanity ruin the oceans: Nasa animation shows how vast 'garbage islands' have taken over the seas in the last 35 years*. 2015 March 31, 2017]; Available from: <http://www.dailymail.co.uk/sciencetech/article-3206442/Watch-humanity-ruin-oceans-Nasa-animation-shows-vast-garbage-islands-taken-seas-35-years.html>.
3. Parker, L. *First of Its Kind Map Reveals Extent of Ocean Plastic*. 2014 March 31, 2017]; Available from: <http://news.nationalgeographic.com/news/2014/07/140715-ocean-plastic-debris-trash-pacific-garbage-patch/>.
4. Lytle, C.I.G. *The great plastic tide*. 2016 April 2016 March 31, 2017]; Available from: <http://plastic-pollution.org/>.
5. *Pollution and Toxin: General*. 2016; Available from: <http://worldcentric.org/about-compostables/traditional-plastic/pollution>.
6. Dicker, M.P.M., P.F. Duckworth, A.B. Baker, G. Francois, M.K. Hazzard, and P.M. Weaver, *Green composites: A review of material attributes and complementary applications*. Composites Part A: Applied Science and Manufacturing, 2014. **56**: pp. 280-289.
7. Bavan, D.S. and G.C.M. Kumar, *Potential use of natural fiber composite materials in India*. Journal of Reinforced Plastics and Composites, 2010. **29**(24): pp. 3600-3613.
8. Ashori, A., *Wood-plastic composites as promising green-composites for automotive industries!* Bioresource Technology, 2008. **99**(11): pp. 4661-4667.
9. Mehta, G., A.K. Mohanty, K. Thayer, M. Misra, and L.T. Drzal, *Novel biocomposites sheet molding compounds for low cost housing panel applications*. Journal of Polymers and the Environment, 2005. **13**(2): pp. 169-175.
10. Chollakup, R., R. Tantatherdtam, S. Ujjin, and K. Sriroth, *Pineapple Leaf Fiber Reinforced Thermoplastic Composites: Effects of Fiber Length and Fiber Content on Their Characteristics*. Journal of Applied Polymer Science, 2011. **119**(4): pp. 1952-1960.
11. John, M.J. and S. Thomas, *Biofibres and biocomposites*. Carbohydrate Polymers, 2008. **71**(3): pp. 343-364.
12. Xu, Y., Q. Wu, Y. Lei, F. Yao, and Q. Zhang, *Natural Fiber Reinforced Poly(vinyl chloride) Composites: Effect of Fiber Type and Impact Modifier*. Journal of Polymers and the Environment, 2008. **16**(4): pp. 250-257.
13. Kim, S.J., J.B. Moon, G.H. Kim, and C.S. Ha, *Mechanical properties of polypropylene/natural fiber composites: Comparison of wood fiber and cotton fiber*. Polymer Testing, 2008. **27**(7): pp. 801-806.
14. Pan, M.-Z., D.-G. Zhou, J. Deng, and S.Y. Zhang, *Preparation and properties of wheat straw fiber-polypropylene composites. I. Investigation of surface treatments on the wheat straw fiber*. Journal of Applied Polymer Science, 2009. **114**(5): pp. 3049-3056.
15. Bourmaud, A. and S. Pimbert, *Investigations on mechanical properties of poly(propylene) and poly(lactic acid) reinforced by miscanthus fibers*. Composites Part A: Applied Science and Manufacturing, 2008. **39**(9): pp. 1444-1454.
16. Chand N., F.M., *Natural fibers and their composites*, in *Tribology of natural fiber polymer composites*, W.P. Limited, Editor 2008, CRC Press LLC: Boca Raton, FL. pp. 2-58.
17. Yao, F., Q.L. Wu, Y. Lei, and Y.J. Xu, *Rice straw fiber-reinforced high-density polyethylene composite: Effect of fiber type and loading*. Industrial Crops and Products, 2008. **28**(1): pp. 63-72.

18. Tajvidi, M. and A. Takemura, *Recycled Natural Fiber Polypropylene Composites: Water Absorption/Desorption Kinetics and Dimensional Stability*. Journal of Polymers and the Environment, 2010. **18**(4): pp. 500-509.
19. Salmah, H. and A. Faisal, *The Effect of Waste Office White Paper Content and Size on the Mechanical and Thermal Properties of Low-Density Polyethylene (LDPE) Composites*. Polymer-Plastics Technology and Engineering, 2010. **49**(7): pp. 672-677.
20. Mohanty, A.K., M. Misra, and L.T. Drzal, *Surface modifications of natural fibers and performance of the resulting biocomposites: An overview*. Composite Interfaces, 2001. **8**(5): pp. 313-343.
21. Faruk, O., A.K. Bledzki, H.-P. Fink, and M. Sain, *Biocomposites reinforced with natural fibers: 2000–2010*. Progress in Polymer Science, 2012. **37**(11): pp. 1552-1596.
22. Shinoj, S., S. Panigrahi, and R. Visvanathan, *Water absorption pattern and dimensional stability of oil palm fiber-linear low density polyethylene composites*. Journal of Applied Polymer Science, 2010. **117**(2): pp. 1064-1075.

## BACKGROUND REFERENCES

1. Nychka, J.A. and G.D. Hibbard. *Rethinking the Materials Paradigm: A Bottom-Up Philosophy*. in *North American Materials Education Symposium - selected oral presentation (1 of 19 from over 100 submissions)*. 2016. University of California Berkeley, Berkeley, CA.
2. Rudin, A. and P. Choi, *Chapter 13 - Biopolymers*, in *The Elements of Polymer Science & Engineering (Third Edition)*2013, Academic Press: Boston. pp. 521-535.
3. Mohanty, A.K., M. Misra, and L.T. Drzal, *Surface modifications of natural fibers and performance of the resulting biocomposites: An overview*. *Composite Interfaces*, 2001. **8**(5): pp. 313-343.
4. Graupner, N., A.S. Herrmann, and J. Mussig, *Natural and man-made cellulose fibre-reinforced poly(lactic acid) (PLA) composites: An overview about mechanical characteristics and application areas*. *Composites Part a-Applied Science and Manufacturing*, 2009. **40**(6-7): pp. 810-821.
5. Mohanty, A.K., M. Misra, and G. Hinrichsen, *Biofibres, biodegradable polymers and biocomposites: An overview*. *Macromolecular Materials and Engineering*, 2000. **276**(3-4): pp. 1-24.
6. Hughes, M., *Defects in natural fibres: their origin, characteristics and implications for natural fibre-reinforced composites*. *Journal of Materials Science*, 2012. **47**(2): pp. 599-609.
7. Thomason, J.L. and J. Carruthers, *Natural fibre cross sectional area, its variability and effects on the determination of fibre properties*. *Journal of Biobased Materials and Bioenergy*, 2012. **6**(4): pp. 424-430.
8. Fernandes, E.M., J.F. Mano, and R.L. Reis, *5. Polyethylene Composites with Lignocellulosic Material*, in *Polyethylene-Based Blends, Composites and Nanocomposites*, V. P. M and M.J.M. Morlanes, Editors. 2015, John Wiley & Sons.
9. Mohanty, A.K., L.T. Drzal, and M. Misra, *Engineered natural fiber reinforced polypropylene composites: influence of surface modifications and novel powder impregnation processing*. *Journal of Adhesion Science and Technology*, 2002. **16**(8): pp. 999-1015.
10. Reddy, N. and Y. Yang, *Biofibers from agricultural byproducts for industrial applications*. *Trends in Biotechnology*, 2005. **23**(1): pp. 22-27.
11. John, M.J. and S. Thomas, *Biofibres and biocomposites*. *Carbohydrate Polymers*, 2008. **71**(3): pp. 343-364.
12. Luo, H. and M.M. Abu-Omar, *Chemicals From Lignin A2 - Abraham, Martin A*, in *Encyclopedia of Sustainable Technologies*2017, Elsevier: Oxford. pp. 573-585.
13. John, M.J. and R.D. Anandjiwala, *Recent developments in chemical modification and characterization of natural fiber-reinforced composites*. *Polymer Composites*, 2008. **29**(2): pp. 187-207.
14. Lu, X., M.Q. Zhang, M.Z. Rong, D.L. Yue, and G.C. Yang, *Environmental degradability of self-reinforced composites made from sisal*. *Composites Science and Technology*, 2004. **64**(9): pp. 1301-1310.
15. Summerscales, J., N.P.J. Dissanayake, A.S. Virk, and W. Hall, *A review of bast fibres and their composites. Part 1 – Fibres as reinforcements*. *Composites Part A: Applied Science and Manufacturing*, 2010. **41**(10): pp. 1329-1335.
16. *Hemicellulose*. Available from: <http://www.lentinplus.net/images/arabinoxylan.gif>.
17. Rong, M.Z., M.Q. Zhang, Y. Liu, G.C. Yang, and H.M. Zeng, *The effect of fiber treatment on the mechanical properties of unidirectional sisal-reinforced epoxy composites*. *Composites Science and Technology*, 2001. **61**(10): pp. 1437-1447.
18. Materialschemist, P.-a.u.k.s.R.Z.S.a.d.w.d.w., *Polymerketten\_ -\_amorph\_und\_kristallin.svg*, Wikimedia Commons.

19. Müssig, J. and R. Martens, *Quality Aspects in Hemp Fibre Production—Influence of Cultivation, Harvesting and Retting*. Journal of Industrial Hemp, 2003. **8**(1): pp. 11-32.
20. Bos, H.L., M.J.A. Van Den Oever, and O.C.J.J. Peters, *Tensile and compressive properties of flax fibres for natural fibre reinforced composites*. Journal of Materials Science, 2002. **37**(8): pp. 1683-1692.
21. Mwaikambo, L.Y. and M.P. Ansell, *Chemical modification of hemp, sisal, jute, and kapok fibers by alkalization*. Journal of Applied Polymer Science, 2002. **84**(12): pp. 2222-2234.
22. Shah, D.U., *Natural fibre composites: Comprehensive Ashby-type materials selection charts*. Materials and Design, 2014. **62**: pp. 21-31.
23. Pickering, K.L., M.G.A. Efenidy, and T.M. Le, *A review of recent developments in natural fibre composites and their mechanical performance*. Composites Part A: Applied Science and Manufacturing, 2016. **83**: pp. 98-112.
24. Cheung, H.-y., M.-p. Ho, K.-t. Lau, F. Cardona, and D. Hui, *Natural fibre-reinforced composites for bioengineering and environmental engineering applications*. Composites Part B: Engineering, 2009. **40**(7): pp. 655-663.
25. Stamboulis, A., C.A. Baillie, S.K. Garkhail, H.G.H. Van Melick, and T. Peijs, *Environmental Durability of Flax Fibres and their Composites based on Polypropylene Matrix*. Applied Composite Materials, 2000(7): pp. 273-294.
26. Nakamura, K., T. Hatakeyama, and H. Hatakeyama, *Studies on Bound Water of Cellulose by Differential Scanning Calorimetry*. Textile Research Journal, 1981. **51**(9): pp. 607-613.
27. Lee, J.M., J.J. Pawlak, and J.A. Heitmann, *Longitudinal and concurrent dimensional changes of cellulose aggregate fibrils during sorption stages*. Materials Characterization, 2010. **61**(5): pp. 507-517.
28. Celino, A., S. Freour, F. Jacquemin, and P. Casari, *The hygroscopic behavior of plant fibers: a review*. Frontiers in Chemistry, 2014. **2**.
29. Céline, A., S. Fréour, F. Jacquemin, and P. Casari, *Characterization and modeling of the moisture diffusion behavior of natural fibers*. Journal of Applied Polymer Science, 2013. **130**(1): pp. 297-306.
30. Saikia, D., *Studies of Water Absorption Behavior of Plant Fibers at Different Temperatures*. International Journal of Thermophysics, 2010. **31**: pp. 1020-1026.
31. Biron, M., *Thermoplastics and Thermoplastics Composites*, 2007.
32. Biron, M., *2 - The Plastics Industry: Economic Overview*, in *Thermoplastics and Thermoplastic Composites (Second Edition)* 2013, William Andrew Publishing. pp. 31-131.
33. Osswald, T.A., *Polymer Processing* 1998, Munich: Hanser Publishers. 229.
34. Freedomia, *World Polyethylene*, in *World Collection* 2014.
35. McKeen, L.W., *9 - Polyolefins, Polyvinyls, and Acrylics*, in *Permeability Properties of Plastics and Elastomers (Third Edition)* 2012, William Andrew Publishing: Oxford. pp. 145-193.
36. Flaconneche, B., J. Matrin, and M.H. Klopffer, *Permeability, Diffusion and Solubility of Gases in Polyethylene, Polyamide 11 and Poly(vinylidene fluoride)*. Oil & Gas Science and Technology, 2001. **56**(3): pp. 261-278.
37. Fotouh, A., J. Wolodko, and M. Lipsett, *Isotherm moisture absorption kinetics in natural-fiber-reinforced polymer under immersion conditions*. Journal of Composite Materials, 2015. **49**(11): pp. 1301-1314.
38. Plastics Design Library, S., *Permeability and Other Film Properties of Plastics and Elastomers*, 1995, William Andrew Publishing/Plastics Design Library.
39. Jasinska, I., *Analysis of thermal decomposition of selected natural fibres on the basis of visual changes during heating*. Industria Textila, 2016. **67**(5): pp. 287-291.
40. Robertson, N.M., J.A. Nychka, and J. Wolodko. *Standardized Thermal Analysis of Natural Fibers in Biocomposites*. in *Faculty of Engineering Graduate Research Symposium*. 2010. Edmonton, Alberta, Canada.

41. *MatWeb: Material Property Data*, 2017, MatWeb, LLC.
42. Chand N., F.M., *Natural fibers and their composites*, in *Tribology of natural fiber polymer composites*, W.P. Limited, Editor 2008, CRC Press LLC: Boca Raton, FL. pp. 2-58.
43. Peltola, H., E. Laatikainen, and P. Jetsu, *Effects of physical treatment of wood fibres on fibre morphology and biocomposite properties*. *Plastics, Rubber and Composites*. **40**: pp. 86-92.
44. Robertson, N.L.M., J.A. Nychka, K. Alemaskin, and J.D. Wolodko, *Mechanical performance and moisture absorption of various natural fiber reinforced thermoplastic composites*. *Journal of Applied Polymer Science*, 2013. **130**(2): pp. 969-980.
45. Mukhopadhyay, S. and R. Fangueiro, *Physical Modification of Natural Fibers and Thermoplastic Films for Composites - A Review*. *Journal of Thermoplastic Composite Materials*, 2009. **22**(2): pp. 135-162.
46. Belgacem, M.N., Bataille P., & Sapiera S., *Effect of Corona Modification on the Mechanical Properties of Polypropylene/Cellulose Composites*. *Journal of Applied Polymer Science*, 1994. **53**: pp. 379 - 385.
47. Cabral, H., M. Cisneros, J.M. Kenny, A. Vázquez, and C.R. Bernal, *Structure-properties relationship of short jute fiber-reinforced polypropylene composites*. *Journal of Composite Materials*, 2005. **39**(1): pp. 51-65.
48. Tajvidi, M. and A. Takemura, *Recycled Natural Fiber Polypropylene Composites: Water Absorption/Desorption Kinetics and Dimensional Stability*. *Journal of Polymers and the Environment*, 2010. **18**(4): pp. 500-509.
49. Wang, W., *Moisture sorption and hygro-thermal expansion of natural fiber plastic composites (NFPC)*, 2005, University of Toronto (Canada): Canada. p. 103.
50. Awal, A., S.B. Ghosh, and M. Sain, *Development and morphological characterization of wood pulp reinforced biocomposite fibers*. *Journal of Materials Science*, 2009. **44**: pp. 2876-2881.
51. Li, X., L.G. Tabil, and S. Panigrahi, *A Study on Flax Fiber-reinforced Polyethylene Biocomposites*. *Applied Engineering in Agriculture*, 2009. **25**(4): pp. 525-531.
52. Agarwal, B.D., L.J. Broutman & Chandrashekhara K., ed. *Analysis and Performance of Fiber Composites*. 3rd ed. 2006, John Wiley & Sons Inc: New Jersey. 562.
53. Zykova, A.K., P.V. Pantyukhov, N.N. Kolesnikova, T.V. Monakhova, and A.A. Popov, *Influence of Filler Particle Size on Physical Properties and Biodegradation of Biocomposites Based on Low-Density Polyethylene and Lignocellulosic Fillers*. 2017: pp. 1-12.
54. Adhikary, K.B., S. Pang, and M.P. Staiger, *Long-term moisture absorption and thickness swelling behaviour of recycled thermoplastics reinforced with Pinus radiata sawdust*. *Chemical Engineering Journal*, 2008. **142**(2): pp. 190-198.
55. Joseph, P.V., M.S. Rabello, L.H.C. Mattoso, K. Joseph, and S. Thomas, *Environmental effects on the degradation behaviour of sisal fibre reinforced polypropylene composites*. *Composites Science and Technology*, 2002. **62**(10): pp. 1357-1372.
56. Tobin, W.J., *Scientific Injection Molding: The Qualifications, Startups, and Tryouts of Injection Molds*. Fourth Edition ed2010: WJT Associates LLC.
57. ASTM, *D1238-13 Standard Test Method for Melt Flow Rates of Thermoplastics by Extrusion Plastometer*, 2013, ASTM International: West Conshohocken, PA.
58. Beg, M.D.H. and K.L. Pickering, *Mechanical performance of Kraft fibre reinforced polypropylene composites: Influence of fibre length, fibre beating and hygrothermal ageing*. *Composites Part A: Applied Science and Manufacturing*, 2008. **39**(11): pp. 1748-1755.
59. *Definition of MECHANISM*, 2017, Merriam-Webster.
60. Azwa, Z.N., B.F. Yousif, A.C. Manalo, and W. Karunasena, *A review on the degradability of polymeric composites based on natural fibres*. *Materials & Design*, 2013. **47**: pp. 424-442.
61. Zammarano, M., P.H. Maupin, L.-P. Sung, J.W. Gilman, E.D. McCarthy, Y.S. Kim, and D.M. Fox, *Revealing the Interface in Polymer Nanocomposites*. *ACS Nano*, 2011. **5**(4): pp. 3391-3399.



62. Le Duigou, A., A. Bourmaud, P. Davies, and C. Baley, *Long term immersion in natural seawater of Flax/PLA biocomposite*. Ocean Engineering, 2014. **90**: pp. 140-148.
63. Kittikorn, T., E. Stromberg, M. Ek, and S. Karlsson, *Comparison of Water Uptake as Function of Surface Modification of Empty Fruit Bunch Oil Palm Fibres in PP Biocomposites*. Bioresources, 2013. **8**(2): pp. 2998-3016.
64. Shakeri, A. and A. Ghasemian, *Water Absorption and Thickness Swelling Behavior of Polypropylene Reinforced with Hybrid Recycled Newspaper and Glass Fiber*. Applied Composite Materials, 2010. **17**: pp. 183-193.
65. Nychka, J.A. and M.M. Gentleman, *Implications of wettability in biological materials science*. JOM, 2010. **62**(7): pp. 39-48.
66. *Percolation Theory and Forest Fires*. [cited 2017; Available from: <http://www1.coe.neu.edu/~emelas/NetForestFires.htm>.
67. Crank, J., *The Mathematics of Diffusion*. Second ed 1975, Great Britain: Oxford University Press.
68. Rudin, A. and P. Choi, *Chapter 6 - Diffusion in Polymers*, in *The Elements of Polymer Science & Engineering (Third Edition)* 2013, Academic Press: Boston. pp. 275-304.
69. Karimi, M., *Diffusion in Polymer Solids and Solutions*, in *Mass Transfer in Chemical Engineering Processes*, J.E. MarkoÅ, Editor 2011, InTech.
70. Alfrey Jr. T, G.E., Lloyd WG., *Diffusion in Glassy Polymers*. J Polym Sci: Part C 1966. **1966**(12).
71. MiSumi. *Plastic Molding Tutorial*. 2011 [cited 2017 August 5]; Available from: <http://www.misumi-techcentral.com/tt/en/mold/2011/12/106-glass-transition-temperature-tg-of-plastics.html>.
72. Espert, A., F. Vilaplana, and S. Karlsson, *Comparison of water absorption in natural cellulosic fibres from wood and one-year crops in polypropylene composites and its influence on their mechanical properties*. Composites Part A: Applied Science and Manufacturing, 2004. **35**(11): pp. 1267-1276.
73. Arbelaiz, A., B. Fernández, J.A. Ramos, A. Retegi, R. Llano-Ponte, and I. Mondragon, *Mechanical properties of short flax fibre bundle/polypropylene composites: Influence of matrix/fibre modification, fibre content, water uptake and recycling*. Composites Science and Technology, 2005. **65**(10): pp. 1582-1592.
74. ISO, *62 - Plastics: Determination of water absorption*, 2008. p. 22.
75. Shen, C.-H. and G.S. Springer, *Moisture Absorption and Desorption of Composite Materials*. Journal of Composite Materials, 1976. **10**(1): pp. 2-20.
76. Jost, W., *Diffusion in Solids, Liquids, Gases*. 3rd ed. PHYSICAL CHEMISTRY: A series of monographs, ed. E. Hutchinson and P.V. Rysselberghe 1960, New York: Academic Press Inc.
77. Lin, Q.F., X.D. Zhou, and G. Dai, *Effect of hydrothermal environment on moisture absorption and mechanical properties of wood flour-filled polypropylene composites*. Journal of Applied Polymer Science, 2002. **85**(14): pp. 2824-2832.
78. ISO, *180 - Plastics - Determination of Izod impact strength*, 2013. p. 10.
79. Xie, Y., C.A.S. Hill, Z. Jalaludin, S.F. Curling, R.D. Anandjiwala, A.J. Norton, and G. Newman, *The dynamic water vapour sorption behaviour of natural fibres and kinetic analysis using the parallel exponential kinetics model*. Journal of Materials Science, 2011. **46**(2): pp. 479-489.
80. Ambrozic, M., A. Dakskobler, M. Valant, and T. Kosmac, *Percolation threshold model and its application to the electrical conductivity of layered BaTiO<sub>3</sub>-Ni*. Materials Science-Poland, 2005. **23**(2): pp. 535-539.
81. Wang, W., M. Sain, and P.A. Cooper, *Study of moisture absorption in natural fiber plastic composites*. Composites Science and Technology, 2006. **66**(3-4): pp. 379-86.
82. Ashby, M.F., *13. Processes and Process Selection*, in *Materials Selection in Mechanical Design (4th Edition)*, Elsevier.

## EXPERIMENTAL DESIGN & DESCRIPTION REFERENCES

1. Ohaus. *MB25 Moisture Analyzer*. 2010 [2015/04/25]; Available from: <http://mea.ohaus.com/mea/en/home/products/product-families/MB25-EU.aspx>.
2. Robertson, N.L.M., J.A. Nychka, K. Alemaskin, and J.D. Wolodko, *Mechanical performance and moisture absorption of various natural fiber reinforced thermoplastic composites*. Journal of Applied Polymer Science, 2013. **130**(2): pp. 969-980.
3. ISO, *294-1 Plastics - Injection moulding of test specimens of thermoplastic materials -*, in *Part 1: General principles, and moulding of multipurpose and bar test specimens* 2000. p. 20.
4. Tobin, W.J., *Scientific Injection Molding: The Qualifications, Startups, and Tryouts of Injection Molds*. Fourth Edition ed 2010: WJT Associates LLC.
5. Truong, M., W. Zhong, S. Boyko, and M. Alcock, *A comparative study on natural fibre density measurement*. Journal of the Textile Institute, 2009. **100**(6): pp. 525-529.
6. PMI. *Gas Pycnometer*. 2009; Available from: <http://www.pmiapp.com/products/productPages/gasPycnometer.html>.
7. Lowell, S., J.E. Shields, M.A. Thomas, and M. Thommes, *Density Measurement, in Characterization of Porous Solids and Powders: Surface Area, Pore Size & Density*, B. Scarlett, Editor 2004, Kluwer Academic Publishers: Boston. p. 347.
8. Technology, N.I.o.S.a., *SRM 1827b - Lead Silica Glass Mass Density Standard*.
9. Adhikary, K.B., S. Pang, and M.P. Staiger, *Long-term moisture absorption and thickness swelling behaviour of recycled thermoplastics reinforced with Pinus radiata sawdust*. Chemical Engineering Journal, 2008. **142**(2): pp. 190-198.
10. Tajvidi, M. and A. Takemura, *Recycled Natural Fiber Polypropylene Composites: Water Absorption/Desorption Kinetics and Dimensional Stability*. Journal of Polymers and the Environment, 2010. **18**(4): pp. 500-509.
11. Wang, W., M. Sain, and P.A. Cooper, *Study of moisture absorption in natural fiber plastic composites*. Composites Science and Technology, 2006. **66**(3-4): pp. 379-86.
12. ASTM, *D570: Standard Test Method for Water Absorption of Plastics*, 1998 (Reapproved 2010). p. 4.
13. ISO, *62 - Plastics: Determination of water absorption*, 2008. p. 22.
14. ASTM, *D638: Standard Test Method for Tensile Properties of Plastics*, 2010. p. 16.
15. *Bluehill 2 Calculations Reference: Reference Manual - Software*, 2012, Instron. pp. 1-224.
16. Schindelin, J., I. Arganda-Carreras, E. Frise, V. Kaynig, M. Longair, T. Pietzsch, S. Preibisch, C. Rueden, S. Saalfeld, B. Schmid, J.-Y. Tinevez, D.J. White, V. Hartenstein, K. Eliceiri, P. Tomancak, and A. Cardona, *Fiji: an open-source platform for biological-image analysis*. Nat Meth, 2012. **9**(7): pp. 676-682.
17. Komuraiah, A., N.S. Kumar, and B.D. Prasad, *Chemical Composition of Natural Fibers and its Influence on their Mechanical Properties*. Mechanics of Composite Materials, 2014. **50**(3): pp. 359-376.
18. Krasowska, K., J. Brzeska, M. Rutkowska, H. Janik, M.S. Sreekala, K. Goda, and T. Sabu, *Environmental Degradation of Ramie Fibre Reinforced Biocomposites*. Polish Journal of Environmental Studies, 2010. **19**(5): pp. 937-945.
19. *Equilibrium Relative Humidity Saturated Salt Solutions*. 2013; Available from: [www.omega.ca/temperature/Z/pdf/z103.pdf](http://www.omega.ca/temperature/Z/pdf/z103.pdf).
20. Scientific, C.-P. *Pyrex 3120-250 Brand 3120 dessicator, 250 mm*. [cited 2017 2017-03-23]; Available from: <https://www.coleparmer.com/i/pyrex-3120-250-brand-3120-dessicator-250-mm/3454923>.

## IMPACT OF WATER ON MECHANICAL PROPERTIES REFERENCES

1. Greenhalgh, E. and M. Hiley, *Fractography of polymer composites: current status and future issues*, in *13th European Conference on Composite Materials* 2008.
2. Agarwal, B.D., L.J. Broutman & Chandrashekhara K., ed. *Analysis and Performance of Fiber Composites*. 3rd ed. 2006, John Wiley & Sons Inc: New Jersey. 562.
3. Rotheron, R.N., *Particulate-filled Polymer Composites* 2003: Rapra Technology Limited.
4. John Bootle, Frank Burzesi, and L. Fiorini, *Design Guidelines*, in *ASM Handbook: Composites* 2001, ASM International. p. 1201.
5. Dicker, M.P.M., P.F. Duckworth, A.B. Baker, G. Francois, M.K. Hazzard, and P.M. Weaver, *Green composites: A review of material attributes and complementary applications*. *Composites Part A: Applied Science and Manufacturing*, 2014. **56**: pp. 280-289.
6. Robertson, N.L.M., J.A. Nychka, K. Alemaskin, and J.D. Wolodko, *Mechanical performance and moisture absorption of various natural fiber reinforced thermoplastic composites*. *Journal of Applied Polymer Science*, 2013. **130**(2): pp. 969-980.
7. Joseph, P.V., M.S. Rabello, L.H.C. Mattoso, K. Joseph, and S. Thomas, *Environmental effects on the degradation behaviour of sisal fibre reinforced polypropylene composites*. *Composites Science and Technology*, 2002. **62**(10): pp. 1357-1372.
8. Arbelaiz, A., B. Fernández, J.A. Ramos, A. Retegi, R. Llano-Ponte, and I. Mondragon, *Mechanical properties of short flax fibre bundle/polypropylene composites: Influence of matrix/fibre modification, fibre content, water uptake and recycling*. *Composites Science and Technology*, 2005. **65**(10): pp. 1582-1592.
9. Beg, M.D.H. and K.L. Pickering, *Mechanical performance of Kraft fibre reinforced polypropylene composites: Influence of fibre length, fibre beating and hygrothermal ageing*. *Composites Part A: Applied Science and Manufacturing*, 2008. **39**(11): pp. 1748-1755.
10. Lin, Q.F., X.D. Zhou, and G. Dai, *Effect of hydrothermal environment on moisture absorption and mechanical properties of wood flour-filled polypropylene composites*. *Journal of Applied Polymer Science*, 2002. **85**(14): pp. 2824-2832.
11. Kittikorn, T., E. Stromberg, M. Ek, and S. Karlsson, *Comparison of Water Uptake as Function of Surface Modification of Empty Fruit Bunch Oil Palm Fibres in PP Biocomposites*. *Bioresources*, 2013. **8**(2): pp. 2998-3016.
12. Stamboulis, A., C.A. Baillie, S.K. Garkhail, H.G.H. Van Melick, and T. Peijs, *Environmental Durability of Flax Fibres and their Composites based on Polypropylene Matrix*. *Applied Composite Materials*, 2000(7): pp. 273-294.
13. Adhikary, K.B., S. Pang, and M.P. Staiger, *Long-term moisture absorption and thickness swelling behaviour of recycled thermoplastics reinforced with Pinus radiata sawdust*. *Chemical Engineering Journal*, 2008. **142**(2): pp. 190-198.
14. Le Duigou, A., A. Bourmaud, P. Davies, and C. Baley, *Long term immersion in natural seawater of Flax/PLA biocomposite*. *Ocean Engineering*, 2014. **90**: pp. 140-148.
15. Espert, A., F. Vilaplana, and S. Karlsson, *Comparison of water absorption in natural cellulosic fibres from wood and one-year crops in polypropylene composites and its influence on their mechanical properties*. *Composites Part A: Applied Science and Manufacturing*, 2004. **35**(11): pp. 1267-1276.
16. *Elongation at Break*. 2016 [cited 2016 July 3, 2017]; Available from: <http://www.ensinger-online.com/en/technical-information/properties-of-plastics/mechanical-properties/elongation-at-break/>.
17. ISO, *180 - Plastics - Determination of Izod impact strength*, 2013. p. 10.
18. ISO, *179-1 Plastics - Determination of Charpy impact properties*, 2010. p. 28.
19. ISO, *8256 - Plastics - Determination of Tensile-Impact Strength*, 2004. p. 22.

20. Truong, M., W. Zhong, S. Boyko, and M. Alcock, *A comparative study on natural fibre density measurement*. Journal of the Textile Institute, 2009. **100**(6): pp. 525-529.

## PHENOMENON, MECHANISM AND PREDICTIVE WATER ABSORPTION MODEL IN BIOCOMPOSITES REFERENCES

1. Sar, B.E., S. Freour, P. Davies, and F. Jacquemin, *Coupling moisture diffusion and internal mechanical states in polymers - A thermodynamical approach*. European Journal of Mechanics A/Solids, 2012(36): pp. 38-43.
2. Sar, B., S. Fréour, A. Céline, and F. Jacquemin, *Accounting for differential swelling in the multi-physics modeling of the diffusive behavior of a tubular polymer structure*. Journal of Composite Materials, 2015. **49**(19): pp. 2375-2387.
3. ISO, *62 - Plastics: Determination of water absorption*, 2008. p. 22.
4. Céline, A., S. Fréour, F. Jacquemin, and P. Casari, *Characterization and modeling of the moisture diffusion behavior of natural fibers*. Journal of Applied Polymer Science, 2013. **130**(1): pp. 297-306.
5. Crank, J. and G.S. Park, *Diffusion in Polymers* 1968: Academic Press. 452.
6. Crank, J., *The Mathematics of Diffusion*. Second ed 1975, Great Britain: Oxford University Press.
7. Jost, W., *Diffusion in Solids, Liquids, Gases*. 3rd ed. PHYSICAL CHEMISTRY: A series of monographs, ed. E. Hutchinson and P.V. Rysselberghe 1960, New York: Academic Press Inc.

## CONCLUSIONS

None

## FUTURE WORK

None

## APPENDICES REFERENCES

1. Bell, S.A. *Measurement Good Practice Guide: A Beginner's Guide to Uncertainty of Measurement*. 2001. 41.
2. *Combined Standard Uncertainty and Propagation of Uncertainty*. 2011 [cited 2015 August 5, 2015]; Available from: <https://www.nde-ed.org/GeneralResources/Uncertainty/Combined.htm>.
3. ASTM, *E4 - 13 Standard Practices for Force Verification of Testing Machines*, 2013, ASTM.

## A. APPENDIX: BIOCOMPOSITES MANUFACTURING PARAMETERS

### A.1 CALIBRATION FEED RATE FOR MATRIX AND FIBER

The auger type feeders utilized demonstrated a linear relationship between average mass rate (g/min) to dial setting for all polymer and fiber types. An example calibration curve has been shown in Figure A.1. In order to establish each feeder's relationship for a particular material type, a minimum of 5 replicate mass samples were taken in 20 second intervals at a minimum of 7 dial settings surrounding the dial setting selected. The mass samples were obtained a minimum 1 hour after the gravimetric feeders had warmed up and been operational. The slope was used to determine the dial setting to both produce targeted fiber fraction and quantity of biocomposite manufactured. The target quantity of manufactured biocomposite mass was between 3.00 – 5.00 kg/hr dependent on the target fiber fraction. The plastic feed rate was kept constant, 0.35 or 0.4, within each matrix fiber combination to limit experimental error in one of the gravimetric feeders.

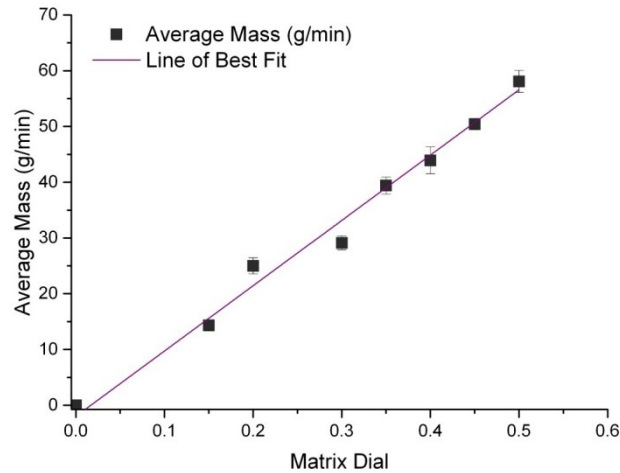


Figure A.1 Example Calibration Curve of High Density Polyethylene Pellets

The equations A.1 to A.3 illustrate the relationship between mass flow and dial setting by the slope of the calibration curve where subscripts  $m$  refers to matrix material and  $f$  refers to fiber. For a specific matrix mass flow rate, the fiber dial setting was calculated to achieve the target weight fraction of fiber,  $W_f$ .

$$\dot{m}_m = dial_m * \mu_{\dot{m}_m} \quad (A.1)$$

$$\dot{m}_f = \frac{\dot{m}_m * W_f}{W_m} \quad (A.2)$$

$$\frac{\dot{m}_f}{\mu_{\dot{m}_f}} = dial_f \quad (A.3)$$

Where:  $\dot{m}$  = mass flow  
 $\mu$  = slope of calibration curve  
 $dial$  = dial speed setting

For both fiber types the gravimetric feed was calibrated at half increments. An example calibration curve is shown in Figure A.2 for pelletized – Wiley milled wood pulp fiber. Natural fibers, unlike polymer pellets, may have a critical dial speed where the auger spins more quickly than the fiber can fall onto the screw due the fibers lightweight fluffy nature. The full range was explored to ensure the fiber dial speeds set with a minimum 1 dial increment buffer.

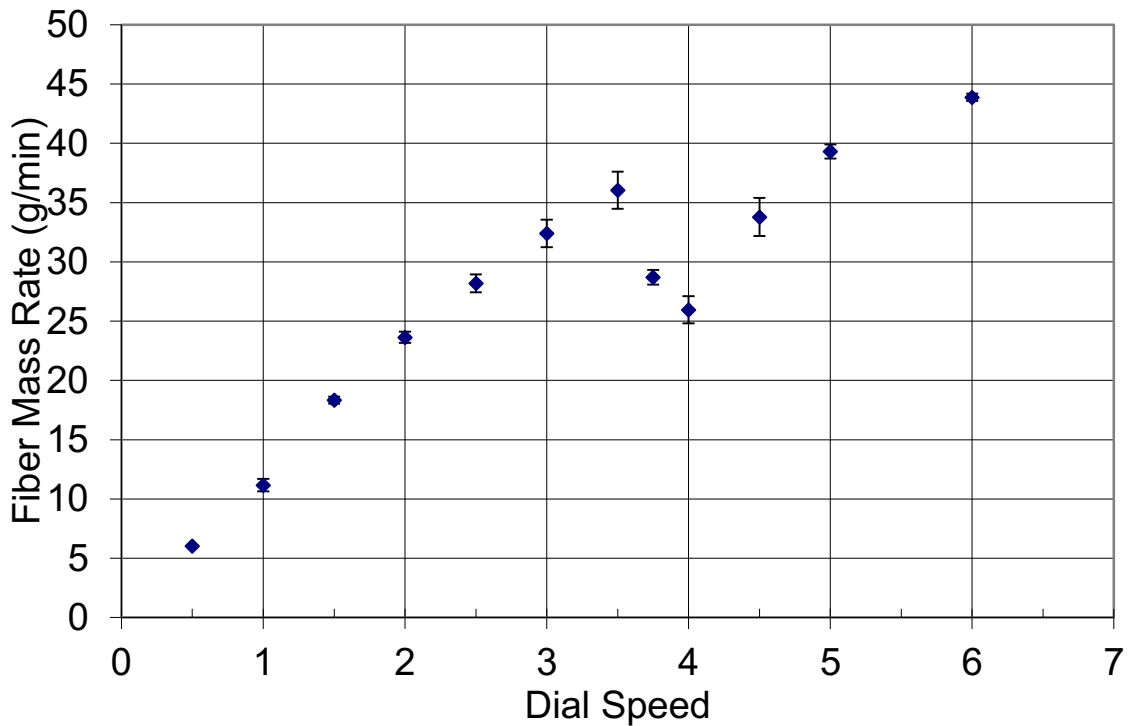


Figure A.2 Example of Wood Pulp Pelletized and Wiley milled gravimetric calibration curve with the error bars graphed with the standard deviation.

## A.2 ADDITIONAL FIBER PROCESSING INFORMATION

The optimized fiber processing trails assessed different methods of fiber compaction to enable the fiber to be gravimetrically fed. The fiber form had to pass both conditions to be considered as a viable option to manufacture the biocomposite:

1. Repeatable fiber mass feed rate where the standard deviation represented less than 10% of the total fiber feed rate measured in 20 second intervals.
2. Slowly fed the processed fiber at very low fiber volume fractions to assess visually if the fiber form had changed form, as shown in Figure A.3.

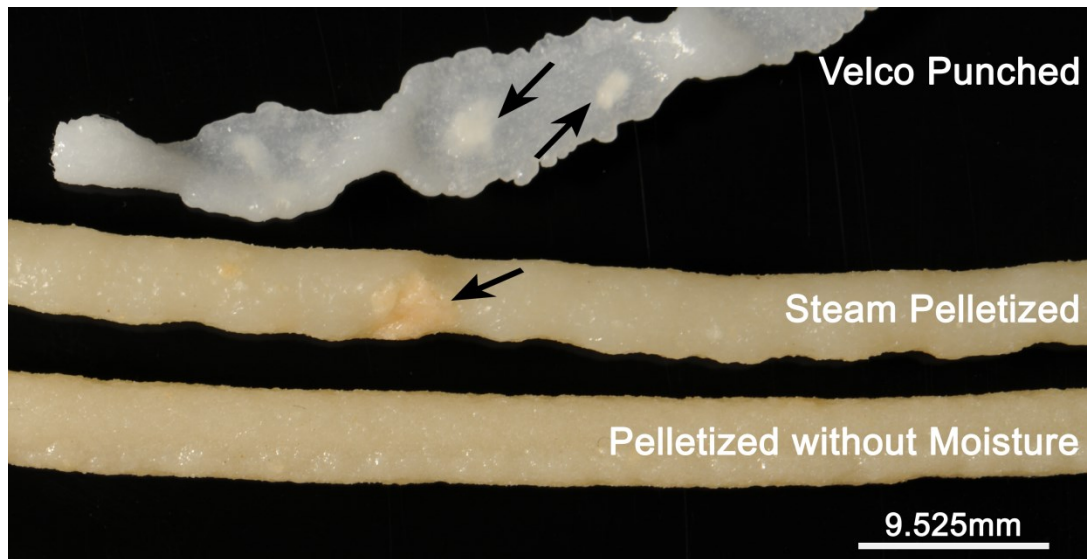


Figure A.3 Example of visual assessment between variations fiber forms of wood pulp (top down) velco punched, steam pelletized and pelletized without addition of moisture extruded with HDPE. From this trail, pelletized without moisture was selected to have promise dispersing into the melt. The black arrows point to locations with noticeable fiber clusters.



### A.3 SUMMARY OF EXTRUSION PARAMETERS

Table A.1 - Summary of Extrusion Parameters

Date YY-MM-DD	Target Material	Feeder Settings			Extruder Settings					Vacuum (bar)	Cutter Speed	
		Plastic Dial	Fiber Dial	Side Feeder Dial	Zone Temp (°C) T <sub>1</sub> -T <sub>2</sub> -T <sub>3</sub> -T <sub>4</sub> -T <sub>5</sub> -T <sub>6</sub> -T <sub>7</sub> -T <sub>8</sub> -T <sub>9</sub> -T <sub>10</sub>	Screw Speed (rpm)	Torque (N-m)	Nozzle Pressure (bar)				
HDPE DMDA8920												
3/22/2012	HH15	0.36	0.5	60	190-190-190-190-190-190-190-180-160-160	120	62	13	-0.22	45		
3/22/2012	HH30	0.35	0.95	70	190-190-190-190-190-190-190-180-160-160	120	65	20	-0.2	45		
3/22/2012	HH45	0.35	1.65	75	190-190-190-190-190-190-190-180-160-160	120	70	38	-0.2	55		
3/2/2012	HW15	0.4	0.58	55.15	190-190-190-190-190-190-190-180-160-140	120	45	10	-0.5	60		
3/2/2012	HW30	0.4	1.41	65	190-190-190-190-190-190-190-180-160-140	120	68	20	-0.5	60		
3/2/2012	HW45	0.4	2.69	80.65	190-190-190-190-190-190-190-180-160-140	120	75	25	-0.5	55		
LDPE AT220												
4/30/2012	LH15	0.4	0.3	50	200-200-200-200-200-200-200-190-160-160	120	35	6	-0.2	45		
5/3/2012	LH30	0.4	0.73	60	200-200-200-200-200-200-200-190-180-160	120	47	26	-0.2	35		
5/3/2012	LH45	0.4	1.4	65	200-200-200-200-200-200-200-190-180-160	120	55	48	-0.2	45		
4/9/2012	LW15	0.4	0.41	60	200-200-200-200-200-200-200-190-160-160	120	50	19	-0.2	35		
4/9/2012	LW30	0.4	0.99	70	200-200-200-200-200-200-200-190-160-160	120	50	27	-0.2	45		
4/12/2012	LW45	0.4	1.88	65	200-200-200-200-200-200-200-190-180-180	120	51	27	-0.2	50		

## A.4 SUMMARY OF INJECTION MOLDING PARAMETERS

Table A.2 - Summary of Injection Molding Parameters

Material	Cycle Time (sec)	Zone Temp (°C) N-T <sub>1</sub> -T <sub>2</sub> -T <sub>3</sub>	INJECTION				HOLDING/TRANSITION				COOLING		RECOVERY	
			Start (mm)	Time (sec)	Speed (%)	Pressure Limit (bar)	Start Position (mm)	Cushion (mm)	Hold Time (sec)	Pressure (bar)	Cooling (sec)	Recovery Time (sec)	Speed (%)	Back Pressure (bar)
HDPE DMDA8920	34-36	190-190-190-190	44.5	0.37	90	130	7	0	5	40	25	10	16.8	5
HH15	26.9	190-190-190-190	54	0.56	60	160	8	4.2	3	40	19	10.5	25	10
HH30	27	190-190-190-190	54	0.56	60	157	8	4.6	3	40	19	11.14	25	10
HH45	29.3	190-190-190-190	54	0.67	50	160	8	2.5	5	70	19	15.85	27	7
HW15	26.5	190-190-190-190	46.3	0.41	80	130	8.5	0.4	4	40-50	19	13	25	0
HW30	28.5	190-190-190-190	46.3	0.44	80	130	5.5	1.8-1.3	4	40	19	16	25	5
HW45	28	190-190-190-190	46.3	0.43	90	130	5.5	1.6-0.9	3	40	19	17	25	5
LDPE AT220	42-42.5	190-190-190-190	46.2	0.56	60	130	6	0.2-0	12	40	25	10.63	16.8	5
LH15	27.8	190-190-190-190	59.5	0.56	60	130	8	3.7	4	50	19	19.5	25	15
LH30	27.38	190-190-190-190	59.4	0.55	60	130	9	3.2	4	60	19	20.67	25	15
LH45 (Tensile)	25.7	190-190-190-190	36	0.86	50	160	5	4.9	3	70	17	16-18	25	15
LH45 (Flex. & Izod)	28.7	190-190-190-190	37.5	0.67	55	160	4	3.9	3	70	17	17-20	25	12
LW15	42-42.5	190-190-190-190	48.9	0.55	70	110	6.5	2.1	12	40	25	19-25	16.8	0
LW30	42-42.7	190-190-190-190	49.7	0.69	70	110	6.5	3.7-4.1	12	40	25	21-25	16.8	0
LW45	41-42	200-200-200-200	51.5	2.3-3.5	100-99	90	7	7	3	50	30	21-25	16.8	10

### A.5 NITROGEN PYCNOMETRY SENSITIVITY OF MINIMUM VOLUME

To verify the required internal volume of sample for the pycnometer, the pycnometer was ran at various fraction of the sample chamber occupied. The testing protocol at each occupied volume fraction were taken as per section 3.2.1. Stainless steel (302) ball bearings were used as the material and were incrementally added into the chamber to obtain minor incremental changes in chamber occupation fraction. The reported average density and corresponding standard deviation at 2% chamber fill was much larger than after the sample occupied 5% or greater of the chamber volume. Once the chamber was approximately 7.5% filled, the change in deviation of the sample remained constant. in the measof the measurements taken of the population decreased used as the material of choice due to the high tolerane wwith the same operating parameters of the pycnometer.

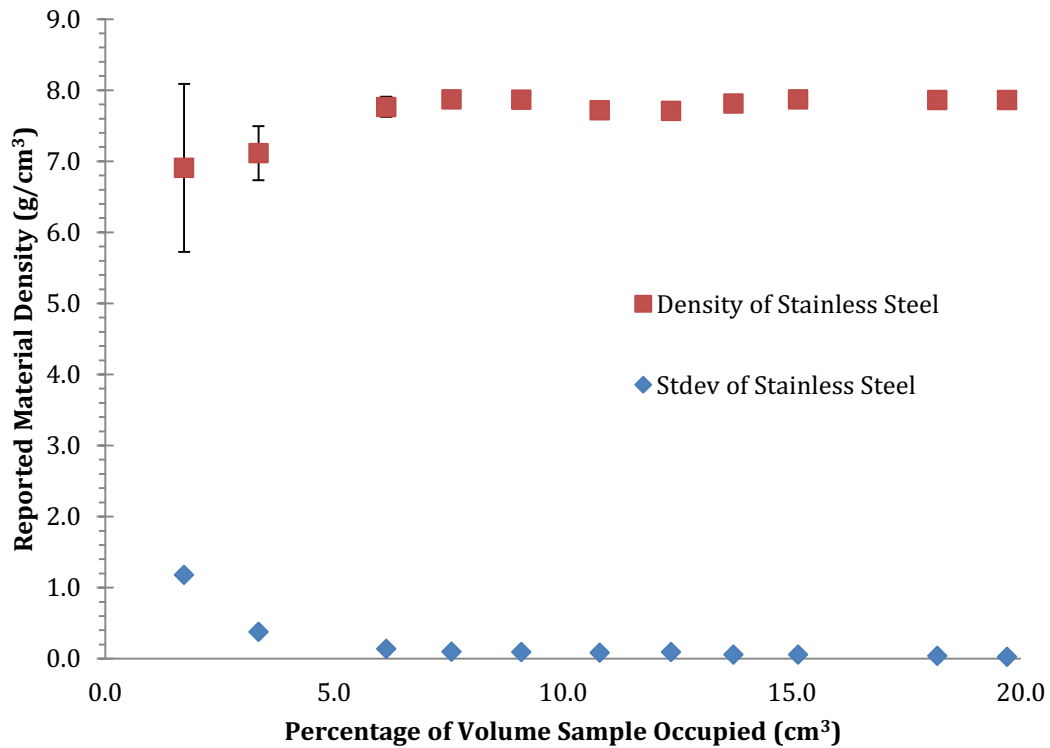


Figure A.4 Example calibration curve of high density polyethylene pellets.

## B. APPENDIX: STATISTICAL ANALYSIS OF UNCERTAINTY

This appendix quantifies the doubt surrounding each measurement and the propagated uncertainty in calculated properties. The quantification of doubt was conducted in accordance with *A Beginner's Guide to Uncertainty of Measurement* [1] and *Combined Standard Uncertainty and Propagation of Uncertainty* [2]. Uncertainty for critical measurements such as weight for analysis of percent weight gain, density to determine fiber fraction, and mechanical properties were assessed. An overview of the types of experimental uncertainty and those types which can be numerically quantified are indicated in Table B.1. The sources of uncertainty indicated will be explored in each section.

Table B.1 Overview of Quantifiable Uncertainty of Experimental Results

Sources of Uncertainty	Fiber Volume Fraction	Weight Gain	Mechanical Properties	
	Density (g/cm <sup>3</sup> )	Percent Weight Gain (%)	Dimensions (mm)	Displacement (mm)
a) Instrument Uncertainty	Yes	Yes	Yes	Yes
b) Environmental Uncertainty	Yes	No	No	No
c) Sampling Issues	No	Yes	Yes	No
d) Item Issue	No		No	No
e) Operator Error / Skill	No		No	No
f) Measurement Process / Protocol	No		No	No
g) Calibration Uncertainty	Yes	No	No	Yes

### B.1 DENSITY MEASUREMENT – UNCERTAINTY ANALYSIS

This section compares three quantitative uncertainties and the corresponding impact on the reported uncertainty of Fiber Volume Fraction ( $V_f$ ):

- 1) Uncertainty based on the calibration reference
- 2) Potential Impact from Temperature
- 3) Combined Uncertainty from the statistical results of the measurement
- 4) Combined Uncertainty from the uncertainty in each measurement from instrumentation

## **1. Calibration Uncertainty**

The standard reference material, Lead Silica Glass Mass Density Standard, used to calibrate the pycnometer and supplied by NIST is certified with a confidence level of 95% to  $\pm 0.000033\text{g/cm}^3$  the average density. This uncertainty in density of measured fiber, matrix and composite density propagated into volume fraction results in the reported  $V_f$  with a range of 0.02-0.03vol% from the reported value. Therefore, this accumulated uncertainty is negligible to the reported volume fraction of fiber.

## **2. Environmental Uncertainty based non-isothermal operating condition**

The sensitivity analysis below illustrates the relative density change corresponding to an incremented ambient chamber temperature deviation between pressure recordings. Increments of 0.1°C, 1°C, 5°C and 10°C were chosen to demonstrate the effect on density, as illustrated in Table B.2. The impact of a slight temperate deviation can potentially result in a drastic influence on density measurement and therefore the calculation of fiber volume fraction. However, the realistic possibility of the temperature changing more than 0.1°C within a measurement is highly unlikely.

Table B.2 Variation in Density with an Ambient Air Temperature deviation during measurement

		$\Delta T$ (°C)			
		0.1	1.0	5.0	10.0
$\Delta P_{\Delta T}$ (kPa)		0.1167	0.2335	1.1675	2.3350
$\Delta \rho$ (g/cm <sup>3</sup> )	HDPE	0.0001	0.0002	0.0010	0.0021
	Hemp Fiber	0.0187	0.0379	0.2111	0.4930
	HH45	0.0054	0.0109	0.0569	0.1199

The calculations used to determine the pressure change are shown in Equation B.1 to B.2. Equation B.3 details where the change in pressure due to temperature,  $\Delta P_{\Delta T}$ , impact the density calculation from the experimental results.

$$\frac{P_1}{T_1} = \frac{P_2}{T_2} \quad (\text{B.1})$$

$$P_2 = \frac{P_1 * T_2}{T_1} \quad (\text{B.2})$$

(B.3)

$$Density = \frac{\left( \frac{[(p_F - p_{F0}) * V_{reference\ chamber}] - [(p_I + \Delta P_{\Delta T} - p_{I0}) - (p_F - p_{F0})] * V_{sample\ chamber}}{p_F - p_{F0}} \right)}{Mass}$$

Due to the importance of ambient chamber temperature on the density measurement, a cooling fan was installed within the machine to minimize the impact of Environmental Uncertainty. Therefore this type of uncertainty is negated from uncertainty analysis of determination of volume fraction due to experimental controls to minimize the impact.

### **3. Combined Uncertainty from the reported densities (Statistical results)**

Evaluation of each fiber type, matrix and biocomposite variation by nitrogen pycnometry resulted in a statistical normal distribution of densities of the sample. The compounded uncertainty has been determined for each biocomposite variation based on its constituent components. The calculation for fiber volume fraction, Equation B.4, determines the calculation required to assess combined uncertainty as outlined in Equation B.5. The range of associated uncertainty for fiber volume fraction,  $u(V_f)$ , ranged from 0.00049 – 0.00136 vol%.

$$V_f = \frac{\rho_c - \rho_m}{\rho_f - \rho_m} \quad (B.4)$$

$$u(V_f) = \sqrt{\left[ \frac{u(\rho_c)}{\rho_c} \right]^2 + 2 * \left[ \frac{u(\rho_m)}{\rho_m} \right]^2 + \left[ \frac{u(\rho_f)}{\rho_f} \right]^2} \quad (B.5)$$

Where:

$$u(\rho_c) = \frac{\text{standard deviation of } \rho_c}{\sqrt{n}}, \text{ where } n = 30 \quad (B.6)$$

### **4. Combined Instrumentation Uncertainty in Density Determination**

The raw data required to calculate density was captured by a pressure gauge (pycnometer) and a gravimetric scale. The combined uncertainty from both instruments were evaluated according to Equation B.8 based on the calculation of raw data in Equation B.7.

$$Density = \frac{\left( \frac{[(p_F - p_{F0}) * V_{reference\ chamber}] - [(p_I - p_{I0}) - (p_F - p_{F0})] * V_{sample\ chamber}}{p_F - p_{F0}} \right)}{Mass} \quad (B.7)$$

Therefore Uncertainty of a density measurement  $u(\rho)$ :

(B.8)

$$= \sqrt{6 * [u(p)]^2 + \left[ \frac{u(v_{sample\ chamber})}{v_{sample\ chamber}} \right]^2 + \left[ \frac{u(v_{reference\ chamber})}{v_{reference\ chamber}} \right]^2 + 2 * \left[ \frac{u(p)}{p_{average}} \right]^2 + \left[ \frac{u(m)}{m_{average}} \right]^2}$$

Where:

$u(p)$  = manufacturer's equipment uncertainty of pressure = 0.001psi

$p_{average}$  = Average Pressure Reading (assumed as 5.5 psi for analysis)

$u(m)$  = manufacturer's equipment uncertainty of mass = 0.0001g

$m_{average}$  = Average Pressure Reading (assumed as 5.5 psi for analysis)

$$u(v_{reference\ chamber}) = \frac{\text{standard deviation}}{\sqrt{n}}, \text{ where } n = 5 \text{ \& stdev} = 0.020905 \text{ cm}^3$$

$$u(v_{sample\ chamber}) = \frac{\text{standard deviation}}{\sqrt{n}}, \text{ where } n = 5 \text{ \& stdev} = 0.034327 \text{ cm}^3$$

The combined uncertainty from instrument sources is 0.002862 g/cm<sup>3</sup> for all reported densities. The propagation of this uncertainty to fiber volume fraction produces a range of uncertainty between 0.93209 – 0.97742 vol% of fiber for all composite material variations. Instrumental uncertainty is the most significant for density. Therefore, both fiber volume fraction and experimental densities will display this uncertainty in all of the results.

## **B.2 WEIGHT MEASUREMENTS & NORMALIZED WEIGHT GAIN**

The analysis below concludes that the statistical variation of water uptake within a material variation due to inherent specimen to specimen variability is greater than either 1) instrument uncertainty or 2) impact of possible residual surface water during measurement on Percent Weight Gain.

### **1. Combined Instrumentation Uncertainty of Percent Weight Gain**

The impact of the combined instrumentation uncertainty is assessed to determine the additive magnitude of uncertainty inherent within all percent weight values. The calculation for percent weight gain, Equation B.9, determines the calculation required to assess combined uncertainty as outlined in Equation B.10. The range of associated uncertainty for percent weight gain,  $u(w_t)$ , ranged from 0.00325 – 0.03183 %.

$$W_t = \frac{w_t - w_i}{w_i} \times 100 \quad (\text{B.9})$$

$$u(W) = \sqrt{3 * \left[ \frac{u(w)}{w} \right]^2} * 100 \quad (\text{B.10})$$

Where:

$u(w)$  = manufacturer's equipment uncertainty of mass = 0.0001g

$w$  = Specimen Weight – utilized heaviest specimen (HH45 Flexural bar – 5.3255g) and lightest specimen (LDPE square – 0.5442g) to determine the range of impact

## **2. Sensitivity Analysis of Residual Water Layers**

The uncertainty related to the quantity of residual water remaining on the specimen surface during gravimetric measurement. Since the measurements were taken by the same operator with the same supplies with a specific protocol the magnitude of uncertainty is repeatable. This combination of uncertainty types is present within all gravimetric measurements for all samples, therefore does not impact the results of the study.

The sensitivity analysis evaluates the impact on percent weight gain corresponding to an incremental thickness of residual water on the surface during gravimetric measurement. Increments of 0.01µm, 0.1µm, 1µm and 10µm were chosen to demonstrate the effect on percent weight gain, detailed in Table B.3. Material variations, LDPE and HH45 were chosen to capture the extremes of the specimen weight. Even with 10µm of water thickness on the surface area of the specimen, the standard deviation of percent weight gain is greater.

Table B.3 Variation in Percent Weight Gain with assumed residual water thickness

		<b>Thickness of Water (µm)</b>				
		<b>0.01</b>	<b>0.1</b>	<b>1</b>	<b>10</b>	
Percent Weight Gain (%)	LDPE	Specimen Type				
		Square	0.001	0.010	0.096	0.956
	Flexural Bar	0.000	0.001	0.012	0.121	
	HH45	Square	0.001	0.008	0.081	0.811
Flexural Bar		0.000	0.001	0.010	0.100	



### **B.3 MECHANICAL PROPERTIES – UNCERTAINTY ANALYSIS**

The below analysis illustrates that the natural scatter present within the population of each material variation is greater than either uncertainty from calibration or instrument measurement. For comparison purposes the smallest standard deviation for yield strength is 0.019 MPa (HH30 at 26 weeks immersion) and 0.001 GPa (LDPE at 24 hours immersion) for tensile modulus.

#### **1. Calibration Uncertainty on Strength and Modulus**

The mechanical testing machine and associated equipment used are annually certified by ASTM E4-13Annex A1.3 [3] to manufacturers specification. The calibration certifies the equipment within  $\pm 1\%$  accuracy, 1% repeatability and zero return tolerance. For HH45 the greatest value in ultimate tensile strength and modulus, results in a standard deviation of 0.26 MPa and 0.0990 GPa which is far below 1% accuracy. Therefore, this accumulated uncertainty is negligible to the reported values for mechanical properties strength and modulus.

#### **2. Combined Instrumentation Uncertainty on Strength and Modulus**

The range of uncertainty for strength, dependent on material variation is 0.00167 – 0.00172 MPa. When compared to the 95% confidence interval of the sample population ranges from 0.10 MPa (L) to 1.53 MPa (HW30). Hence combined instrumentation uncertainty is captured within the natural statistical scatter of the data.

Strength

$$\sigma_c = \frac{Force}{width_{crosssection} * thickness_{cross section}} \quad (B.11)$$

$$u(\sigma_c) = \sqrt{\left[\frac{u(F)}{F}\right]^2 + \left[\frac{u(width)}{width}\right]^2 + \left[\frac{u(thickness)}{thickness}\right]^2} \quad (B.12)$$

Where:

$u(F) = \text{manufacturer's equipment uncertainty of Force} = 0.15$

$u(\text{dimension}) = \text{manufacturer's equipment uncertainty of dimension} = 0.005$

The range of uncertainty for modulus based on combined instrumentation uncertainty ranges from 0.000018 GPa – 0.000141 GPa nears closer to the statistical variation within the population ranging from 0.011 GPa (L) to 0.174 GPa (HW30).

Modulus

$$E_c = \frac{\sigma_2 - \sigma_1}{\varepsilon_2 - \varepsilon_1} \quad (\text{B.13})$$

$$u(E_c) = \sqrt{2 * \left[ \frac{u(\sigma_c)}{\sigma_c} \right]^2 + 2 * \left[ \frac{u(\varepsilon)}{\varepsilon} \right]^2} \quad (\text{B.14})$$

Where:

$u(\varepsilon)$  = manufacturer's equipment uncertainty of strain = 0.0001 mm/mm

$u(\sigma_c)$  = calculated uncertainty in Equation B.12

## REFERENCES

1. Bell, S.A. Measurement Good Practice Guide: A Beginner's Guide to Uncertainty of Measurement. 2001. 41.
2. *Combined Standard Uncertainty and Propagation of Uncertainty*. 2011 [cited 2015 August 5, 2015]; Available from: <https://www.nde-ed.org/GeneralResources/Uncertainty/Combined.htm>.
3. ASTM, E4 - 13 Standard Practices for Force Verification of Testing Machines, 2013, ASTM.

## C. APPENDIX: MECHANICAL PROPERTY DATA LIBRARY

This appendix serves as a compilation of all tensile test data. Seven specimens were tested for each condition. The average and standard deviation are reported for tensile yield stress at 2%, stress at maximum load, modulus, strain at break and toughness as well as the number of included fractured specimens. The order of the results presented includes: matrix material Table C.1 , hemp reinforced biocomposites Table C.2 and Table C.3 followed by wood pulp reinforced biocomposite Table C.4 and Table C.5.

Table C.1 Matrix Material – LDPE and HDPE

	Immersion Time (hours)	Tensile Stress at 2% Yield (MPa)		Tensile Stress at Max Load (MPa)		Modulus (GPa)		Tensile Strain at break (%)		Toughness (J)	
		Avg	Stdev	Avg	Stdev	Avg	Stdev	Avg	Stdev	Avg	Stdev
LDPE	0	5.86	0.08	12.60	0.32	0.03	0.00	170.67	7.70	32.60	2.11
	24	5.97	0.15	12.37	0.10	0.03	0.00	169.99	5.03	32.00	1.36
	168	5.84	0.14	12.37	0.21	0.03	0.00	175.58	6.80	33.47	1.48
	336	5.97	0.09	12.48	0.25	0.03	0.00	153.14	12.74	29.50	2.72
	672	5.92	0.16	12.52	0.10	0.03	0.00	172.52	4.60	33.03	1.11
	1344	6.07	0.12	12.61	0.12	0.03	0.00	165.08	4.36	32.19	1.26
	4374	5.86	0.05	12.27	0.09	0.03	0.00	167.85	11.18	32.29	2.41
	6578	6.00	0.08	11.08	0.10	0.03	0.01	138.45	17.30	32.16	0.73
	6552	5.62	0.20	12.73	0.44	0.03	0.00	172.59	10.33	33.62	2.40
HDPE	0	15.55	0.21	19.78	0.19	0.53	0.01	Did not break		*see footnote	
	24	15.38	0.25	19.44	0.25	0.54	0.03	Did not break			
	168	16.16	0.22	20.16	0.16	0.60	0.04	Did not break			
	336	15.93	0.13	20.20	0.20	0.55	0.01	Did not break			
	672	15.92	0.23	20.04	0.27	0.57	0.01	Did not break			
	1344	16.02	0.35	20.07	0.32	0.58	0.03	Did not break			
	4375	15.53	0.18	19.57	0.19	0.56	0.04	Did not break			
	6578	15.70	0.13	19.64	0.11	0.55	0.02	Did not break			
	6552	15.12	0.25	19.48	0.13	0.49	0.06	Did not break			

\*inconclusive as only 1 out of 7 specimens was tested to maximum load frame extension

Table C.2 Hemp Reinforced LDPE Biocomposites

	Immersion Time (hours)	Tensile Stress at 2% Yield (MPa)		Tensile Stress at Max Load (MPa)		Modulus (GPa)		Tensile Strain at break (%)		Toughness (J)	
		Avg	Stdev	Avg	Stdev	Avg	Stdev	Avg	Stdev	Avg	Stdev
LH15	0	7.86	0.07	10.97	0.20	0.12	0.03	51.27	13.08	9.53	2.64
	24	7.92	0.04	11.11	0.05	0.11	0.01	57.74	5.24	11.42	1.01
	168	7.59	0.20	10.82	0.14	0.11	0.02	52.36	7.49	9.63	1.42
	336	7.74	0.07	11.01	0.05	0.11	0.01	54.12	7.07	10.34	1.41
	672	7.65	0.11	11.15	0.20	0.11	0.01	56.11	7.40	10.73	1.54
	1344	7.74	0.09	11.30	0.09	0.11	0.01	55.89	7.58	10.88	1.61
	4373	6.88	0.43	10.38	0.63	0.09	0.01	61.36	10.92	11.77	2.25
	6553	6.92	0.04	10.74	0.10	0.09	0.01	63.14	6.04	11.97	1.20
	6552	7.99	0.47	11.15	0.11	0.10	0.01	59.03	3.80	11.33	0.82
LH30	0	11.89	0.14	12.74	0.21	0.72	0.02	6.81	0.53	1.47	0.30
	24	11.63	0.16	12.69	0.12	0.69	0.02	7.14	0.30	1.43	0.15
	168	10.89	0.28	11.99	0.28	0.62	0.05	6.99	0.83	1.32	0.25
	336	11.04	0.07	12.35	0.06	0.62	0.03	7.98	1.05	1.52	0.32
	672	10.98	0.10	12.37	0.11	0.61	0.02	7.86	0.92	1.48	0.31
	1344	10.91	0.23	12.56	0.25	0.59	0.03	8.01	0.72	1.59	0.26
	4397	9.94	0.25	12.28	0.09	0.48	0.04	10.36	1.99	2.12	0.49
	6553	9.44	0.20	12.23	0.18	0.40	0.05	11.83	2.85	2.44	0.67
	6552	11.03	0.15	12.31	0.14	0.59	0.03	8.58	1.30	1.62	0.47
LH45	0	11.74	0.52	11.91	0.24	1.59	0.09	3.63	0.21	0.46	0.13
	5	11.27	0.22	11.28	0.22	1.41	0.05	3.03	0.22	0.54	0.07
	24	11.15	0.19	11.26	0.17	1.32	0.08	3.52	0.36	0.64	0.14
	168	9.65	0.11	10.15	0.10	0.90	0.05	4.45	0.40	0.77	0.09
	336	9.35	0.30	10.22	0.26	0.76	0.05	5.06	0.35	0.96	0.10
	672	8.00	0.18	9.55	0.18	0.51	0.04	6.28	0.71	0.93	0.23
	1344	7.05	0.14	9.39	0.15	0.36	0.01	8.06	0.50	1.21	0.19
	4373	6.64	0.11	8.86	0.13	0.33	0.02	8.08	0.95	1.16	0.23
	6553	6.67	0.08	8.80	0.11	0.35	0.02	7.69	0.51	1.06	0.13
	6552	9.61	0.08	10.27	0.10	0.79	0.03	4.82	0.42	0.72	0.18

Table C.3 Hemp Reinforced HDPE Biocomposites

	Immersion Time (hours)	Tensile Stress at 2% Yield (MPa)		Tensile Stress at Max Load (MPa)		Modulus (GPa)		Tensile Strain at break (%)		Toughness (J)	
		Avg	Stdev	Avg	Stdev	Avg	Stdev	Avg	Stdev	Avg	Stdev
HH15	0	17.60	0.17	19.09	0.13	1.26	0.03	8.94	0.91	2.93	0.30
	24	17.64	0.06	19.16	0.03	1.28	0.01	7.61	0.27	2.45	0.14
	168	16.65	0.21	18.42	0.24	1.13	0.06	8.37	1.54	2.68	0.47
	336	17.58	0.31	19.22	0.30	1.22	0.04	8.00	1.00	2.53	0.58
	672	17.07	0.12	18.97	0.13	1.11	0.03	8.35	1.09	2.68	0.43
	1344	16.92	0.11	18.94	0.11	1.06	0.04	8.80	1.75	2.77	0.70
	4370	15.33	0.12	17.89	0.12	0.81	0.02	10.86	1.21	3.35	0.43
	6553	14.24	0.16	17.34	0.17	0.73	0.04	10.29	1.83	2.97	0.67
	6552	16.19	0.17	18.52	0.14	0.98	0.04	8.80	1.03	2.75	0.32
HH30	0	19.09	0.52	18.79	0.71	2.34	0.14	3.16	0.46	1.02	0.20
	24	18.95	0.22	19.40	0.27	2.15	0.05	3.84	0.47	1.25	0.33
	168	17.01	0.26	17.94	0.35	1.58	0.10	4.75	0.55	1.48	0.23
	336	16.53	0.22	17.58	0.21	1.49	0.12	4.52	0.49	1.30	0.10
	672	15.04	0.47	17.05	0.20	1.07	0.12	5.73	0.99	1.60	0.44
	1344	13.72	0.24	16.38	0.29	0.78	0.06	7.42	1.04	1.98	0.33
	4370	13.63	0.33	15.94	0.19	0.82	0.11	7.00	0.73	1.75	0.34
	6553	13.43	0.02	15.83	0.10	0.78	0.02	7.26	0.59	1.98	0.19
	6552	16.35	0.48	17.68	0.48	1.39	0.09	4.89	0.51	1.42	0.16
HH45	0	18.82	0.26	19.27	0.26	3.13	0.10	2.69	0.29	0.89	0.20
	5	18.08	1.79	18.88	0.13	3.13	0.20	2.61	0.28	0.94	0.16
	24	17.19	0.13	17.49	0.11	2.10	0.08	2.67	0.23	1.02	0.22
	168	13.03	0.17	14.57	0.15	0.92	0.05	5.92	0.50	1.49	0.28
	336	12.08	0.19	14.02	0.18	0.76	0.06	6.63	0.91	1.58	0.43
	672	11.70	0.18	13.67	0.16	0.71	0.03	6.34	0.27	1.69	0.13
	1344	12.01	0.17	13.85	0.13	0.77	0.04	6.46	0.43	1.61	0.19
	4369	11.93	0.15	13.75	0.16	0.77	0.08	6.74	0.46	1.77	0.10
	6553	12.31	0.17	14.15	0.22	0.81	0.02	6.53	0.51	1.66	0.24
	6552	15.64	0.42	16.47	0.44	1.49	0.09	4.20	0.38	1.09	0.23

Table C.4 Wood Pulp Reinforced LDPE Biocomposites

	Immersion Time (hours)	Tensile Stress at 2% Yield (MPa)		Tensile Stress at Max Load (MPa)		Modulus (GPa)		Tensile Strain at break (%)		Toughness (J)	
		Avg	Stdev	Avg	Stdev	Avg	Stdev	Avg	Stdev	Avg	Stdev
LW15	0	8.73	0.06	11.67	0.34	0.20	0.04	30.31	5.36	6.07	1.22
	24	8.88	0.11	11.68	0.17	0.20	0.02	29.98	2.18	6.16	0.50
	168	8.39	0.09	11.46	0.21	0.17	0.01	31.90	4.14	6.34	0.91
	336	8.46	0.07	11.51	0.07	0.18	0.01	31.42	2.46	6.39	0.58
	672	8.23	0.20	30.65	6.08	0.17	0.03	33.60	6.45	6.74	1.37
	1344	8.23	0.07	11.62	0.17	0.17	0.02	31.72	4.75	6.39	1.04
	4372	7.87	0.13	11.32	0.11	0.17	0.02	31.31	5.01	6.31	1.11
	6553	7.68	0.23	11.26	0.19	0.16	0.02	31.94	5.90	6.27	1.29
	6552	8.25	0.09	11.28	0.14	0.17	0.02	34.23	6.23	6.70	1.31
LW30	0	10.69	0.24	11.08	0.36	0.56	0.02	6.79	0.54	1.22	0.21
	24	10.93	0.14	12.12	0.13	0.60	0.04	6.54	1.02	1.20	0.28
	168	10.206	0.08	11.58	0.14	0.52	0.03	7.26	0.89	1.13	0.32
	336	10.28	0.19	11.73	0.20	0.53	0.01	7.10	0.50	1.19	0.26
	672	10.02	0.25	11.79	0.22	0.50	0.02	8.19	0.73	1.46	0.24
	1344	9.87	0.12	11.76	0.15	0.50	0.02	8.04	0.94	1.45	0.22
	4372	9.60	0.15	11.96	0.12	0.46	0.01	9.12	0.49	1.73	0.13
	6553	9.24	0.34	11.76	0.26	0.41	0.02	9.11	1.20	1.64	0.30
	6552	10.83	0.43	11.93	0.17	0.54	0.03	6.80	1.33	1.20	0.37
LW45	0	12.08	0.56	12.14	0.56	0.92	0.06	3.63	0.21	0.68	0.17
	24	12.01	0.29	12.14	0.30	0.96	0.02	3.62	0.26	0.63	0.23
	168	11.08	0.38	11.24	0.45	0.86	0.03	3.80	0.23	0.65	0.10
	336	11.23	0.14	11.50	0.23	0.87	0.02	4.11	0.34	0.74	0.13
	672	10.63	0.25	10.96	0.29	0.82	0.02	3.86	0.30	0.63	0.13
	1344	10.65	0.27	11.14	0.34	0.81	0.02	4.38	0.44	0.76	0.15
	4371	9.46	0.54	10.44	0.74	0.64	0.02	5.11	0.37	0.85	0.19
	6553	8.84	0.21	10.14	0.28	0.54	0.03	5.81	0.34	1.03	0.16
	6552	11.72	0.33	11.92	0.28	0.84	0.05	3.84	0.42	0.64	0.17

Table C.5 Wood Pulp Reinforced HDPE Biocomposites

	Immersion Time (hours)	Tensile Stress at 2% Yield (MPa)		Tensile Stress at Max Load (MPa)		Modulus (GPa)		Tensile Strain at break (%)		Toughness (J)	
		Avg	Stdev	Avg	Stdev	Avg	Stdev	Avg	Stdev	Avg	Stdev
HW15	0	14.99	0.14	17.30	0.22	0.89	0.04	8.87	1.56	2.48	0.51
	24	15.20	0.25	17.37	0.24	0.97	0.07	7.32	1.00	1.85	0.56
	168	15.44	0.27	17.61	0.38	0.95	0.07	7.92	1.49	2.34	0.49
	336	15.71	0.19	17.77	0.14	0.97	0.02	7.58	0.34	2.16	0.15
	672	15.59	0.15	17.76	0.25	0.95	0.05	7.97	0.78	2.21	0.34
	1344	15.59	0.08	17.84	0.12	0.92	0.04	8.47	0.80	2.37	0.49
	4398	15.49	0.26	17.48	0.35	0.94	0.09	7.54	1.33	2.12	0.54
	6564	14.98	0.26	16.86	0.33	0.93	0.08	7.74	1.84	2.16	0.61
	6552	15.07	0.15	17.61	0.30	0.88	0.07	15.07	0.15	2.46	0.54
HW30	0	15.91	0.27	16.51	0.31	1.53	0.10	4.54	0.69	1.28	0.20
	24	15.60	1.24	16.59	1.33	1.38	0.14	5.06	0.54	1.35	0.23
	168	15.71	0.32	16.59	0.24	1.41	0.07	5.10	0.42	1.47	0.12
	336	15.88	0.16	16.89	0.18	1.37	0.12	5.13	0.63	1.36	0.22
	672	15.40	0.18	16.47	0.17	1.27	0.08	5.53	0.66	1.59	0.25
	1344	15.35	0.18	16.05	0.34	1.39	0.09	4.58	0.69	1.24	0.25
	4398	14.24	0.14	15.54	0.11	1.04	0.06	6.12	0.46	1.69	0.20
	6564	13.93	0.37	15.51	0.48	0.92	0.06	6.93	0.73	1.93	0.27
	6552	15.13	0.16	16.62	0.21	1.17	0.10	5.99	0.63	1.74	0.19
HW45	0	15.61	0.10	15.87	0.21	1.81	0.09	3.61	0.46	0.94	0.18
	24	15.69	0.33	16.00	0.41	1.85	0.11	3.54	0.53	0.88	0.20
	168	14.89	0.18	15.41	0.26	1.56	0.08	4.13	0.58	1.03	0.35
	336	14.82	0.25	15.25	0.34	1.59	0.12	3.74	0.52	0.84	0.25
	672	14.02	0.25	14.56	0.43	1.44	0.14	3.94	0.71	0.92	0.21
	1344	13.78	0.15	14.52	0.29	1.27	0.09	4.42	0.55	1.00	0.17
	4373	11.83	0.17	13.06	0.26	0.89	0.03	5.40	0.44	1.12	0.15
	6564	12.37	0.14	13.41	0.27	0.99	0.07	5.07	0.87	1.07	0.23
	6552	14.43	0.18	15.13	0.30	1.41	0.05	3.91	0.30	0.99	0.13

## D. APPENDIX: WATER ABSORPTION DATA LIBRARY

This appendix serves as a compilation of all water absorption data. The duration, hours, of immersion along with the average mass gain and standard deviation are reported for each material variation and specimen type. The order of the results presented includes:



Table D.1 Water Absorption for LDPE specimen types

L - Square			L - 4 Cut			L - 2 Long Cut			L - 2 Short Cut			L - 1 Long Cut			L - No Cut			L - Tensile		
Time	Mass	Stddev	Time	Mass	Stddev	Time	Mass	Stddev	Time	Mass	Stddev	Time	Mass	Stddev	Time	Mass	Stddev	Time	Mass	Stddev
0.0	0.00	0.00	0.0	0.00	0.00	0.0	0.00	0.00	0.0	0.00	0.00	0.0	0.00	0.00	0.0	0.00	0.00	0.0	0.00	0.00
2.0	0.002	0.025	2.1	0.04	0.07	2.1	-0.01	0.03	2.1	-0.01	0.03	2.1	0.15	0.26	2.0	0.05	0.16	24.0	0.01	0.0063
4.0	0.011	0.025	6.8	0.00	0.02	6.8	-0.05	0.05	6.8	-0.05	0.05	6.8	0.06	0.02	6.8	0.62	0.04	168.0	0.01	0.0144
13.5	0.004	0.022	17.5	0.01	0.02	17.4	-0.04	0.05	17.4	-0.04	0.05	17.4	-0.01	0.04	17.3	0.76	0.11	336.0	0.00	0.0025
25	0.002	0.021	24.0	0.01	0.18	24.0	0.08	0.07	24.0	0.08	0.07	24.1	0.31	0.25	24.1	0.09	0.05	672.0	0.01	0.0229
48	0.0	0.026	48.1	0.10	0.02	48.1	0.24	0.18	48.1	0.24	0.18	48.1	0.15	0.07	48.0	0.04	0.07	1344.0	0.00	0.0096
72	0.006	0.015	72.1	0.28	0.07	72.1	0.16	0.06	72.1	0.16	0.06	72.1	0.13	0.13	72.1	0.08	0.11	4373.6	-0.06	0.0173
100	0.023	0.033	119.9	0.85	0.29	119.9	0.84	0.29	119.9	0.84	0.29	119.9	0.31	0.11	119.8	0.23	0.25	6578.0	-0.08	0.0222
168	0.047	0.049	167.8	0.48	0.20	167.8	0.21	0.03	167.8	0.21	0.03	167.8	0.18	0.13	167.8	0.09	0.07	6552.0	-0.19	0.0246
336	0.041	0.026	185.5	0.20	0.02	185.5	0.09	0.05	185.5	0.09	0.05	185.5	0.02	0.04	185.5	0.01	0.08			
504	0.033	0.039	2301.9	0.00	0.01	2301.9	0.03	0.19	2301.9	0.03	0.19	2301.9	0.08	0.19	2301.9	0.56	0.46			
672	0.076	0.034	3589.0	0.04	0.05	3589.0	0.01	0.04	3589.0	0.01	0.04	3589.0	-0.02	0.05	3589.0	0.04	0.18			
1421	0.098	0.073	5108.0	0.01	0.03	5108.0	-0.05	0.04	5108.0	-0.05	0.04	5108.0	-0.02	0.08	5108.0	-0.03	0.08			
4368	0.026	0.024	6594.0	0.01	0.03	6594.0	-0.03	0.05	6594.0	-0.03	0.05	6594.0	-0.03	0.06	6594.0	-0.03	0.08			
8736	0.022	0.028	6762.0	-0.07	0.02	6762.0	-0.12	0.04	6762.0	-0.12	0.04	6762.0	-0.09	0.05	6762.0	0.00	0.10			

Table D.2 Water Absorption for HDPE specimen types

H-Square			H-4 Cut			H-2 Long Cut			H-2 Short Cut			H-1 Long Cut			H-No Cut			H-Tensile		
Time	Mass	Stdev	Time	Mass	Stdev	Time	Mass	Stdev	Time	Mass	Stdev	Time	Mass	Stdev	Time	Mass	Stdev	Time	Mass	Stdev
0.0	0.00	0.00	0.0	0.00	0.00	0.0	0.00	0.00	0.0	0.00	0.00	0.0	0.00	0.00	0.0	0.00	0.00	0	0.00	0.00
2.0	0.010	0.011	2.0	0.988	0.178	2.0	1.764	0.981	2.0	1.436	1.244	2.0	0.596	0.664	2.0	-0.286	1.832	24.0	0.06	0.04
4.0	0.004	0.011	4.0	0.192	0.524	4.0	0.468	0.284	4.0	0.132	0.085	4.0	0.283	0.123	4.0	0.148	0.812	168.0	0.02	0.01
13.5	0.007	0.003	9.2	0.207	0.090	9.2	0.072	0.460	9.2	0.307	0.253	9.2	0.294	0.248	9.2	-0.319	1.316	336.0	0.05	0.02
25.0	0.006	0.007	25.0	0.274	0.151	25.0	0.063	0.315	25.0	0.354	0.373	25.0	0.291	0.668	25.0	-0.483	1.421	672.0	0.02	0.02
48.0	0.015	0.011	36.2	0.019	0.133	36.2	0.141	0.369	36.2	0.417	0.469	36.2	-0.155	0.196	36.2	-0.519	1.270	1344.0	0.03	0.03
72.7	0.010	0.008	49.0	0.011	0.095	49.0	0.475	0.285	49.0	0.130	0.461	49.0	-0.372	0.381	49.0	-0.948	1.260	4375.4	0.02	0.01
100.0	0.013	0.010	75.0	0.140	0.320	75.0	0.338	0.414	75.0	0.096	0.258	75.0	-0.289	0.482	75.0	-0.661	1.174	6578.0	0.02	0.02
168.0	0.015	0.015	100.0	0.211	0.395	100.0	0.032	0.616	100.0	0.652	0.232	100.0	0.393	0.894	100.0	-0.789	1.361	6552	-0.07	0.02
336.0	0.011	0.007	216.2	0.084	0.054	216.2	0.508	0.297	216.2	0.066	0.117	216.2	-0.189	0.320	216.2	-0.524	1.213			
504.0	0.007	0.014	336.0	0.073	0.039	336.0	0.468	0.325	336.0	0.044	0.305	336.0	-0.219	0.206	336.0	-0.795	1.330			
672.0	0.024	0.029	504.0	0.046	0.050	504.0	0.363	0.466	504.0	0.123	0.228	504.0	-0.376	0.442	504.0	-0.692	1.403			
1421	0.027	0.012	744.0	0.046	0.063	744.0	0.307	0.223	744.0	1.541	0.965	744.0	0.836	0.780	744.0	-0.741	1.384			
4368	0.016	0.007	1008.0	0.010	0.049	1008.0	0.335	0.250	1008.0	0.212	0.362	1008.0	-0.387	0.445	1008.0	-0.317	0.435			
8736	0.13	0.015	1512.0	0.903	0.908	1512.0	0.309	0.123	1512.0	0.934	0.218	1512.0	-0.102	0.569	1512.0	0.394	0.499			
			2016.0	-	0.016	2016.0	-	0.349	2016.0	-	0.222	2016.0	-0.190	0.592	2016.0	-0.051	0.411			
			3000.0	-	0.049	3000.0	-	0.291	3000.0	0.083	0.151	3000.0	-0.003	0.185	3000.0	-0.360	0.702			
			4045.0	0.048	0.048	4045.0	0.465	0.307	4045.0	0.143	0.181	4045.0	-0.372	0.430	4045.0	-0.923	1.186			
			6552.0	-	0.036	6552.0	-	0.181	6552.0	0.464	0.477	6552.0	0.021	0.436	6552.0	-0.103	0.410			
				-	0.067		0.448													

Table D.3 Water Absorption for LH15 specimen types

LH15 -Square			LH15 -4 Cut			LH15 -2 Long Cut			LH15 -2 Short Cut			LH15 -1 Long Cut			LH15 -No Cut			LH15 -Tensile		
Time	Mass	Stdev	Time	Mass	Stdev	Time	Mass	Stdev	Time	Mass	Stdev	Time	Mass	Stdev	Time	Mass	Stdev	Time	Mass	Stdev
0.0	0.00	0.00	0.0	0.00	0.00	0.0	0.00	0.00	0.0	0.00	0.00	0.0	0.00	0.00	0.0	0.00	0.00	0	0.00	0.00
2.0	0.19	0.02	2.1	0.27	0.05	2.1	0.25	0.08	2.1	0.11	0.03	2.1	0.18	0.05	2.1	0.09	0.19	24.0	0.18	0.02
4.0	0.21	0.02	6.8	0.23	0.06	6.8	0.25	0.02	6.8	0.12	0.01	6.8	0.21	0.06	6.8	0.05	0.12	168.0	0.36	0.02
13.5	0.28	0.01	17.9	0.33	0.01	18.0	0.33	0.03	18.0	0.16	0.01	18.0	0.23	0.02	18.0	0.19	0.11	33.6	0.48	0.02
25.0	0.33	0.02	23.7	0.46	0.02	23.7	0.49	0.09	23.7	0.24	0.04	23.7	0.33	0.00	23.7	0.13	0.06	672.0	0.62	0.01
48.0	0.41	0.04	48.1	0.54	0.06	48.1	0.48	0.05	48.1	0.38	0.05	48.1	0.57	0.24	48.1	0.24	0.05	1344.0	0.86	0.04
72.7	0.44	0.01	71.9	0.57	0.05	72.0	0.57	0.13	72.0	0.32	0.02	72.0	0.41	0.01	72.0	0.26	0.12	4373.2	1.34	0.02
100.0	0.50	0.02	119.9	1.56	0.40	119.9	1.15	0.17	119.9	1.04	0.39	119.9	0.94	0.07	119.9	0.61	0.16	6553.0	1.56	0.03
168.0	0.68	0.05	167.8	1.12	0.13	167.8	1.06	0.14	167.8	0.76	0.11	167.8	1.08	0.16	167.8	0.60	0.14			
336.0	0.92	0.08	185.5	0.74	0.02	185.5	1.05	0.26	185.5	0.45	0.02	185.5	0.78	0.07	185.5	0.38	0.09			
504.0	1.08	0.15	2301.4	1.45	0.06	2301.4	1.42	0.04	2301.4	1.11	0.03	2301.4	1.22	0.03	2301.3	1.05	0.05			
672.0	1.16	0.05	3589.0	1.67	0.05	3589.0	1.67	0.05	3589.0	1.31	0.04	3589.0	1.47	0.04	3589.0	1.23	0.07			
1421.0	1.47	0.10	5108.0	1.81	0.03	5108.0	1.79	0.05	5108.0	1.48	0.03	5108.0	1.63	0.05	5108.0	1.39	0.06			
4368.0	2.00	0.07	6594.0	2.00	0.05	6594.0	2.00	0.03	6594.0	1.60	0.02	6594.0	1.79	0.05	6594.0	1.53	0.06			
8736.0	2.28	0.19																		

Table D.4 Water Absorption for LH30 specimen types

LH30 -Square			LH30 -4 Cut			LH30 -2 Long Cut			LH30 -2 Short Cut			LH30 -1 Long Cut			LH30 -No Cut			LH30 -Tensile		
Time	Mass	Stdev	Time	Mass	95% Cl	Stdev	Time	Mass	Time	Mass	Stdev	Time	Mass	Stdev	Time	Mass	Stdev	Time	Mass	Stdev
0.0	0.00	0.00	0.0	0.00	0.00	0.00	0.0	0.00	0.0	0.00	0.00	0.0	0.00	0.00	0.0	0.00	0.00	0.0	0.00	0.00
2.0	0.50	0.02	2.1	0.57	0.10	0.04	2.1	0.60	2.1	0.24	0.02	2.1	0.43	0.01	2.1	0.25	0.01	24.0	0.54	0.02
4.0	0.62	0.02	6.8	0.74	0.12	0.05	6.8	0.75	6.8	0.36	0.03	6.7	0.55	0.02	6.7	0.37	0.02	168.0	1.09	0.05
13.5	0.84	0.04	18.0	1.16	0.19	0.08	17.9	0.56	17.9	1.12	0.06	17.8	0.89	0.09	17.8	0.63	0.06	336.0	1.34	0.06
25.0	1.00	0.04	23.8	1.21	0.16	0.07	23.9	1.21	23.9	0.64	0.02	23.8	0.86	0.05	23.8	0.58	0.02	672.0	1.82	0.03
48.0	1.25	0.06	48.1	1.38	0.20	0.16	48.1	1.60	48.1	0.75	0.47	48.1	1.24	0.06	48.1	0.77	0.06	1344.0	2.45	0.04
72.0	1.51	0.09	72.0	1.71	0.20	0.08	72.0	1.69	72.0	0.87	0.02	72.0	1.31	0.08	72.0	0.84	0.03	4397.1	3.99	0.10
100	1.67	0.07	9	2.30	0.27	0.11	119.9	2.19	119.9	1.50	0.05	119.9	2.06	0.25	119.9	1.50	0.19	6553.0	4.63	0.06
168	2.07	0.10	167.8	2.28	0.15	0.06	167.8	2.47	167.8	1.33	0.19	167.8	1.86	0.17	167.8	1.52	0.20			
336	2.79	0.11	185.5	2.16	0.29	0.12	185.5	2.28	185.5	1.18	0.11	185.5	1.71	0.06	185.5	1.20	0.02			
504	3.23	0.13	2301.9	4.82	0.59	0.24	2301.9	5.16	2301.9	2.93	0.07	2301.9	3.93	0.08	2301.9	2.99	0.23			
672	3.64	0.14	3589.0	5.62	0.27	0.91	3589.0	5.68	3589.0	3.56	0.16	3589.0	4.68	0.09	3589.0	3.64	0.03			
1421	4.84	0.30	5108.0	6.14	0.37	0.15	5108.0	6.25	5108.0	4.07	0.09	5108.0	5.20	0.09	5108.0	4.10	0.04			
4368.0	6.99	0.34	6594.0	6.64	0.37	0.15	6594.0	6.76	6594.0	4.46	0.16	6594.0	5.66	0.06	6594.0	4.53	0.08			
8736.0	7.48	0.23																		

Table D.5 Water Absorption for LH45 specimen types

LH45 -Square			LH45 -4 Cut			LH45 -2 Long Cut			LH45 -2 Short Cut			LH45 -1 Long Cut			LH45 -No Cut			LH45 -Tensile		
Time	Mass	Stdev	Time	Mass	Stdev	Time	Mass	Stdev	Time	Mass	Stdev	Time	Mass	Stdev	Time	Mass	Stdev	Time	Mass	Stdev
0.0	0.00	0.00	0.0	0.00	0.00	0.0	0.00	0.00	0.0	0.00	0.00	0.0	0.00	0.00	0.0	0.00	0.00	0.0	0.00	0.00
2.0	1.39	0.11	2.1	1.45	0.05	2.1	1.50	0.06	2.1	0.88	0.02	2.2	1.19	0.07	2.2	0.82	0.08	24.0	1.88	0.04
4.0	1.77	0.14	6.8	2.20	0.10	6.8	2.16	0.03	6.8	1.32	0.04	6.8	1.64	0.06	6.8	1.24	0.05	168.0	4.87	0.09
13.5	2.79	0.31	17.8	3.42	0.12	17.8	3.37	0.05	17.6	2.08	0.21	17.5	2.61	0.13	17.5	1.94	0.07	33.6	7.03	0.19
25.0	3.55	0.41	23.9	3.69	0.10	23.9	3.72	0.00	23.9	2.23	0.08	24.0	2.82	0.07	24.0	2.13	0.10	672.0	10.0	0.13
48.0	4.73	0.59	48.1	4.99	0.28	48.0	4.91	0.09	48.0	3.05	0.09	48.0	3.75	0.17	48.0	2.91	0.12	1344.0	13.4	0.13
72.7	5.79	0.73	72.0	5.85	0.16	72.0	5.98	0.11	72.0	3.75	0.08	72.0	4.64	0.15	72.0	3.72	0.16	4372.7	16.4	0.14
100.0	6.74	0.87	119.9	8.24	0.93	119.9	7.80	0.19	119.9	5.02	0.12	119.9	6.02	0.24	119.9	5.00	0.21	6553.0	16.1	0.17
168.0	8.71	1.07	167.8	8.66	0.07	167.8	8.67	0.07	167.8	5.86	0.16	167.8	6.80	0.32	167.8	5.48	0.19			
336.0	11.95	1.23	185.5	8.92	0.15	185.5	8.83	0.05	185.5	6.04	0.13	185.5	7.07	0.24	185.5	5.75	0.17			
504.0	13.75	1.17	2302.5	18.10	0.10	2302.5	17.85	0.24	2302.4	16.34	0.12	2302.4	17.28	0.12	2302.4	16.38	0.22			
672.0	15.02	0.89	3589.0	17.53	0.38	3589.0	17.40	0.12	3589.0	16.14	0.14	3589.0	16.72	0.26	3589.0	16.14	0.16			
1421	16.62	0.35	5108.0	17.25	0.47	5108.0	17.10	0.21	5108.0	15.85	0.24	5108.0	16.50	0.28	5108.0	15.89	0.23			
4368	16.55	0.20	6594.0	17.09	0.44	6594.0	16.95	0.29	6594.0	15.71	0.29	6594.0	16.36	0.30	6594.0	15.57	0.24			
8736	15.67	0.07																		

Table D.6 Water Absorption for HH15 specimen types

HH15 - Square			HH15 - 4 Cut			HH15 - 2 Long Cut			HH15 - 2 Short Cut			HH15 - 1 Long Cut			HH15 - No Cut			HH15 - Tensile		
Time	Mass	Stddev	Time	Mass	Stddev	Time	Mass	Stddev	Time	Mass	Stddev	Time	Mass	Stddev	Time	Mass	Stddev	Time	Mass	Stddev
0.0	0.00	0.00	0.0	0.00	0.00	0.0	0.00	0.00	0.0	0.00	0.00	0.0	0.00	0.00	0.0	0.00	0.00	0.0	0.0000	0.00
2.0	0.21	0.02	2.0	0.26	0.00	2.0	0.23	0.02	2.0	0.02	0.03	2.0	0.14	0.02	2.0	0.11	0.02	24.0	0.32	0.03
4.0	0.27	0.02	4.0	0.33	0.02	4.0	0.30	0.04	4.0	0.05	0.03	4.0	0.16	0.02	4.0	0.15	0.02	168.0	0.66	0.02
13.5	0.39	0.02	9.2	0.43	0.00	9.2	0.39	0.04	9.2	0.11	0.04	9.2	0.24	0.02	9.2	0.20	0.03	336.0	0.90	0.04
25.0	0.50	0.02	25.0	0.61	0.01	25.0	0.52	0.04	25.0	0.22	0.03	25.0	0.37	0.03	25.0	0.30	0.01	672.0	1.27	0.03
48.0	0.63	0.03	36.2	0.69	0.01	36.2	0.64	0.04	36.2	0.25	0.03	36.2	0.44	0.02	36.2	0.35	0.01	1344.0	1.86	0.16
72.7	0.78	0.06	49.0	0.78	0.00	49.0	0.81	0.01	49.0	0.30	0.03	49.0	0.52	0.00	49.0	0.40	0.01	4370.3	3.78	0.03
100.0	0.90	0.04	75.0	0.86	0.01	75.0	0.87	0.01	75.0	0.38	0.03	75.0	0.58	0.01	75.0	0.48	0.02	6553.0	4.34	0.07
168.0	1.16	0.07	100.0	1.03	0.00	100.0	0.98	0.01	100.0	0.45	0.04	100.0	0.70	0.01	100.0	0.54	0.02			
336.0	1.65	0.11	216.2	1.32	0.02	216.2	1.26	0.06	216.2	0.64	0.03	216.2	0.93	0.02	216.2	0.75	0.02			
504.0	1.95	0.12	336.0	1.62	0.02	336.0	1.56	0.17	336.0	0.82	0.03	336.0	1.16	0.03	336.0	0.91	0.02			
672.0	2.23	0.17	504.0	1.95	0.02	504.0	1.79	0.15	504.0	1.02	0.03	504.0	1.37	0.04	504.0	1.10	0.03			
1421	3.11	0.23	744.0	2.34	0.01	744.0	2.15	0.19	744.0	1.27	0.04	744.0	1.65	0.06	744.0	1.34	0.06			
4368	4.55	0.04	1008.0	2.62	0.02	1008.0	2.41	0.21	1008.0	1.50	0.03	1008.0	1.93	0.05	1008.0	1.58	0.09			
8736	4.20	0.17	1512.0	3.15	0.08	1512.0	2.90	0.23	1512.0	1.88	0.04	1512.0	2.34	0.06	1512.0	1.96	0.13			
			2016.0	3.72	0.02	2016.0	3.56	0.14	2016.0	2.25	0.02	2016.0	2.77	0.03	2016.0	2.32	0.16			
			3000.0	4.28	0.07	3000.0	3.82	0.33	3000.0	2.85	0.04	3000.0	3.41	0.08	3000.0	2.94	0.22			
			4045.0	4.73	0.10	4045.0	4.56	0.15	4045.0	3.71	0.05	4045.0	4.17	0.09	4045.0	3.83	0.25			
			6552.0	4.66	0.04	6552.0	4.65	0.07	6552.0	4.09	0.04	6552.0	4.43	0.08	6552.0	4.23	0.23			

Table D.7 Water Absorption for HH30 specimen types

HH30 - Square			HH30 - 4 Cut			HH30 - 2 Long Cut			HH30 - 2 Short Cut			HH30 - 1 Long Cut			HH30 - No Cut			HH30 - Tensile		
Time	Mass	Stdev	Time	Mass	Stdev	Time	Mass	Stdev	Time	Mass	Stdev	Time	Mass	Stdev	Time	Mass	Stdev	Time	Mass	Stdev
0.0	0.00	0.00	0.0	0.00	0.00	0.0	0.00	0.00	0.0	0.00	0.00	0.0	0.00	0.00	0.0	0.00	0.00	0.0	0.00	0.00
2.0	0.47	0.06	2.0	0.57	0.01	2.0	0.64	0.06	2.0	0.44	0.02	2.0	0.44	0.02	2.0	0.28	0.02	2.0	0.91	0.02
4.0	0.63	0.08	4.0	0.78	0.01	4.0	0.79	0.01	4.0	0.62	0.01	4.0	0.62	0.01	4.0	0.41	0.02	4.0	2.65	0.10
13.5	1.04	0.11	9.2	1.05	0.03	9.2	1.04	0.03	9.2	0.85	0.07	9.2	0.85	0.07	9.2	0.57	0.02	336.0	4.09	0.12
25.0	1.38	0.16	25.0	1.66	0.02	25.0	1.65	0.01	25.0	1.39	0.09	25.0	1.39	0.09	25.0	0.93	0.03	672.0	5.90	0.36
48.0	1.93	0.23	36.2	1.96	0.03	36.2	1.94	0.05	36.2	1.73	0.06	36.2	1.73	0.06	36.2	1.13	0.03	1344.0	8.34	0.23
72.7	2.45	0.27	49.0	2.33	0.04	49.0	2.31	0.01	49.0	1.98	0.14	49.0	1.98	0.14	49.0	1.33	0.05	4369.7	9.73	0.16
100.0	2.93	0.32	75.0	2.74	0.04	75.0	2.80	0.05	75.0	2.43	0.18	75.0	2.43	0.18	75.0	1.66	0.04	6553.0	9.56	0.17
168.0	3.89	0.39	100.0	3.19	0.06	100.0	3.23	0.05	100.0	2.80	0.23	100.0	2.80	0.23	100.0	2.01	0.04			
336.0	5.62	0.46	216.2	4.68	0.10	216.2	4.82	0.11	216.2	4.14	0.37	216.2	4.14	0.37	216.2	3.08	0.11			
504.0	6.71	0.46	336.0	5.91	0.10	336.0	5.89	0.09	336.0	5.14	0.49	336.0	5.14	0.49	336.0	4.10	0.15			
672.0	7.46	0.40	504.0	7.19	0.02	504.0	7.19	0.13	504.0	6.31	0.69	504.0	6.31	0.69	504.0	5.22	0.21			
1421	8.21	0.26	744.0	8.35	0.02	744.0	8.32	0.08	744.0	7.67	0.74	744.0	7.67	0.74	744.0	6.52	0.24			
4368	7.74	0.24	1008.0	8.79	0.10	1008.0	8.92	0.10	1008.0	8.73	0.85	1008.0	8.73	0.85	1008.0	7.44	0.24			
8736	7.04	0.20	1512.0	8.98	0.13	1512.0	9.06	0.14	1512.0	10.03	0.82	1512.0	10.03	0.82	1512.0	8.21	0.19			
			2016.0	8.90	0.19	2016.0	9.03	0.04	2016.0	10.83	1.03	2016.0	10.83	1.03	2016.0	8.41	0.18			
			3000.0	8.80	0.20	3000.0	8.84	0.15	3000.0	11.47	0.57	3000.0	11.47	0.57	3000.0	8.25	0.19			
			4045.0	8.64	0.21	4045.0	8.64	0.27	4045.0	11.94	0.16	4045.0	11.94	0.16	4045.0	8.06	0.15			
			6552.0	8.46	0.24	6552.0	8.48	0.18	6552.0	11.91	0.52	6552.0	11.91	0.52	6552.0	7.88	0.19			

Table D.8 Water Absorption for HH45 specimen types

HH45 - Square		HH45 -4 Cut			HH45 -2 Long Cut			HH45 -2 Short Cut			HH45 -1 Long Cut			HH45 -No Cut			HH45 -Tensile		
Time	Mass	Stdev	Time	Mass	Stdev	Time	Mass	Stdev	Time	Mass	Stdev	Time	Mass	Stdev	Time	Mass	Stdev		
0.0	0.00	0.00	0.0	0.00	0.00	0.0	0.00	0.00	0.0	0.00	0.00	0.0	0.00	0.00	0.0	0.00	0.00		
2.0	1.26	0.38	2.0	1.41	0.03	2.0	0.85	0.01	2.0	1.07	0.04	2.0	0.87	0.02	24.0	2.79	0.06		
4.0	1.70	0.50	4.0	2.03	0.13	4.0	1.23	0.03	4.0	1.55	0.16	4.0	1.22	0.02	168.0	8.34	0.14		
13.5	3.00	0.77	9.2	2.81	0.18	9.2	1.83	0.07	9.2	2.23	0.03	9.2	1.81	0.04	336.0	11.66	0.09		
25.0	4.08	0.88	25.0	4.91	0.26	25.0	2.97	0.07	25.0	3.76	0.04	25.0	2.96	0.02	672.0	13.81	0.12		
48.0	5.83	1.02	36.2	5.89	0.25	36.2	3.58	0.05	36.2	4.60	0.08	36.2	3.59	0.01	1344.0	13.72	0.05		
72.7	7.28	1.10	49.0	7.06	0.31	49.0	4.29	0.06	49.0	5.37	0.17	49.0	4.29	0.02	4369.2	13.63	0.18		
100	8.66	1.18	75.0	8.81	0.21	75.0	5.44	0.06	75.0	6.82	0.14	75.0	5.45	0.02	6553.0	13.33	0.15		
168	11.03	1.09	100.0	9.86	0.26	100.0	6.39	0.11	100.0	7.80	0.22	100.0	6.31	0.01					
336	13.96	0.62	216.2	13.55	0.06	216.2	9.77	0.18	216.2	11.41	0.32	216.2	9.66	0.07					
504	14.39	0.42	336.0	14.89	0.04	336.0	12.00	0.08	336.0	13.53	0.38	336.0	11.92	0.06					
672	14.42	0.37	504.0	14.93	0.08	504.0	13.41	0.08	504.0	14.16	0.16	504.0	13.40	0.05					
1421	14.11	0.38	744.0	14.87	0.01	744.0	13.61	0.08	744.0	14.18	0.12	744.0	13.73	0.02					
4368	13.42	0.56	1008.0	14.68	0.02	1008.0	13.59	0.06	1008.0	14.03	0.09	1008.0	13.66	0.03					
8736	12.65	0.32	1512.0	14.70	0.10	1512.0	13.44	0.09	1512.0	13.90	0.09	1512.0	13.42	0.04					
			2016.0	14.66	0.04	2016.0	13.51	0.09	2016.0	13.94	0.09	2016.0	13.51	0.08					
			3000.0	14.34	0.05	3000.0	13.24	0.08	3000.0	13.72	0.03	3000.0	13.35	0.05					
			4045.0	14.15	0.01	4045.0	13.09	0.11	4045.0	13.49	0.01	4045.0	13.16	0.08					
			6552.0	13.85	0.03	6552.0	12.91	0.13	6552.0	13.35	0.03	6552.0	12.90	0.08					



Table D.9 Water Absorption for LW15 specimen types

LW15 -Square			LW15 -4 Cut			LW15 -2 Long Cut			LW15 -2 Short Cut			LW15 -1 Long Cut			LW15 -No Cut			LW15 -Tensile		
Time	Mass	Stdev	Time	Mass	Stdev	Time	Mass	Stdev	Time	Mass	Stdev	Time	Mass	Stdev	Time	Mass	Stdev	Time	Mass	Stdev
0.0	0.00	0.00	0.0	0.00	0.00	0.0	0.00	0.00	0.0	0.00	0.00	0.0	0.00	0.00	0.0	0.00	0.00	0.0	0.00	0.00
2.0	0.14	0.02	2.0	0.17	0.02	2.0	0.19	0.01	2.0	0.10	0.05	2.0	0.12	0.05	2.0	0.02	0.08	24.0	0.20	0.01
4.0	0.19	0.02	4.0	0.22	0.03	4.0	0.24	0.01	4.0	0.08	0.02	4.0	0.01	0.05	4.0	0.05	0.05	168.0	0.36	0.02
13.5	0.28	0.05	9.2	0.29	0.04	9.2	0.29	0.04	9.2	0.12	0.02	9.2	0.18	0.04	9.2	0.09	0.06	336.0	0.52	0.02
25.0	0.32	0.04	24.0	0.36	0.02	24.0	0.39	0.02	24.0	0.19	0.02	24.0	0.27	0.06	24.0	0.16	0.07	672.0	0.67	0.03
48.0	0.39	0.05	36.0	0.41	0.02	36.0	0.42	0.02	36.0	0.21	0.03	36.0	0.30	0.05	36.0	0.18	0.06	1344.0	0.92	0.03
72.7	0.45	0.04	49.5	0.46	0.04	49.5	0.48	0.03	49.5	0.24	0.02	49.5	0.34	0.05	49.5	0.21	0.06	4372.0	1.50	0.03
100.0	0.52	0.03	72.0	0.50	0.03	72.0	0.52	0.01	72.0	0.29	0.02	72.0	0.39	0.04	72.0	0.24	0.06	6553.0	1.72	0.07
168.0	0.66	0.06	100.0	0.54	0.03	100.0	0.57	0.03	100.0	0.33	0.03	100.0	0.46	0.07	100.0	0.30	0.07			
336.0	0.88	0.03	168.2	0.67	0.04	168.2	0.71	0.04	168.2	0.41	0.03	168.2	0.54	0.06	168.2	0.36	0.06			
504.0	1.03	0.09	340.1	0.78	0.05	340.1	0.89	0.06	340.1	0.56	0.01	340.1	0.71	0.09	340.1	0.50	0.06			
672.0	1.16	0.07	510.5	0.95	0.07	510.5	1.01	0.05	510.5	0.65	0.03	510.5	0.82	0.09	510.5	0.60	0.06			
1421	1.47	0.06	672.0	1.00	0.05	672.0	1.06	0.03	672.0	0.74	0.02	672.0	0.86	0.05	672.0	0.68	0.07			
4368	2.11	0.09	1032.5	1.25	0.01	1032.5	1.24	0.02	1032.5	0.90	0.01	1032.5	1.03	0.07	1032.5	0.82	0.06			
8736	2.17	0.15	1347.7	1.30	0.01	1347.7	1.36	0.12	1347.7	0.98	0.03	1347.7	1.11	0.07	1347.7	0.93	0.05			
			1891.0	1.40	0.06	1891.0	1.45	0.07	1891.0	1.13	0.03	1891.0	1.25	0.07	1891.0	1.06	0.06			
			3000.0	1.63	0.09	3000.0	1.71	0.08	3000.0	1.36	0.04	3000.0	1.52	0.08	3000.0	1.30	0.06			
			4043.0	1.86	0.07	4043.0	1.96	0.06	4043.0	1.58	0.04	4043.0	1.76	0.08	4043.0	1.50	0.06			
			6552.0	1.96	0.11	6552.0	2.09	0.09	6552.0	1.79	0.05	6552.0	1.91	0.09	6552.0	1.73	0.05			



Table D.11 Water Absorption for LW45 specimen types

LW45 -Square			LW45 -4 Cut			LW45 -2 Long Cut			LW45 -2 Short Cut			LW45 -1 Long Cut			LW45 -No Cut			LW45 -Tensile		
Time	Mass	Stdev	Time	Mass	Stdev	Time	Mass	Stdev	Time	Mass	Stdev	Time	Mass	Stdev	Time	Mass	Stdev	Time	Mass	Stdev
0.0	0.00	0.00	0.0	0.00	0.00	0.0	0.00	0.00	0.0	0.00	0.00	0.0	0.00	0.00	0.0	0.00	0.00	0.0	0.00	0.00
2.0	0.52	0.02	2.0	0.75	0.06	2.0	0.69	0.05	2.0	0.43	0.03	2.0	0.57	0.05	2.0	0.36	0.04	24.0	0.97	0.04
4.0	0.69	0.02	4.0	0.85	0.06	4.0	0.79	0.05	4.0	0.54	0.02	4.0	0.67	0.10	4.0	0.54	0.04	168.0	1.89	0.16
13.5	1.06	0.10	9.0	1.08	0.05	9.0	1.05	0.08	9.0	0.71	0.04	9.0	0.86	0.04	9.0	0.68	0.01	336.0	2.19	0.10
25.0	1.24	0.10	24.0	1.50	0.06	24.0	1.37	0.06	24.0	1.02	0.04	24.0	1.24	0.05	24.0	0.99	0.08	672.0	2.84	0.10
48.0	1.57	0.12	36.0	1.62	0.06	36.0	1.53	0.11	36.0	1.10	0.06	36.0	1.34	0.12	36.0	1.12	0.02	1344.0	3.47	0.09
72.2	1.81	0.12	49.5	1.80	0.05	49.5	1.69	0.11	49.5	1.25	0.08	49.5	1.57	0.13	49.5	1.29	0.05	4370.9	5.27	0.25
100.0	2.10	0.17	72.0	2.00	0.06	72.0	1.93	0.07	72.0	1.41	0.12	72.0	1.71	0.11	72.0	1.41	0.04	6553.0	5.59	0.33
168.0	2.55	0.18	100.0	2.28	0.13	100.0	2.11	0.08	100.0	1.65	0.12	100.0	1.86	0.14	100.0	1.56	0.08			
336.0	3.28	0.25	168.2	2.62	0.08	168.2	2.42	0.07	168.2	1.82	0.10	168.2	2.14	0.14	168.2	1.87	0.10			
504.0	3.74	0.31	340.1	3.17	0.10	340.1	3.04	0.16	340.1	2.22	0.13	340.1	2.64	0.18	340.1	2.21	0.15			
672.0	4.28	0.33	510.5	3.64	0.03	510.5	3.59	0.11	510.5	2.62	0.11	510.5	3.03	0.10	510.5	2.59	0.11			
1421.0	5.33	0.42	672.0	3.92	0.12	672.0	3.82	0.18	672.0	2.85	0.11	672.0	3.29	0.06	672.0	2.74	0.18			
4368.0	7.31	0.46	1032.5	4.54	0.14	1032.5	4.43	0.21	1032.5	3.35	0.16	1032.5	3.88	0.20	1032.5	3.32	0.12			
8736.0	7.22	0.44	1347.7	4.87	0.15	1347.7	4.71	0.20	1347.7	3.59	0.15	1347.7	4.10	0.21	1347.7	3.58	0.24			
			1891.0	5.28	0.13	1891.0	5.21	0.24	1891.0	3.99	0.19	1891.0	4.52	0.25	1891.0	3.98	0.33			
			3000.0	6.17	0.14	3000.0	6.13	0.27	3000.0	4.82	0.18	3000.0	5.48	0.26	3000.0	4.76	0.44			
			4043.0	6.71	0.13	4043.0	6.75	0.29	4043.0	5.34	0.15	4043.0	6.01	0.23	4043.0	5.22	0.54			
			6552.0	7.21	0.11	6552.0	7.19	0.28	6552.0	5.92	0.21	6552.0	6.56	0.21	6552.0	5.81	0.52			

Table D.12 Water Absorption for HW15 specimen types

HW15 - Square			HW15 - 4 Cut			HW15 - 2 Long Cut			HW15 - 2 Short Cut			HW15 - 1 Long Cut			HW15 - No Cut			HW15 - Tensile		
Time	Mass	Stddev	Time	Mass	Stddev	Time	Mass	Stddev	Time	Mass	Stddev	Time	Mass	Stddev	Time	Mass	Stddev	Time	Mass	Stddev
0.0	0.00	0.00	0.0	0.00	0.00	0.0	0.00	0.00	0.0	0.00	0.00	0.0	0.00	0.00	0.0	0.00	0.00	0.0	0.00	0.00
2.0	0.06	0.02	2.0	0.12	0.01	2.0	0.09	0.08	2.0	0.11	0.08	2.0	0.06	0.10	2.0	0.05	0.05	2.0	0.13	0.01
4.0	0.09	0.02	4.0	0.16	0.02	4.0	0.12	0.07	4.0	0.07	0.05	4.0	0.03	0.05	4.0	0.06	0.05	4.0	0.28	0.03
13.5	0.14	0.03	9.0	0.21	0.01	9.0	0.15	0.04	9.0	0.05	0.02	9.0	0.07	0.06	9.0	0.07	0.04	336.0	0.36	0.03
25.0	0.18	0.04	24.0	0.27	0.01	24.0	0.22	0.07	24.0	0.10	0.02	24.0	0.14	0.09	24.0	0.13	0.07	672.0	0.53	0.10
48.0	0.24	0.05	36.0	0.31	0.02	36.0	0.23	0.05	36.0	0.11	0.02	36.0	0.13	0.05	36.0	0.12	0.04	1344.0	0.68	0.06
72.0	0.28	0.05	48.0	0.32	0.00	48.0	0.27	0.05	48.0	0.13	0.02	48.0	0.15	0.06	48.0	0.18	0.05	4398.3	1.08	0.05
100.0	0.31	0.07	72.0	0.36	0.02	72.0	0.29	0.05	72.0	0.16	0.02	72.0	0.18	0.05	72.0	0.16	0.05	6564.0	1.34	0.08
168.0	0.38	0.07	96.0	0.37	0.01	96.0	0.31	0.05	96.0	0.18	0.02	96.0	0.20	0.06	96.0	0.19	0.05			
336.0	0.53	0.11	123.5	0.41	0.01	123.5	0.34	0.05	123.5	0.20	0.01	123.5	0.23	0.06	123.5	0.22	0.05			
504.0	0.59	0.09	168.0	0.44	0.02	168.0	0.38	0.07	168.0	0.23	0.02	168.0	0.26	0.07	168.0	0.24	0.05			
672.0	0.69	0.10	336.0	0.59	0.02	336.0	0.53	0.07	336.0	0.35	0.03	336.0	0.40	0.07	336.0	0.36	0.05			
1421.0	0.92	0.14	504.0	0.63	0.02	504.0	0.57	0.08	504.0	0.38	0.03	504.0	0.43	0.07	504.0	0.40	0.03			
4368.0	1.41	0.19	672.0	0.68	0.02	672.0	0.63	0.07	672.0	0.43	0.02	672.0	0.49	0.08	672.0	0.44	0.04			
8736.0	1.60	0.25	1344.0	0.86	0.02	1344.0	0.77	0.05	1344.0	0.54	0.00	1344.0	0.63	0.07	1344.0	0.54	0.04			
			2016.0	1.03	0.05	2016.0	0.98	0.07	2016.0	0.72	0.02	2016.0	0.77	0.07	2016.0	0.71	0.06			
			2688.0	1.24	0.06	2688.0	1.15	0.06	2688.0	0.89	0.03	2688.0	0.93	0.07	2688.0	0.87	0.07			
			4007.0	1.33	0.07	4007.0	1.23	0.08	4007.0	1.02	0.02	4007.0	1.04	0.07	4007.0	0.97	0.06			
			5040.0	1.40	0.08	5040.0	1.31	0.09	5040.0	1.09	0.03	5040.0	1.13	0.07	5040.0	1.07	0.05			
			6552.0	1.54	0.08	6552.0	1.44	0.09	6552.0	1.23	0.04	6552.0	1.26	0.07	6552.0	1.20	0.06			

Table D.13 Water Absorption for HW30 specimen types

HW30 - Square			HW30 - 4 Cut			HW30 - 2 Long Cut			HW30 - 2 Short Cut			HW30 - 1 Long Cut			HW30 - No Cut			HW30 - Tensile		
Time	Mass	Stdev	Time	Mass	Stdev	Time	Mass	Stdev	Time	Mass	Stdev	Time	Mass	Stdev	Time	Mass	Stdev	Time	Mass	Stdev
0.0	0.00	0.00	0.0	0.00	0.00	0.0	0.00	0.00	0.0	0.00	0.00	0.0	0.00	0.00	0.0	0.00	0.00	0.0	0.00	0.00
2.0	0.15	0.02	2.0	0.28	0.03	2.0	0.27	0.02	2.0	0.10	0.01	2.0	0.16	0.02	2.0	0.08	0.04	2.0	0.31	0.03
4.0	0.19	0.02	4.0	0.33	0.02	4.0	0.35	0.02	4.0	0.14	0.01	4.0	0.22	0.03	4.0	0.12	0.06	4.0	0.80	0.05
13.5	0.33	0.04	9.0	0.44	0.01	9.0	0.41	0.04	9.0	0.21	0.02	9.0	0.31	0.02	9.0	0.20	0.05	9.0	1.10	0.17
25.0	0.44	0.08	24.0	0.61	0.01	24.0	0.57	0.03	24.0	0.32	0.01	24.0	0.43	0.02	24.0	0.33	0.03	24.0	1.51	0.08
48.0	0.59	0.10	36.0	0.70	0.01	36.0	0.65	0.05	36.0	0.36	0.02	36.0	0.49	0.03	36.0	0.39	0.03	36.0	2.31	0.13
71.6	0.73	0.12	48.0	0.79	0.02	48.0	0.78	0.02	48.0	0.41	0.02	48.0	0.57	0.02	48.0	0.45	0.04	48.0	3.52	0.05
100.0	0.84	0.15	72.0	0.90	0.03	72.0	0.92	0.03	72.0	0.48	0.02	72.0	0.65	0.02	72.0	0.50	0.04	72.0	6.56	0.11
168.0	1.09	0.18	96.0	1.03	0.01	96.0	1.00	0.07	96.0	0.54	0.02	96.0	0.73	0.03	96.0	0.58	0.03	96.0		
336.0	1.60	0.29	123.5	1.10	0.06	123.5	1.06	0.06	123.5	0.61	0.02	123.5	0.83	0.03	123.5	0.63	0.07	123.5		
504.0	1.90	0.38	168.0	1.26	0.08	168.0	1.24	0.09	168.0	0.71	0.01	168.0	0.93	0.03	168.0	0.71	0.06	168.0		
672.0	2.21	0.42	336.0	1.86	0.10	336.0	1.85	0.13	336.0	1.13	0.02	336.0	1.40	0.03	336.0	1.16	0.06	336.0		
1421.0	3.13	0.59	504.0	1.98	0.10	504.0	2.03	0.24	504.0	1.23	0.02	504.0	1.52	0.02	504.0	1.27	0.07	504.0		
4368.0	4.49	0.56	672.0	2.28	0.10	672.0	2.31	0.29	672.0	1.45	0.01	672.0	1.76	0.02	672.0	1.50	0.07	672.0		
8736.0	4.26	0.49	1344.0	2.77	0.14	1344.0	2.85	0.36	1344.0	1.88	0.03	1344.0	2.20	0.05	1344.0	1.91	0.07	1344.0		
			2016.0	3.52	0.18	2016.0	3.63	0.42	2016.0	2.65	0.02	2016.0	2.95	0.10	2016.0	2.69	0.06	2016.0		
			2688.0	4.12	0.16	2688.0	4.24	0.41	2688.0	3.27	0.04	2688.0	3.56	0.07	2688.0	3.26	0.06	2688.0		
			4007.0	4.30	0.13	4007.0	4.43	0.38	4007.0	3.63	0.05	4007.0	3.89	0.09	4007.0	3.60	0.06	4007.0		
			5040.0	4.39	0.10	5040.0	4.53	0.35	5040.0	3.92	0.05	5040.0	4.10	0.09	5040.0	3.88	0.05	5040.0		
			6552.0	4.43	0.13	6552.0	4.57	0.36	6552.0	4.19	0.04	6552.0	4.28	0.10	6552.0	4.16	0.05	6552.0		

Table D.14 Water Absorption for HW45 specimen types

HW45 - Square			HW45 - 4 Cut			HW45 - 2 Long Cut			HW45 - 2 Short Cut			HW45 - 1 Long Cut			HW45 - No Cut			HW45 - Tensile		
Time	Mass	Stdev	Time	Mass	Stdev	Time	Mass	Stdev	Time	Mass	Stdev	Time	Mass	Stdev	Time	Mass	Stdev	Time	Mass	Stdev
0.0	0.00	0.00	0.0	0.00	0.00	0.0	0.00	0.00	0.0	0.00	0.00	0.0	0.00	0.00	0.0	0.00	0.00	0.0	0.00	0.00
2.0	0.31	0.07	2.0	0.50	0.03	2.0	0.45	0.01	2.0	0.17	0.01	2.0	0.30	0.02	2.0	0.12	0.00	24.0	0.63	0.02
4.0	0.38	0.07	4.0	0.63	0.03	4.0	0.55	0.01	4.0	0.27	0.01	4.0	0.44	0.12	4.0	0.22	0.00	168.0	1.69	0.04
13.5	0.68	0.07	9.0	0.82	0.02	9.0	0.77	0.01	9.0	0.42	0.01	9.0	0.61	0.02	9.0	0.35	0.02	336.0	2.35	0.11
25.0	0.91	0.11	24.0	1.23	0.03	24.0	1.18	0.01	24.0	0.64	0.02	24.0	0.96	0.02	24.0	0.56	0.04	672.0	3.79	0.17
48.0	1.25	0.17	36.0	1.41	0.04	36.0	1.34	0.01	36.0	0.75	0.02	36.0	1.06	0.06	36.0	0.69	0.03	1344.0	5.01	0.08
71.6	1.54	0.23	48.0	1.77	0.07	48.0	1.59	0.02	48.0	0.88	0.02	48.0	1.23	0.05	48.0	0.79	0.04	4373.4	6.91	0.06
100.0	1.82	0.30	72.0	1.96	0.07	72.0	1.90	0.01	72.0	1.07	0.01	72.0	1.49	0.03	72.0	1.02	0.03	6564.0	7.19	0.07
168.0	2.46	0.42	96.0	2.20	0.10	96.0	2.14	0.02	96.0	1.22	0.02	96.0	1.68	0.05	96.0	1.15	0.07			
336.0	3.58	0.64	123.5	2.56	0.16	123.5	2.47	0.04	123.5	1.37	0.04	123.5	1.93	0.03	123.5	1.33	0.09			
504.0	4.36	0.77	168.0	2.92	0.24	168.0	2.81	0.03	168.0	1.64	0.09	168.0	2.25	0.06	168.0	1.56	0.15			
672.0	5.01	0.86	336.0	4.66	0.22	336.0	4.45	0.01	336.0	2.96	0.15	336.0	3.74	0.07	336.0	2.87	0.17			
1421.0	6.45	0.73	504.0	4.91	0.25	504.0	4.71	0.03	504.0	3.25	0.17	504.0	4.05	0.07	504.0	3.17	0.16			
4368.0	7.40	0.47	672.0	5.60	0.23	672.0	5.36	0.09	672.0	3.86	0.20	672.0	4.69	0.07	672.0	3.76	0.15			
8736.0	7.04	0.51	1344.0	6.59	0.21	1344.0	6.30	0.15	1344.0	4.71	0.28	1344.0	5.63	0.11	1344.0	4.59	0.13			
			2016.0	7.68	0.14	2016.0	7.32	0.10	2016.0	6.15	0.19	2016.0	6.85	0.04	2016.0	6.15	0.16			
			2688.0	7.87	0.16	2688.0	7.60	0.12	2688.0	6.81	0.09	2688.0	7.25	0.07	2688.0	6.72	0.10			
			4007.0	7.88	0.14	4007.0	7.56	0.19	4007.0	6.99	0.01	4007.0	7.31	0.03	4007.0	6.89	0.10			
			5040.0	7.93	0.12	5040.0	7.62	0.17	5040.0	7.12	0.05	5040.0	7.41	0.08	5040.0	7.05	0.10			
			6552.0	7.95	0.11	6552.0	7.61	0.21	6552.0	7.28	0.18	6552.0	7.48	0.08	6552.0	7.21	0.09			

## E. APPENDIX: WATER ABSORPTION MODEL PARAMETERS

This appendix serves as a full library of water absorption model parameters for all 84 material biocomposite variations.

Table E.1 Hemp fiber reinforced LDPE specimen model parameters

		Model Parameters						R <sup>2</sup> <sub>DOF</sub>
		A	B	C	D	E	F	
LH 15	Tensile	0.34	7.79E-06	1.78	8.65E-08	0.38	8.71E-08	0.990
	No Cut	0.51	4.09E-06	3.00	6.11E-08	0.40	6.47E-08	0.983
	1 Longitudinal Cut	0.46	1.71E-05	1.76	8.24E-08	0.22	8.47E-08	0.968
	2 Latitudinal Cut	0.34	1.38E-05	1.70	9.29E-08	0.30	8.90E-08	0.991
	2 Longitudinal Cut	1.12	4.34E-06	3.78	1.49E-08	0.40	4.19E-08	0.971
	4 Cut	0.60	1.54E-05	2.42	9.53E-08	0.91	9.38E-08	0.971
	Square	0.46	1.64E-05	2.34	1.76E-07	0.56	1.75E-07	0.984
LH 30	Tensile	0.97	8.51E-06	4.89	8.21E-08	0.62	8.29E-08	0.994
	No Cut	1.21	7.10E-06	4.43	6.85E-08	0.32	6.66E-08	0.982
	1 Longitudinal Cut	1.58	1.00E-05	5.12	8.32E-08	0.42	8.46E-08	0.985
	2 Latitudinal Cut	0.99	2.40E-05	4.81	7.84E-08	0.74	7.88E-08	0.970
	2 Longitudinal Cut	1.75	1.15E-05	5.20	1.28E-07	0.46	1.17E-08	0.981
	4 Cut	1.75	1.51E-05	5.26	1.11E-07	0.10	1.43E-07	0.986
	Square	1.27	2.29E-05	6.28	1.94E-07	0.18	1.98E-07	0.990
LH 45	Tensile	2.60	1.01E-04	15.18	2.87E-07	2.80	3.50E-08	1.000
	No Cut	1.66	4.86E-04	16.06	4.82E-07	2.92	5.56E-08	0.999
	1 Longitudinal Cut	2.18	5.84E-04	17.85	5.48E-07	3.83	1.40E-07	0.999
	2 Latitudinal Cut	1.65	6.11E-04	16.20	5.18E-07	2.41	9.32E-08	0.999
	2 Longitudinal Cut	2.85	5.63E-04	16.02	7.77E-07	2.41	6.97E-08	0.998
	4 Cut	2.85	5.59E-04	16.63	7.67E-07	2.75	8.87E-08	0.996
	Square	2.63	7.12E-04	14.35	8.82E-07	3.77	1.30E-08	0.999

Table E.2 Wood Pulp reinforced LDPE specimen model parameters

		Model Parameters						R <sup>2</sup> <sub>Dof</sub>
		A	B	C	D	E	F	
LW15	Tensile	0.32	1.02E-05	1.83	1.00E-07	0.29	1.00E-07	0.993
	No Cut	0.30	7.48E-06	2.24	9.85E-08	0.73	6.62E-08	0.996
	1 Longitudinal Cut	0.45	8.26E-06	3.07	1.29E-07	1.52	1.40E-07	0.995
	2 Latitudinal Cut	0.36	5.46E-06	2.30	9.86E-08	0.74	8.86E-08	0.998
	2 Longitudinal Cut	0.49	2.83E-05	1.89	1.56E-07	0.26	1.56E-07	0.993
	4 Cut	0.45	3.62E-05	1.89	1.72E-07	0.35	1.71E-07	0.994
	Square	0.38	2.99E-05	2.26	2.23E-07	0.47	2.28E-07	0.996
LW30	Tensile	0.69	9.21E-05	3.72	1.05E-07	0.66	1.05E-07	0.995
	No Cut	0.69	1.01E-04	3.62	1.08E-07	0.64	1.06E-07	0.994
	1 Longitudinal Cut	0.85	1.39E-04	3.62	1.19E-07	0.53	1.17E-07	0.995
	2 Latitudinal Cut	0.66	9.33E-05	2.99	1.08E-07	0.11	1.07E-07	0.993
	2 Longitudinal Cut	1.04	2.33E-04	4.19	1.64E-07	0.77	1.65E-07	0.984
	4 Cut	1.15	1.19E-04	3.36	1.33E-07	0.00	7.07E-09	0.983
	Square	0.96	1.65E-04	4.59	1.85E-07	0.57	1.85E-07	0.988
LW45	Tensile	1.40	1.25E-04	5.56	1.65E-07	1.29	2.07E-07	0.984
	No Cut	1.40	1.40E-04	5.31	1.32E-07	0.90	8.83E-08	0.991
	1 Longitudinal Cut	1.50	1.75E-04	6.05	1.47E-07	0.86	1.28E-07	0.993
	2 Latitudinal Cut	1.42	1.48E-04	5.64	1.35E-07	1.06	1.33E-07	0.989
	2 Longitudinal Cut	1.75	2.80E-04	6.84	1.61E-07	1.33	1.34E-07	0.993
	4 Cut	1.80	3.23E-04	7.97	1.94E-07	2.76	1.94E-07	0.984
	Square	1.55	2.26E-04	6.37	2.54E-07	0.66	2.54E-07	0.988



Table E.3 Hemp fiber reinforced HDPE specimen model parameters

		Model Parameters						R <sup>2</sup> <sub>Dof</sub>
		A	B	C	D	E	F	
HH15	Tensile	0.51	9.52E-05	6.52	5.82E-08	2.70	1.92E-08	0.998
	No Cut	0.55	6.56E-06	5.93	1.07E-07	1.71	2.12E-07	0.994
	1 Longitudinal Cut	0.67	6.86E-06	6.23	1.34E-07	2.14	2.16E-07	0.995
	2 Latitudinal Cut	0.56	3.39E-06	5.94	1.17E-07	1.98	2.43E-07	0.995
	2 Longitudinal Cut	0.81	1.23E-05	4.71	1.29E-07	1.26	2.82E-08	0.993
	4 Cut	0.71	2.86E-05	4.61	1.64E-07	1.97	1.23E-08	0.995
	Square	0.66	1.35E-04	4.79	1.79E-07	2.00	2.86E-08	0.993
HH30	Tensile	2.24	7.08E-08	9.00	4.64E-07	2.51	2.78E-08	0.994
	No Cut	0.62	5.35E-05	8.46	4.77E-07	1.70	5.08E-08	0.999
	1 Longitudinal Cut	1.65	1.45E-05	11.00	3.30E-07	0.80	3.30E-07	0.999
	2 Latitudinal Cut	0.63	5.17E-05	9.88	4.27E-07	2.69	1.28E-07	0.999
	2 Longitudinal Cut	1.25	5.36E-05	9.44	6.59E-07	2.26	1.62E-07	0.999
	4 Cut	1.26	4.97E-05	9.79	6.45E-07	2.58	2.03E-07	0.999
	Square	0.91	1.00E-04	7.75	1.02E-06	2.23	4.16E-08	0.988
HH45	Tensile	0.95	8.72E-05	15.08	1.22E-06	2.55	4.00E-07	0.992
	No Cut	1.44	8.39E-05	13.73	1.31E-06	2.13	2.44E-07	0.999
	1 Longitudinal Cut	1.70	8.92E-05	13.36	1.81E-06	1.66	1.96E-07	0.999
	2 Latitudinal Cut	1.38	8.91E-05	13.61	1.36E-06	1.99	2.37E-07	0.999
	2 Longitudinal Cut	1.70	8.92E-05	13.86	1.81E-06	1.66	1.96E-07	0.999
	4 Cut	1.88	1.20E-04	13.40	2.70E-06	1.66	7.95E-08	0.999
	Square	2.45	1.50E-04	12.75	2.13E-06	2.73	5.49E-08	0.999

Table E.4 Wood Pulp reinforced HDPE specimen model parameters

		Model Parameters						R <sup>2</sup> <sub>DOF</sub>
		A	B	C	D	E	F	
HW15	Tensile	0.42	1.39E-05	2.07	2.81E-08	0.17	2.94E-08	0.959
	No Cut	0.22	5.08E-06	1.13	8.16E-08	0.40	1.05E-09	0.990
	1 Longitudinal Cut	0.26	3.97E-06	1.25	8.55E-08	0.12	8.49E-08	0.993
	2 Latitudinal Cut	0.20	4.79E-06	1.27	8.09E-08	0.08	8.46E-08	0.988
	2 Longitudinal Cut	0.27	2.27E-05	1.53	1.32E-07	0.35	1.34E-07	0.989
	4 Cut	0.33	3.57E-05	1.57	1.32E-07	0.35	1.33E-07	0.989
	Square	0.29	8.88E-05	1.71	1.33E-07	0.40	1.31E-07	0.993
HW30	Tensile	0.62	6.21E-06	3.91	1.20E-07	0.38	1.22E-07	0.990
	No Cut	0.49	9.17E-06	4.18	1.13E-07	0.25	1.15E-07	0.994
	1 Longitudinal Cut	0.64	1.05E-05	4.02	1.29E-07	0.23	6.51E-08	0.993
	2 Latitudinal Cut	0.46	9.43E-06	4.10	1.09E-07	0.08	4.50E-08	0.994
	2 Longitudinal Cut	0.77	1.69E-05	4.03	1.98E-07	0.16	1.87E-07	0.991
	4 Cut	0.79	1.91E-05	3.98	1.98E-07	0.28	1.89E-07	0.990
	Square	0.63	9.85E-06	4.67	1.82E-07	1.75	2.68E-08	0.997
HW45	Tensile	1.08	6.41E-05	7.28	1.99E-07	1.29	1.00E-07	0.99
	No Cut	1.73	2.70E-06	7.01	2.50E-07	1.50	5.11E-07	0.993
	1 Longitudinal Cut	1.01	2.12E-05	7.35	3.51E-07	0.99	3.54E-07	0.993
	2 Latitudinal Cut	1.93	2.25E-06	6.89	2.26E-07	1.50	5.43E-07	0.993
	2 Longitudinal Cut	1.20	2.81E-05	6.71	4.60E-07	0.37	4.53E-07	0.992
	4 Cut	1.26	3.16E-05	7.09	4.53E-07	0.45	4.48E-07	0.994
	Square	1.12	9.98E-06	6.56	3.75E-07	1.18	2.29E-08	0.997

## F. APPENDIX: SURFACE EXPOSED FIBER – BACK SCATTERED SEM IMAGE ANALYSIS RESULTS

This appendix presents the full data set of the assessed surface area of fiber on each type of surface, F.1, and the calculated surface area of fiber for each specimen type, F.2. The four surface types have been classified as: As-molded, As-molded perimeter, Latitudinal cut and Longitudinal cut were imaged by back scattered scanning electron microscopy (BS-SEM) with the micrographs analyzed according to section 2.2.6 methodology. Each type of prepared comprises one or more of the 7 specimen types.

### F.1 ASSESSMENT OF PERCENT FIBER ON MANUFACTURED SURFACES

The results within are presented for all fiber fractions for each matrix fiber combination, such as LH, LW, HH and HW.

Table F.1 Percent Fiber on each surface type for Hemp fiber reinforced LDPE

		Surface Area Percent Fiber (%)		Number of Micrographs
		Average	Stdev	n
LH15	As-molded	2.90	0.69	18
	As-molded Perimeter	3.02	0.77	10
	Transverse cut	16.28	9.12	27
	Longitudinal cut	20.23	2.01	20
LH30	As-molded	8.03	1.88	20
	As-molded Perimeter	7.24	0.78	12
	Transverse cut	27.93	9.38	25
	Longitudinal cut	32.04	2.77	20
LH45	As-molded	15.70	2.32	20
	As-molded Perimeter	20.70	2.11	13
	Transverse cut	37.13	2.55	20
	Longitudinal cut	47.93	1.16	20

Table F.2 Percent Fiber on each surface type for Wood Pulp reinforced HDPE

		Surface Area Percent Fiber (%)		Number of Micrographs
		Average	Stdev	n
LW15	As-molded	5.18	1.07	20
	As-molded Perimeter	3.97	0.74	12
	Transverse cut	19.23	8.09	30
	Longitudinal cut	24.75	2.75	20
LW30	As-molded	9.75	1.30	20
	As-molded Perimeter	8.53	1.48	12
	Transverse cut	31.30	8.25	29
	Longitudinal cut	31.03	4.77	20
LW45	As-molded	21.56	2.30	20
	As-molded Perimeter	17.52	1.62	11
	Transverse cut	34.80	8.04	27
	Longitudinal cut	37.68	3.26	20

Table F.3 Percent Fiber on each surface type for Hemp fiber reinforced HDPE

		Surface Area Percent Fiber (%)		Number of Micrographs
		Average	Stdev	n
HH15	As-molded	4.47	0.85	22
	As-molded Perimeter	1.87	0.50	12
	Transverse cut	24.12	5.23	26
	Longitudinal cut	21.72	2.18	12
HH30	As-molded	8.07	1.17	14
	As-molded Perimeter	9.66	1.29	12
	Transverse cut	34.20	6.75	30
	Longitudinal cut	36.07	2.62	9
HH45	As-molded	12.42	1.35	12
	As-molded Perimeter	15.56	2.22	12
	Transverse cut	45.68	8.48	29
	Longitudinal cut	44.43	2.78	10

Table F.4 Percent Fiber on each surface type for Wood Pulp reinforced HDPE

		Surface Area Percent Fiber (%)		Number of Micrographs
		Average	Stdev	n
HW15	As-molded	2.46	0.44	16
	As-molded Perimeter	0.67	0.30	12
	Transverse cut	18.24	5.84	18
	Longitudinal cut	14.34	3.06	15
HW30	As-molded	4.76	0.89	17
	As-molded Perimeter	2.89	0.66	12
	Transverse cut	29.54	4.46	21
	Longitudinal cut	19.72	2.24	16
HW45	As-molded	5.78	1.70	23
	As-molded Perimeter	8.09	1.33	12
	Transverse cut	35.84	5.07	21
	Longitudinal cut	35.54	4.83	19

## F.2 CALCULATED SURFACE AREA OF FIBER

The calculated accessible fiber for each specimen type were calculated using ( F.1 to (F.8. The dimensions referenced in each equation are relative to the measured dimensions of each specimen type: length (l), width (w) and thickness (t). The area fraction of fiber on the surface is denoted as  $A_f$ .

$$\text{Surface Area of Fiber}_{Tensile}^1 = SA_{Perimeter} * A_{f_{AM Perimeter}} + 2 * SA_{As Molded} * A_{f_{AM}} \quad (F.1)$$

$$\text{Surface Area of Fiber}_{No Cut} = (2 * l * w + 2 * l * t) * A_{f_{AM Perimeter}} + 2 * w * l * A_{f_{AM}} \quad (F.2)$$

$$\begin{aligned} \text{Surface Area of Fiber}_{1 Longitudinal Cut} \\ = (l * t + 2 * w * t) * A_{f_{AM Perimeter}} + 2 * w * l * A_{f_{AM}} + l * t * A_{f_{Longitudinal Cut}} \end{aligned} \quad (F.3)$$

$$\begin{aligned} \text{Surface Area of Fiber}_{2 Transverse Cut} \\ = 2 * w * t * A_{f_{Latitudinal Cut}} + 2 * l * t * A_{f_{As Molded-Perimeter}} + 2 * l * w * A_{f_{As Molded}} \end{aligned} \quad (F.4)$$

$$\begin{aligned} \text{Surface Area of Fiber}_{2 Longitudinal Cut} \\ = 2 * w * t * A_{f_{AM Perimeter}} + 2 * (w * l) * A_{f_{AM}} + 2 * (l * t) * A_{f_{Longitudinal Cut}} \end{aligned} \quad (F.5)$$

$$\text{Surface Area of Fiber}_{4 Cut} = 2 * w * t * A_{f_{Latitudinal Cut}} + 2 * w * l * A_{f_{AM}} + 2 * l * t * A_{f_{Longitudinal Cut}} \quad (F.6)$$

$$\text{Surface Area of Fiber}_{Square} = 2 * w * t * A_{f_{Latitudinal Cut}} + 2 * l * t * A_{f_{As Molded-Perimeter}} + 2 * l * w * A_{f_{As Molded}} \quad (F.7)$$

$$\text{Percent Surface Area of Fiber} [\%] = \frac{\text{Surface Area}_{Fiber}}{\text{Surface Area}_{Specimen}} * 100 \quad (F.8)$$

---

<sup>1</sup> A Solidworks model was created based on the tensile specimen model parameters. The model was used to calculate the Perimeter and SA of the top of the specimen. These values were used for all material variations.

Table F.5 Total Calculated Accessible Fiber for Hemp reinforced LDPE specimen types

		Accessible Fiber		$SA_{\text{specimen}}/V_{\text{specimen}}$ (1/mm)	$SA_f/V_{\text{specimen}}$ (1/mm)
		Percent Surface Area Fiber (%)	SA Fiber (mm <sup>2</sup> )		
LH 15	Tensile	2.92	183.53	0.79	0.02
	No Cut	2.93	115.62	0.83	0.02
	1 Longitudinal Cut	4.84	167.49	0.85	0.04
	2 Transverse Cut	3.20	115.62	0.82	0.03
	2 Longitudinal Cut	7.24	217.58	0.90	0.07
	4 Cut	7.47	216.60	0.90	0.07
	Square	4.76	26.79	0.94	0.04
LH 30	Tensile	7.89	496.04	0.79	0.06
	No Cut	7.87	316.90	0.82	0.06
	1 Longitudinal Cut	10.55	379.11	0.84	0.09
	2 Transverse Cut	8.29	316.90	0.81	0.07
	2 Longitudinal Cut	14.08	429.68	0.90	0.13
	4 Cut	14.46	416.87	0.90	0.13
	Square	10.68	59.24	0.94	0.10
LH 45	Tensile	16.61	1046.95	0.78	0.13
	No Cut	16.77	677.36	0.82	0.14
	1 Longitudinal Cut	19.88	716.96	0.84	0.17
	2 Transverse Cut	17.11	677.36	0.82	0.15
	2 Longitudinal Cut	24.11	746.50	0.88	0.21
	4 Cut	24.42	716.65	0.87	0.21
	Square	19.53	110.74	0.93	0.18

Table F.6 Total Calculated Accessible Fiber for Wood Pulp reinforced LDPE specimens

		Accessible Fiber		SA <sub>specimen</sub> /V <sub>specimen</sub> (1/mm)	SA <sub>f</sub> /V <sub>specimen</sub> (1/mm)
		Percent Surface Area Fiber (%)	SA Fiber (mm <sup>2</sup> )		
LW15	Tensile	4.96	311.64	0.79	0.04
	No Cut	4.92	195.96	0.82	0.04
	1 Longitudinal Cut	7.25	246.94	0.85	0.06
	2 Transverse Cut	5.23	195.96	0.81	0.04
	2 Longitudinal Cut	10.15	305.95	0.89	0.09
	4 Cut	10.40	301.42	0.89	0.09
	Square	6.92	38.97	0.94	0.06
LW30	Tensile	9.53	599.61	0.79	0.07
	No Cut	9.49	379.25	0.82	0.08
	1 Longitudinal Cut	11.95	420.25	0.85	0.10
	2 Transverse Cut	9.95	379.25	0.82	0.08
	2 Longitudinal Cut	15.08	459.93	0.90	0.14
	4 Cut	15.54	449.84	0.89	0.14
	Square	12.56	69.84	0.93	0.12
LW45	Tensile	20.82	1312.03	0.78	0.16
	No Cut	20.69	833.02	0.82	0.17
	1 Longitudinal Cut	22.82	809.28	0.84	0.19
	2 Transverse Cut	21.04	833.02	0.82	0.18
	2 Longitudinal Cut	25.53	777.93	0.90	0.23
	4 Cut	25.83	747.03	0.90	0.23
	Square	22.71	128.75	0.93	0.21



Table F.7 Total Calculated Accessible Fiber for Hemp reinforced HDPE specimens

		Accessible Fiber		SA <sub>specimen</sub> /V <sub>specimen</sub> (1/mm)	SA <sub>f</sub> /V <sub>specimen</sub> (1/mm)
		Percent Surface Area Fiber (%)	SA Fiber (mm <sup>2</sup> )		
HH15	Tensile	4.00	251.30	0.79	0.03
	No Cut	3.91	155.28	0.82	0.03
	1 Longitudinal Cut	6.04	211.86	0.85	0.05
	2 Transverse Cut	4.36	155.28	0.82	0.03
	2 Longitudinal Cut	8.77	268.38	0.89	0.08
	4 Cut	9.14	267.09	0.89	0.08
	Square	6.71	37.41	0.94	0.06
HH30	Tensile	8.36	525.64	0.79	0.07
	No Cut	8.41	335.49	0.82	0.07
	1 Longitudinal Cut	11.34	404.41	0.85	0.10
	2 Transverse Cut	8.91	335.49	0.82	0.07
	2 Longitudinal Cut	15.05	461.45	0.90	0.14
	4 Cut	15.46	445.26	0.91	0.14
	Square	11.94	66.81	0.94	0.11
HH45	Tensile	12.99	817.75	0.79	0.10
	No Cut	13.09	527.54	0.82	0.11
	1 Longitudinal Cut	16.52	574.05	0.84	0.14
	2 Transverse Cut	13.71	527.54	0.82	0.11
	2 Longitudinal Cut	21.17	613.39	0.90	0.19
	4 Cut	21.72	591.36	0.91	0.20
	Square	17.55	98.82	0.93	0.16

Table F.8 Total Calculated Accessible Fiber for Wood Pulp reinforced HDPE specimens

		Accessible Fiber		SA <sub>specimen</sub> /V <sub>specimen</sub> (1/mm)	SA <sub>f</sub> /V <sub>specimen</sub> (1/mm)
		Percent Surface Area Fiber (%)	SA Fiber (mm <sup>2</sup> )		
HW15	Tensile	2.13	134.00	0.79	0.02
	No Cut	2.07	80.68	0.82	0.02
	1 Longitudinal Cut	3.52	123.38	0.85	0.03
	2 Transverse Cut	2.43	80.68	0.83	0.02
	2 Longitudinal Cut	5.39	160.74	0.91	0.05
	4 Cut	5.71	165.78	0.90	0.05
	Square	4.31	24.02	0.94	0.04
HW30	Tensile	4.42	277.78	0.79	0.03
	No Cut	4.35	171.84	0.82	0.04
	1 Longitudinal Cut	6.19	214.90	0.85	0.05
	2 Transverse Cut	4.89	171.84	0.82	0.04
	2 Longitudinal Cut	8.44	256.83	0.90	0.08
	4 Cut	8.95	260.40	0.90	0.08
	Square	7.86	43.99	0.93	0.07
HW45	Tensile	6.20	390.23	0.79	0.05
	No Cut	6.28	249.47	0.82	0.05
	1 Longitudinal Cut	9.35	330.16	0.85	0.08
	2 Transverse Cut	8.66	249.47	0.82	0.05
	2 Longitudinal Cut	13.27	404.08	0.90	0.12
	4 Cut	13.81	400.77	0.90	0.12
	Square	10.32	58.14	0.93	0.10